Evaluation of combined CO_2 and O_2 measurements taken by the CARIBIC passenger aircraft

Master's Thesis
Faculty of Science
University of Bern

presented by
Iwan Bigler
2013

Supervisor:
Prof. Dr. Markus Leuenberger
Physics Institute and Oeschger Centre for Climate Change Research

Advisor:
Michael Schibig
Physics Institute and Oeschger Centre for Climate Change Research

ACKNOWLEDGMENTS

My grateful appreciation goes to Markus Leuenberger for supervising this thesis and his support throughout my time at the division for Climate and Environmental Physics, Peter Nyfeler for patiently explaining the technical aspects behind this project, Michael Schibig for always taking his time whenever I had questions, and Doris Rätz who handled the administrative work.

I further wish to extend my gratitude to Carl Brenninkmeijer and the welcoming people that are his working group in Mainz, who keep the CARIBIC project running and make data acquisition possible. I would particularly like to thank Tanja Schuck for introducing me into the CARIBIC project, Angela Baker and Taku Umezawa for the encouraging discussions in times when the data looked less than perfect, Armin Rauthe-Schöch to whom I owe much of the Matlab script, and Dieter Scharffe for his support on all things technical about the aircraft and container.

I am also thankful to the people at the division for Climate and Environmental Physics in Bern, for providing such a pleasant working environment and all the delicious treats.

Contents

List of Figures

List of Tables

List of Abbreviations

CARIBIC	Civil Aircraft for the Regular Investigation of the atmosphere Based on an Instrumented Container
CG1	Calibration gas 1 (high-span for CO_2, low-span for O_2)
CG2	Calibration gas 2 (low-span for CO_2, high-span for O_2)
ECMWF	European Centre for Medium-Range Weather Forecasts
HS	High-span
IMK	Institute for Climate Research, Karlsruhe Institute of Technology, Karlsruhe
IRMS	Isotope Ratio Mass Spectrometer
KNMI	Koninklijk Nederlands Meteorologisch Instituut, De Bilt
LS	Low-span
LSCE	Laboratoire des Sciences du Climat et de l'Environnement, Gif-sur-Yvette
MPI	Max-Planck-Institute, Mainz
NDIR	Non-dispersive infrared
PIUB	Physics Institute, University of Bern
SIO	Scripps Institution of Oceanography
UTC	Coordinated Universal Time
WG	working gas

Chapter 1

Introduction

Climate change and its causes and consequences have been subject of extensive research in the last decades. Anthropogenically emitted carbon dioxide (CO_2) is a significant contributor to global warming and has been accumulating in the atmosphere since the beginning of the industrial era. It is therefore essential to comprehend the global carbon cycle for reliable future projections of CO_2 levels and their effects on climate change. For a better understanding of the carbon cycle and in particular to partition the oceanic and terrestrial sinks of atmospheric CO_2, oxygen-to-nitrogen (O_2/N_2) ratio observations can be carried out (e.g. Keeling et al. 1993). As changes of O_2 in the atmosphere are in most processes directly related to changes in atmospheric CO_2 concentrations, they occur in the same order of magnitude (Laan-Luijkx et al., 2010b). These variations in O_2 are much more difficult to detect against the very large background concentration of 21 %. Since the first high precision O_2 measurement systems in 1988 (Keeling, 1988b), there has been an increase in the number of measurement sites. Observations of the atmospheric O_2/N_2 ratio have been made stationarily on land and at sea (e.g. Bender et al. 1996; Laan-Luijkx et al. 2010b; Manning and Keeling 2006; Stephens et al. 2007b; Tohjima et al. 2008), and on moving platforms such as ships (Battle et al., 2006; Thompson et al., 2007; Tohjima et al., 2005), balloons (Ishidoya et al., 2006) and aircrafts (Ishidoya et al., 2012; Langenfelds, 2002; Sturm et al., 2005). With the exception of the study by Ishidoya et al. (2012), past research was mostly conducted sporadically in the form of campaigns and focused on surface sites or vertical profiles of O_2/N_2. While they contributed to an understanding of the variations in O_2/N_2 locally and on short time scales, there is still insufficient long-term global data coverage and few observations of systematic temporal and spatial variations of O_2/N_2 in the free troposphere (Goto, 2011; Ishidoya et al., 2006; Sturm et al., 2005). Apart from numerous ground-based stations, satellite technology has recently emerged to monitor the CO_2 concentration on a broad scale but their produced distribution maps so far have usually been of insufficient resolution to give a detailed and accurate view. Research aircraft projects on the other hand usually suffer from small data sets and low spatial

and temporal coverage (Sawa et al., 2012). More observations of CO_2 on longer time scales in the free troposphere and the lowermost stratosphere can provide valuable information for the evaluation of the much improved atmospheric transport models available to date (Brenninkmeijer et al., 2007; Matsueda et al., 2002b).

Within the framework of the CARIBIC project (Civil Aircraft for the Regular Investigation of the atmosphere Based on an Instrumented Container, www.caribic-atmospheric.com), the Physics Institute at the University of Bern (PIUB) has developed a semi-continuous O_2 and CO_2 analyzer for automated operation on a commercial airplane (Valentino, 2007). As the cruise altitudes of passenger aircrafts coincide with the interesting, yet largely unexplored area of the upper troposphere/lowermost stratosphere, CARIBIC can extend the global climate data network. Using an advanced multi-probe inlet system attached to an Airbus A340-600, in-situ measurements of atmospheric O_2 and CO_2 measurements are conducted based on fuel cell and non-dispersive infrared (NDIR) sensor technology, covering large parts of the globe. As of yet, in-situ analyses of O_2 aboard a fast-moving civil aircraft have not been attempted and pose a great challenge in terms of gas handling and automation. Therefore, the scientific payload added by the PIUB has been stated to be of experimental nature (Brenninkmeijer et al., 2007). Since 2005, the equipment has been aboard the aircraft for roughly one campaign per month, resulting in a vast data set, which has not been analyzed in detail. Extending initial work presented by Valentino (2007), it was the goal of this Master's Thesis to develop a data processing routine, as well as to evaluate the O_2 and CO_2 data collected so far in order to draw conclusions as to whether this kind of measurement system incorporated into an aircraft yields precise enough data for meaningful interpretation. I first provide some background information and the theoretical aspects relevant for this thesis in chapter 2, then continue with a description of the current experimental setup in chapter 3, in which I will also illustrate the methodology of the analysis of data, followed by the presentation of some example flights in chapter 4. My thesis will be concluded with a discussion of the problems that were encountered with the current setup and by providing options for future improvements.

Chapter 2

Theory

2.1 The global carbon cycle

Throughout Earth's history, the climate has changed substantially numerous times (IPCC, 2007). The past variability in the climate system prior to industrialization was natural in origin and caused by variations in factors such as solar insolation, Earth albedo, atmospheric composition, ocean currents or volcanic eruptions. Increasing evidence points out that during the last century however, human activities have had dramatic influence on the climate additionally (IPCC, 2007). The scientific opinion as expressed by the Intergovernmental Panel on Climate Change (IPCC) states that most of the observed rise in global surface temperatures of the past 50 years is attributable to man-made emissions of atmospheric greenhouse gases (IPCC, 2007). These greenhouse gases present a characteristic to absorb infrared radiation. Incoming shortwave radiation from the sun is absorbed by the surface on Earth and subsequently re-emitted in the form of thermal infrared radiation of longer wave length. While greenhouse gases are transparent to short-wave radiation, they absorb large parts of long-wave radiation, thus trapping heat within the atmosphere rather than allowing it to pass into space. The primary greenhouse gases giving rise to this so called greenhouse effect are water vapor (H_2O), carbon dioxide (CO_2), methane (CH_4), nitrous oxide (N_2O), tropospheric ozone (O_3) and chlorofluorocarbons (CFC) (IPCC, 2007). Yet, the greenhouse effect is not harmful per se. In fact, without it, the global surface temperature—currently at about 14 °C—would only be −19 °C (IPCC, 2007). Hence, the natural greenhouse effect also generates the temperature prerequisite for life on Earth as we know it today (Laan-Luijkx, 2010). Furthermore, the most important greenhouse gas in the atmosphere is water vapour, which is only marginally affected by direct anthropogenic activities (IPCC, 2007). What is alarming though is that the second most important greenhouse gas, CO_2, constitutes by far the largest radiative forcing of 1.66 $\mathrm{W\,m^{-2}}$ since the pre-industrial time 1750 (IPCC, 2007) and the current concentration of 397 ppmv (parts per million by volume) in the atmosphere has not been

exceeded during the last 650 000 years (IPCC, 2007). The increase from 280 ppmv in pre-industrial times to the present-day level has also occurred on an unusually short time scale (IPCC, 2007). Since concentrations of CO_2 and other greenhouse gases are expected to increase further within this century, it is therefore essential to understand the global biogeochemical cycles in order to quantify the implications of anthropogenic emissions of greenhouse gases on the climate (Sturm et al., 2005).

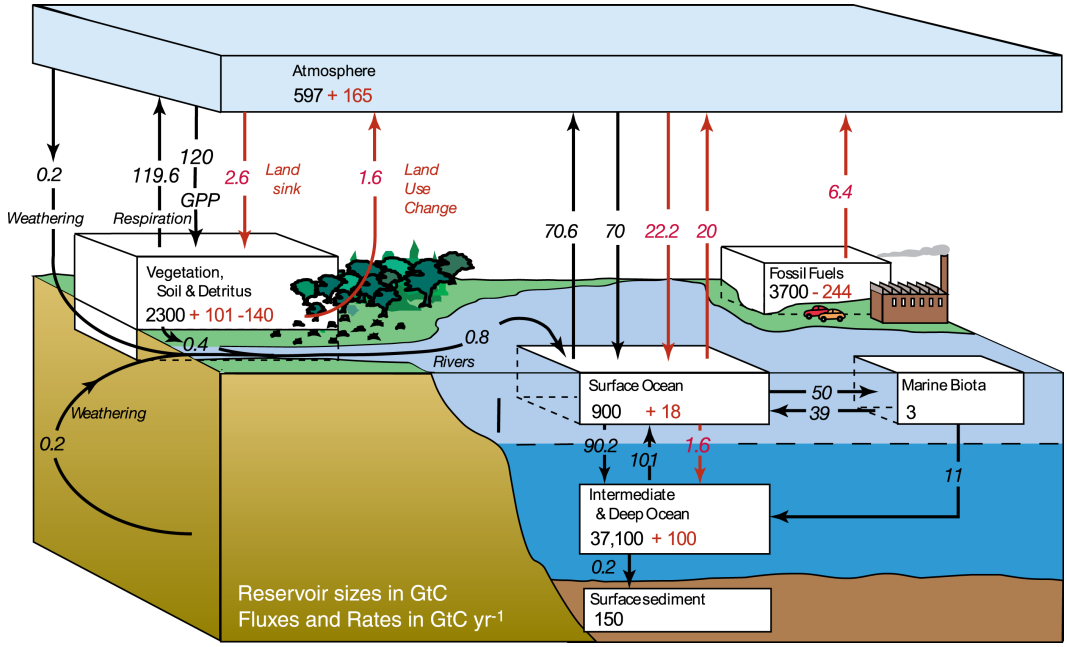

Figure 2.1 The global carbon cycle for the 1990s with the main reservoirs atmosphere, terrestrial biosphere, ocean and fossil fuels, and the fluxes between them. Black arrows and numbers indicate pre-industrial natural fluxes and pool sizes, and anthropogenic changes in net carbon fluxes and reservoirs are depicted in red. Figure from IPCC (2007).

The inventory of the Earth's carbon can be split up into four main pools: the atmosphere, the terrestrial biosphere, the ocean, and sediments including fossil fuels. Through processes that take place over seconds to millenia, carbon is constantly being transferred between these various reservoirs, which is referred to as the global carbon cycle.

The atmospheric carbon content sums up to approximately 810 Gt, most of which is present in the form of CO_2, with much smaller amounts of CH_4 and carbon monoxide (CO) (Joos, 2012). Even so, CO_2 only makes up 0.04 % of the atmosphere, besides primarily the much more abundant species N_2 with 78.08 %, O_2 with 20.95 % (Machta and Hughes, 1970) and Argon (Ar) with 0.93 %. Despite this being a considerably smaller amount compared to the other pools, carbon in the atmosphere is of vital importance due to its impact on the greenhouse effect, thereby providing the direct link with climate change. Before the industrial revolution, the size of the atmospheric reservoir was substantially smaller at 600 GtC. The fact that the CO_2 mixing ratio in the atmosphere has only varied between 260 ppmv and 280 ppmv in the 10 kyr before the industrialization indicates that the

global carbon system was close to equilibrium (IPCC, 2007; Joos, 2012). Estimates suggest that of the human activities that caused this increase, fossil fuel burning has contributed two thirds and land use change one third (IPCC, 2007). Land use change is dominated by deforestation and its associated biomass burning, as well as changes in agricultural practices (IPCC, 2007). Atmospheric CO_2 exhibits inter-annual variability caused by variations in land use emissions and global air-to-land and air-to-ocean net carbon fluxes. During El Niño/Southern Oscillation (ENSO) events for example, when the combination of land use activities and dry conditions lead to release of carbon from forest fires, the CO_2 mixing ratio is particularly elevated (Joos, 2012). By dividing the atmospheric carbon stock by the gross fluxes into the ocean and the biosphere, one can estimate that the mean residence time for an atom of carbon in the atmosphere is 3 to 4 years (Malhi, 2002).

The terrestrial biosphere is composed of vegetation, soil and detritus, with the majority of carbon being stored in the soil. It is currently estimated that the biospheric carbon inventory comprises about 2500 GtC to 3800 GtC with an average residence time of 17 years (Joos, 2012; Malhi, 2002). Via the processes of photosynthesis and respiration the atmosphere and the biosphere exchange carbon with each other. During photosynthesis, plants take up CO_2 from the atmosphere and convert the carbon to plant biomass as shown in the following simplified reaction.

$$6\,CO_2 + 6\,H_2O + \text{light} \longrightarrow C_6H_{12}O_6 + 6\,O_2 \tag{2.1}$$

This gross primary production (GPP) by vegetation accounts for a carbon uptake of about 120 GtC/yr. Around half of the assimilated carbon is released again by the plant itself in the process of autotrophic respiration as the plants metabolize their produced sugars:

$$C_6H_{12}O_6 + 6\,O_2 \longrightarrow 6\,CO_2 + 6\,H_2O \tag{2.2}$$

If we also consider the release of carbon into the atmosphere by microbial decomposition of dead organic material (50 GtC/yr) and disturbances such as fires, deforestation or herbivory (9 GtC/yr) we end up with a resulting net carbon flux from the atmosphere to the terrestrial biosphere of about 1 GtC each year (Joos, 2012).

The upper curve in Figure 2.2 depicts the famous Keeling curve, an atmospheric long-term CO_2 record collected in Hawaii. The distinct seasonal signal in CO_2 concentration mainly reflects the biospheric activity, when periods of predominant respiration alternate with periods of elevated photosynthetic activity (Assonov et al., 2009). Due to its larger land mass for vegetation to grow on compared to the southern hemisphere, the northern hemisphere generally shows a more pronounced seasonal signal in the atmospheric CO_2 mixing ratio. CO_2 builds up slowly during the northern winter when the vegetation is dormant and reaches the highest levels in April, depending on the latitude. In spring the plants start to grow and remain photosynthetically active throughout the summer, which leads to a CO_2 minimum around August. While the peak-to-peak signal of the seasonal cycle around

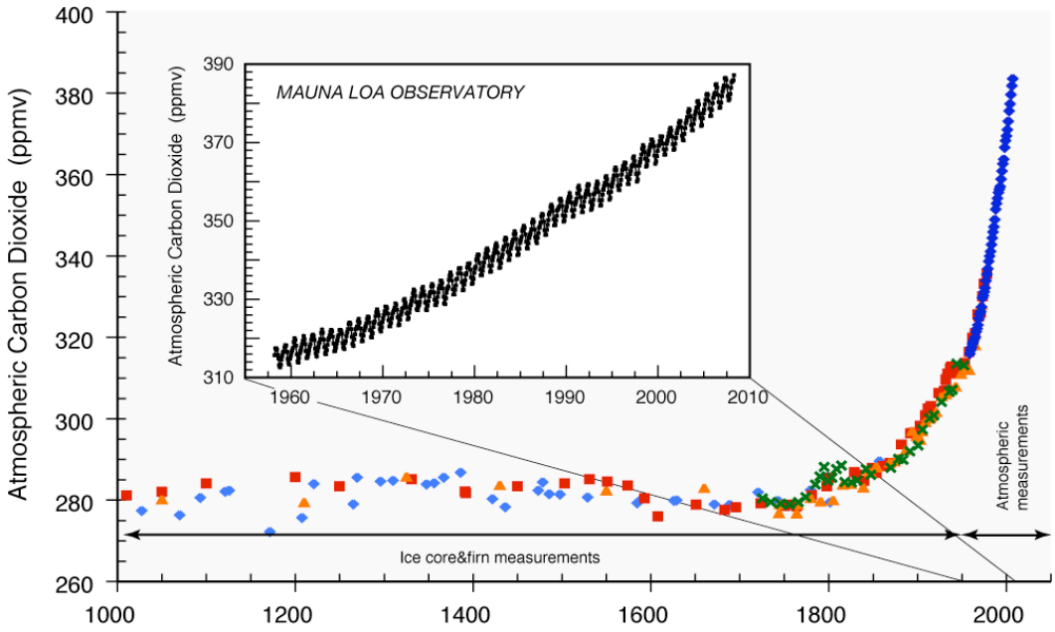

Figure 2.2 The evolution of atmospheric CO_2 since 1000 AD. CO_2 data prior to 1958 consist of measurements of air bubbles trapped in ice cores sampled at sites in Antarctica (Barnola, 1999). Dark blue diamond-shaped symbols and the data in the inset denote direct measurements of air samples taken by Keeling and Whorf (2000) since 1958 at Mauna Loa, Hawaii. Figure updated by Gruber from Sarmiento and Gruber (2002).

the equator amounts to only about 3 ppmv, the amplitude in the far north can reach values of up to 20 ppmv. This discrepancy can be explained by the increasing seasonality of plant activity towards higher latitudes owing to the climate (Keeling et al., 1996). Keeling et al. (1996) further report that the seasonal amplitude has increased since the measurements on Mauna Loa started in the 1960s and that there have been shifts in the timing of the seasonal cycle with the decrease occurring 7 days earlier. These findings indicate an increased exchange of carbon with the terrestrial biosphere because of a CO_2 fertilization effect and land use change (McGuire et al., 2001), as well as a lengthening of the growing season (Keeling et al., 1996). Most of the spatial variation in carbon storage density in the biosphere can be attributed to differences in characteristics of vegetation types. Tropical forest biomes exhibit the largest capacity to store carbon in the vegetation and soil (Joos, 2012). Some of the carbon is also transported laterally from the terrestrial biosphere to the ocean by rivers. It was assumed that this transport remained unchanged since pre-industrial times. Regnier et al. (2013) have recently estimated that the total carbon flux from soils, bedrock and sewage to aquatic systems today is 2.5 GtC/yr, of which 1.0 GtC/yr can be attributed to anthropogenic perturbation. They suggest, that only 0.1 GtC/yr of the initial perturbation are eventually transported to the open ocean.

With a carbon content of 38 000 Gt, the ocean is the largest fast exchanging carbon pool and as such exerts a dominant control on the CO_2 levels in the atmosphere (Sturm, 2005). Prior to the onset of industrialization, the ocean had stored 60 times more carbon than the atmosphere and 20 times

the amount contained in the land biosphere (IPCC, 2007). The main exchange occurs between the atmosphere and the surface ocean, and starts via the process of dissolution.

$$CO_2(aq) + H_2O \longleftrightarrow H_2CO_3 \rightleftharpoons H^+ + HCO_3^- \rightleftharpoons 2\,H^+ + CO_3^{2-} \tag{2.3}$$

CO_2 in the atmosphere dissolves in the surface ocean and reacts with water to form carbonic acid (H_2CO_3), only to rapidly dissociate again into bicarbonate (HCO_3^-) and carbonate (CO_3^{2-}). The sum of these carbonic species is termed dissolved inorganic carbon (DIC), where carbon is most abundant in the form of HCO_3^-. It is estimated that the amount of time the carbon in the form of DIC resides in the well mixed upper ocean is less than a decade before it is transported to the intermediate ocean where DIC enriched waters may stay out of contact with the atmosphere for thousands of years (IPCC, 2007). Two mechanisms are responsible for the flux of DIC from the upper ocean to the depth corresponding to 90 GtC/yr. As the solubility of CO_2 is greater in colder waters, areas of increased carbon uptake coincide with areas where cooler and more saline water masses sink due to their increased density. We call this first mechanism, associated with the meridional overturning circulation, the solubility pump. Prominent example for a location with a strong solubility pump is the North Atlantic. The second means of carbon transport from the surface ocean to the intermediate and deep ocean is the biological pump. Just like the biosphere on land, phytoplankton in the euphotic zone of the ocean takes up carbon through photosynthesis and fix it in organic form. DIC is also the form in which carbon is used by marine organisms for the synthesis of carbonate shells (Malhi, 2002). Sinking of particulate material such as faecal pellets and dead organisms, followed by conversion of this soft tissue material first into particulate organic carbon or dissolved organic carbon (DOC) and then back into DIC at depth by bacteria through respiration, pumps some of the carbon from the ocean surface into the depth. This recycled CO_2 is then transported by the global thermohaline circulation and after a long time eventually upwelled to the surface ocean at a different location such as the Equator or western margins of continents (Malhi, 2002). DOC can also enter the ocean via river input (IPCC, 2007). It is believed that the biological pump accounts for about 80 % of the vertical gradient in DIC, whereas the remaining 20 % are attributable to the solubility pump (Siegenthaler and Sarmiento, 1993). Only a very small fraction of 1 % of the sinking biological particles leaving the surface ocean reach the ocean floor, where it may be buried in the sediments (IPCC, 2007).

Finally, a vast amount of carbon is stored in the relatively inactive form of sediments. Due to their very slow exchanging nature, they are only considered to be important on timescales of thousands of years (Joos, 2012). Depicted in figure 2.1 are only the fractions existing in surface sediment and fossil fuels that do exchange carbon; the remainder of several millions of GtC, most commonly present as $CaCO_3$ and $MgCO_3$, is not illustrated. Since the 1750s, fossil fuels have become an increasingly important energy source. Carbon, which has accumulated in coal, petroleum and natural gas over millions of years is now re-emitted into the atmosphere on extremely short timescales. The process of

stoichiometric combustion of hydrocarbons (Goto, 2011) can generally be expressed by

$$C_xH_y + (x + \frac{y}{4})O_2 \longrightarrow xCO_2 + \frac{y}{2}H_2O \tag{2.4}$$

The present-day value of total carbon emission is roughly 10 GtC/yr. If all the CO_2 remained airborne, the atmospheric CO_2 concentration would increase by almost 5 ppmv each year, with 1 ppmv corresponding to 2.123 GtC (Joos, 2012). However, measurements from 1995 to 2005 showed an average increase rate of 1.9 ppmv/yr. The reason for this is that 30 % of the anthropogenically emitted CO_2 is absorbed by the oceans, 25 % is taken up by the terrestrial biosphere, while a little less than half of it remains in the atmosphere (IPCC, 2007). This way, the system is able to remove about half of a CO_2 disturbance to the atmosphere within 30 years and 80 % over a time scale of a couple of centuries. The remaining 20 % however will typically stay in the atmosphere for many millenia (IPCC, 2007).

2.2 Atmospheric oxygen as a tracer for carbon cycle processes

While it is possible to directly measure the changes in CO_2 concentration in the atmosphere with high precision, it is very difficult to quantitatively determine carbon inventory changes in the terrestrial biosphere and the ocean (Malhi, 2002). One reason for this is that the atmospheric CO_2 content is considered relatively well-mixed globally, whereas the spatial heterogeneity in the terrestrial biosphere and the ocean reservoirs complicate the assessment of the carbon source and sink strengths. Another reason is that these relative net changes in the carbon pool sizes for the biosphere and the ocean are much smaller compared to the changes in the atmospheric carbon (Sturm, 2005). Hence, several indirect approaches have been conducted in order to estimate the partitioning of anthropogenic CO_2 between the biosphere and the ocean. For example, observed CO_2 partial pressure differences between the surface ocean and the atmosphere were analyzed to estimate the atmosphere-ocean CO_2 flux (Tans et al., 1990). Ciais et al. (1995) based another approach on the fact that plants preferably assimilate the lighter ^{12}C isotope in CO_2 resulting in enriched ^{13}C in the atmosphere. Because exchange of CO_2 between the air and the ocean does not strongly alter the $^{13}C/^{12}C$ ratio, combined measurements of the CO_2 mixing ration in the atmosphere and the carbon isotopic ratio can be used to separate the carbon uptake by vegetation and the ocean (Sturm, 2005). More recently, studies have also deployed three-dimensional global-scale models which include ocean circulation and biogeochemistry (Le Quéré et al., 2000).

Keeling and Shertz (1992) suggested a fourth methodology to constrain the partitioning of oceanic and terrestrial CO_2 uptake, and to gain a better understanding of the global carbon cycle. In their approach, variations in atmospheric CO_2 are simultaneously measured in combination with atmospheric oxygen. The different behaviors of CO_2 and O_2 in the exchange between the atmospheric and

oceanic reservoirs can give us valuable information about the marine uptake of CO_2, which cannot be obtained by CO_2 concentration measurements alone (Laan-Luijkx, 2010): For most processes, changes in CO_2 are accompanied by inverse changes in O_2 according to process-specific stoichiometric ratios. This is the case for fossil fuel combustion (reaction 2.4), photosynthesis (reaction 2.1) and respiration (reaction 2.2). For each mole of CO_2 that is released during fossil fuel burning, one expects a global average of 1.4 mol of O_2 to be removed from the atmosphere (Keeling, 1988b). In contrast, the ratio is on average 1.1 mol O_2 for every mole of CO_2 for photosynthesis and likewise for respiration (Severinghaus, 1995). An exception to the anti-correlated relationship forms the air-surface ocean interface. The reactions 2.3 indicate that O_2 is irrelevant to the dissolution of CO_2 in the ocean and hence, only the exchange of CO_2 by the biosphere will leave an imprint on the atmospheric O_2 signal. Independent of the CO_2 uptake, there is also dissolution of O_2 in the ocean, determined by partial pressure differences between the reservoirs, which in turn depends on the solubility of oxygen in seawater, biological activities in the ocean and upwelling of deep water (Goto, 2011). O_2 is not only less soluble in the ocean than CO_2 but it is also is not involved in the oceanic carbonate-buffersystem as CO_2 once it is dissolved, so that variability in the ocean O_2 inventory usually affect the atmospheric concentration only little (Valentino, 2007). Still, the effect of marine O_2 outgassing caused by rising sea surface temperatures and changes in biological pumps offset the observed atmospheric O_2 decrease and have to be taken into account when calculating the global carbon budget accurately (Manning and Keeling, 2006).

Knowing the stoichiometric ratios and the amount of CO_2 release through fossil fuel burning makes it possible to discern the marine and terrestrial CO_2 uptake components of the anthropogenic emissions that do not accumulate in the atmosphere (Sturm, 2005). The global budgets for O_2 and CO_2 can be illustrated by the following equations (Laan-Luijkx, 2010; Valentino, 2007):

$$\Delta CO_2 = F - B - O \tag{2.5}$$

$$\Delta O_2 = -\alpha_F \cdot F + \alpha_B \cdot B + Z \tag{2.6}$$

$$B = \frac{\Delta O_2 + \alpha_F \cdot F - Z}{\alpha_B} \tag{2.7}$$

$$O = F - \left(\frac{\Delta O_2 + \alpha_F \cdot F - Z}{\alpha_B} \right) - \Delta CO_2 \tag{2.8}$$

ΔCO_2 and ΔO_2 refer to the observed change in atmospheric CO_2 and O_2 respectively, F is the fossil fuel CO_2 source, B is the net land biotic CO_2 sink, O is the net marine CO_2 sink, Z is the net O_2 flux between the ocean and the atmosphere, α_B and α_F are the stoichiometric ratios of O_2 to CO_2 for photosynthesis and respiration, and for fossil fuel combustion, respectively.

Strictly speaking, this method can only differentiate between the non-biological CO_2 uptake by the ocean and the biological uptake that occurs in both the land and the ocean reservoirs. The biospheric

uptake of carbon is however attributed to the land, since the biological oxygen uptake in the ocean is not expected to have changed substantially during recent decades (IPCC, 2003).

Studies that applied the method of O_2/N_2 measurements quantified the ocean sink for CO_2 during the 1990s at $1.7 \pm 0.5\,GtC/yr$ (Manning, 2001) and $2.1 \pm 0.5\,GtC/yr$ (Bender et al., 2005).

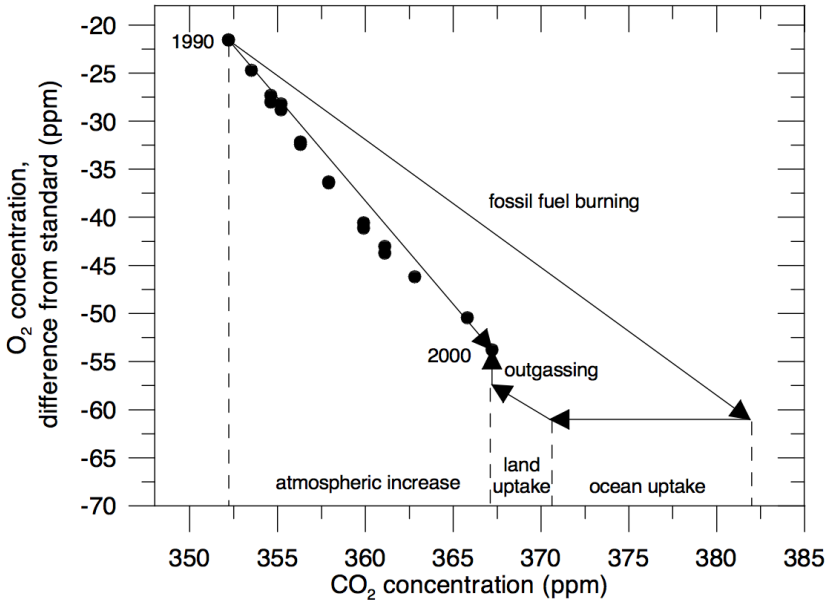

Figure 2.3 Schematic overview of the relationship between the changes in atmospheric O_2 and CO_2 concentrations for partitioning of fossil fuel carbon using combined measurement (Laan-Luijkx, 2010). Solid circles represent annual averages of measured O_2 (y-axis) and CO_2 (x-axis) concentrations for the years 1990 to 2000. The arrow labeled "fossil fuel burning" indicates the change in atmospheric O_2 and CO_2 concentrations that would have occurred if all CO_2 emitted remained in the atmosphere. Carbon uptake by land and ocean is constrained by the known O_2:CO_2 stoichiometric ratios of these processes, determining the slopes of the respective arrows (Plattner et al., 2002). Figure from Sturm (2005), modified from Plattner et al. (2002).

2.3 Measuring atmospheric oxygen

The expected absolute variations of O_2 in the atmosphere are about in the same range as the variations in CO_2. However, in contrast to CO_2 measurements, the changes in O_2 content need to be detected against a large background concentration of 20.95 % (Laan-Luijkx, 2010). Achieving the same relative precision as for CO_2 to be able to constrain the global carbon budget poses a great analytical challenge and makes high demands on the gas handling and equipment used (Sturm, 2005). The high O_2 content in air further causes some complications when measuring changes in the percentage of atmospheric O_2 in background air (Keeling and Shertz, 1992). For example, suppose one molecule of CO_2 is added to a sample air mass containing one million molecules, of which 390 are CO_2 and 209460 are O_2. The resulting mixing ratio in CO_2 is $391/1000001 \cdot 10^6 = 390.999609$, yielding a change in the

mixing ratio by almost exactly 1 ppmv. If one molecule of O_2 is added to the sample and the same principle is applied, the mixing ratio becomes $209461/1000001 \cdot 10^6 = 209460.791$. The increase in O_2 is noticeably smaller than 1 ppmv (by ppmv O_2 I mean µmol O_2 per mol of dry air on a CO_2-free basis (Valentino, 2007)) caused by the increased total number of molecules, which partly offsets the increase in O_2. The same dilution effect is negligible for CO_2. The O_2 concentration even decreases by 0.2095 ppmv by the mere addition of a CO_2 molecule. Since CO_2 is considered a trace gas, its concentrations are commonly reported as mole fractions or mixing ratios (ppmv). The benefit of volume per volume units is that gaseous concentrations expressed in these units are not altered when the gas is expanded or compressed. Using mole fraction units does not represent well fluxes of O_2 and appears to be a confusing basis for tracking O_2 and CO_2 simultaneously. To avoid confusion, changes in the atmospheric O_2 concentration are usually expressed through changes in the ratio of O_2 to N_2 following the convention originally suggested by Keeling and Shertz (1992). Because the variations in atmospheric N_2 are substantially smaller and superimposed on a larger background concentration than those for O_2, one can assume that changes in O_2/N_2 predominantly reflect variations in the abundance of O_2. O_2/N_2 ratios of a sample are reported as relative deviations ($\delta(O_2/N_2)$) from an arbitrary reference gas (Keeling and Shertz, 1992):

$$\delta(O_2/N_2) = \left(\frac{(O_2/N_2)_{\text{sample}}}{(O_2/N_2)_{\text{reference}}} - 1 \right) \tag{2.9}$$

By multiplying $\delta(O_2/N_2)$ by 10^6 and thereby expressing the ratio in units of "per meg" one can avoid very small $\delta(O_2/N_2)$ values common for natural air (Keeling and Shertz, 1992). 4.77 per meg is equivalent to 1 ppmv. This expression has the advantage of being insensitive to varying concentrations in other atmospheric gases such as CO_2 or Ar (Laan-Luijkx, 2010). Keeling et al. (1993) report of interannual trends of -15 per meg/yr, interhemispheric differences of 30 per meg and seasonal cycle amplitudes of up to 100 per meg, and recommended that for oxygen a measurement precision of about 5 per meg should be aimed at in order to resolve these features accurately.

Inversely to CO_2, the O_2/N_2 ratio is decreasing globally and depending on location exhibits a seasonal cycle, as can be seen in figure 2.4. The O_2/N_2 ratio is higher in summer and lower in winter in each hemisphere. The amplitude exhibited by the O_2/N_2 cycle however is larger than would be expected from the variations in CO_2 (Keeling and Shertz, 1992). In the southern hemisphere, the cycle can be primarily explained by seasonal variations in O_2 solubility in the ocean caused by changes in water temperature and salinity (Keeling et al., 1998b). In the northern hemisphere, two components contribute mainly to the seasonal variations. One component is the terrestrial biosphere: In spring and summer, net photosynthesis by plants consumes CO_2 and releases O_2, thereby increasing the O_2/N_2 ratio. This is reversed in autumn and winter, when respiration dominates. The second component reinforcing the amplitude is the marine biosphere. Warming in spring leads to a more stratified ocean, which in turn results in a more efficient biological pump due to less upward transport of nutrient-rich,

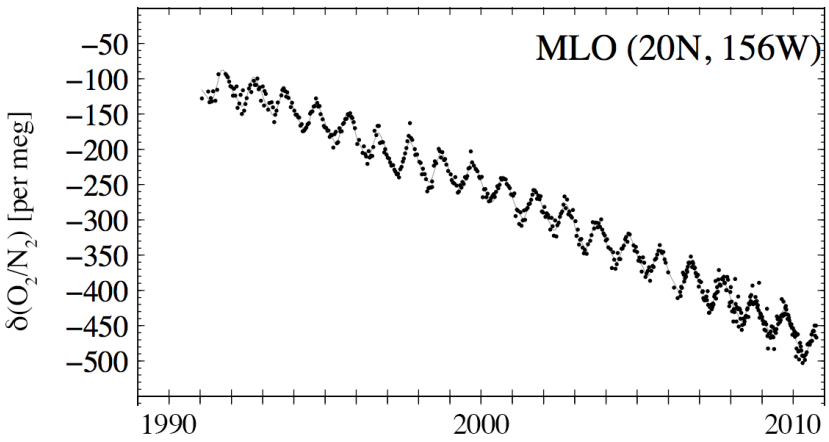

Figure 2.4 Atmospheric $\delta(O_2/N_2)$ ratio recorded at Mauna Loa, Hawaii from 1990 to 2010. Figure from Keeling (2010).

O_2-poor waters. O_2 produced by the biosphere supersaturates the water and induces a flux of oxygen to the atmosphere. When the water starts to cool in autumn the mixing in the ocean interior is picked up and brings O_2-depleted water masses to the surface, resulting in a net air-sea flux of O_2 (Bender, 2006). While the thermal and biological forcings reinforce each other in the case of O_2/N_2 ratio, these effects partially compensate each other for CO_2, hence resulting in smaller seasonal air-sea fluxes in CO_2 (Keeling and Shertz, 1992). Combustion of fossil fuels is responsible for the long-term decrease in the ratio of O_2/N_2, with land biosphere growth attenuating the fossil decrease (Bender, 2006).

By combining data on the concentrations of O_2 and CO_2, one can constrain the physical and biological processes in the ocean (Stephens et al., 2003). For this, Stephens et al. (1998) introduced the quantity "atmospheric potential oxygen" (APO), which is defined as

$$\delta APO = \delta\left(O_2/N_2\right) + \frac{1.1}{X_{O_2}} \cdot \left([CO_2] - 350\right) \tag{2.10}$$

APO is the sum of the O_2 concentration $\delta(O_2/N_2)$ and 1.1 times the CO_2 concentration, with 1.1 being the global average stoichiometric ratio between O_2 and CO_2 in photosynthesis and respiration (α_B). By dividing by the standard mole fraction of O_2 in dry air (X_{O_2}), the units of ppmv are converted into per meg equivalent. 350 ppmv is an arbitrary reference that is used on the Scripps Institution of Oceanography (SIO) per meg scale for APO (Manning and Keeling, 2006). This equation is simplified from the original formula of Stephens et al. (1998), in that the minor influences from oxidation of CH_4 and CO are neglected here. APO is also reported in per meg units and represents the atmospheric O_2/N_2 ratio one would measure if all CO_2 was converted to O_2 through terrestrial photosynthesis (Stephens et al., 1998). The definition implies that this tracer is insensitive to photosynthesis on land and hence, is affected only by O_2 and CO_2 fluxes between the atmosphere and the ocean, and combustion of fossil fuels, which has a higher stoichiometric ratio (Laan-Luijkx et al., 2010b; Manning and Keeling, 2006). Generally, one would expect a maximum in APO around the

equator, which is a region of oceanic upwelling particularly in the Pacific. When O_2-poor, nutrient-rich waters reach the surface, they absorb O_2 from the atmosphere. At the same time, the nutrients that are brought to the surface enhance the production of O_2 by plankton, leading to a counter-flux of O_2 to the atmosphere which overcompensates the opposite effect initiated by undersaturation. Upwelling furthermore transports water masses abundant in CO_2 to the surface where they warm and degas CO_2 to the atmosphere (Bender, 2006). The sum of these fluxes results in a pronounced equatorial bulge in APO, dependent on the strength of the upwelling (Battle et al., 2006).

To date, numerous measurement techniques have been introduced in order to tackle the challenge of precise O_2 measurements. The first one to succeed was Keeling (1988a), who developed a method based on interferometry. His approach used changes in the refractive index of air to derive variations in the composition of the sampled air to quantify the detection of spatial, seasonal and inter-annual variations in O_2. Bender et al. (1994) was able to measure the atomic masses 32 of $^{16}O_2$, and 29 of $^{15}N^{14}N$ on an isotope mass spectrometer, in which the O_2/N_2 ratio is the directly observed quantity. A third method proposed by Tohjima (2000) involved a gas chromatograph equipped with a thermal conductivity detector. All of these methods make use of rather expensive or large instruments, which limits their deployability to laboratories and consequently require the collection of flask samples. In order to refine the temporal and spatial resolution of existing O_2 data, continuously measuring field-based techniques have been developed more recently. Manning et al. (1999), for example, made continuous high-precision measurements with a modified paramagnetic analyzer. This approach is based on the fact that O_2 is paramagnetic and therefore attracted to the point of maximum magnetic field strength. Since the O_2 partial pressure is determined by the degree of deflection of a dumbbell produced by the attraction, this device exhibits a high degree of vibration sensitivity. This limitation precludes the method for application on any moving platform such as a ship or an airplane. By means of measuring the absorption of vacuum ultraviolet radiation by oxygen when it passes through an air sample, this limitation can be overcome (Stephens, 1999; Stephens et al., 2003). Finally, observations of the atmospheric O_2 mole fraction meeting the intended precision have also been carried out with a fuel cell-based technique introduced by Stephens et al. (2007b), which also do not necessitate stationary operation. The functional principle of fuel cells will be discussed in chapter 3.2.5.

2.4 Atmospheric air measurements using commercial aircrafts

Using a commercial airliner to conduct measurements is unique in that a large fraction of the globe can be covered, that tropospheric background air is probed, that most of the data is collected in the tropopause region, and that vertical profiles near airports can be theoretically investigated as well (Machida et al., 2002; Schuck et al., 2009). The extendable set of in-situ analyzers in combination with air and aerosol samplers turns the CARIBIC project into what Brenninkmeijer et al. (2007) called

a "flying observatory". However, the reliance on an airplane entails restrictions: The scientific and analytical requirements have to be met within the constraints of the aircraft's structure, safety and operation at all times, and the equipment has to pass a thorough safety certification process first. All the instruments aboard the aircraft must abide by the mechanical and electrical restrictions, be free of compounds classified as hazardous such as liquid nitrogen and exhibit minimal levels of radiated and conducted electromagnetic interference according to the environmental test of avionics hardware, DO-160 (Scharffe et al., 2012). The inlet system as well needs to be checked among others on its effects on the aerodynamics, stability on the aircraft hull, and its behavior at icing conditions. Additionally, it proves difficult to obtain precise measurements aboard an aircraft due to challenging conditions of changing pressure and temperature, as well as mechanical stress in terms of shock and vibration (Chen et al., 2010). Therefore, some compromises with respect to analytical capabilities have to be made (see section Instrumentation). At the same time, employment of scientific equipment demands high standards of automation in case of unmanned projects such as CARIBIC. A further disadvantage of using a commercial aircraft concerns the data constraints resulting from the facts that the data profiles are confined to predefined airports and cruise level, and that the time of observations are restricted to the scheduled flights (one campaign per month). Furthermore, the fitting of an aircraft with the necessary equipment is costly and demands high engineering efforts.

The idea of measuring the atmospheric composition via civil aircraft is not a novelty. Reports on carbon dioxide assessments by airliner go back to as early as 1962 (Bischof, 1970). One of the first routine projects to use fully automated air sampling systems on board of a commercial aircraft was GASP (Global Atmospheric Sampling Project), a program initiated by NASA in 1975 (Falconer and Holdeman, 1976). After successfully having collected information on O_3, CO and particle densities, the project was terminated in 1979 (Dattore, 2011). With the launch of several projects in the 1990s in-flight measurements seemed to have once again awaken the scientific community's interest. The Swiss project NOXAR (Nitrogen Oxides and Ozone along Air Routes) measured nitrogen oxides and O_3 concentrations over a one year period ending in 1996 (Dias-Lalcaca et al., 1998). During the first phase of the Japan Airlines airliner observational project from 1993 to 2005, an automated flask sampling system was used to obtain a long-term record of CO_2 and other trace gases. For the start of phase two in 2005, the instruments were transferred to a newer aircraft type, a continuous CO_2 measuring device was installed for in-situ measurements and the project was renamed CONTRAIL (Comprehensive Observation Network for Trace gases by Airliner) (Machida et al., 2008; Matsueda et al., 2008). Under this name the project is still running today. Yet another project worth mentioning is MOZAIC (Measurements of Ozone and water vapor by in-service Airbus aircraft). It was launched in 1993 by several European airlines as an EU-funded research project and used autonomous scientific instruments installed on five commercial aircrafts to daily monitor the atmosphere for O_3, water vapor, and later on also CO and nitrogen oxides (IAGOS, 2012). The MOZAIC project can be considered the

predecessor of a project entitled Integration of routine Aircraft measurements into a Global Observing System (IAGOS), as it went on hiatus in 2009 and picked up its measurements again in 2011 under this new name. IAGOS-ERI is an European initiative and seeks to establish a sustainable infrastructure for global observations of atmospheric composition from a large fleet of in-service aircraft. This is achieved by installing autonomous instrument packages aboard 10 to 20 long-range aircraft of internationally operating airlines. Whilst the initiative originated from the MOZAIC project, close links are established with other routine aircraft programs such as the CARIBIC project.

2.5 Transport processes in the atmosphere

Measuring the spatial distribution of CO_2 is useful not only for expanding our present knowledge about the global carbon cycle but also for providing information on the transport of air masses and the atmospheric structure (Machida et al., 2002). Especially upper tropospheric CO_2 data can be a powerful tool to improve our understanding of transport processes like convection, inter-hemispheric transport and exchange between the upper troposphere and the lowermost stratosphere (Matsueda et al., 2002b). Near the Earth's surface fossil fuel emissions, biomass burning, photosynthesis, respiration, oxidation of organic matter and air-sea exchange strongly influence the CO_2 concentration in the atmosphere. In contrast, sources and sinks of CO_2 in the free troposphere in the form of chemical reactions is small (Machida et al., 2002). Combined measurements of O_2 and CO_2 therefore have the potential to act as tracers to determine the origin of air masses, such as biomass burning or contact with the biosphere (Brenninkmeijer et al., 2007). CO_2 measurements have been used in the past for tracing troposphere-stratosphere exchange processes (Boering et al., 1996; Hintsa et al., 1998; James and Legras, 2009; Park et al., 2007).

By definition, the tropopause is the boundary between the well-mixed troposphere and the stratified stratosphere, and is located at the point where the environmental lapse rate changes from positive in the troposphere to negative values in the stratosphere. As such, the tropopause can be seen as a mixing barrier, across which tracer species exhibit a jump in the vertical gradient (James and Legras, 2009). Besides the traditional definition of the thermal tropopause, studies have used potential vorticity as a measure to determine a dynamic tropopause and to divide measurements into tropospheric and stratospheric air by commonly incorporating a threshold of 2 PVU (Potential Vorticity Units, 1 PVU $= 10^{-6}\,\mathrm{m^2\,s^{-1}\,K\,kg^{-1}}$) (e.g. Hoor et al. 2004; Sawa et al. 2008). Under adiabatic conditions potential vorticity is a conservative tracer (Sawa et al., 2008). Once the stratosphere is reached, potential vorticity exhibits a sharp increase due to a jump in static stability across the tropopause (Valentino, 2007). Because O_3 is present in such large quantities in the stratosphere compared to the troposphere, it is frequently used to define a chemical tropopause as well (Yates et al., 2013). Due to deep convection in the tropics, the height of the tropical tropopause layer is at around 17 km and at the poles, the

tropopause is roughly at 8 km. Tropospheric air is believed to predominantly enter the stratosphere in the tropics, be uplifted and then transported towards the poles, where it descends back into the troposphere. This simple picture driven by the Brewer-Dobson circulation applies only above the mean potential temperature of the tropical tropopause of 380 K. The tropopause as defined by PVU units exhibits a stronger decrease in tropopause height with increasing latitudes outside the tropics. Closer to the poles, the tropopause can be located as low as 300 K. The region between the local tropopause and the potential temperature of the tropical tropopause is the "lowermost stratosphere", which commonly falls within the altitude range of passenger aircraft flights in higher latitudes. The region above the potential temperature of the tropical tropopause on the other hand is known as the "overworld". Hintsa et al. (1998) mentioned three alternative paths for air to reach the lowermost stratosphere region as indicated in figure 2.5: 1) Diabatic descent from the overworld associated with the Brewer-Dobson circulation, 2) adiabatic transport along isentropes from the upper troposphere across the tropopause, and 3) transport across isentropes caused by diabatic heating and turbulent mixing at midlatitudes. As CO_2 mixing ratios differ from each other in the lower latitude and midlatitude upper troposphere, CO_2 can for example be used to trace back the origin of air that crossed the tropopause and hence allow for distinction of path 1) and 2) originating in the lower latitudes from path 3) originating in the midlatitudes (Hintsa et al., 1998).

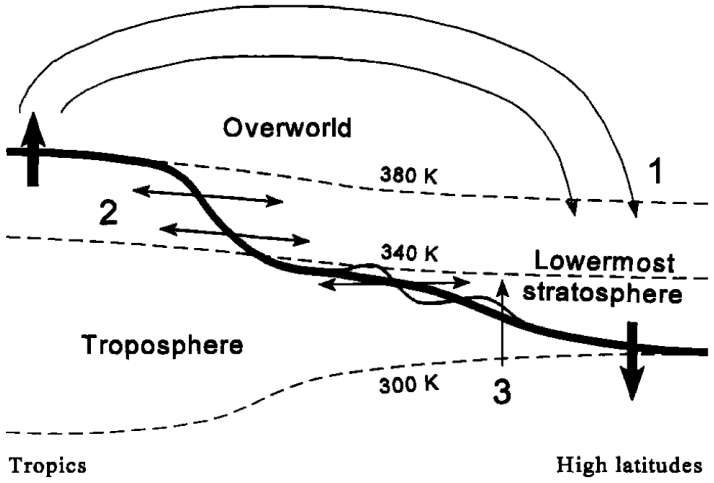

Figure 2.5 Schematic of the upper troposphere/lowermost stratosphere at different latitudes. Depicted are the average tropopause (thick line), isentropes along potential temperatures (dashed lines), the Brewer-Dobson circulation (thick arrows), and transport pathways from the throposphere to the lowermost stratosphere (thin arrows). Numbers describe the three different ways of transport as described in the text. Figure from Hintsa et al. (1998).

Another interesting application of CO_2 data is the assessment of the phase lag times of a trace gas, which is the time it takes for a periodically varying mixing ratio signal to propagate to the sampled region. Because CO_2 is very long-lived and its mixing ratio follows a well known, annual cycle also in high altitudes, it qualifies to trace the time since an air mass has left the near-surface

environment (Waugh and Hall, 2002). Communication of changes in CO_2 concentration between the planetary boundary layer and the free troposphere is often slow and incomplete, particularly over mid to high northern latitude regions (Anderson et al., 1996). This leads to CO_2 cycles in the lowermost stratosphere being characterized by dampened amplitudes and seasonal maxima occurring several months later relative to the troposphere (Sawa et al., 2008). Studies have reported of a phase lag between the tropical troposphere to the mid-latitude lowermost stratosphere of 2 to 3 months (Boering et al., 1996; Hoor et al., 2004; Nakazawa et al., 1991).

Chapter 3

Methods

3.1 CARIBIC project overview

CARIBIC is a long-term atmospheric measurement program based on the use of a commercial passenger aircraft. The project provides the possibility of regularly monitoring the chemistry and composition of the Earth's atmosphere over a time span of several years (Brenninkmeijer et al., 2007). Before take-off, a specially developed freight container fitted with analytical instruments is loaded into the cargo compartment of the passenger aircraft. In transit, an air inlet system attached underneath the aircraft transports ambient air via a tube system to the container in the cargo bay for automatic in-situ analyses and concentration assessments. In addition to real time measurements of numerous trace constituents and aerosols (see table 3.1), the CARIBIC instrument container is also capable of collecting air samples in flasks for later analysis (Schuck et al., 2009). After each flight campaign, which consists of two or four individual flights, the container is unloaded until the next flight campaign. Since the CARIBIC project uses Frankfurt Airport as its base airport, each campaign starts and ends in Frankfurt. Destination airports are spread over different areas on the globe including North America (USA: Denver, Houston, Orlando, Chicago; Canada: Vancouver, Toronto), South America (Bogotá, Columbia; Caracas, Venezuela; Buenos Aires, Argentina; São Paulo, Brazil; Santiago de Chile, Chile), Africa (Cape Town, South Africa; Johannesburg, South Africa) and Asia (Guangzhou, China; Osaka, Japan; Manila, Philippines; Bangkok, Thailand; Kuala Lumpur, Malaysia; Seoul, South Korea; Chennai, India). The flight routes change from season to season and can be chosen by the CARIBIC scientists to some extent. In April and October, Lufthansa releases the flight schedules of its modified aircraft for the following winter and summer seasons. The routes that meet Lufthansa's own criteria for carrying the CARIBIC container are offered to the CARIBIC community, which then gets to select a route that is most suitable from an analytical point of view and covers the most scientifically interesting regions such as the Indian monsoon region for example. Figure 3.1 depicts

the flight trajectories for all the flight campaigns conducted thus far. It is apparent that the flight routes do not only cover narrow corridors. This wider coverage is due to the fact that airlines sometimes use meteorological conditions in order to optimize their fuel consumption. Variations in the exact route and altitude mean that exhaust plumes caused by other airplanes generally have little to no direct influence on the intercepted air. Occasionally local peaks of aerosols and trace gases indicate other air traffic, but these effects can easily be identified (Brenninkmeijer et al., 2007). As the cruising altitude of a passenger aircraft is limited to a range of about 8.5 km to 12.5 km (Schuck et al., 2009), the CARIBIC project provides information on the chemical composition in the upper troposphere/lowermost stratosphere region at mid-latitudes, whereas information is obtained mainly on the free troposphere in the tropics (Brenninkmeijer et al., 2007).

The CARIBIC project is coordinated by the Max-Planck-Institute for Chemistry in Mainz (MPI), but several institutes throughout Europe are collaborating and have added their own measuring devices to the container (see table 3.1). The participating institutes include the Institute for Climate Research, Karlsruhe, Germany (IMK), Deutsches Zentrum für Luft- und Raumfahrt, Oberpfaffenhofen, Germany (DLR), Laboratoire des Sciences du Climat et de l'Environnement, Gif-sur-Yvette, France (LSCE), Helmholtz-Zentrum Geesthacht, Geesthacht, Germany (HZG), Leibniz Institute for Tropospheric Research, Leipzig, Germany (TROPOS), University of Lund, Lund, Sweden (U. Lund), University of East Anglia, Norwich, Great Britain (UEA), and the Institut für Umweltphysik, University of Heidelberg, Heidelberg, Germany (IUP). Furthermore, the Koninklijk Nederlands Meteorologisch Instituut, De Bilt, Netherlands (KNMI) provides meteorological plots for the CARIBIC flights such as forward and backward trajectories, maps and vertical cross-sections of relevant parameters using ECMWF (European Centre for Medium-Range Weather Forecasts) model data. Funding for operation and flight cost, which amount to up to € 16 000 per flight campaign (Volz-Thomas et al., 2007), is contributed by Fraport AG operating Frankfurt Airport, the German Federal Ministry of Education and Research, the research infrastructure IAGOS, IGAS (IAGOS for the GMES Atmosphere Service) and GMOS (Global Mercury Observation System). There has also been substantial cooperation and financial support by Lufthansa German Airlines, which made this project possible in the first place. Data obtained by the CARIBIC aircraft is available upon request and is used by modelers interested in the evaluation of their models or other researchers for the validation of remote sensing based assessments and other observations.

The CARIBIC project started with its first regular flights in November 1997 (Brenninkmeijer et al., 1999). However, it was only after a major revision of the project in 2005 that the PIUB installed the O_2 and CO_2 instruments. Besides the addition of new devices, the revision also included technical improvements and the switch from the previously used Boeing 767 to a newer Airbus A340-600 from Lufthansa German Airlines, which has a longer range. After eight years in use, the CARIBIC container is still transported roughly once a month by one single modified aircraft and has recently traveled its

Table 3.1 List of species analyzed and instrumentation aboard the Airbus A340-600 aircraft in the scope of the CARIBIC project. Modified from Brenninkmeijer et al. (2007).

Species	Analysis	Principle	Resolution	Institute
O_3	In-situ	UV absorption	8 s	IMK
O_3	In-situ	Chemiluminescence	0.2 s	IMK
CO	In-situ	Vacuum UV fluorescence	5 s	MPI
CO	In-situ	Condensation particle counter >4 nm	2 s	MPI
H_2O total	In-situ	Laser photoacoustic	10–90 s	IMK
H_2O gaseous	In-situ	Dew point	10–90 s	IMK
H_2O gaseous	In-situ	Laser photoacoustic	10–90 s	IMK
NOx	In-situ	Chemiluminescence	10 s	DLR
NOy	In-situ	Chemiluminescence with Au converter	10 s	DLR
CO_2	In-situ	NDIR	15 s	LSCE
O_2	In-situ	Electrochemical cells	12 min	PIUB
CO_2	In-situ	NDIR	1 s	PIUB
Oxygenated volatile organic compounds	In-situ	Proton-transfer-reaction mass spectrometry	20–60 s	IMK
Hg	In-situ	Enrichment and atomic fluorescence	10 min	HZG
CH_4, CO_2	In-situ	Cavity ring-down spectrometry	?	IMK
H_2O isotopes	In-situ	Cavity ring-down spectrometry	?	IMK
Clouds	In-situ	Video camera	0.5 s	TROPOS
Aerosol concentration	In-situ	Condensation particle counter >12 nm	2 s	TROPOS
Aerosol concentration	In-situ	Condensation particle counter >18 nm	2 s	TROPOS
Aerosol size distribution 150–5000 nm	In-situ	Optical particle counter	20 s	TROPOS
Aerosol composition	Laboratory	Impactor, particle-induced X-ray emission analysis, particle elastic scattering analysis	16 samples	U. Lund
Aerosol morphology	Laboratory	Impactor, electron microscope	16 samples	U. Lund
CO_2, CH_4, N_2O, SF_6	Laboratory	Glass canisters, gas chromatography-flame ionization detector-electron capture detector	28 samples	MPI
Non-methane hydrocarbons	Laboratory	Glass canisters, gas chromatography-flame ionization detector	28 samples	MPI
Halocarbons	Laboratory	Glass canisters, gas chromatography-mass spectrometry	28 samples	UEA
Halogen oxides, NO_2, O_3 SO_2	Remote	Differential optical absorption spectroscopy	30 s	IUP

two millionth kilometer. The new CARIBIC project was intended to be in operation for at least ten years. By 2013 the CARIBIC project will become a member of the IAGOS-ERI project, which will act as an umbrella organization for all European civil aircraft projects (Volz-Thomas et al., 2007).

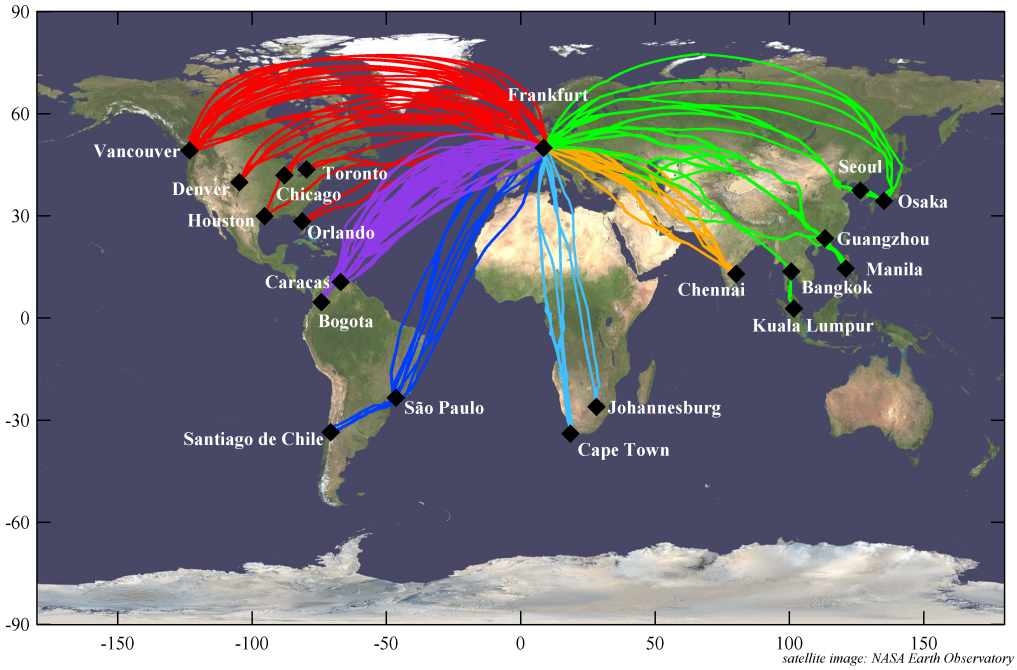

Figure 3.1 World map showing the coverage of flights to all destinations during the CARIBIC project since 2005. Figure from NASA (2013).

3.2 Instrumentation

The integration of the CARIBIC system into the A340-600 aircraft required numerous modifications. Most important were the structural changes to the hull around the mounting position of the inlet system, followed by the installation of the air tubing and cables. Also required were a container connector interface, a control panel in the cockpit, and modifications to electrical hardware, electronics and software. Here, only the main aspects of the air sampling relevant for the O_2 and CO_2 measurements discussed in this thesis, are summarized. Further information, in particular about the inlet system and the container, are published in more detail by Brenninkmeijer et al. (2007).

3.2.1 Inlet

The inlet system basically consists of a a hollow aluminum spar protruding at the shell of the fuselage underbelly, to which three tubular probes for aerosols, trace gases and water are attached, facing in flight direction. The spar, acting as a pylon, holds the probes in place and houses the tubings to

connect the probes with the container inside the aircraft. Furthermore, it comprises heater elements, insulation, temperature sensors, an exhaust, three DOAS telescopes adding remote sensing capabilities, and a video camera for post-flight cloud observation. In order to ensure stability of the assembly, the spar is coated with additional hulls in the front and the back, and all essential parts exposed into the direction of flight are nickel plated. A flange at the base of the pylon doubles the fuselage skin. The pylon is installed in front of the wing box and sticks out at a slight angle when viewed from direction of flight because it is not exactly centered due to the presence of an internal stringer in the middle of the fuselage. The inlet system was developed in close cooperation with Garner CAD Technics GmbH and KOLT Engineering GmbH (Oberpfaffenhofen, Germany) and manufactured by Heggeman Aerospace (Büren, Germany). As a whole, it measures 34 cm in height, 55 cm in length and 18 cm in width, and weighs 3.5 kg. The height of the inlet system is basically a trade-off between a structural and an analytical point of view. On one hand the height should be minimal to reduce stress but on the other hand it is desirable to sample outside of the aircraft's boundary layer. Data from Airbus Hamburg concerning the airflow field and pressure distribution around the aircraft indicated that the boundary layer thickness at the position of the inlet is about 25 cm.

Both O_2 and CO_2 analyzers incorporated by the PIUB are attached to the water probe, through which the IMK obtains its water vapor and cloud water measurements. The water probe is mounted on the right-hand side when looking in flight direction, 1 cm above the centered aerosol probe. There are two openings on the water probe allowing ambient air intake. A forward facing, heated inlet tip with an inner diameter of 4 mm uses ram pressure to collect air for the determination of the water in gas phase and in form of droplets or crystals (total water content). Air for the measurement of gaseous water is provided via a second, heated opening, which is facing sidewards and hence, acts like a static port at near neutral pressure. As fluid dynamical calculations done by Airbus Hamburg indicate, air displacement at the nose of the aircraft causes an enrichment of cloud particles at the total water inlet of 12–19 %, depending on the angle of attack. Additionally, cloud particle count at this intake is further elevated by 220–500 % due to the non-isokinetic inlet configuration as proposed by Liu et al. (1989). The extent of this effect is determined by the airplane's cruise speed as well as the inlet sample flow (Brenninkmeijer et al., 2007). This needs to be taken into account when comparing the PIUB H_2O values with the ones obtained by the IMK as up to flight number 293 the total water inlet at the tip was used to obtain the O_2 and CO_2 measurements (see section 3.3 and figure 4.2). Since flight 294 in the beginning of 2010 the setup is such that air is sucked in through the sidewards facing inlet, which is only capable of seeing water vapor, not droplets or crystals. However, I do not apply any of the above mentioned water corrections when calculating the CO_2 mixing ratios, since in order to correct for the water dilution effect I require the H_2O mixing ratios that the CO_2 analyzer is actually subjected to, rather than the water content existent in the ambient air in reality.

The upper rear side of the pylon is equipped with an exhaust, through which the sampled air is

expelled again after it has passed the various instruments in the container.

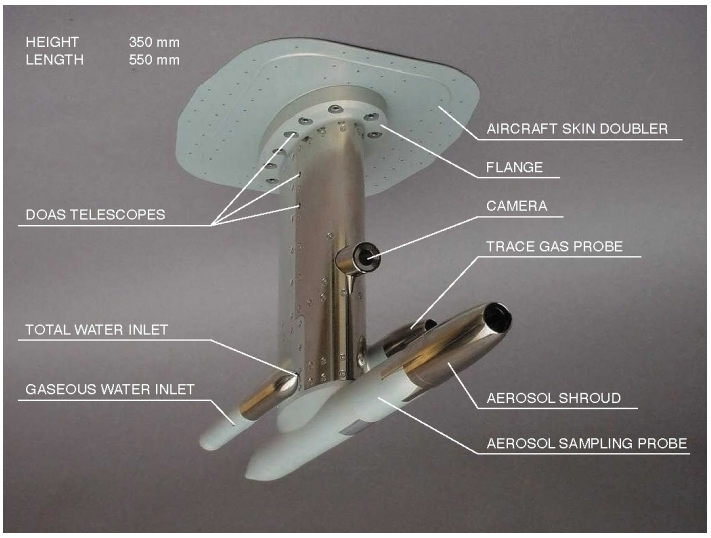

Figure 3.2 The CARIBIC inlet system prototype. The exhaust orifice in the back of the pylon is not visible from this angle of view.

3.2.2 Container

The measurement devices are installed in a modified LD-11 airfreight container manufactured by Alcan Singen GmbH with the dimensions 3.1 m × 1.5 m × 1.6 m. A requirement is that the CARIBIC container is loaded into the aircraft first, prior to all the regular cargo containers and pallets. This ensures that the measurement container can stay in place for up to four succeeding flights without obstructing unloading of the standard freight after each flight. Upon return to Frankfurt Airport, the cargo is discharged first, followed by the careful de-installation of the container and transport back to the MPI. Hence, the container needs to be always placed furthest from the cargo door, at the very back of the cargo compartment. As for the Airbus A340-600, the cargo loading door of the forward cargo bay is located in the front. This means that the measurement container is positioned 25 m away from the aircraft nose, towards the wing box above the leading edge of the belly fairing. Ideally, the inlet system should be located directly underneath the container because short tubes minimize contamination and loss of gases and aerosol particles. However, positioning of the inlet below the container is not possible because the belly fairing is located there, which is too thin to support it. As a result the actual position of the inlet system is shifted forward by 2 m, 23 m from the aircraft nose.

In the following, the major modifications on the original LD-11 container carried out by Enviscope GmbH (Frankfurt, Germany) are discussed. On the inside of the aircraft, the inlet system is attached to a connector bracket incorporated into the cargo floor underneath the container. This connector bracket contains connectors for power and data from the aircraft, and provides all the necessary

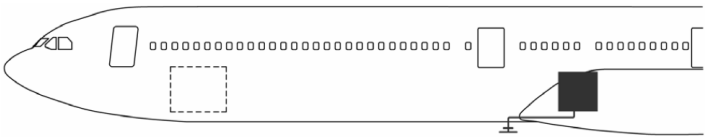

Figure 3.3 Position of the inlet system and the measurement container (black square) on the Airbus A340-600. The dashed rectangle indicates the cargo loading door of the forward cargo bay. Figure from Brenninkmeijer et al. (2007).

linkages to the inlet system for the air measurements. To provide space for connecting the instruments to the container connector bracket, a rectangular opening was cut in the double floor of the container. The rear wall of the container housing on the longer side was replaced by three removable panels and its front opening was equipped with two doors. This facilitates access of the instruments from both sides for maintenance and improves the mechanical stability of the container. In order to minimize electromagnetic interference, the edges along the container doors are sealed with chromatized, nylon-encapsulated foam tape. Six aluminum purpose-built racks are installed to carry the measuring instruments, auxiliary equipment such as the calibration gas cylinders, and a master computer. All the racks measure 136 cm in height and either 19 inches or 65 cm in width. A ventilation system has been added composed of seven fans. Four of them, located at the bottom of the right side panel, suck air from the cargo bay, which in turn is cooled via the aircraft's air conditioning system, into the container and blow it in the perforated sandwich flooring space from where it is evenly distributed around the equipment racks for improved heat dissipation. Two fans beneath the top on the opposite side vent heat generated by the instruments out of the container. The small revision in 2009 after flight 293 also included the addition of another fan in the center of the back panel with the aim of reducing the observed heat build-up in the middle of the container. Eight temperature sensors are used to monitor the temperatures at various locations within the container. Two additional smoke and overheating detectors (model SD9472-00) by Apparatebau Gauting GmbH (Gauting, Germany) have been installed as well.

When the container is not on board, the cables are coiled inside a drum placed in the tub. The tube openings are sealed with blind connector plugs and the container connector bracket opening in the aircraft is covered by a floor panel. The container is based at MPI in Mainz and placed on a hydraulic platform. Prior to a flight campaign the container is lifted upwards, rolled into a truck equipped with a roller system and transported to Frankfurt Airport, where a high loader takes over the container and lifts it into the aircraft followed by the installation under the supervision of a Lufthansa technician.

With the current scientific load the container weighs 1470 kg in total. Since the LD-11 container allows a gross weight of 3175 kg and the cost of freight is not determined by the actual weight but solely based on the container volume, there is substantial potential for the CARIBIC project to improve the measurement capability by adding more scientific instruments at the same operational costs. The

only constraints to expandability are the available space, electrical power and the amount of heat that can be dissipated into the cargo bay during the flight (Brenninkmeijer et al., 2007).

3.2.3 Sample tubing, electric system and general data handling

The air from both intakes on the water probe is transported from the inlet connector bracket to the container connector bracket through 2.5 m of 3/8 inch O.D. electro-polished stainless steel tubes heated to 60 °C. Either end of each tube consists of flexible, armored PTFE tubing sections to prevent mechanical strains, and quick-connect couplings by Swagelok. Heating is achieved using silicone-rubber-based ribbon heaters by Adel Wiggins (Los Angeles, CA, USA) and 1000 Ω Pt temperature sensors by Minco (Minneapolis, MN, USA) control the temperature. Within the container, a 2 m heated tube links the connector bracket to the frost point hygrometer and the laser photoacoustic analyzer for the water mixing ratio determination by the IMK. This is the point where the line branches off into an unheated 1/8 inch stainless steel tube of 2.5 m length, through which the O_2 and CO_2 measurement unit pumps the sample air. Prior to flight 294 the length of the pipe from the split to the PIUB unit was shorter by about 1.5 m. After analyses, the air is collected in a 3/4 inch stainless steel tube and flushed out the exhaust located in the back of the pylon.

The so called data distribution box is situated in a 19 inches rack (6 HU), weighs 20 kg and forms another interface between the container and the aircraft. Its duties include the transfer of smoke detector signals, as well as a signal indicating the presence of the container aboard to the aircraft, and the transfer of ARINC data from the aircraft to the master computer. Furthermore, it provides power for the camera in the pylon and controls the temperature of 18 heaters in the pylon, tubes, container and cargo compartment (Brenninkmeijer et al., 2007).

Of great importance is that the power usage by the container is kept low to minimize heat generation, save energy and to not affect any aircraft functions. To meet these requirements, the scientific equipment is powered by two power supplies with different priorities that convert the three phase 115 VAC (400 Hz) into 24 and 28 VDC. The smaller of these supplies, termed Base Power Supply, is a EL 4 kW MegaPAC by Vicor (Sunnyvale, CA, USA) and is allowed to be switched on while the aircraft is still docked at the airport apron, when the aircraft receives power via a ground cable. During push back and taxiing, the Base Power Supply looses power to pick it up again when the aircraft receives energy through the turbines. It provides 2 kW for most instruments including the O_2 and CO_2 measurement unit and the master computer for essential functions when the power consumption is limited. This is particularly beneficial for devices that need to be evacuated first or warmed up to a stable level for reliable data collection. When the aircraft is powered by the Base Power Supply none of the instruments is allowed to take measurements, they are solely running in a standby mode. There is no guarantee that the CARIBIC container and the Base Power Supply receives electricity at all prior to take-off. Therefore, instrument spin-up time varies from flight to flight between several

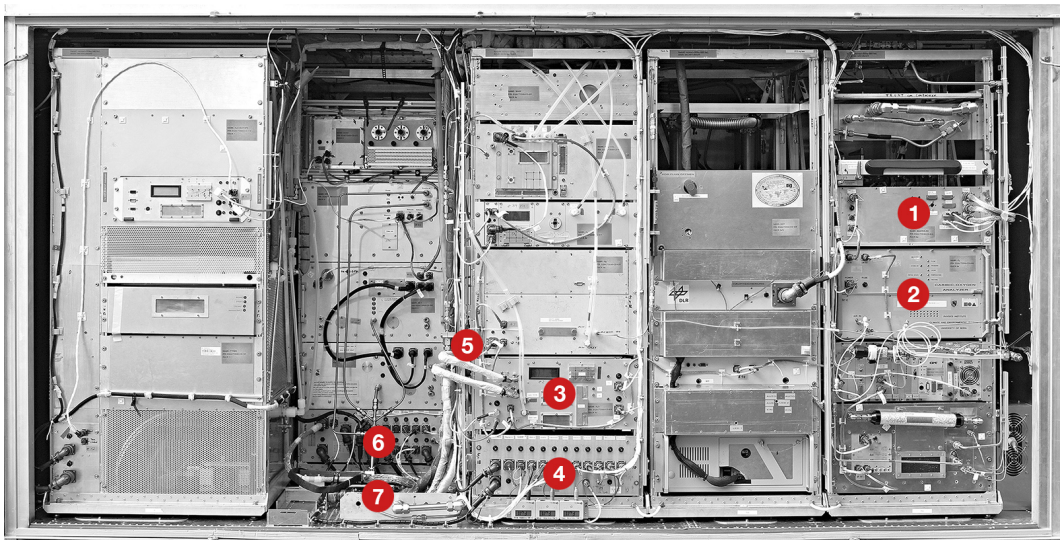

(a) Frontal view of the CARIBIC container

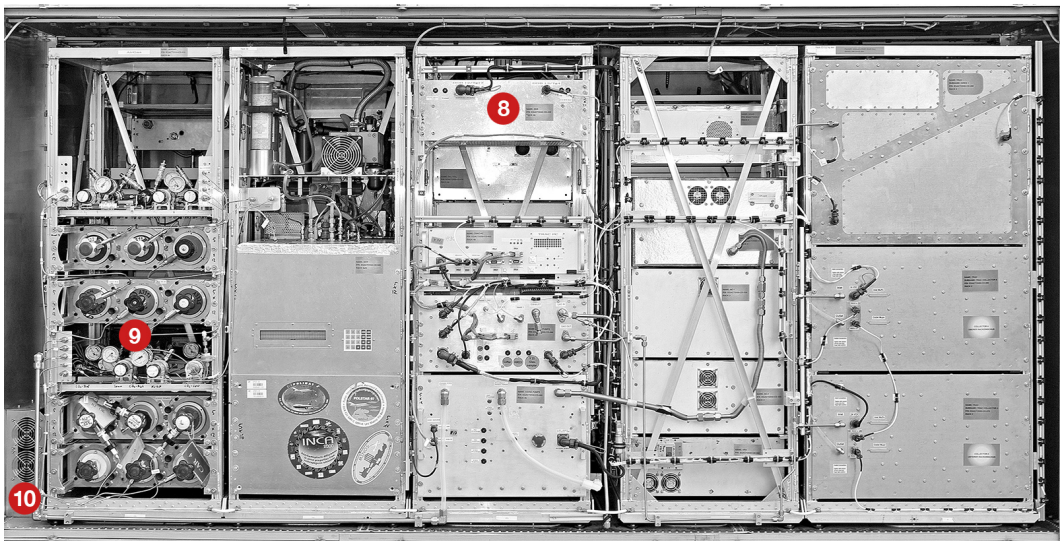

(b) Rear view of the CARIBIC container

Figure 3.4 Two photographs of the CARIBIC container with its doors and panels removed in order to get a view of all the instruments inside located in the front (a) and in the back (b). 1: Master computer, 2: O_2 & CO_2 analyzer unit (PIUB), 3: Water content measurement device (IMK), 4: base power supply, 5: Point where O_2 & CO_2 sample gas split from the shared H_2O sampling line, 6: main power supply, 7: container connector bracket acting as an aircraft-container interface, 8: data distribution box, 9: calibration gas rack, 10: four ventilators sucking air into the container to even out temperature differences. Also visible are the numerous measuring devices by the other groups, which are not directly relevant to the PIUB instruments.

hours to none before the ascent. As soon as the weight-on-wheel signal disappears at take-off, the second power supply, named Transformer Rectifier Unit, is switched on. This main supply by Aircraft Electronics Engineering GmbH (Seefeld, Germany) has a capacity of 8 kW and remains active during the entire flight. The actual total power consumption of the fully instrumented container currently is 5.5 kW with a peak load of 7.0 kW.

The power output by both of the power supplies is logged by a master computer located in the container. An essential task of the master computer is the control of all the individual analytical devices. With the main power supply after take-off the master computer is turned on and activates the measurement modes of the individual instruments successively in order to prevent power surges. Since all the CARIBIC groups expressed a keen interest in monitoring the background air composition outside of the boundary layer, sampling in the vicinity of airports is avoided by using a pressure threshold monitored with sensors in the tubing. During take-off the master computer starts to send the measurement signal when the pressure drops below 630 mbar, whereas the standby signal is sent when the outside pressure exceeds 660 mbar again during landing, corresponding to a height level of approximately 3000 m above sea level (a.s.l.). For flights bound to elevated airports such as the ones in Johannesburg or Bogotá, the pressure threshold values may be manually altered to lower pressures in order to ensure that pollution nearby is excluded. In flight, the master computer communicates with each of the measuring devices via an Ethernet network to check their status through simple algorithms. In case any instrument is not responding, the master computer can initiate its reboot or shut down. The communication between the devices is logged. The master computer also monitors the conditions in the container, the inlet and the tubing system, and reports smoke or overheat detection to a CARIBIC control panel in the cockpit via an optical and acoustic signal. The pilots are able to switch off the container's power supply at any time. This happened for example during flight 426 (B). Surveillance of the parameters is achieved using four internal pressure sensors, the two above mentioned external temperature sensors and the signals from 18 temperature controllers in the data distribution box. The third major function of the master computer is the retention of the aircraft's ARINC 429 data. ARINC is the technical standard for the predominant data bus system in civil aviation. ARINC data is collected by the aircraft itself and provides parameters such as altitude, outside temperature, GPS location, time and cruise speed, among others. By storing this extensive set of flight data on the master computer, these parameters are also available for analysis of the CARIBIC measurements. Any data related to ambient air measurements is not stored on the master computer as each instrument in the container is responsible for its own data storage. After each campaign, when the container is back at the MPI in Mainz, the data stored by each device is extracted and uploaded to an FTP server, which all the CARIBIC team members have access to.

3.2.4 Calibration and working gases

A set of three high pressure gas cylinders is employed to calibrate the measurements. All three gases are contained in 2.16 l, 200 bar aluminum cylinders (Luxfer) fitted with stainless steel valves (Linde), which are placed in the dedicated calibration gas rack in the back of the CARIBIC container. As suggested by Keeling et al. (2007), all cylinders within the container are stored horizontally in order to minimize gravimetric fractionation. High-span (HS) and a low-span (LS) calibration gases are used in conjunction with each other to determine the sensitivity of both devices. While calibration gas 1 (CG1) acts as the high-span for the Licor and corresponds to the low O_2 calibration gas at the same time, calibration gas 2 (CG2) is both the low concentration CO_2 concentration gas and the high-span for the oxygen measurement. Using inverted O_2 and CO_2 ranges for the calibration gases is more closely in accordance with the natural variations (Stephens et al., 2007a). Additionally, a third cylinder holds the working gas (WG), which is used as such for the oxygen device only. By frequently comparing sample air to a reference gas under closely identical conditions a more precise, relative oxygen measurement is obtained, which is corrected for most sources of drift with time scales longer than 12 min (Stephens et al., 2007a; Valentino, 2007). While fuel cells exhibit significant short-term drift, the Licor device has shown to be less prone to drift. Thus, the WG is only used for the determination of O_2 and never passes the Licor sample cell.

Well before their employment, the three cylinders are filled and prepared in the laboratory at the PIUB. Dry compressed air in 50 l steel tanks are retrieved from Carbagas, Switzerland, which are used as bases for the three calibration and working gases. First, the $\delta(O_2/N_2)$ ratios (atomic masses 32/28), the CO_2 mixing ratios, as well as the $\delta(Ar/N_2)$ ratios (42/28) in the three 50 l cylinders are determined in the laboratory using an Isotope Ratio Mass Spectrometer (IRMS) modified with a new inlet system based on an open split design as known from gas chromatography/mass spectrometry systems (Valentino, 2007). Gases are analyzed relative to a working gas, which in turn is calibrated against four secondary standards from NOAA/CCGG (Boulder, CO, USA). The CO_2 mixing ratios are inferred from $\delta(CO_2/N_2)$ (44/28), determined by mass spectrometry. The precision of this CO_2 measuring method is somewhat impaired by the production of N_2O^+, NO_2^+ and NO^+ from excited N_2 and O_2 or fragments thereof in the ion source, which yields a signal in the same mass-to-charge ratio as CO_2 (Leuenberger et al., 2000). The extent of this effect can be derived by measuring CO_2-free air at the end of each measurement day. Because CO_2 preferentially adsorbs on metal surfaces or porous ceramic compared to other gas components, a significant background level is measured even after long evacuation times (Leuenberger et al., 2000). This also needs to be accounted for. Using the known CO_2 mixing ratio of the working standard and the correction for the background signal and the production of N_2O^+, NO_2^+ and NO^+, the $\delta(CO_2/N_2)$ can be converted into a CO_2 mixing ratio with a stated accuracy of ± 0.5 ppmv (Sturm et al., 2005). However, the error largely depends on the sample size.

Measuring O_2, Ar as well as CO_2 on the mass spectrometer has two main benefits. Firstly, this method allows simultaneous measurements of all three gases at once using the same measurement principle. Secondly, mass spectrometers require much less gas volumes to yield accurate values—an important factor considering the limited size of gas cylinders currently in use. More detailed information on the mass spectrometrical measurement system are given in Leuenberger et al. (2000) and the diploma thesis by Sturm (2001). Since during the process of drying the gases and filling the cylinders at Carbagas, O_2 was consumed and the O_2/N_2 ratio substantially altered towards more negative values, it is necessary that the 50 l cylinders be spiked with pure O_2 to reach reasonable, naturally occurring values. CG1 and CG2 are intended to span the full range of $\delta(O_2/N_2)$ and CO_2 observations, with the WG preferably having values closely matching the current air sample. However, these values can be difficult to achieve using natural air only, especially for the calibration gases, and require further alteration of the O_2 and CO_2 mole fractions by spiking the tanks with synthetic gases. The nominal CO_2 mixing ratios of approximately 432 ppmv for the high span and 357 ppmv for the low span are usually reached to a good degree. However, desired O_2/N_2 ratios are far more difficult to achieve, as they are highly sensible to spiking, and it repeatedly occurred that the oxygen high span cylinder contained a lesser amount of oxygen than the WG or the ambient air.

Once the three large cylinders are set, they can be used repeatedly to fill the 2.16 l aluminum cylinders, which will eventually fly aboard the aircraft. When re-filling the small cylinders, air from the large tanks is added on top of the residual pressure without emptying it and the filling hose is first evacuated to avoid contamination from lab air. Before the cylinders are transported in bulk to the MPI in Mainz, the composition of the air in the cylinders is determined in the same manner as the large tanks. Appendix D includes a list of all the calibration and working gases used during the project. The precision of the IRMS system improves with increasing sample size. Due to time limitation some calibration cylinders could only be measured for half an hour, resulting in only four measurement replicates. There were also cases where the IRMS did not measure properly and the calibration cylinder values could not be determined. For example, the CG2, which has been in use since flight 329, was affected by this. In that case the values of the large tank, from which it was filled, were assumed. This practice obviously introduces uncertainties in the O_2, CO_2 and Ar values of the calibration gases that eventually manifest themselves in all of the data collected during the flights.

Upon completion of each campaign, the remaining pressure of all three cylinders is checked in Mainz. When the remaining pressure drops below 20 bar, the cylinder is replaced. Because they are only used for calibration, both calibration gases generally last for more than 26 campaigns corresponding to a timespan of more than two and a half years. For campaigns with a total airborne time of more than 40 h including four flights of long air routes, it occurs regularly that the working gas cylinder runs empty during the last leg of the campaign. Unless the previous campaign contained only two flights or there was a power failure, the working gas is replaced after each campaign.

Out of the above mentioned methods to measure atmospheric O_2 contents, only mass spectrometers can be configured to measure $\delta(O_2/N_2)$ ratios directly, whereas the others measure signals more related to the mole fraction of O_2, which is sensitive to variations in other gases. When using fuel cells, it is thus necessary to convert from units of ppmv to per meg and to correct for variations in CO_2 to be able to compare the results of different methods (Stephens et al., 2003) (equation 3.9). Vice versa, for the calibration of the fuel cells, I first convert the calibration gas $\delta(O_2/N_2)$ values in per meg as determined by the mass spectrometer in the laboratory into apparent mole fraction differences (δX_{O_2}) in ppmv using equation 3.1 (Stephens et al., 2007a; Uglietti, 2009).

$$\delta X_{O_2} = \delta(O_2/N_2) \cdot X_{O_2}(1 - X_{O_2}) - (([CO_2] - 384.5) + \delta(Ar/N_2) \cdot X_{Ar})\, X_{O_2} \tag{3.1}$$

The O_2 mole fraction in air X_{O_2} is 0.20946, $[CO_2]$ is the measured CO_2 concentration in the calibration gas in ppmv, 384.5 is the average CO_2 concentration of the reference cylinders defining zero on the local PIUB O_2 scale, $\delta(Ar/N_2)$ is the measured argon (Ar) to nitrogen ratio in the calibration cylinder, and X_{Ar} is the Ar mole fraction in air (0.009393). The equation not only takes into account changes in the CO_2 content but also applies a correction for Ar. Correcting for argon is necessary in this case because the concentration of argon in the calibration and working gases was strongly modified in the process of making the gases through spiking (Popa, 2007; Uglietti, 2009). For the calibration gases, storage drift over time is expected to be insignificant and I do not correct the calibration gases for any kind of drift during their employment. Due to the challenging shortage of space in the container the employment of additional calibration gases is ineligible (Sturm, 2005).

3.2.5 Oxygen and carbon dioxide measurement unit

The incorporation of analytical devices in an aircraft demands a high degree of automation and reliability of the system. When not in transit, the device is located in Mainz, Germany, and is not projected to return to the PIUB in Switzerland for maintenance work. Especially so because the CARIBIC container is only allowed on board in the state in which it abode by the regulations, meaning fully fitted with all the devices. Thus, if a device is faulty and needs to be worked on, it must be transported, fixed and transported back to the MPI between two flight campaigns, corresponding to a time frame of roughly three weeks. The device has to fly in the container, even if it means the device not collecting any data and being turned off during the flight. Furthermore, any additions of electronic equipment to a device would require the entire container to go through the testing protocol again. Changes to the setup design are therefore not easily implemented and an extensive testing phase in the laboratory was required preceding the first flights.

The measurement unit consists of the O_2 analyzer, the CO_2 analyzer and a tubing system. Of crucial importance is to reach and maintain stable conditions in the system in order to obtain precise measurements, while at the same time attain a good resolution throughout the flight. The biggest

challenge is the pressure and temperature control of the oxygen cells (Valentino, 2007). A gas handling scheme allowing for switching between ambient air, two calibration gases and a working gas is required. In the following sections, the components and layout in the measurement unit added to the CARIBIC container by the PIUB to obtain O_2 and CO_2 mixing ratios are described.

3.2.5.1 Oxygen analyzer

The in-situ assessment of the O_2 content relies on the fuel cell technology. Hereby a chemical reaction is used to generate an electric current. A fuel cell, in this case, is a lead-oxygen battery, composed of a gold-plated cathode, an anode made of lead, a weak acid acting as an electrolyte and a non-porous, gas-permeable Teflon FEP membrane attached to the cathode. O_2 in the incoming air stream diffuses into the sensor through the membrane and is reduced at the cathode. In the cell the net reaction

$$O_2 + 4\,H^+ + 2\,Pb \longrightarrow 2\,H_2O + 2\,Pb^{2+} \tag{3.2}$$

takes place. This reaction generates a current across the cell which is linearly proportional to the rate at which oxygen diffuses across the membrane, or in other words the partial pressure of O_2 in the analyzed air sample (Stephens et al., 2007a). The above reaction generates PbO, which dissolves into the electrolyte as long as it is not saturated with PbO. However, life expectancy is a function of usage and at some point after the fuel cell has been in use, the lead oxide will start to precipitate onto the lead anode (Maxtec, 2003). When all available surface area of the lead anode has been converted to PbO, the electrochemical sensitivity will cease, and the sensor will have to be replaced (Boettern, 2000). It is important to note that unlike mass spectrometers, the application of fuel cells results in an output in the O_2 mole fraction, therefore requiring a conversion (see 3.2.4). Another important consideration is that oxygen sensors are influenced by the temperature of the atmosphere they are being used to measure, since higher temperatures lead to faster electrochemical reactions in the cell (Boettern, 2000). For this reason the O_2 analyzer is placed in a thermostable environment within the container. The O_2 analyzer is home made and consists of four Max-250 fuel cells arranged in sequence. The second fuel cell is not functional as it was modified to act as a temperature sensor in order to be able to keep track of the temperature stability precisely where O_2 is measured. Hence, sample air is serially analyzed three times for O_2 and the same gas is run through the four fuel cells at all times. To improve upon the precision and stability of the measurement, the system switches every 6 min between sample gas and a reference working gas (WG) using a set of 13 valves in total. By subtracting the mean voltages from the preceding and following working gas from the voltages for the sample gas for each fuel cell, most sources of signal drift with time on longer time scales can be eliminated.

The PIUB opted for Max-250 oxygen sensors by Maxtec since tests in the lab have shown that these sensors exhibit lower noise signals (root mean square of 15–100 per meg at 1 s resolution) and less short-term variability (15–30 per meg for 10 s intervals) compared to competing products (Valentino,

2007). Furthermore, through the use of an acid electrolyte, the Max-250 series sensor is virtually insensitive to CO_2 and other background gases related to emissions such as SO_2 and NOx (Maxtec, 2003). The stronger long-term drift in the signals that Max-250 cells appeared to exhibit can be eliminated by frequently switching sample air with the working gas as described in section Gas handling scheme. The voltage output by a fuel cell for 0.2 bar partial pressure of O_2 is typically 1 mV and the sensitivity is in the order of 10 nV/per meg. This demands an electronic amplification of the weak electrical signal to yield a adequate signal-to-noise ratio at ambient O_2 concentrations of about 21 % with a resolution of 0.0001 % O_2 in order to match the CO_2 resolution (Brenninkmeijer et al., 2007). For amplifying the signal, an electronic system was added with an internal noise of 5 per meg for a 120 s period (Valentino, 2007). Moreover, as part of the system revision in 2009, dynamic resistance potentiometers were interposed between the fuel cells and the ADC. The principle of fuel cells has specific benefits, which make them an appropriate tool for oxygen analysis on such a fast-moving platform: They are small, light and relatively cost-effective compared to other methods because fuel cells can be commercially produced in large quantities. In addition, they do not require extensive construction and they can run without frequent maintenance for long times. The main advantage of fuel cells in contrast to paramagnetic cells, however, is that they are are unaffected with regards to motion or vibration (Stephens et al., 2007a). This property renders fuel cells suited for the employment on an aircraft. The lifetime of a fuel cell is largely dependent on the amount of electrolyte and material present for the reaction, but also the exposure to oxygen, and in this case adds up to roughly two years. As soon as a fuel cell exhibits continuous clipping due to the signal being out of the range, its range is adjusted using potentiometers (after flight 294) or the fuel cell is replaced with a new one. The determination of the atmospheric O_2/N_2 ratio becomes most valuable with concurrent CO_2 measurements. Therefore, despite a device dedicated to CO_2 detection being already placed in the instrument container and operated by another team, the PIUB decided to employ a similar analyzer to complement the oxygen measurements (Sturm, 2005).

3.2.5.2 Carbon dioxide analyzer

The CO_2 analyzer deployed in this setup is the now discontinued LI-6262 model by LI-COR Biosciences, which was first introduced in 1990 (LI-COR, 1996). This dual detector system bases its simultaneous analysis of both CO_2 and H_2O in the same gas stream on the principle of NDIR technology. Infrared techniques make use of the fact that many gases exhibit very characteristic absorption in the infrared region between 2 µm and 20 µm due to transitions in their vibration-rotation energy levels. Key is the selection of the wavelength at which the absorption is measured: By careful choice of wavebands the direct infrared absorption by water vapor can be eliminated (LI-COR, 1996). At a wavelength of 4.26 µm the absorption spectrum for CO_2 is a narrow and near-non-overlapping band, and therefore virtually unique to CO_2. For the assessment of the water concentration in an analogous

manner the device measures IR absorption of water molecules at 2.59 µm.

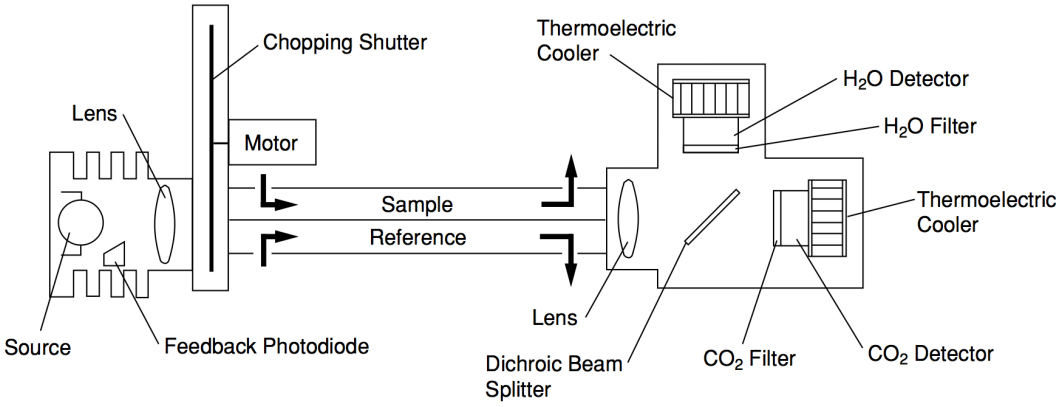

Figure 3.5 Scheme of the LI-6262 NDIR CO_2 analyzer. Figure from LI-COR (1996).

The LI-6262 device is equipped with a sample cell and a reference cell. The CO_2 and H_2O measurements are based on the difference of infrared radiation passing through both cells to get rid of any variation in the ground signal. By pumping gases around a closed loop containing chemical scrubbers to remove water vapor and CO_2 after the sample cell, only dried gas with a zero CO_2 concentration is swept through the reference cell, which allows for operation of the CO_2 analyzer in absolute mode. Thus, the difference between the sample and the reference cell in this case directly corresponds to the absolute CO_2 and H_2O mixing ratios in the gas sample analyzed. Moreover, as space is too limiting to convey a separate CO_2 reference gas just for the reference cell, half of the time the analyzer is run in serial mode, where the reference cell is subjected to the same gas that has been injected into the sample cell (Sturm, 2005).

The vacuum sealed light source is kept at a constant color temperature of 1250 K using a separate optical feedback circuit with a photodiode and directs IR radiation through the two chambers. In order to send the light alternatively through the sample and the reference cell at a frequency of 500 Hz, a motor controls the rotation of a chopping shutter disc. The optical path is sealed and continuously purged of CO_2 and H_2O by an attached tube containing soda lime and magnesium perchlorate, eliminating interference due to ambient CO_2 and water vapor. Additionally, the cells are plated with gold to enhance IR reflection and resist tarnishing over time. Maximal signal sensitivity is increased by focusing the radiation on the detectors, which is achieved by placing a lens at each end of the optical bench. The dichroic beam splitter feeds the transmitted radiation simultaneously to a CO_2 detector and a separate detector for H_2O. The detectors on the other end of the chambers are lead selenide sensors cooled to $-5\,°C$ by thermoelectric coolers. Electronic circuits monitor the detector sensitivities and make sure it stays constant. Two optical filters installed in front of the sensors tune the CO_2 and H_2O detectors to 4.5 µm and 2.59 µm respectively (Gibert et al., 2009; LI-COR, 1996). The intensity of IR light that reaches the detector is inversely related to the concentration of CO_2

and water vapor in the sampled air. A built-in temperature sensor enables the LI-6262 to log its temperature.

Even when carefully choosing distinct wavebands for measuring CO_2 and H_2O, there are two ways how water vapor concentrations can still influence the infrared detection of CO_2. The first one is a dilution effect of water, which needs to be corrected for using a well known method (equation 3.5). The second type is called pressure broadening. Gas phase absorption of infrared radiation is due to energy-induced changes in vibrational and rotational energy states. When the pressure is increased, intermolecular collisions which alter these energy states increase in number, thereby causing a spreading of spectral lines (LI-COR, 1996). This effect is also embodied in equation 3.5.

The benefit of NDIR technology is that its detectors are insensitive to vibration, therefore making it feasible for operation on moving platforms. Numerous studies have reported precise CO_2 measurements using infrared gas analyzers (Gibert et al., 2009; Keeling et al., 1976; Pandey and Kim, 2007; Thoning et al., 1995).

3.2.5.3 Gas handling scheme

Just like all equipment involved in the project, the measurement unit containing the O_2 and CO_2 analyzer has to comply with the strict safety regulations. A commercially available case (19 inches, 6 HU) that is shielded against EMR is used. Including the analytical instrumentation, it weighs 39 kg. The box is protected from damage caused by electric overload or short circuit using aviation type circuit breakers and is mechanically stable with all components securely fastened (Valentino, 2007).

1/8 inch stainless steel pipes for the internal tubing are employed. A set of 13 two-way standard valves (ET-2-24, Clippard S.A.) switches the system between calibration gas, working gas and sample gas, and to determine which gas is expelled through the exhaust. These solenoid valves are switched electronically by a modular industrial FBCube bus computer (Syslogic) according to six different configurations (A, B, C, D, E and F). Each mode is engaged sequentially for 6 min before the system switches to the next mode. The first mode at the very beginning of each flight is always configuration D, followed by A. For most of the time, the system alternates configurations A and D, and only during calibration phases the configurations B, C, E and F are run. Because configuration D is used to introduce the working gas for drift correction in the fuel cells, only CO_2 is analyzed in sample air during configuration D (see table 3.2), while the fuel cells as well as the reference cell analyze the working gas. This split into two lines is achieved by including a branch-off downstream the Licor sample cell (valves V5–8 on figure 3.6), allowing to separate the Licor sample cell from the reference cell and the fuel cells, and allow passage of two different gases. Comparison between the CO_2 analyzer sample and reference cell output in this case requires that the measurement be absolute, where water vapor and CO_2 are removed in the reference cell. The computer-controlled valves V5, V7 and V6, V8 can only be switched in pairs and determine whether either the working gas or any one of the two

Table 3.2 Overview of the gases that are introduced through the inlet, pass the O_2 and CO_2 analyzer, and get expelled again during the six different modes.

Mode	Air in	O_2 analyzer	CO_2 analyzer sample cell	CO_2 analyzer reference cell	Air out
A	Ambient	Ambient (dried)	Ambient	Ambient (dried, CO_2 removed)	Ambient
B	Ambient	CG1 (dried)	Ambient	CG1 (dried, CO_2 removed)	Ambient, CG1
C	Ambient	CG2 (dried)	Ambient	CG2 (dried, CO_2 removed)	Ambient, CG2
D	Ambient	WG (dried)	Ambient	WG (dried, CO_2 removed)	Ambient, WG
E	-	WG (dried)	CG1	WG (dried, CO_2 removed)	WG, CG1
F	-	WG (dried)	CG2	WG (dried, CO_2 removed)	CG2, WG

calibration gases and the air sample is sent to the O_2 analyzer according to the current configuration. The fuel cells and the Licor reference cell downstream always see the same gas with the exception that CO_2 is removed after the O_2 analyzer. During configuration A the valves V5 and V7 are open, and V6 and V8 closed, so that both analyzers probe outside air brought in through the inlet. Therefore, mode A is when the Licor device is operated in serial mode. Configurations B and C serve the purpose of O_2 analyzer calibration, whereas configurations E and F are used to calibrate the CO_2 analyzer. As illustrated in figure 3.8, the HS for the calibration of CO_2 is introduced during configuration E, the LS for CO_2 during F, the LS for O_2 during B and the HS for O_2 during C. Both analyzers are hence not calibrated synchronously, but offset by one configuration. This is advantageous in that both devices can be calibrated individually and during the calibration of one device, the other analyzer can continue to take measurements. The computer runs a program written in Turbo Pascal to trigger calibrations three hours after take-off and a second calibration phase six hours after the first calibrations, flight duration permitting. The sequence of modes during the calibration phase is E - B - F - C, with each calibration cycle thus lasting a total of 24 min.

A 7 µm pore size in-line filter (Swagelok) upfront ensures that no particles such as aerosols contained in the incoming air stream can enter the system. In order to preserve a sample flow of 85 ml min^{-1} a custom-made membrane pump (PM20196-86.3 by KNF Neuberger GmbH) is used. Depending on the aircraft's altitude, the ambient air pressure exhibits large changes between roughly 200 hPa at cruise altitude and 1000 hPa at ground level. To counterbalance the changes in outside pressure and to obtain a constant inlet pressure, a micro valve fluistor (NC 1500 by Redwood Microsystems) upstream the diaphragm pump fine-tunes the pump capacity to a pressure of 1550 hPa. The pressure is maintained somewhat above any ambient pressure the system experiences. The fluistor pressure adjustments are driven by a dTRON 16.1 microprocessor controller (JUMO) in conjunction with a 40.4366 dTRANS p30 pressure transmitter (JUMO), which logs the pressure after the air has passed the sample cell of the CO_2 analyzer. In the current setup, any air that enters the sample cell of the LI-6262 CO_2 detector is not dried prior to analysis. Depending on the transported goods that

share the same cargo compartment with the CARIBIC container as well as the heat produced by the scientific instruments, temperature within the measurement unit can vary greatly between 15 °C to 50 °C, with temperature changes during single flights of up to 28 °C. From a scientific point of view, a consistently cooled cargo bay is most favorable, but the CARIBIC container is considered low priority cargo by the pilots. In contrast, living organisms for example are high priority and may require a heated environment. Since the LI-6262 device is placed in a temperature uncontrolled environment it is subjected to these temperature variations. For later temperature effect correction the CO_2 analyzer comes with a built-in temperature sensor. Temperature profiles logged by the CO_2 analyzer usually start at values corresponding to outside temperature at the respective airport and then typically start to increase with heat generated in the container or decrease in case air conditioning is active in the cargo compartment.

After the sample cell, gases bound for the fuel cells first pass through a drying unit consisting of a stainless steel tube filled with 50 g of anhydrous magnesium perchlorate ($Mg(ClO_4)_2$) followed by a second filter, which prevents any dust from the desiccant to enter the O_2 analyzer. Upon return to Mainz, the magnesium perchlorate is replaced to ensure its efficacy for the following campaign. The tubing segment between valve V7 and the differential pressure gauge experiences large deviations in gas flow of 85 ml min^{-1} in the configuration A when outside air is introduced compared to 110 ml min^{-1} in the configuration D when the WG is introduced. These changes in flow are compensated downstream using a differential pressure gauge as described below. The fuel cells are housed in a temperature controlled enclosure insulated with non-inflammable isoTHERM 1000 needle fleece (Frenzelit Werke GmbH), a safety regulation implemented whenever heating elements are used, limiting the unit's heat dissipation. The temperature is set to 48 °C with a stability better than 0.1 °C and recorded by a dTRON 16.1 controller (JUMO) using a Pt100 temperature probe (Minco) (Valentino, 2007). A heating foil (Minco) is used to reach a constant temperature. Temperature is maintained at a rather high level due to large temperature variations in the cargo bay and the fact that there is currently no space to include a cooling element. Precise and constant fuel cell input pressure is achieved using a Type 250E PID feedback control module (MKS), which maintains the same pressure as a reference volume across a differential pressure transducer (Type 223 Baratron, MKS) by adjusting a bypass flow via a solenoid control valve (Type 248, MKS). On the reference side of the differential pressure gauge is a reference volume filled with air at room temperature to 1120 hPa, which translates to a pressure of roughly 1236 hPa in the heated environment aboard. The precision of the pressure control is 0.005 mbar (Valentino, 2007). The adjustable waste flux controlled by the control module is measured and logged downstream by an AWM3100V airflow sensor (Honeywell). Next, the air enters the O_2 analyzer, where it passes three fuel cells and a Pt100 temperature sensor (Minco). An Ascarite trap in a stainless steel tube containing sodium hydroxide-coated silica scrubs the CO_2 before it flows into the reference cell of the CO_2 analyzer makin it possible to measure dry, CO_2-free air. Magnesium

perchlorate is placed at both ends of the Ascarite in order to remove water, which is formed as a by-product of the CO_2 absorption process (Sturm, 2005). Together with the magnesium perchlorate trap, the Ascarite is substituted after each campaign. While the fluistor obtains a constant inlet pressure at the sample cell of the Licor, the inlet pressure at its reference cell is controlled by the electronic MKS 250E controller upstream of the fuel cells, and with 1550 hPa and 1100 hPa respectively, these pressures are not equal for the two cells. An electronic pressure controller (Type 640, MKS) placed in the thermostable enclosure for increased precision, is used to sustain a constant outlet pressure of the CO_2 analyzer. Before it is expelled out of the system and transported to the exhaust, the total air flow is measured by a Type 179A all-metal mass-flow meter (MKS). Five capillaries are built in to down-regulate the pressure and flow, and to smooth any pulsing pressure signals. Additionally, a total of three needle valves restrict the flow and guarantee base pressure. Because the unit generates more signals than can individually be processed by the eight analog-to-digital converters (ADC), a multiplexer (MUX) is used to add four more inputs at 60 s intervals. The system is operated by the unit's own computer, which also has a 128 MB CompactFlash memory card slot for data storage. The parameters are recorded at a resolution of 1 s and include the date, time, configuration active, voltage output of the fuel cells, fuel cell temperature, Licor sample cell inlet pressure, temperature in the temperature controlled box harboring the fuel cells, total flux at MKS 179, differential CO_2 and H_2O voltage output by the Licor device, Licor temperature, Licor reference cell pressure, waste flux passing the Honeywell AWM3100 (MUX), the pressure at the differential pressure gauge (MUX), outlet pressure as measured at the MKS 640 (MUX), as well as the actual input voltage of 12 V provided for the unit with a DC-to-DC converter (MUX). Via the Ethernet port, the unit's own computer receives instructions from the master computer in the container and synchronizes its time.

3.3 Data processing and calculations

The computer within the measurement unit merely stores the raw value outputs directly from both the O_2 and CO_2 devices and does not perform any calculations on site. One of the main goals of this thesis was to develop a routine to process the voltage values from both devices into final data of $\delta(O_2/N_2)$ ratios in per meg and mixing ratios of CO_2 in ppmv for interpretation. With the benefit of being platform-independent in mind, the code was written in the numerical computing environment MATLAB R2011b (MathWorks), which is also widely used in scientific research. The underlying idea was to obtain a fast, reliable and simple-to-use automation of the calculations to remove any user biases that may arise in manual data processing. The script requires manual input of the raw files as well as minor user interaction and is run on a flight-by-flight basis. Its main tasks include the combination of the individual text files, the application of the necessary corrections and calculations of the CO_2 and $\delta(O_2/N_2)$ values, and the saving of the final data in the NASA Ames Format for

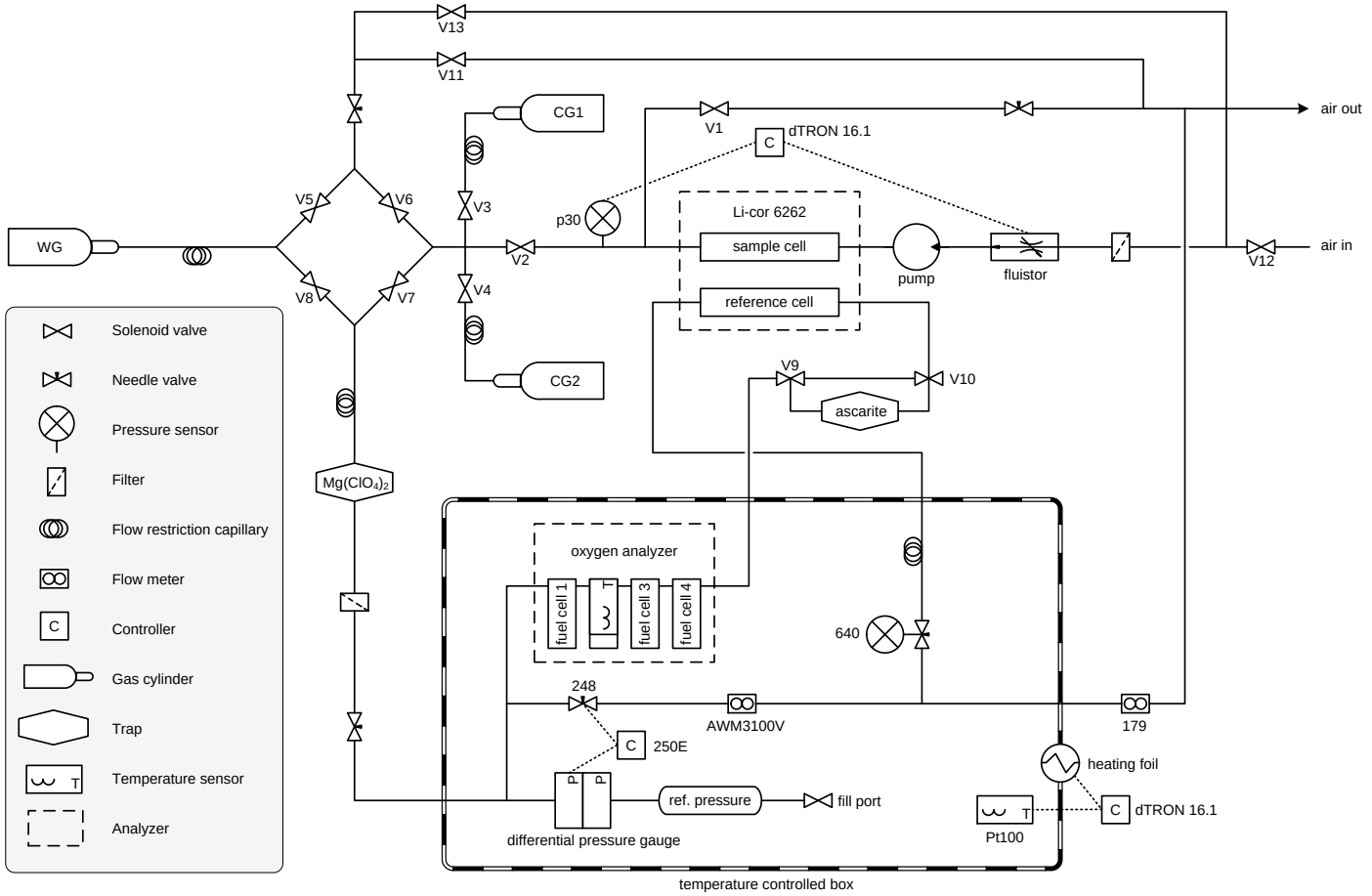

Figure 3.6 General tubing scheme of the O_2 and CO_2 measuring unit in the CARIBIC container. See description in the text for more details and appendix A for flow charts of all the individual configurations.

Data Exchange in a project-wide uniform time resolution, followed by the joining of the PIUB data with other CARIBIC measurements and the aircraft ARINC parameters. In the following the data processing routine is described. The full code of the main script is listed in Appendix C.

The computer in the PIUB measurement unit that writes the data to text files creates a new file every two hours containing two and a half hours worth of data in 1 s temporal resolution, with half an hour of data overlap. Thus, by default, flight data is divided into up to seven text files. As a first step, the separate files were combined and the overlap between them removed. For some flights, it frequently occurred that the unit's computer lost the communication to the master computer in the container, which triggered a reboot in the PIUB system. This not only resulted in an increased number of files but also approximately 1 min of missing data for the duration it takes the system to boot up again. Fuel cell and Licor data of the entire affected configuration were skipped in these cases, in order to remove any break-in effects during startup.

The CARIBIC project uses the Coordinated Universal Time (UTC) as a coherent time axis for all flights. It is paramount for all the measurements to be synchronous, which sometimes required a time correction of the data either because the master computer was asynchronous with the aircraft time or because the PIUB device failed to synchronize time with the master computer.

Data points of all parameters were considered invalid or missing if values were negative or zero, and in the case of the fuel cells clipping at a voltage of 10 V. As a means of a first coarse outlier removal, individual fuel cells and Licor data points were removed if their raw values lied outside three standard deviations (3σ) of the mean for each individual configuration.

For the calibration of both analyzers as well as the calculation of the $\delta(O_2/N_2)$ values, it is crucial that the pressure has been equilibrated after each configuration switch. To allow for stabilization of the system, the first 4 min as well as the last 10 s of each configuration were discarded and the readings of all the parameters and measurements for the remaining 110 s were averaged. Data for each flight therefore exists in two time resolutions: one in a 6 min resolution with a value for each configuration and the original 1 s resolution. While the O_2 measurements are reported in the low resolution, CO_2 values are calculated on the temporal resolution of 1 s.

3.3.1 Calculations concerning the NDIR analyzer

3.3.1.1 Water vapor calculation

Water vapor is removed from the air sample only after it has passed the Licor sample cell. Since water affects the CO_2 measurements through pressure broadening and dilution it is therefore required that I first calculate the H_2O mixing ratio in the sampled air in order to correct the CO_2 readings. The

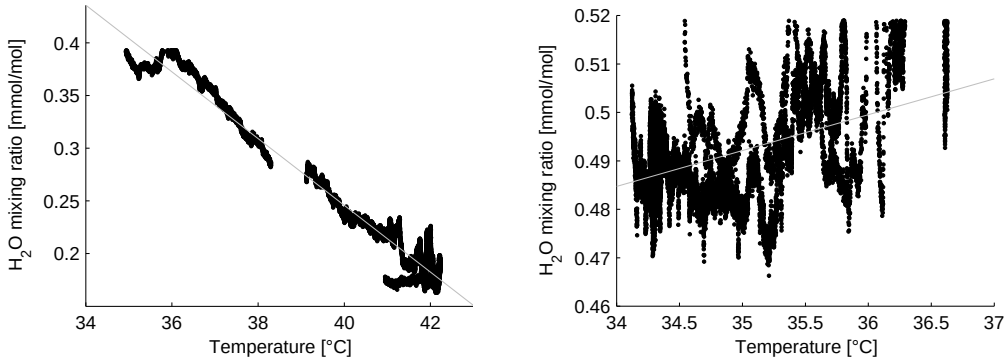

(a) Flight 313 **(b)** Flight 314

Figure 3.7 Example of a strong and a weak temperature dependence in the H_2O mixing ratio during flight 313 (a) and 314 (b). Black points are water measurements obtained by the LI-6262 and the gray line represents the linear relationship with a least-squares line by which the H_2O data was corrected in the case of flight 313.

expression relating water signal output V_w to water vapor concentration in mmol mol^{-1} w is

$$w = F_w \left[V_w \cdot \left(\frac{p_0}{p} \right)^{0.9} \right] \cdot \left(\frac{T + 273.15}{T_0 + 273.15} \right) \tag{3.3}$$

as given in (LI-COR, 1996), where F_w is a third order polynomial function specific to the PIUB device that relates V to water vapor concentration, p_0 is the standard barometric pressure (101.325 kPa, p is the barometric pressure in the sample cell in kPa, T is the temperature of the Licor device in °C and T_0 is the temperature at which the Licor device was calibrated in °C.

Despite the temperature normalization, the Licor device still seemed to exhibit a temperature dependent drift in water content. This dependence, due to reasons yet unknown, appeared to be very variable from flight to flight. Furthermore, when comparing the raw H_2O measurements with the ones taken by the IMK, there was a noticeable positive offset in the PIUB measurement of variable extent (up to several hundred ppmv). There is no reason for me to believe that more water vapor actually did enter the system than was measured by the IMK after flight 294, as from this flight onwards the same inlet was shared. I attributed this discrepancy between the measurements to the fact that the CO_2 analyzer is not calibrated for H_2O content. To roughly correct for the temperature effect, a simple linear regression was applied to the voltages for configurations A and D over the entire flight excluding the first and last 42 min and which did not deviate by more than four times the median, as well as for which the R squared value was larger than 0.5. The correction is based on the assumption that on cruise altitude, there is very little variation in the H_2O signal. However, this method yielded diminished correlations for earlier flights up to 293, because the PIUB system was attached to the forward facing water inlet, resulting in the emergence of H_2O signals due to clouds.

The variable offset in the atmospheric H_2O content was corrected for using the calibrations with the following procedure. First, the average H_2O mixing ratios in the deployed CG1 (passing the

Licor during configuration E) and CG2 (configuration F) gas cylinders were estimated by comparing the mean differences between the water content measured in configuration E and F for all flights that used the same cylinders, and an assumed overall average H_2O mixing ratio in the cylinders of 50 ppmv based on H_2O determinations by mass spectrometry. Then, the very last 10 s of the E and F configurations of each flight were discarded and the absolute H_2O readings of the seconds 340 to 350 were averaged. The disagreement between the measured and estimated average water content in the calibration gases corresponded to the extent of the offset, and I subtracted the smallest difference from all the H_2O values. Any negative water values which resulted form this correction were treated as zero water content. In case of unavailable water values during calibrations or for shorter flights without any calibrations, the H_2O offset was corrected by simply subtracting the lowest measured raw voltage value for H_2O from all the values and then adding 1 mV, crudely assuming that at some point in the flight an average minimum mixing ratio of 4.5 ppmv is reached.

3.3.1.2 Carbon dioxide calculation

Over much of its range the LI-6262 output voltage is proportional to the number of photons reaching the detector and therefore to absorptance. Absorptance on the other hand is not a linear function of the CO_2 mole fraction. Both analyzer output voltage and absorptance increase with increasing CO_2 concentration in the sample cell. A fifth order polynomial function $F(V)$ relates the output voltage V to CO_2 mole fraction (LI-COR, 1996).

$$F_c(V) = a_1 V + a_2 V^2 + a_3 V^3 + a_4 V^4 + a_5 V^5 \tag{3.4}$$

The coefficients a_1 through a_5 are unique to each device and need to be determined by sending it in for factory calibration. The calibration polynomial $F_c(V)$ is valid only for the temperature and pressure at which it was determined and therefore requires that corrections be made for operation under different environmental conditions as it is the case in-flight. The gas concentration is affected by absolute temperature in a linear fashion, whereas pressure has a linear effect on the signal output V. To calculate the temperature, pressure and water vapor corrected CO_2 mole fraction C in the PIUB setup, I used the following expression from LI-COR (1996) (their equation 3-4, combined with equation 3-20 and 3-32 for added water vapor correction)

$$C = \frac{F_c \left[\left(\frac{V \cdot S + b}{1 + (a_w - 1)\frac{w}{1000}} \right) \left(\frac{p_0}{p} \right) \right] \left(1 + (a_w - 1)\frac{w}{1000} \right) \left(\frac{T + 273.15}{T_0 + 273.15} \right)}{1 - \frac{w}{1000}} \tag{3.5}$$

V is the voltage output from the LI-6262 expressed as the difference between sample cell and reference cell, S is the sensitivity of the instrument expressed as a span factor in $\mathrm{mV\,mV^{-1}}$, b is the offset in mV (see section 3.3.1.3), a_w is a weighting factor with a value of 1.57 representing the pressure broadening effectiveness of water vapor relative to a reference of dry air, w corresponds to the water vapor mole fraction in units of $\mathrm{mmol\,mol^{-1}}$ calculated in equation 3.3 above.

By comparing the CO_2 mixing ratios resulting from this calculation procedure with the CO_2 data obtained by the LSCE, I discovered that the LI-6262 device sometimes still exhibited a strong dependence on temperature despite the temperature correction applied above. Similar to the temperature dependence in the H_2O mixing ratios, the drift in the CO_2 mV values seemed variable from flight to flight and was estimated to be -0.244 ± 0.223 ppmv/°C by averaging the relationships of the first and last flights where temperature explains more than 30 % of the difference between the PIUB CO_2 data and the LSCE CO_2 data. At a temperature of 30.055 ± 4.360 °C, PIUB and LSCE values seemed to agree. In contrast to the individually derived H_2O corrections, it was not possible to determine the dependence flight-by-flight because the natural signals in CO_2 mixing ratio was generally larger than the drift with temperature. There also did not seem to be any correlation between temperature dependence in the H_2O values and the CO_2 values. In order not to make the PIUB CO_2 measurements dependent on the measurements by the LSCE, I applied the average correction $V_{\mathrm{cor}} = V_{\mathrm{uncor}} + ((T - 30.055) \cdot 0.244/0.241)$ to the raw mV values in the beginning, with 30.055 and 0.244 being the derived coefficients of the dependence, and 0.241 being the factor relating the units of ppmv to mV assuming a linear relationship between the LS and HS that were used.

According to the LI-6262 manual the device has a warm-up time of 5 min, which was the reason why I excluded the very first 6 min of each flight. For the 1 s resolution CO_2 data the values for each first minute after switching to configurations A and D were discarded. As visible in figure 3.8a it took longer until the signal from the LI-6262 device was stabilized again after the configurations E and F that are used to calibrate the CO_2 measurements. Hence, when the subsequent modes B and C were active, 3 min were omitted before further analysis. The CO_2 mixing ratios are reported on the WMO07 CO_2 mole fraction scale.

3.3.1.3 NDIR calibration

For the calculation of the CO_2 analyzer calibration, the 110 s averaged data was used, in order to avoid abrupt changes occurring during switching between the gases (Uglietti, 2009). The assigned CO_2 mixing ratios ($CO_{2\,\mathrm{as}}$) in ppmv of both calibration cylinders CG1 and CG2 were first converted into values of mV (V_{as}) expected to result from the LI-6262 system is measuring the two gases using equation 3.6:

$$V_{\mathrm{as}} = F_c^{-1}\left[CO_{2\,\mathrm{as}}\left(1 - \frac{w}{1000}\right)\left(\frac{T_0 + 273.15}{T + 273.15}\right)\left(\frac{1}{1 + (a_w - 1)\frac{w}{1000}}\right)\right]\left(1 + (a_w - 1)\frac{w}{1000}\right)\left(\frac{p}{p_0}\right) \tag{3.6}$$

This equation is basically the same as equation 3.5 described in the previous section, solved for V. F_c^{-1} is an inverse polynomial function (3.4), whose result I derive iteratively to a precision of ±0.2 mV, corresponding to roughly ±0.035 ppmv in CO_2. The instrument sensitivity expressed as $mV_{\mathrm{as}}/mV_{\mathrm{me}}$, here defined as the span factor, is then determined by the ratio between the difference of the assigned mean high ($V_{\mathrm{HS,\,as}}$) and low span CO_2 calibration gas voltages ($V_{\mathrm{LS,\,as}}$) and the difference of the

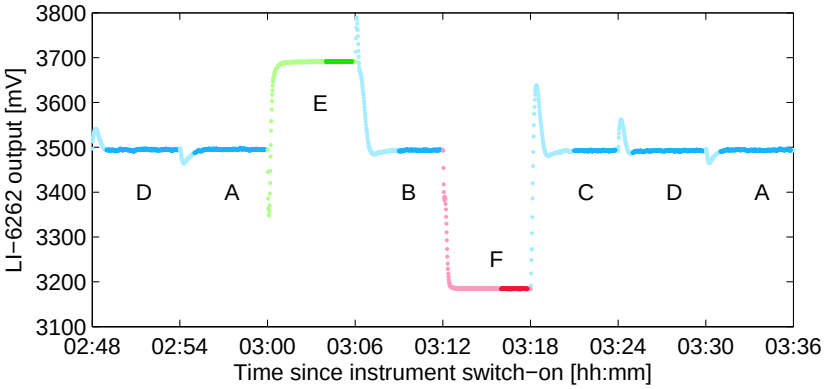

(a) CO_2 calibration scheme

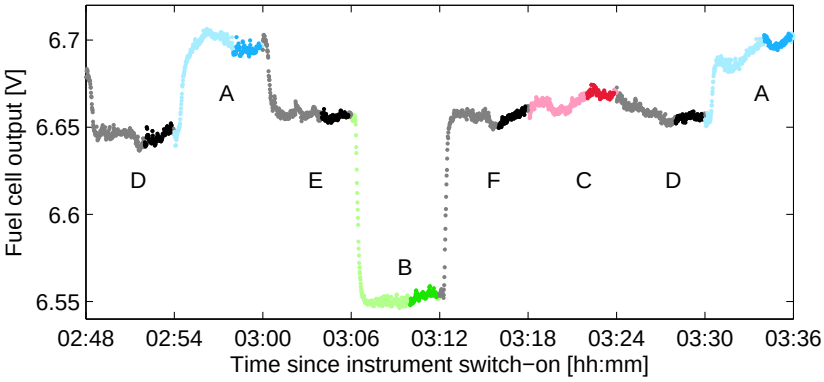

(b) O_2 calibration scheme

Figure 3.8 Examples of output signals of the LI-6262 CO_2 analyzer (a) and one of the fuel cells of the O_2 analyzer (b) during a calibration procedure. The graphs show a 48 min extract approximately 3 h after take-off, thus including the first calibration procedure of a flight. Letters indicate the active configurations. Green, red, blue and gray points indicate outputs for CG1 (HS for CO_2, LS for O_2), CG2 (LS for CO_2, HS for O_2), sample air and for WG, respectively. Lighter colors represent data points that were excluded.

measured mean high ($V_{\mathrm{HS,\ me}}$) and low span CO_2 calibration gas voltages ($V_{\mathrm{LS,\ me}}$).

$$S = \frac{V_{\mathrm{HS,\ as}} - V_{\mathrm{LS,\ as}}}{V_{\mathrm{HS,\ me}} - V_{\mathrm{LS,\ me}}} \tag{3.7}$$

The offset b from this relationship is calculated with the equation

$$b = V_{\mathrm{HS,\ as}} - S \cdot V_{\mathrm{HS,\ me}} \tag{3.8}$$

To illustrate the noise of the instrument and to give an overview of the calibration procedure, figure 3.8 shows an example of O_2 and CO_2 signals recorded for a calibration during a flight. The bottom panel further illustrates the above mentioned issue of the O_2 HS containing an apparent O_2 mole fraction too low to span the spectrum of natural variations.

3.3.2 Calculations concerning the fuel cell analyzer

3.3.2.1 Oxygen calculation

Valentino (2007) reported of issues with the temperature stability of the fuel cells in this project. Of particular concern is the seemingly long time it takes the fuel cells to equilibrate with the temperature within the box after take-off, since the thermal mass of the sensors typically slow down any transient temperature effects on the sensor (Maxtec, 2003). As a consequence the oxygen signal consistently exhibited severe drifts approximately in the initial 2 h (see figure 3.9). The graph visualizes that whereas temperature is most likely the main factor affecting signal drift in the beginning, the fuel cells did not drift depending on temperature alone. It is highlighted that each fuel cell behaves in a unique manner. In the case of flight 393, the FC3 signal displays a prominent dip at 15:00 from 7.2 V to 6.6 V. Furthermore, one can recognize that the three fuel cells suffer from different amounts of noise and sensitivities.

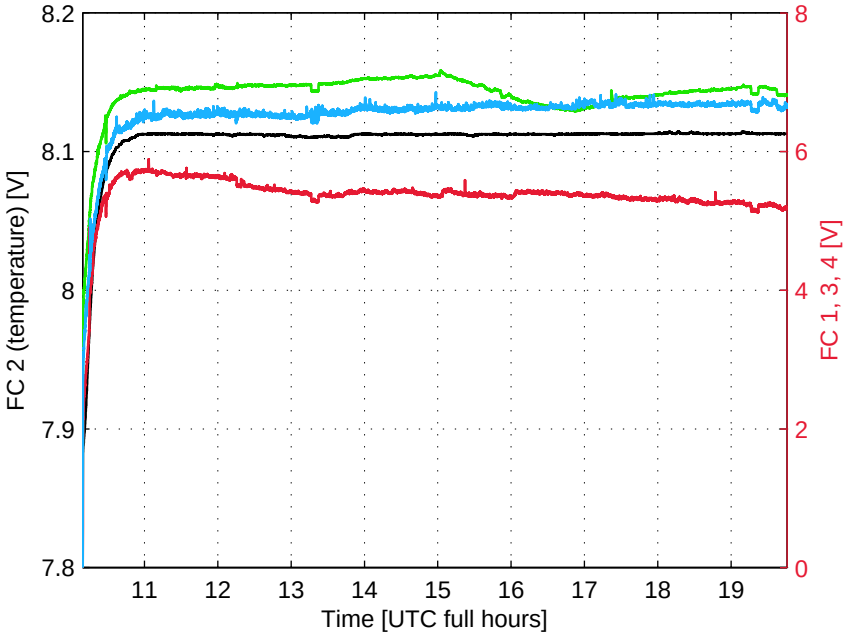

Figure 3.9 Graph showing the raw signal outputs by the three fuel cells 1 (red), 3 (green) and 4 (blue) on the right y-axis, and the temperature sensor in fuel cell 2 (black) on the left y-axis. Data was taken from flight 393.

In order to address the problem of drift, I used the averaged low resolution data of configuration D (when the WG was measured) for each individual fuel cell separately to obtain a cubic smoothing spline function with a cut-off period of 12 min, which I subsequently subtracted from the raw voltage signal. This procedure flattened the curves and to a great extent removed long-term drift from the data. Whereas the original fuel cell signal in figure 3.10 exhibits substantial drift, the corrected curve

is almost flattened out without losing the signal in the sampled air. As visible in flight 393, the spline is not able to successfully resolve the sharp changes in the beginning and end of a flight. It appears that FC3 has less noise towards the end of the flight relative to the first 2 h.

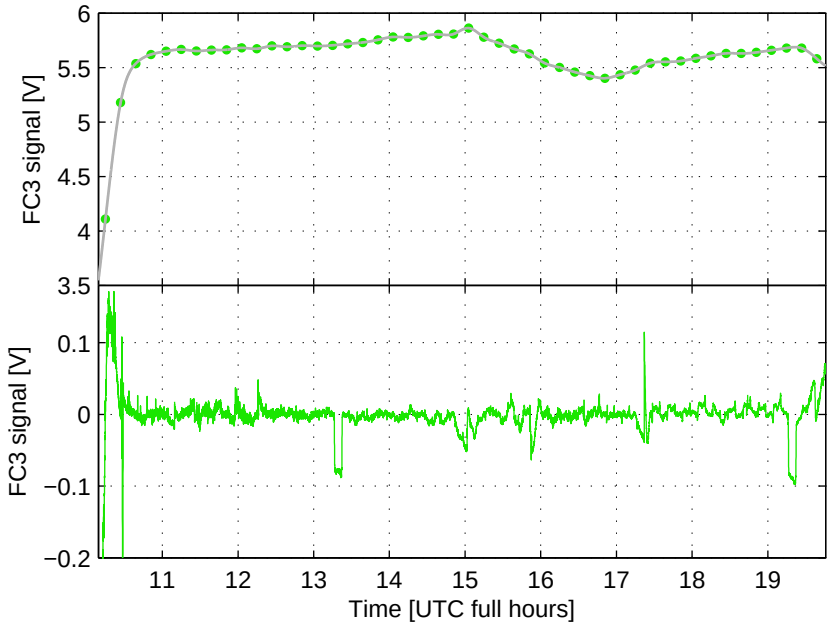

Figure 3.10 Cubic smoothing spline fit using the example of fuel cell 3 of flight 393. The upper panel shows the fuel cell 3 data after it has been normalized to standard pressure. Green dots indicate averaged mean values for all D configurations when WG is measured, to which a cubic smoothing spline (gray line) is fitted. The green line below is the same fuel cell signal after the spline function has been subtracted.

Furthermore, a correction for pressure variability was added as well. I used the Baratron pressure for this as it delivered the most precise pressure measurement right before the air enters the O_2 analyzer. To disentangle the influences of temperature and pressure the Baratron pressure was first temperature corrected with a second order polynomial regression model for each flight. The coefficients were derived by fitting the polynomial to the data for the configurations A and D only, and during the first 1.5 h of the flight in a least squares sense. A threshold of 1.5 h was chosen because the beginning of each flight is when the temperature change is most significant and, for the following correction of the other fuel cell values, the influence of actual O_2 signals from outside air the lowest. The temperature corrected pressure values were calculated by subtracting the polynomial function from the raw values and subsequently adding the median value of the pressure over the entire flight.

For the multiplexed parameters waste flux, Baratron pressure and MKS640 pressure values are only recorded for 1 or 2 min out of the 6 min long configurations. In order to obtain a value at each time step for the multiplexed parameters as well, the median value for each configuration was calculated

and assumed constant for the entire configuration. The fuel cell voltages were then normalized to standard pressure ($V_{\mathrm{cor}} = V_{\mathrm{uncor}} \cdot (1013.25/p)$).

To express the fuel cell output for the sample air in per meg unit allowing the results to be directly compared with results of other laboratories that employ the mass spectrometric method, the following formula was applied.

$$\delta(\mathrm{O_2/N_2}) = \frac{(\Delta V \cdot S + \delta[\mathrm{O_2}]_{\mathrm{WG,\,as}}) + ([\mathrm{CO_2}] - 384.5) \cdot X_{\mathrm{O_2}}}{X_{\mathrm{O_2}} \cdot (1 - X_{\mathrm{O_2}})}, \tag{3.9}$$

where ΔV is the voltage output from the fuel cell, expressed as the difference between sample gas and the mean of the preceding and following WG, S is the sensitivity factor unique to each fuel cell in units of ppmv/V calculated during the calibration by analyzing CG1 and CG2 with known O_2 concentrations (see section 3.2.4), $\delta[\mathrm{O_2}]_{\mathrm{WG,\,as}}$ is the assigned O_2 mixing ratio deviation from an arbitrary reference gas in ppmv contained in the WG cylinder, $X_{\mathrm{O_2}}$ is the standard mole fraction of O_2 in dry air for which I used 0.20946 (Machta and Hughes, 1970), $[\mathrm{CO_2}]$ is the CO_2 mixing ratio averaged over the configuration as determined by the NDIR analyzer in ppmv, 384.5 is the CO_2 concentration of the arbitrary reference cylinder defining zero on the local PIUB O_2 scale. This conversion takes into account the correction for the diluting effect of changing CO_2 concentrations according to the theory by Manning et al. (1999). I assumed that dilution caused by variations in trace gas species other than CO_2, such as Ar, is negligible due to the variations in air being too small to affect the oxygen measurement significantly. It is therefore important to only use equation 3.9 for calculations concerning natural sample air. For calculating the $\delta(\mathrm{O_2/N_2})$ ratio of the standards CG1 and CG2, which should in theory conform with the assigned mass spectrometer values, a slight variant of equation 3.9 was used including a correction for changes in Ar content between the cylinders denoted by the term $\delta(\mathrm{Ar/N_2})$ (also see equation 3.1).

$$\delta(\mathrm{O_2/N_2}) = \frac{(\Delta V \cdot S + \delta[\mathrm{O_2}]_{\mathrm{WG,\,as}}) + ([\mathrm{CO_2}] - 384.5) \cdot X_{\mathrm{O_2}} + \delta(\mathrm{Ar/N_2}) \cdot X_{\mathrm{Ar}} \cdot X_{\mathrm{O_2}}}{X_{\mathrm{O_2}} \cdot (1 - X_{\mathrm{O_2}})}, \tag{3.10}$$

An international standard is not established yet for oxygen measurements, but the SIO $\delta(\mathrm{O_2/N_2})$ scale is the most widely used one. All the values for $\delta(\mathrm{O_2/N_2})$ are reported in per meg on the SIO scale after conversion from the local PIUB scale using the equation:

$$\delta(\mathrm{O_2/N_2})_{\mathrm{Scripps}} = \left(\left(\frac{\delta(\mathrm{O_2/N_2})_{\mathrm{PIUB}}}{10^6} + 1\right) \cdot \left(\frac{-550}{10^6} + 1\right) - 1\right) \cdot 10^6 \tag{3.11}$$

3.3.2.2 Fuel cell calibration

The fuel cell sensitivity for each of the three fuel cells was determined via the HS and LS gases in a similar fashion as the NDIR calibration, with the difference that drifts in the measured WG signal ($V_{\mathrm{WG,\,me}}$) were taken into account.

$$S = \frac{V_{\mathrm{HS,\ as}} - V_{\mathrm{LS,\ as}}}{(V_{\mathrm{HS,\ me}} - V_{\mathrm{WG,\ me}}) + (V_{\mathrm{WG,\ me}} - V_{\mathrm{LS,\ me}})} \tag{3.12}$$

Here, the terms $V_{\mathrm{WG,\ me}}$ represent the interpolated WG voltages derived by averaging the output values of the embedding D configurations for both HS and LS. All the assigned values are apparent oxygen mole fraction differences from an arbitrary standard, hence yielding the fuel cell sensitivities in units of ppmv/V. The offset, in this case, is directly defined as the value of the assigned WG apparent mole fraction deviation. This approach of calibration assumes that the fuel cell outputs behave linearly with changing O_2 content.

3.3.3 General considerations

Most flights undertaken with the CARIBIC equipment onboard are long distance and include at least one calibration procedure, which are triggered at the third and ninth hour of the flight. If there was one calibration, the sensitivities (and the offset for CO_2) of both the O_2 and the CO_2 analyzer were assumed constant for the entire flight. For long flights containing two calibration procedures, the span and offset values were linearly inter- and extrapolated in time over the duration of the flight. In case the second calibration occurred within the last 42 min of the flight it was excluded and only the values calculated for the first calibration considered in order to make sure that calibrations were not affected by the descent phase of the flight. Whenever the WG cylinder ran out of gas a clear pressure collapse during configuration D could be detected by the Licor reference cell pressure logger. Such drastic changes in reference pressure were used to identify empty WG cylinders and any fuel cell data after the first occurrence was automatically discarded. Since the computer is programmed to always trigger the first calibration 3 h after instrument switch-on, the inevitable problem arises of short flights without any calibration values. For these flights the calibration values of the next closest calibration in time were assumed, which were usually the second calibration values of the first flight if the second leg of a campaign was too short, and the first calibration values of the fourth flight if the third leg was short. Flights lasting less than 3 h should thus be interpreted with caution.

The CARIBIC partners have settled on a project-wide uniform time resolution of 10 s for in-situ measurements and the ARINC data output. CO_2 data collected by the PIUB was therefore averaged into 10 s bins and together with the O_2 data saved in the NASA Ames data format. This convention allows for easy comparison with other greenhouse gas measurements by partner institutes as well as the ARINC parameters provided by the aircraft. When merging the data sets, the PIUB data matched the LSCE CO_2 data best when a lag of 7 s was corrected for.

Airborne observations of greenhouse gases commonly determine the tropopause height by using 2 PVU (Gurk et al., 2008; Sawa et al., 2008, 2012). Despite available potential vorticity values for all flights, I chose a different approach for distinguishing tropospheric from stratospheric air for the

flight trajectory plots and used O_3 as a measure of relative height above the tropopause by comparing measured O_3 concentration with a known vertical ozone profile as derived from currently 12 stations north of 35° N. These values were already calculated by the IMK. This method is able to capture the fine-scale dynamics around the tropopause much better than the tropopause information from ECMWF model in KNMI data, which is known to suffer from coarse model resolution. The resulting unit of measurement is the representative height above the tropopause in km. This technique is described in more detail in Sprung and Zahn (2010).

Within the scope of this thesis, the CARIBIC flights numbered 190 through 432 were processed. The reason for not including all the CARIBIC flights since flight 102 is that numerous changes had been applied to the system in the early stages, in particular concerning the handling of calibrations and improvements of previously dominant inlet pressure fluctuations.

Chapter 4

Results

The CARIBIC container was installed in the Airbus A340-600 during a total of 242 flights in 65 campaigns, corresponding to a time frame between May, 2007 and June, 2013. Various problems that were encountered throughout this time however, lead to a substantially lower amount of flights with suitable data sets. Some of these problems were universal and affected the entire CARIBIC community. During the flights 200 and 201 the tubing connecting the inlet and the container was broken so that no ambient air was measured. It also happened several times that the container did not receive any power (flights 217, 267, 277, 318, 320, 410–412, 425–428). Other issues were specific to the O_2 and CO_2 analyzer measurement unit. These included situations in which the unit was inoperable (flights 365–372), the Licor device did not function (flights 209, 236–239, 261, 271, 272), the computer lost communication and constantly rebooted (flights 270, 273, 275), data was not saved (flights 242, 284) or the equipment regulating constant conditions failed (flights 321, 346, 347, 349–352, 355, 356, 364). There were also six flights (205, 257, 297–300) where data acquisition terminated mid-flight. Additionally, the flights 294–296 in April and March 2010 were ignored, because those were special volcanic cloud flights in the vicinity of Iceland with the aim of investigating the aftermath of the erupted Eyjafjallajökull volcano and did not intend to measure background air.

A total of 195 flights were eligible and analyzed yielding 386 354 data points in 10 s resolution, of which 66 % were assigned to the troposphere. Figure 4.1 depicts that most data collected at low latitudes did not include stratospheric air, which is consistent with the fact that the tropopause height is higher in the tropics. Appendix B includes a complete list of flights. CO_2 data was discarded when the following conditions were not met: a reference cell pressure in the range of 1098 hPa to 1102 hPa, Baratron pressure range of 1232 hPa to 1241 hPa, MKS 640 pressure range of 1020 hPa to 1040 hPa. Likewise for the O_2 measurements, with the additional exclusion if the temperature in the box fell below 47.8 °C or exceeded 48.3 °C.

Table 4.1 List of all the destinations covered between May 2007 and June 2013. Numbers indicate the number of times the destinations were approached.

	2007	2008	2009	2010	2011	2012	2013
Frankfurt	6	16	11	12	15	16	6
Denver	1						
Houston	1						
Toronto	1						
Manila	6	2					
Guangzhou	11	4					
Chennai		14				2	
Chicago			1				
Orlando			1				
Cape Town			2		2		
Caracas			4	5	6	6	3
Vancouver			3		5	4	2
Johannesburg				1	1		
Bogotá				2	2		
Osaka				5	1		
Seoul						2	
Kuala Lumpur						2	2
Bangkok						4	5

4.1 Water vapor measurements

Figure 4.2 depicts a comparison between the H_2O measurements conducted by the PIUB LI-6262 device and the laser photoacoustic analyzer specialized on the detection of water in the atmosphere. Whereas the analyzer incorporated by the IMK can distinguish between water vapor and cloud water/ice content by using two distinct lines, the LI-6262 cannot. Figure 4.2a shows water data as obtained in June 2007 during one of the earlier flights 194, where the PIUB O_2 and CO_2 analyzer was attached to the forward facing inlet and measured total water. One would therefore expect the PIUB device to measure the summed up effect of both water phases for flight numbers lower than 293. ECMWF data in panel 4.2c indicates that at around 23:00 on that flight, the aircraft passed through an ice cloud right after reaching cruise altitude. The cloud signal is clearly represented by the IMK device as well as the NDIR analyzer. The finding that the peak is overestimated by a factor of three by the NDIR device can be explained by the air displacement and the anisokinetic inlet mentioned in section 3.2.1. Both cloud particle enhancement factors are considered when calculating the amount of cloud water or ice in the IMK device (Brenninkmeijer et al., 2007). In the PIUB device, correction for these effects is non-essential as the water measurements are solely used to correct the CO_2 data. Comparing the uncorrected and the corrected values, one can detect that a temperature dependence was found and applied for in this case, and the calibration values visible as two flattening peaks at 1 am had been successfully used to correct for the offset of about 1000 ppmv. In panel 4.2b the offset for flight 309 in September 2010 is 800 ppmv and no temperature dependence was detected. This plot

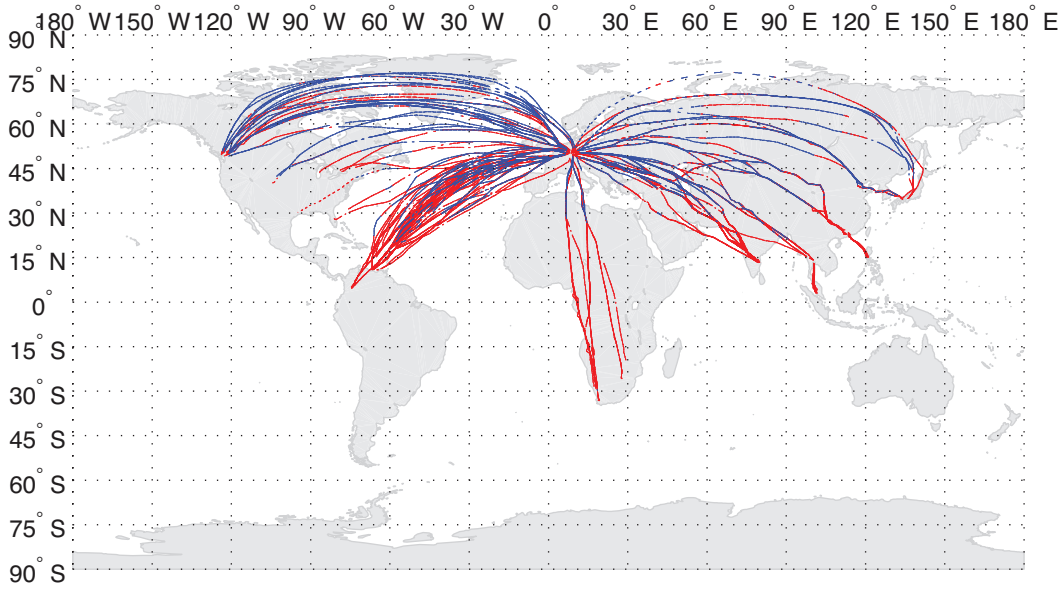

Figure 4.1 Map of the locations where all the data points were collected between May 2007 and June 2013 during the CARIBIC project. Red and blue dots denote measurements in the troposphere and stratosphere, respectively. The quasi-dashed line trajectories, such as the northernmost flight from Osaka to Frankfurt, are from flights during which the WG run out, leading to the Licor reference cell pressure to drop and data from the affected mode D to be excluded.

shows the same comparison after the line had been switched to the perpendicular inlet resulting in the detection of water exclusively in the gaseous phase, so that the green and black curves should match more closely. In fact, the LI-6262 does not pick up the ice cloud signal at 12:00 and 18:30. The strong variations in the PIUB H_2O measurement towards the end of flight 309 was caused by the second calibration procedure which was taking place.

The mean deviation of the H_2O values obtained by the LI-6262 device and the IMK device (PIUB - IMK) amounted to 33.2 ± 352.0 ppmv for flights with numbers 297 or higher, whereas before the difference was 84.2 ± 300.8 ppmv. Generally, the corrected H_2O values parallel the actual water values much better than the uncorrected ones, particularly at cruising altitude. The small-scale structures in the PIUB and IMK curves are in accordance, which is an indication that there is a time or temperature dependent offset rather than a memory effect due to adsorption of water vapor in the tubings. The most likely reason for the pronounced positive offset in the data is that the LI-6262 is not calibrated for water vapor during flights. Despite the H_2O values that are used to correct CO_2 only being roughly corrected using rudimentary methods, the CO_2 measurements are only marginally affected for applications at higher altitudes, where the water vapor content is usually very low at values of usually below 50 ppmv, and the resulting water dilution effect lower than the error. However, during take-off and landing, passage over the convective regions at the Intertropical Convergence Zone (ITCZ), where humid air is upwelled, as well as passage through clouds for earlier flights, the water mixing

ratio in air can become significantly large with values of 5000 ppmv and more. A deviation from the actual H_2O values of 100 ppmv corresponds to a deviation in CO_2 of roughly 0.039 ppmv at an initial CO_2 mixing ratio of 390 ppmv due to the dilution alone.

On the basis of the peak in H_2O at 23:00 of flight 194 (figure 4.3), one can estimate the combined effect of the cloud particle enhancement and the non-isokinetic inlet factors in this case to $((6400\,\text{ppmv} - 400\,\text{ppmv})\,/1900\,\text{ppmv}) \cdot 100 = 316\,\%$.

4.2 Carbon dioxide measurements

The instrument package in the CARIBIC container also includes two additional devices measuring atmospheric CO_2. The first one is a second NDIR device for real-time measurements operated by the LSCE, which is based on the same type LI-6262 analyzer. Secondly, there is a whole air sampler installed by the MPI allowing for subsequent analysis in the lab by means of gas chromatography. If available for a given flight, both these data sets can be used to cross-validate the PIUB measurements of CO_2. Schuck et al. (2009) reported of ranges in absolute differences between the laboratory analysis and the in-situ data from 0.03 ppmv to 0.3 ppmv with an average difference of 0.12 ppmv when comparing the results for flight 214. They concluded that the results agree within their 1-σ-errors, considering an absolute error of 0.2 ppmv for the flask measurement and a precision of 0.18 ppmv for the in-situ instrument. It is important to note that these statistics are only based on a single flight. All things considered, the LSCE data did agree well with the flask data. Since their setup is similar and the time resolution exactly the same, the CO_2 data acquired by the LSCE was used to evaluate the reliabilities of the PIUB CO_2 data. The differences between the LSCE and the PIUB (LSCE - PIUB) measurements deviated from a clear normal distribution in that they were rather fat-tailed, with a main peak at -1, indicating a systematic offset between the measurements. The frequency distribution (figure 4.4) depicts a range of differences (PIUB minus LSCE) from -16.0 to 19.3 ppmv with a mean of -1.11 ± 1.51 ppmv. From this I estimated the analytical accuracy of the PIUB CO_2 analyzer to be 2.61 ppmv. The large range in deviations originates from ascent and descent phases of several flights during which both the PIUB and the LSCE NDIR analyzer recorded unnaturally high or low values due to measure artifacts such as prolonged warm-up times. There were two notable issues that were discovered and need to be addressed in the future to lower uncertainties in the CO_2 data.

4.2.1 Carbon dioxide offset

The first issue is a constant offset throughout a flight between the PIUB CO_2 data and the data by LSCE. This offset changed from flight to flight and amounted to roughly -7.18 to 0.98 ppmv. The PIUB determined mixing ratios were almost exclusively lower than the LSCE values, with only eight

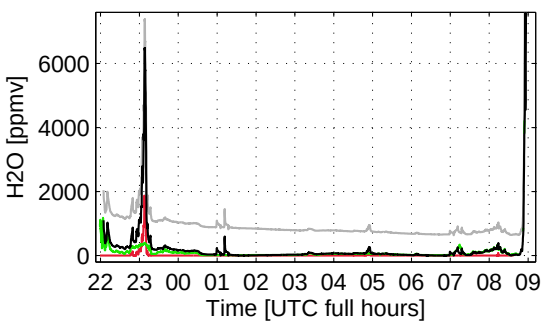

(a) H_2O mixing ratio comparison for flight 194 on 21.06.2007

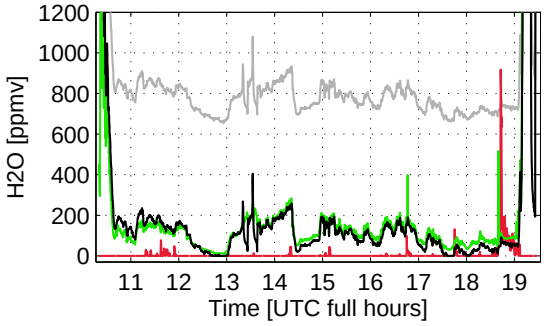

(b) H_2O mixing ratio comparison for flight 309 on 22.09.2010

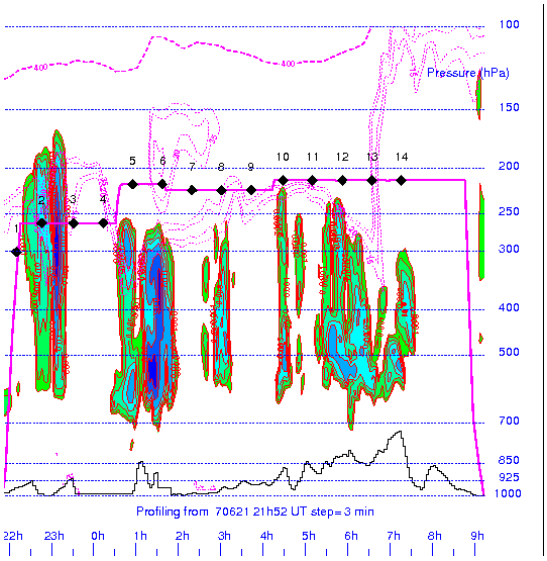

(c) Vertical cloud ice cross-section for flight 194

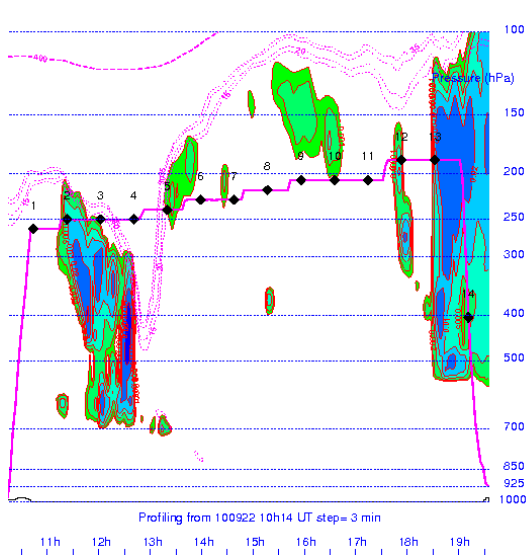

(d) Vertical cloud ice cross-section for flight 309

Figure 4.2 Comparison of the H_2O data obtained by the PIUB LI-6262 and data obtained by the dedicated laser photoacoustic analyzer by the IMK. The upper two panels show in-flight measurements of the H_2O mixing ratios for the flight 194 (a), and flight 309 (b). Gray, black, green and red represent uncorrected data obtained by the LI-6262, corrected data obtained by the LI-6262, gaseous H_2O data obtained by the laser photoacoustic device, and cloud H_2O data obtained by the laser photoacoustic device, respectively. A magnification of the peak in flight 194 is shown in figure 4.3. The bottom panels depict the presence of cloud ice contents in $kg\,m^{-3}$ for flight 194 (c) and flight 309 (d) derived from 6-hourly ECMWF model forecasts calculated by the KNMI. Potential temperature (quasi-horizontal blue dot-dashed), equivalent potential temperature (green dot-dashed), selected PV-values typical of the tropopause (purple dotted) and the 400 K isentrope (purple dashed) are indicated as well.

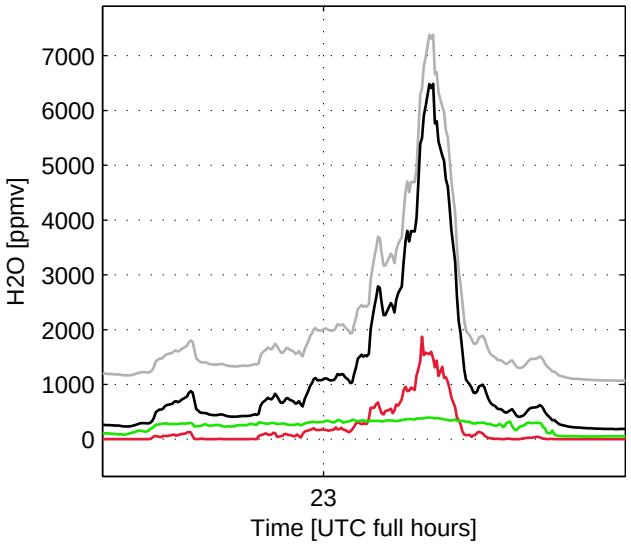

Figure 4.3 Magnified section of the H_2O comparison containing the ice cloud peak during flight 194. For explanation see figure 4.2.

flights showing higher mean values compared to the LSCE data. Short flights with missing calibrations proofed to be problematic. In figure 4.6, six out of the seven most negative and the three most positive offsets were recorded on short flights.

4.2.2 Visible cycling in carbon dioxide

The second problem that was encountered concerned the visible switching between the configurations. Sometimes this cycling behavior persisted over entire flights, sometimes it appeared towards the end. The issue was observed for about one third of all flights to various extent up to approximately 4 ppmv (figure 4.7a). For example, for flight 194 the cycling could be attributed to a failure in the regulation of the reference cell pressure. Flight 417 also showed significantly different CO_2 values for the A and D configurations due to inlet pressure drops. Persistent cycling behavior was observed starting in February 2011 until August 2012, affecting flights 331 through 389. In the beginning of 2012 all the flights suffered from increasingly strong jumps in CO_2 as well as in H_2O up to flight 389 when the inlet pump was replaced after breaking down during flight 387. This is also visible as the incremental standard deviation between flight 373 and 387 in figure 4.6. Both CO_2 and H_2O raw data had elevated voltages when configuration D was active. As this problem vanished when the defective pump was replaced, one would expect the inlet pressure to be the reason, but as figure 4.7b shows, none of the parameters that are logged were able to explain the observed cycles. Figure 4.7b also reveals that the inlet pressure during the configurations E and F however, when the NDIR analyzer is calibrated, drops by 150 hPa to 180 hPa in this case. Inlet pressure was lower during calibrations for all flights,

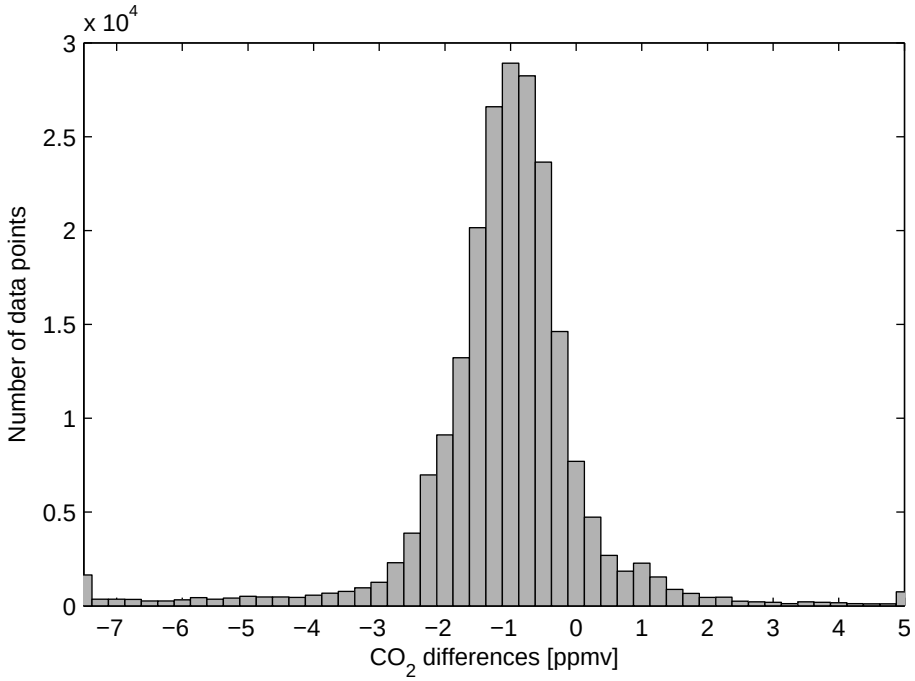

Figure 4.4 Histogram of the differences between the LSCE and the PIUB CO_2 measurements (PIUB - LSCE) over all flights where LSCE data was available.

but to variable extent.

4.3 Oxygen measurements

Figure 4.8 shows a plot of all the O_2 data collected between 2007 and 2013, regardless of the position on the globe plotted against time. Whereas the span of the fuel cells is calculated using the HS and LS gases, the offset is determined with the WG. Thus, by shifting the offset so it matches the assigned WG O_2 value, the assigned HS and LS values did not necessarily agree with the measured values if the relationship was not exactly linear. The mean difference from the assigned calibration values of 22.8 per meg and its standard deviation of 219.2 per meg was used to estimate the accuracy in the O_2 measurements to 242 per meg. Variations that were observed during flights were of several hundred per meg, far larger than expected. Fuel cells, in the way they are employed in this setup, do not seem to be able to resolve natural variations in air properly. From flight 190 in May 2007 to flight 297 in June 2010 the data shows a decrease in the $\delta(O_2/N_2)$ data in accordance with the expectations, albeit with a too steep trend. Other studies have found a trend in O_2/N_2 of around -20 per meg/yr (Ishidoya et al., 2006, 2012; Laan-Luijkx et al., 2010b). One would expect the ratios to lie between -350 per meg and -600 per meg for the past six years (Laan-Luijkx et al., 2010b). Hence, it looks like the first phase up to the revision is displaced towards lower ratios, whereas after the revision the values are too high. An unlikely increase in the ratio in mid-2010 coincided with the

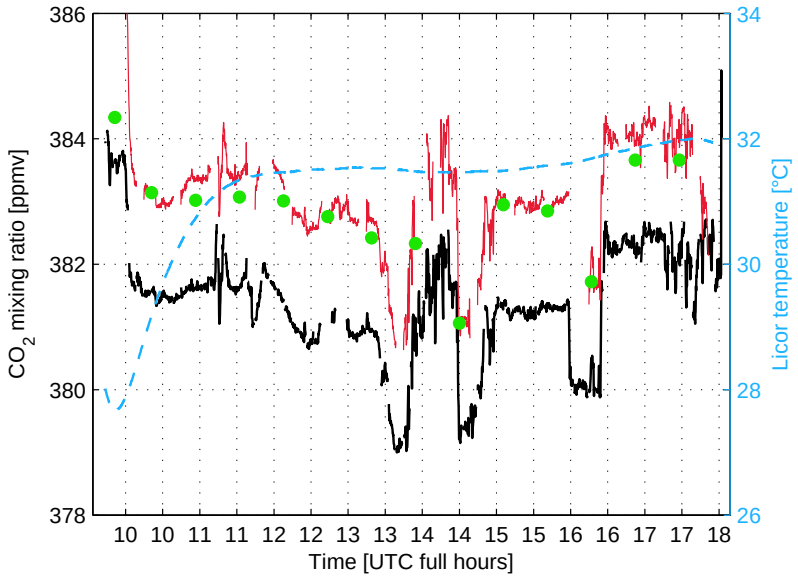

(a) Flight 252 from Frankfurt to Chennai, India on 15.10.2008

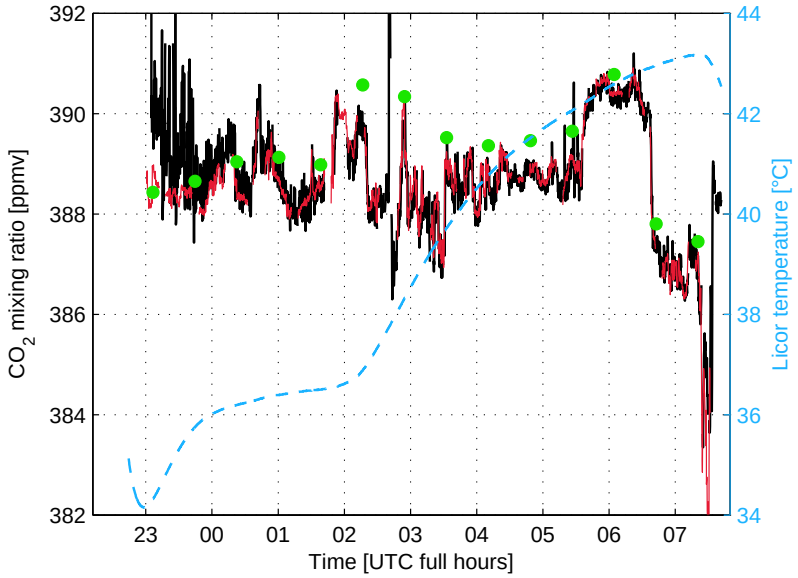

(b) Flight 302 from Caracas, Venezuela to Frankfurt on 27.07.2010

Figure 4.5 Comparison of CO_2 data obtained by the in-situ analyzers and the flask measurements for two example flights. Figure (a) shows data comparison for the flight 252 from Frankfurt to Chennai, India on 15.10.2008, figure (b) for the flight 302 from Caracas, Venezuela to Frankfurt on 27.07.2010. The black line (PIUB data), red line (LSCE data) and green dots (MPI flask data) use the left y-axis. Licor temperature is also plotted in a blue dashed line and uses the right y-axis.

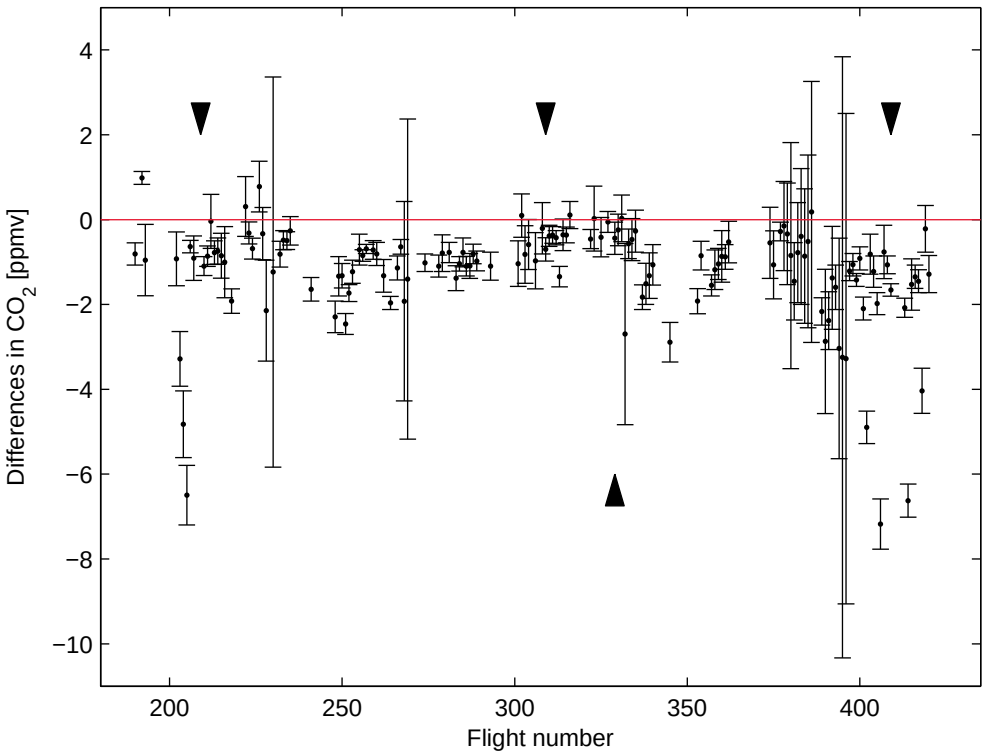

Figure 4.6 Differences (PIUB - LSCE) in the CO_2 data for each flight in chronological order of the flights. The error bars indicate the standard deviation for that flight, the red line indicates agreement between the data sets. Black arrows mark the points when the HS gases (top) and the LS gas (bottom) were exchanged (see appendix D for values).

project revision at the end of 2009. The increase is consistently observed for all fuel cells. In 2011, a similar decrease rate is observed as in the phase prior to the inlet switch. One can also see that for large parts fuel cells did not yield any data, which holds especially true for fuel cells 3 and 4. This happened when the fuel cell raw signal amplification was not adjusted correctly for the voltages to fall into the ADC range of 0 V to 10 V. Measured $\delta(O_2/N_2)$ values for flights are presented in section 4.4. In virtue of the large spread present even in the 12 min-resolved O_2 data, I decided to only plot the averaged low resolution data.

4.4 Example flights

In the following, O_2 and CO_2 data is reported against UTC time and described for example flights, during which the PIUB unit worked as expected and there was good agreement with the CO_2 data obtained by the LSCE, or there was a constant offset without cycling or drift behavior. Additional information such as the flight trajectories, potential vorticity, altitude, carbon monoxide concentrations

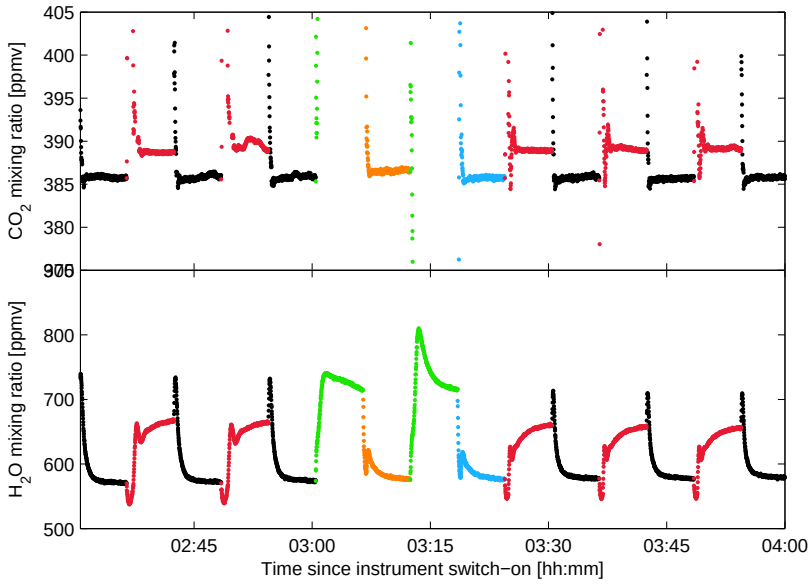

(a) NDIR data for flight 385

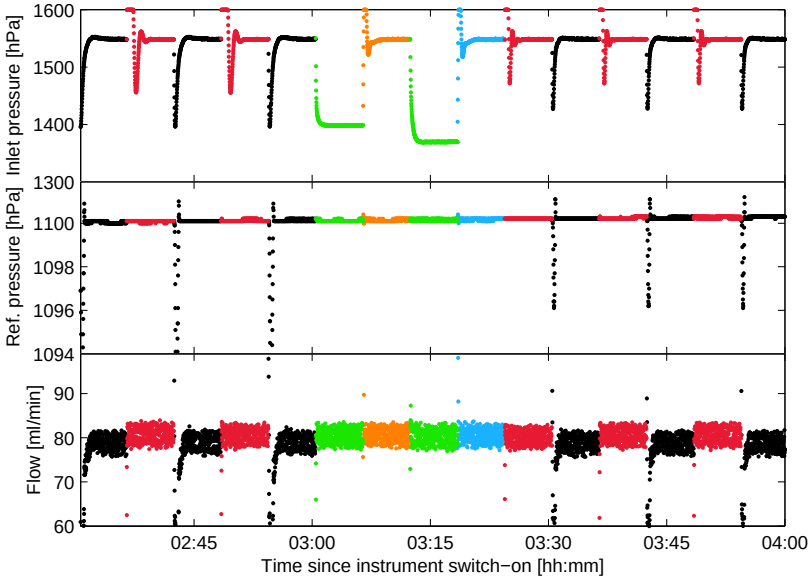

(b) Parameters for flight 385

Figure 4.7 1.5 h extract of NDIR data (a) and measured parameters (b) for flight 385 showing distinctly elevated values in CO_2 and H_2O during the D mode. Black, red, orange, blue and green dots represent the modes A, D, B, C and both modes E and F, respectively. For the CO_2 values, the leveled off HS and LS values for modes E and F are not visible because they fall outside of the range of the graph.

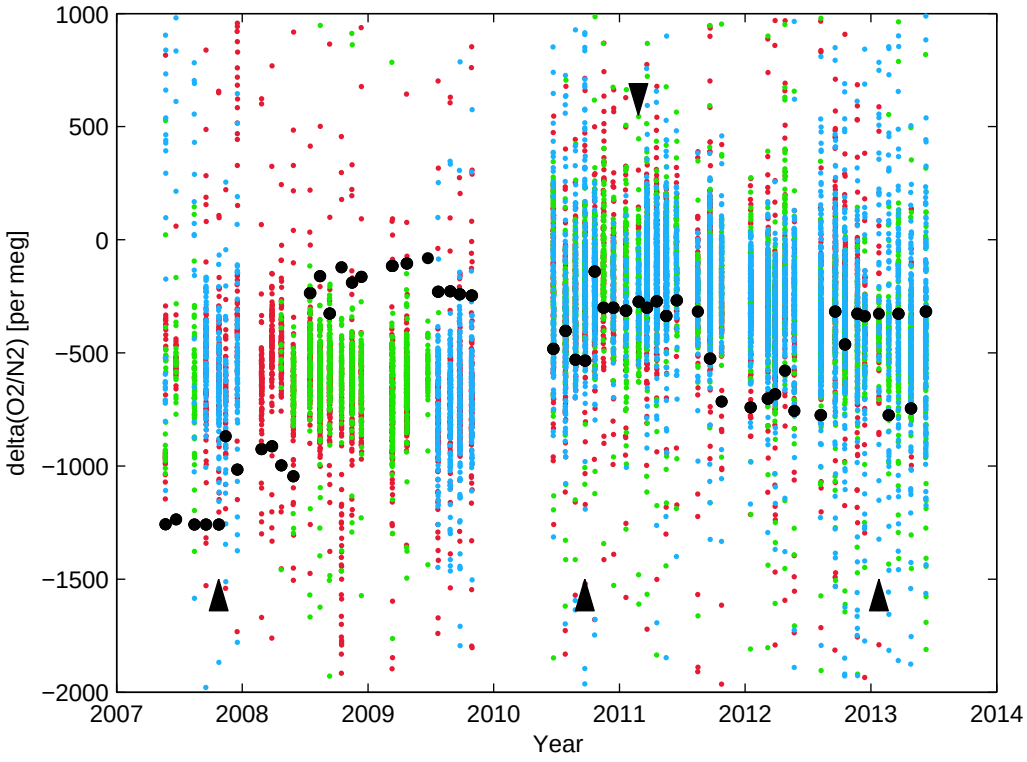

Figure 4.8 All the 12 min-resolved O_2 data points from flight 190 to flight 432. Red, green and blue dots respectively indicate measurements by fuel cell 1, 3 and 4. Also plotted in black dots are the assigned $\delta(O_2/N_2)$ values of the WG used in the flights on the SIO O_2/N_2 scale. Black arrows mark the points when the HS gas (top) and the LS gases (bottom) were exchanged (see appendix D for values). The data gap between the end of 2009 and mid-2010 is when the revision after flight 294 was undertaken and the inlet position changed from front-facing to perpendicular to flight direction.

monitored by the MPI (see Scharffe et al. (2012)) and ECMWF-generated 5-day backward trajectories of air masses are included to help with the interpretation of the data. The flight trajectory plots show the aircraft's position provided by the ARINC data, where red points stand for data collected in the troposphere, blue points for stratospheric data derived from O_3 height profiles, and the numbers next to black dots indicate the full hours in UTC on the day of departure. In the data plots the altitude is plotted in the uppermost panel in black, and the potential vorticity as calculated from wind and temperature fields by ECMWF in red. CO can be used as a tracer for the terrestrial surface processes of biomass burning and fossil fuel combustion (Matsueda et al., 2002a) and is plotted in the middle panel. The lowermost panel shows the PIUB data, where a black line is used for CO_2 data by the NDIR and the red, green and blue dots represent O_2 data measured by the fuel cells 1, 3 and 4, respectively. The data plots are set up in a way such that the dotted vertical lines correspond to the position of the aircraft at the black dots on the associated flight trajectory plot. In the ECMWF backward

trajectory plots, black dots represent the flight path, and the different pressure levels are indicated by the colors dark blue (< 200 hPa), light blue (201 hPa to 250 hPa), green (251 hPa to 300 hPa), olive (301 hPa to 400 hPa), orange (401 hPa to 500 hPa), red (501 hPa to 850 hPa) and purple (> 850 hPa).

On December 17, 2007 the CARIBIC equipment was aboard flight 218 from Frankfurt, Germany to Denver, USA. PIUB CO_2 data were lower than the LSCE CO_2 data by 1.92 ± 0.29 ppmv. However, agreement to the MPI flask measurements was better (-0.95 ± 0.19 ppmv) and otherwise matched the variations detected by the LSCE NDIR nicely. No CO data was available. This flight is interesting in that it featured a sharp-edged period between 16:30 and 22:30 (corresponding to a longitude of 33° W and 100° W) in which the sampled air was of stratospheric nature with values greater than 6 PVU. This feature was explicitly mirrored in the CO_2 data. Even the local increase in potential vorticity over Scotland seemed to result in a decrease in CO_2 levels by about 1.5 ppmv. The difference in CO_2 mixing ratios between the upper troposphere and the lowermost stratosphere in this case of northern hemisphere summer was around 3 ppmv. This is in accordance with the theory that air encountered in the winter stratosphere is older and hence preserves the lower CO_2 mixing ratios of the previous summer caused by the seasonal cycle (Boenisch et al., 2009; Hoor et al., 2004). Another noticeable property is that larger variations in the mixing ratio in the order of 2 ppmv were associated with tropospheric measurements, while variations in the stratosphere were limited to about 0.5 ppmv. 5-day back trajectories by the ECMWF (figure 4.10) show how tropospheric air tends to stay in the troposphere. As soon as the tropopause is crossed at 16:30, air masses stem from vastly different regions and higher altitudes (figure 4.10b). Fuel cell 3 was out of range during this flight and fuel cell 4 was clipping for the initial 2.5 h of this flight as well. Fuel cells 1 and 4 did not seem to correlate with each other or exhibit features like in CO_2 and scattered between -100 per meg to -700 per meg, which is unlikely to represent natural variations in the atmosphere. Both fuel cells display outliers.

CARIBIC flight 266 with destination Caracas, Venezuela took off in Frankfurt on April 22, 2009. The CO_2 mixing ratios registered by the PIUB device were 1.13 ± 0.20 ppmv lower compared to the LSCE values. This flight shows the same prominent feature of enriched CO_2 in the troposphere compared to the stratosphere as flight 218. In this case the difference is even more pronounced at 5.5 ppmv which can be understood as a consequence of the seasonal cycle in the troposphere being at its peak in April with the highest mixing ratios in the northern hemisphere. Tropospheric air sampled around 50° N before 12:00 showed higher mixing ratios than the values recorded in the troposphere after 15:30, south of 35° N, which was attributed to the amplitude of the seasonal cycle at higher latitudes being larger than at lower latitudes (NOAA, 2012). In general, CO_2 varied inversely with potential vorticity, as expected in spring, and showed a visible positive correlation with CO. The trajectories suggest that the encountered air masses on flight 266 were dominantly transported by westerly winds from higher altitude levels, which implies that the sampled air was representative for background air. Fuel cell 4 did not record any values because they lay outside of the range. The

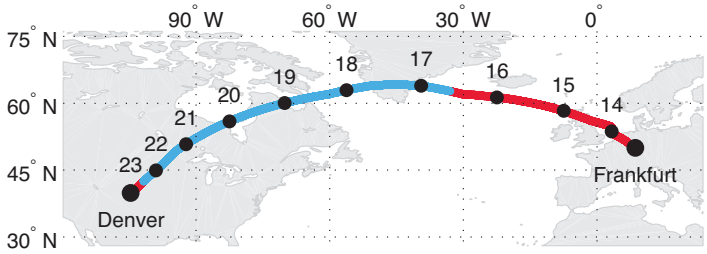

(a) Flight trajectory

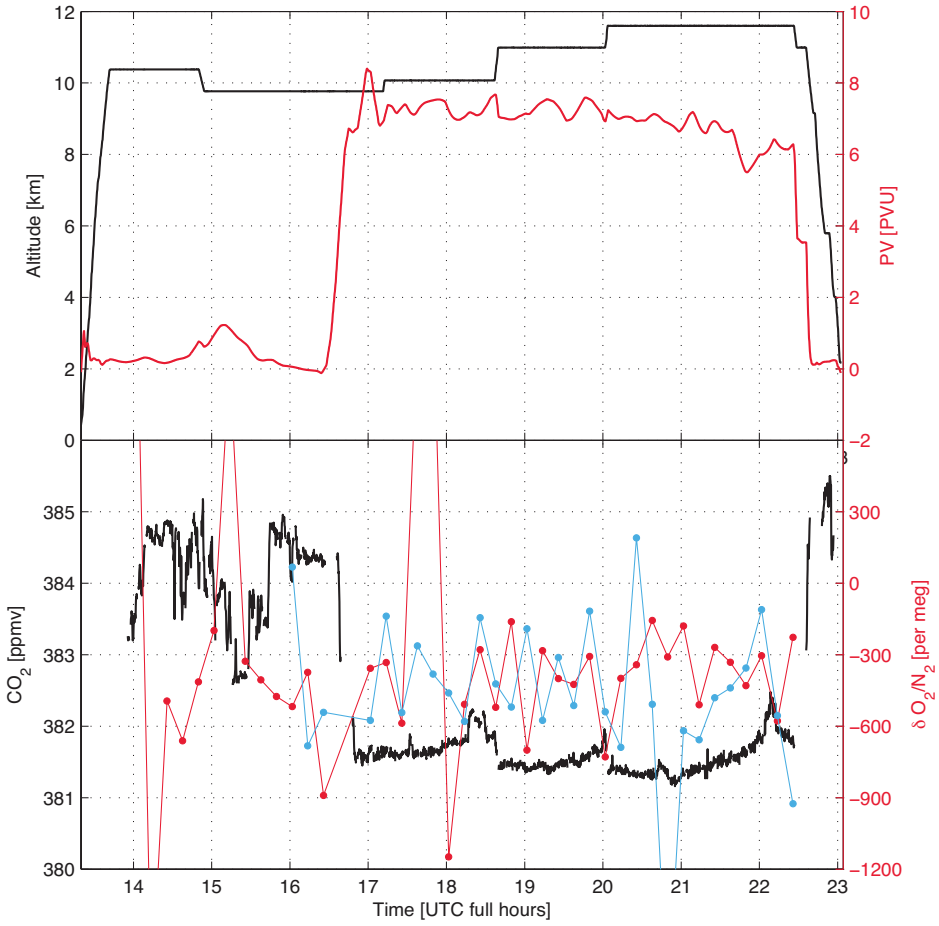

(b) Data

Figure 4.9 Measurements for flight 218 from Frankfurt to Denver on 17.12.2007.

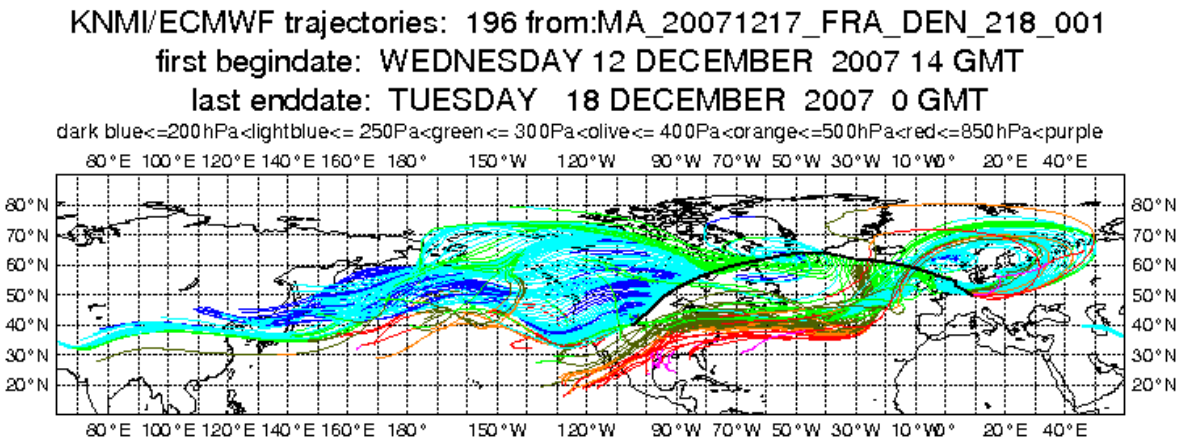

(a) 5-day back trajectories for the entire flight

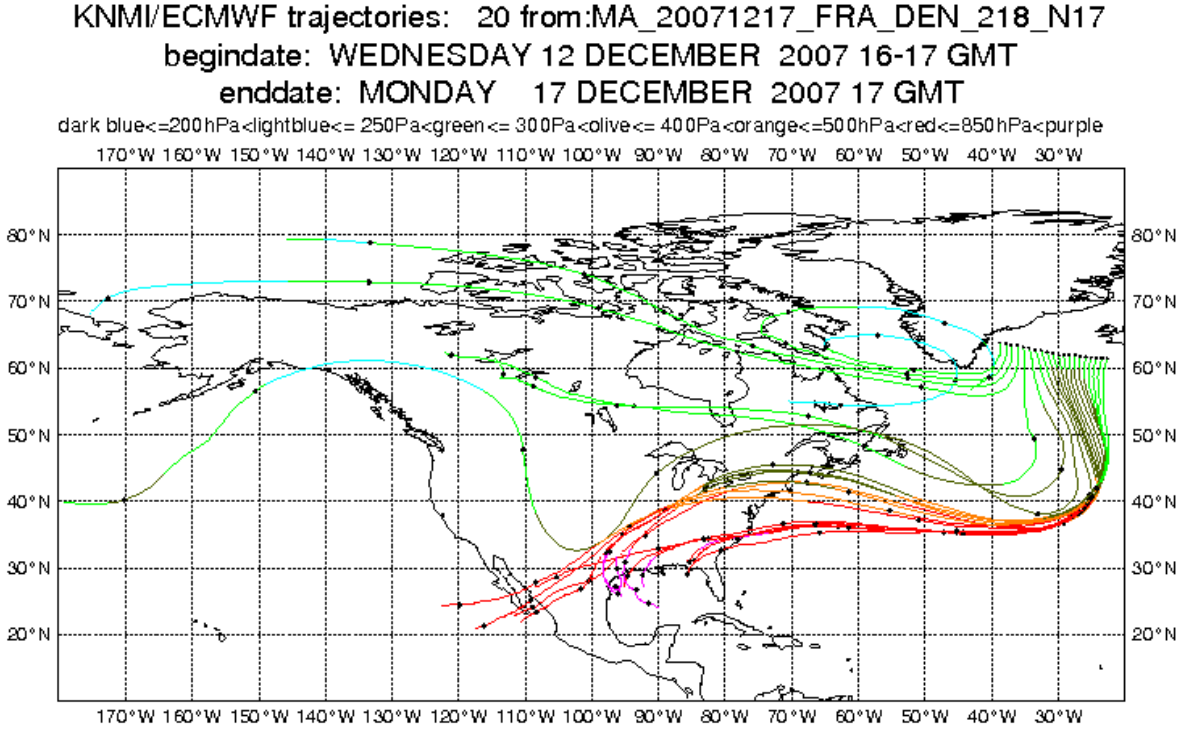

(b) 5-day back trajectories 16:00–17:00

Figure 4.10 Additional plots for interpretation of the data collected during flight 218 from Frankfurt to Denver on 17.12.2007.

other two fuel cells did not reveal any anti-correlation with CO_2 and varied strongly in the beginning. Towards the end, fuel cell 1 and 3 behaved synchronously but it remains questionable if this was a real signal in O_2 or caused by variations in temperature or pressure.

Figure 4.13 shows data collected aboard a flight from Frankfurt to Vancouver, Canada on July 23, 2009, which showed a discrepancy to the LSCE data of -0.88 ± 0.23 ppmv. This flight covered the northernmost route in the CARIBIC project and was therefore characterized by stratospheric influence. Stratospheric CO_2 values amounted to 385 ppmv, clearly higher than for the flights 218 and 266 owing to the secular increase caused by fossil fuel burning over the years and a superimposed seasonal cycle. CO_2 mixing ratios should be higher in the stratosphere compared to the troposphere in the summer in the northern high latitudes (Machida et al., 2002): The lowermost stratosphere contains air that has been transported across the tropopause before, still carrying the elevated CO_2 load of spring, so that high potential vorticity now coincides with elevated CO_2 mixing ratios, while this was reversed in winter (figure 4.11b)(Schuck et al., 2009). In the case of flight 280 this was observed in the troposphere over Greenland and Nunavut, Canada. The drop over Greenland however stands out with extremely low CO_2 values with a difference to the stratospheric values of about 12 ppmv. The same decrease was also observed by the LSCE. Surface data from the Earth System Research Laboratory (ESRL) global network reveals monthly CO_2 averages at Summit, Greenland (73° N, 38° W, 3216 m above sea level) to reach down to 382.5 ppmv and 378.3 ppmv in July and August, respectively. The values that were recorded by the NDIR analyzer were still substantially lower than the expected background concentration for summer. Wada et al. (2007) also reported of extremely low CO_2 events in summer with values lower than up to 8 ppmv at Minamitorishima Island in the northwestern Pacific Ocean. They concluded that low-CO_2 air masses were formed by an active uptake of CO_2 by the terrestrial biosphere over sink regions. Such a reasoning should theoretically be verifiable in this case using O_2/N_2 data, since a decrease of CO_2 of 12 ppmv should correspond to an increase in $\delta(O_2/N_2)$ of about 60 per meg. However, even such a strong change in CO_2 is not reflected in the oxygen data, which shows large variations between -1100 per meg to -500 per meg. As Greenland does not have much vegetation it is supposed that the drop in CO_2 is not due to a local influence, but rather likewise driven by rapid long-range transport of continental air masses associated with active biospheric uptake in the summer season. Figure 4.14b in fact depicts the passage of these low CO_2 air masses over the heavily forested CO_2-sink areas in northwestern Russia.

On July 27, 2010 the CARIBIC container was aboard flight 302 from Caracas, Venezuela to Frankfurt, Germany (figure 4.15). During the 9 h flight, the NDIR analyzer registered CO_2 mixing ratios around 389 ppmv, which was in agreement with the LSCE data (mean difference 0.10 ± 0.51 ppmv). The large variability in CO_2 at the beginning of the flight were not detected by the LSCE (figure 4.5b) and can be explained by the pump in the PIUB system not being able to maintain a constant pressure. Another feature that is imprinted by the inlet pressure is the peak at 02:40. The ascent performed

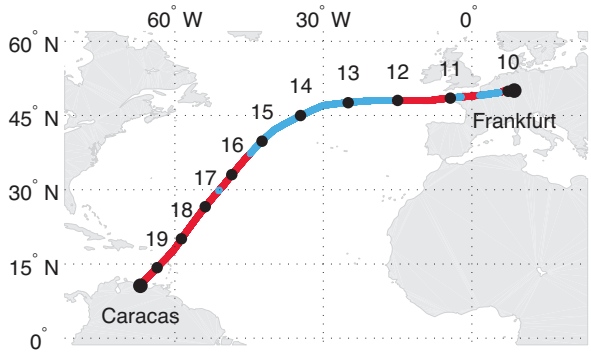

(a) Flight trajectory

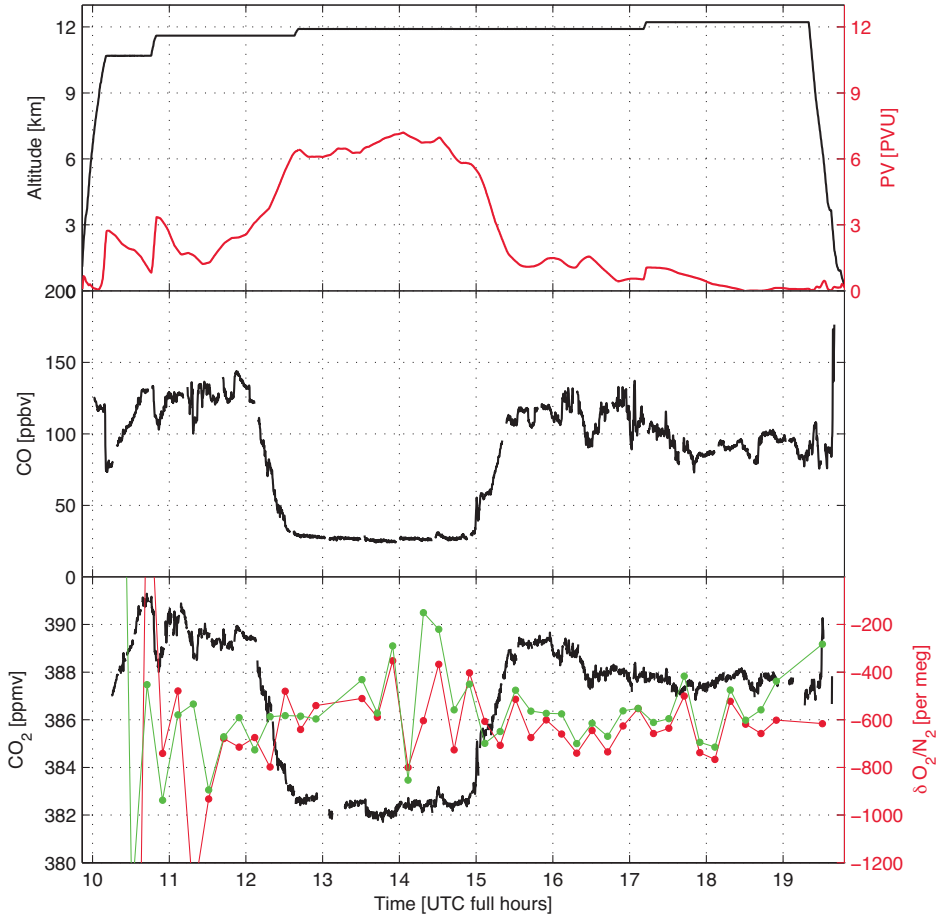

(b) Data

Figure 4.11 Measurements for flight 266 from Frankfurt to Caracas on 22.04.2009.

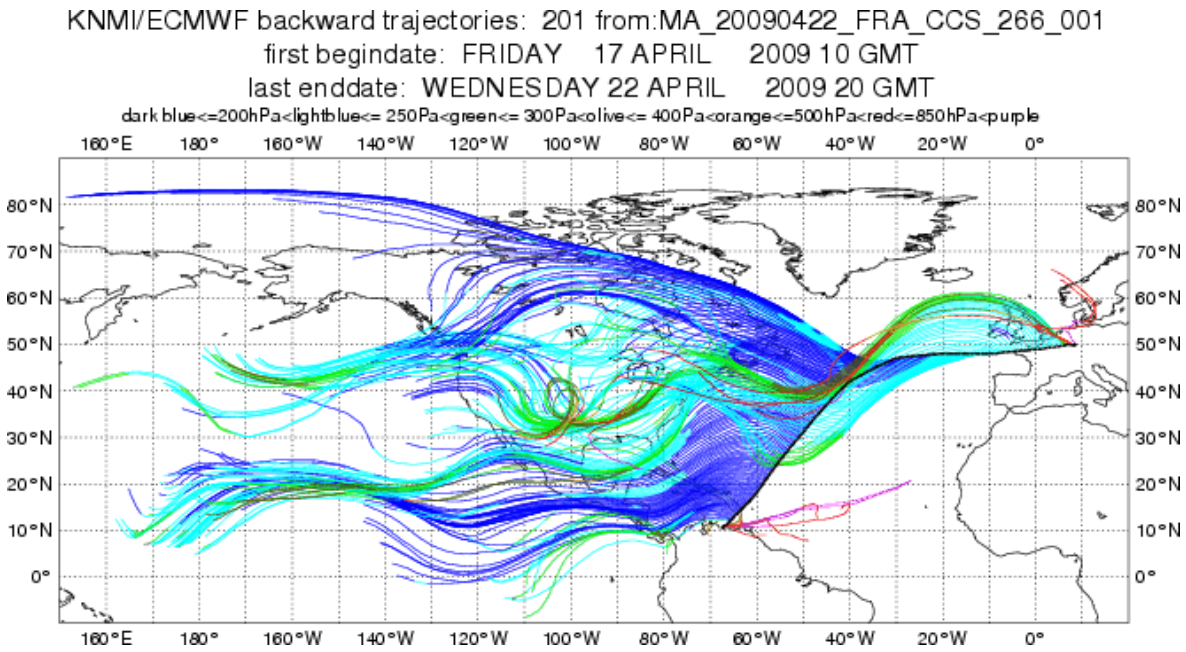

Figure 4.12 5-day back trajectories for the entire flight 266 from Frankfurt to Caracas on 22.04.2009.

by the aircraft at that time was enough to trigger a dip in inlet pressure for about 1 min. Counter-intuitively, this lead to a rise in CO_2 up to 396 ppmv, as well as a distinct increase in all the fuel cells since it occurred during the last minute of an A configuration, which is in accordance with the expectations. Towards the end, O_2 values were excluded because the box temperature began to increase by 1 °C. Apparently, the aircraft received power via the Base Power Supply half an hour prior to take-off at Caracas airport, as visible in the altitude plot. Therefore, the enclosure hosting the O_2 analyzer was allowed to start warming up earlier on, reaching 48 °C faster, which benefited the fuel cell measurements. Nonetheless, the $\delta(O_2/N_2)$ still exhibits large variations, particularly in the first two hours of the flight. Until 05:00, CO_2 measurements suggest that the sampled air is representative for tropospheric background air for the northern hemisphere summer. This is also reflected in the back trajectories showing that only the start and beginning of flight 302 were largely in contact with the surface. The step-like increase in CO_2 at 05:30 can be explained with the crossing of the tropopause after which air originates from a different area over the Pacific (figure 4.16b).

Flight 330 depicted in figure 4.17 was from Cape Town, South Africa to Frankfurt, Germany and took place on February 25, 2011. For this particular flight the mean deviation to the LSCE device was -0.25 ± 0.37 ppmv. Due to Frankfurt and Cape Town being located in a similar degree of longitude on the north and south hemisphere, flight 330 represents an example of meridional O_2 and CO_2 distributions. CO_2 for this flight varied between 379 ppmv to 397 ppmv and exhibited lower values in the southern hemisphere compared to the northern hemisphere. There were two maxima in

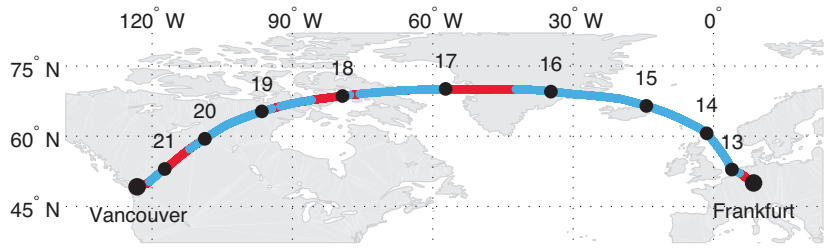

(a) Flight trajectory

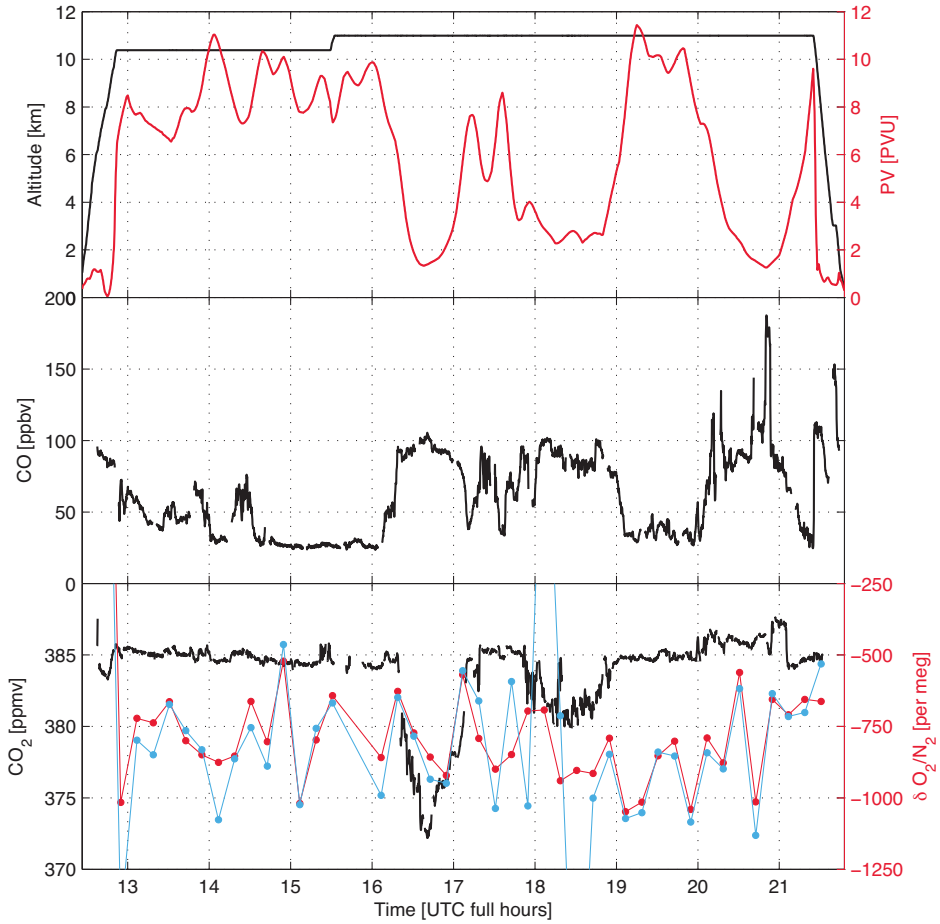

(b) Data

Figure 4.13 Measurements for flight 280 on 23.07.2009 from Frankfurt to Vancouver.

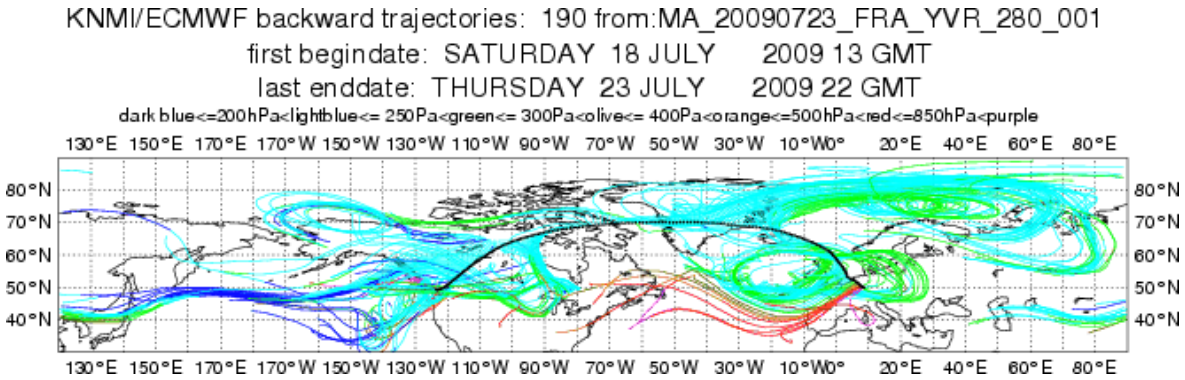

(a) 5-day back trajectories for the entire flight

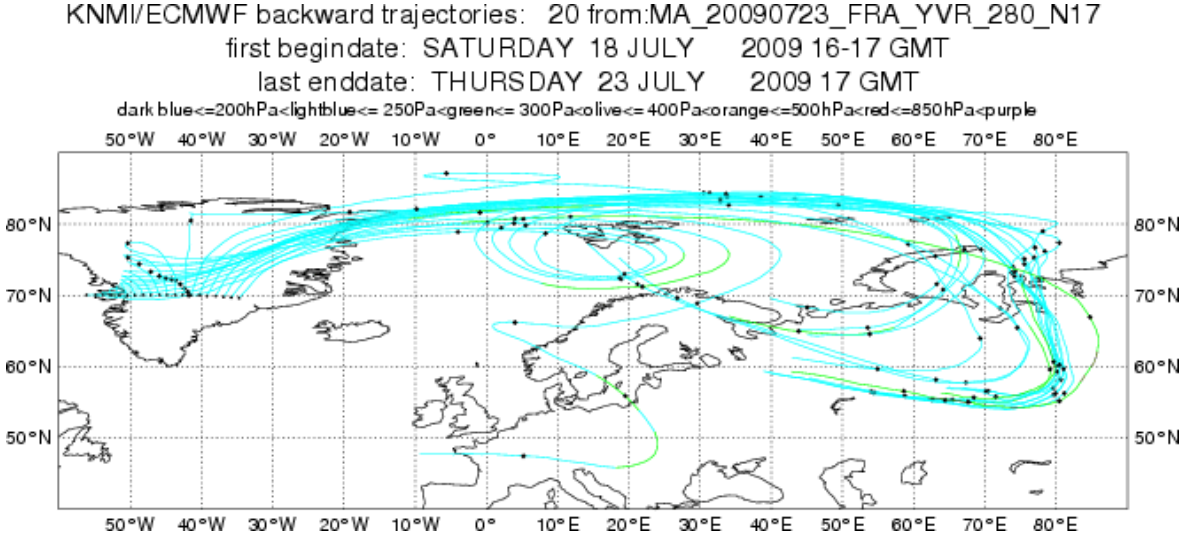

(b) 5-day back trajectories, 16:00–17:00

Figure 4.14 Additional plots for interpretation of the data collected during flight 280 from Frankfurt to Vancouver on 23.07.2009.

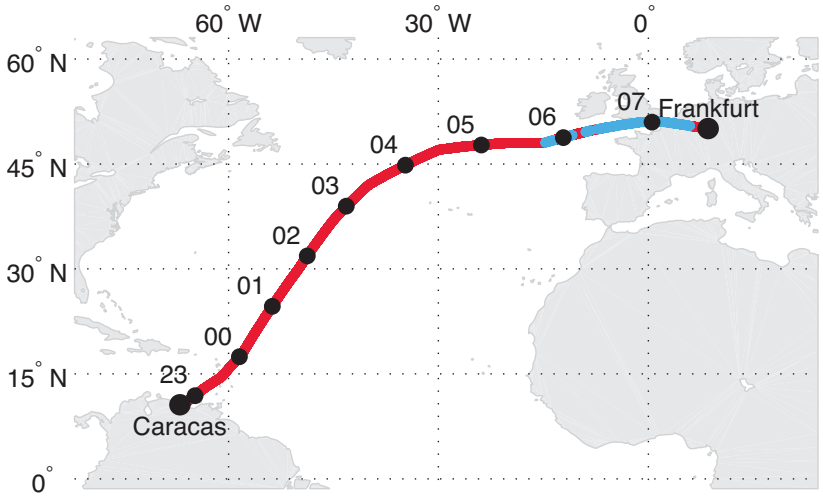

(a) Flight trajectory

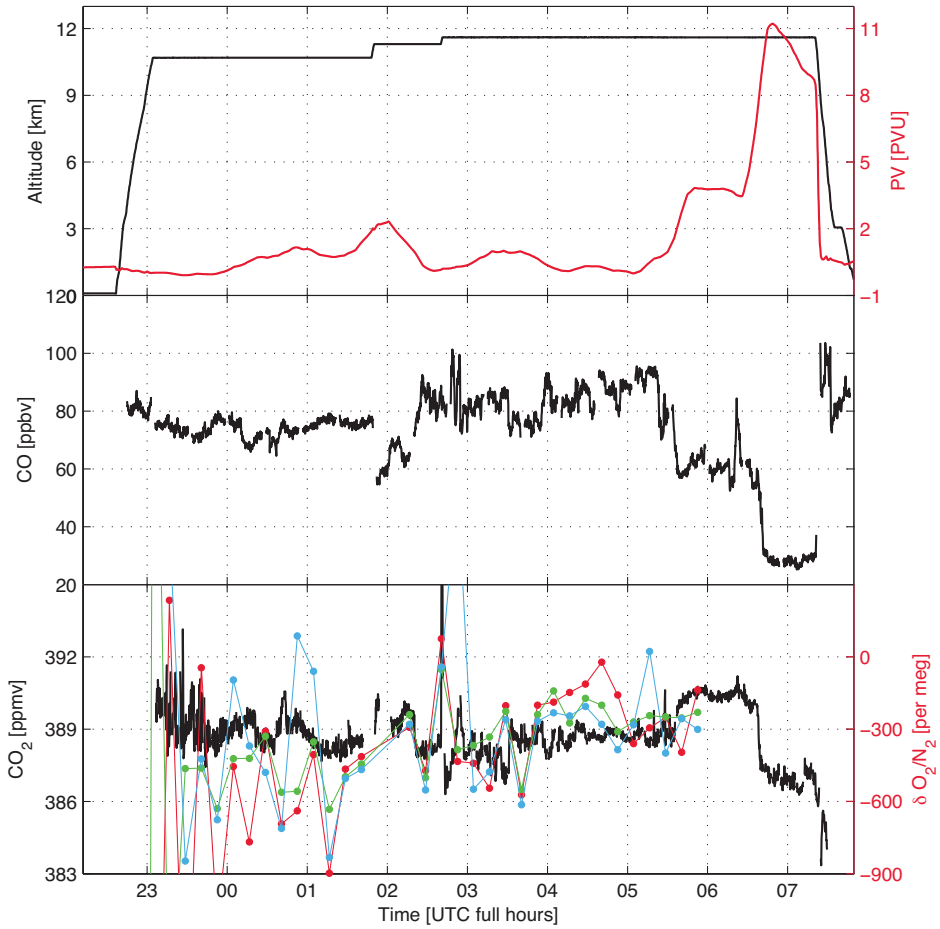

(b) Data

Figure 4.15 Measurements for flight 302 from Caracas to Frankfurt on 27.07.2010.

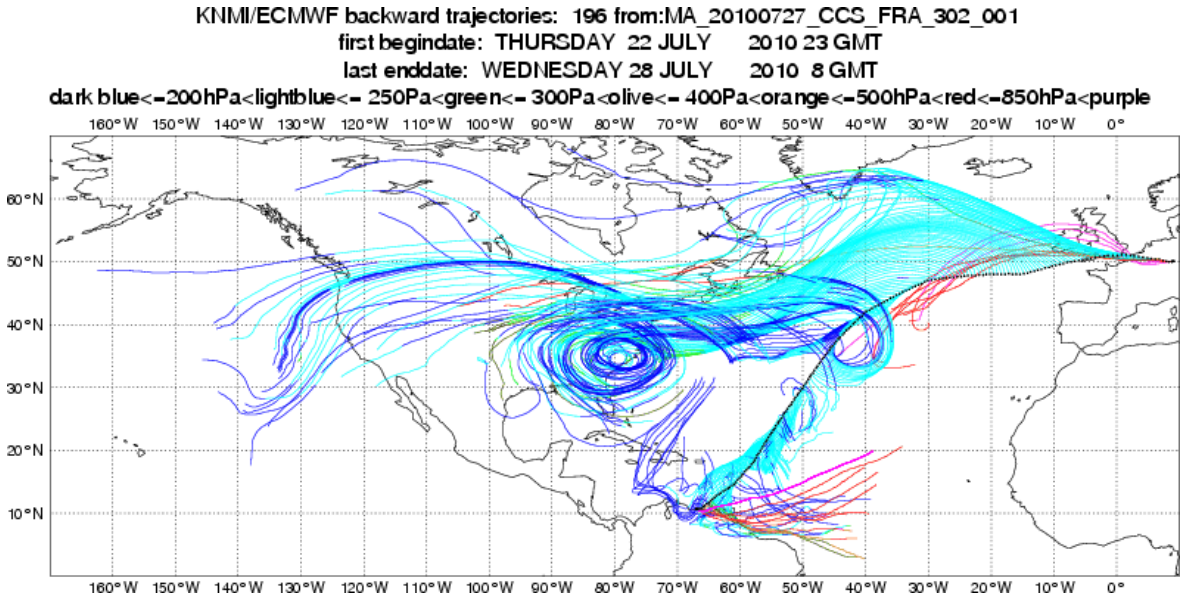

(a) 5-day back trajectories for the entire flight

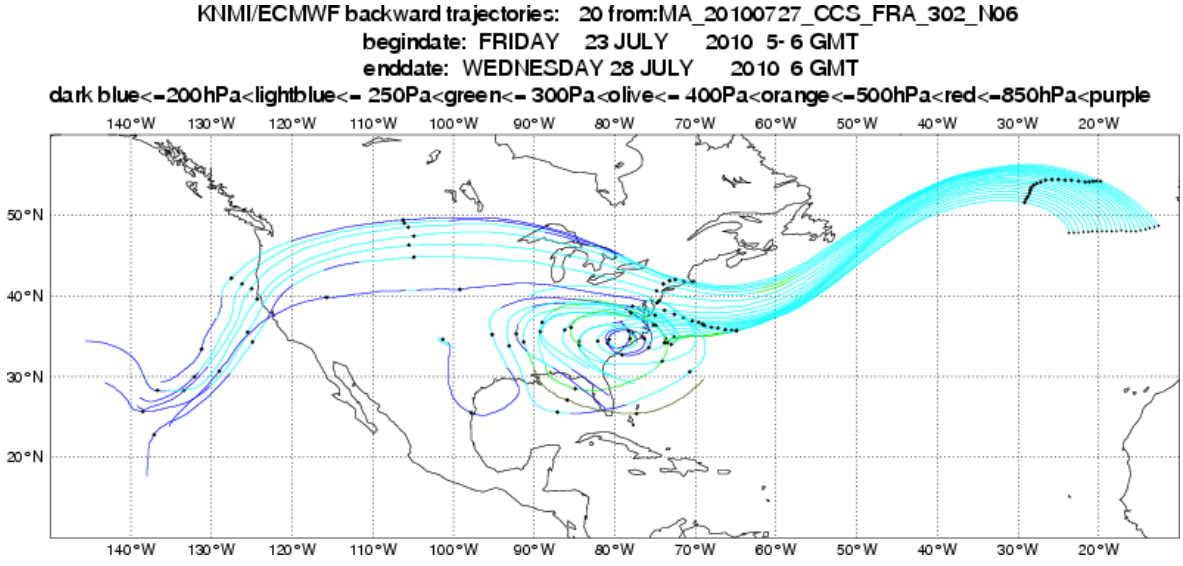

(b) 5-day back trajectories, 05:00–06:00

Figure 4.16 Additional plots for interpretation of the data of flight 302 from Caracas to Frankfurt on 27.07.2010.

CO_2, one at the equator and one close to Frankfurt. When the aircraft crossed the tropopause into the stratosphere at around 01:00, the CO_2 mixing ratios decreased by about 3 ppmv and increased again substantially when potential vorticity weakened towards the end. CO values were strongly elevated after passing the equator into the northern hemisphere. The CO curve shows a very similar shape as the CO_2 curve and even some small-scale structures such as the local peaks between 22:00 and 23:00 and around 02:00, suggesting that flight 330 was largely influenced by biomass burning and anthropogenic emissions. 5-day backward trajectories by ECMWF visualize that the air masses sampled before midnight when the maxima occurred were transported to the cruising altitude from much lower altitudes in the East. The ITCZ is still located just south of the equator in February in Africa, with the areas north of it experiencing very little precipitation and hence being prone to wildfires. Satellite observations using Moderate-Resolution Imaging Spectroradiometer (MODIS) in figure 4.18b further consolidates the idea that the air masses intercepted around the equator had recently been in contact with burning biomass. O_2 data shows large variability in the range of −600 per meg to 100 per meg. For any measurement, the three fuel cells matched each other only to about 100 per meg. The general picture suggests that the fuel cells agreed on the sign of changes, which could however also be attributed to pressure or temperature changes to which all fuel cells were subjected equally.

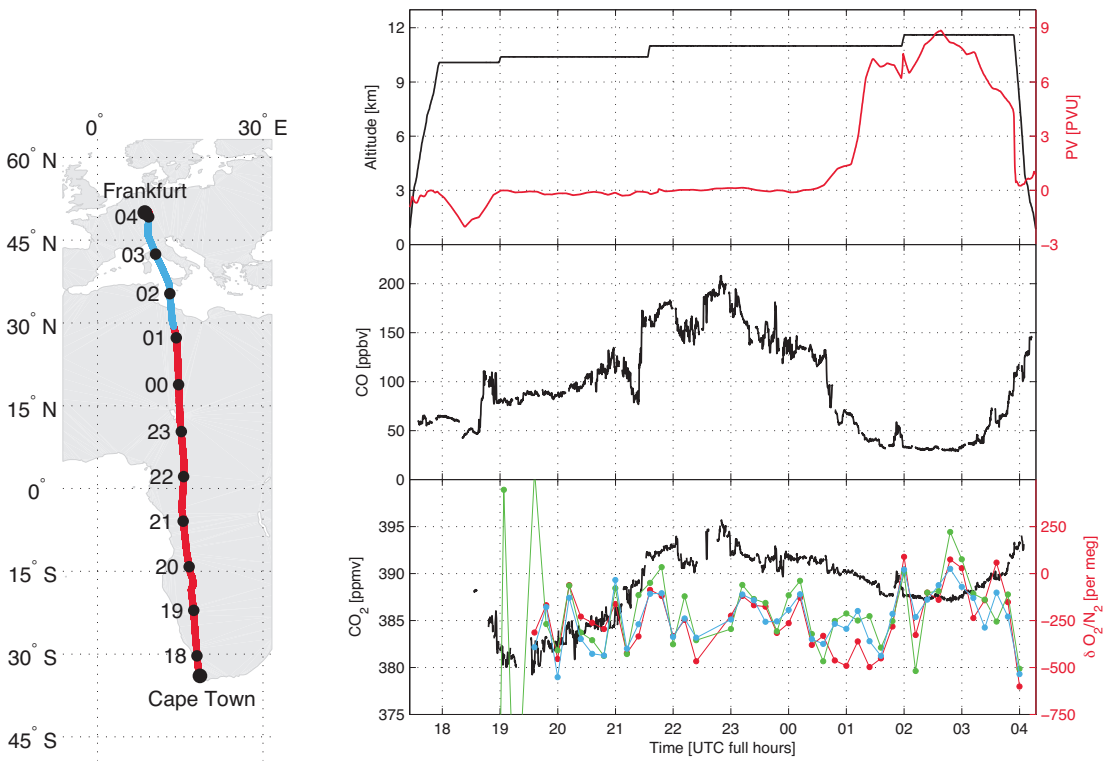

(a) Flight trajectory **(b)** Data

Figure 4.17 Measurements for flight 330 from Cape Town to Frankfurt on 25.02.2011.

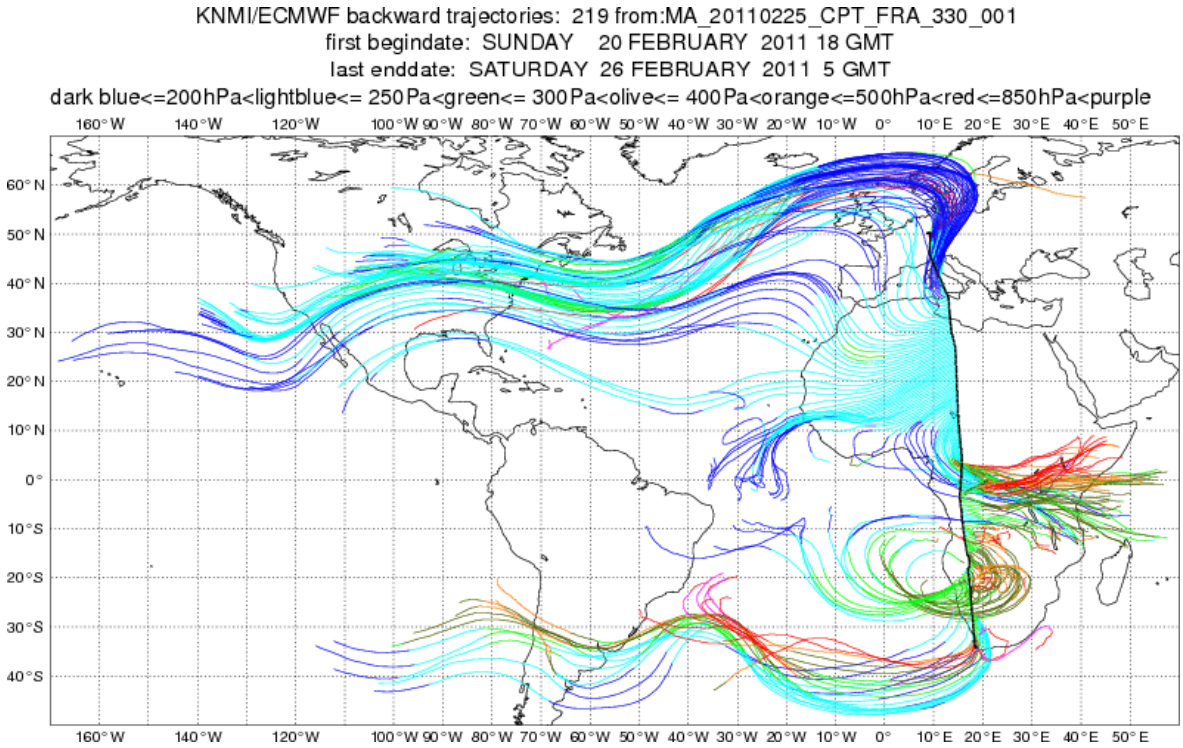

(a) 5-day back trajectories for the entire flight

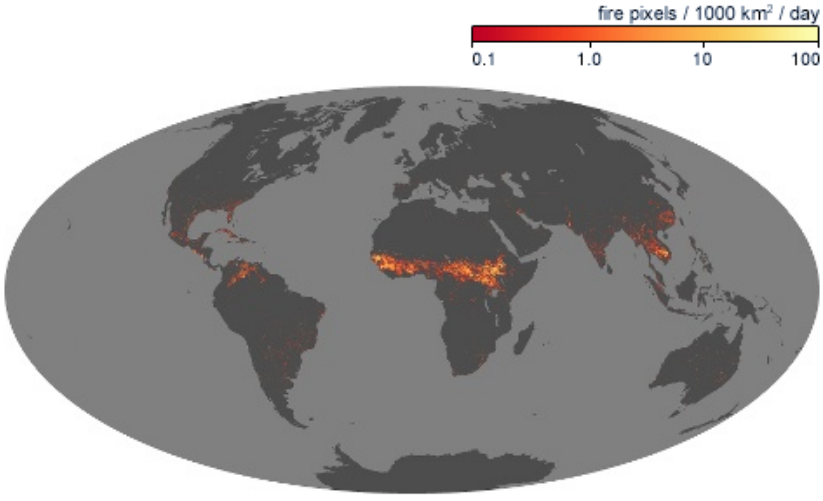

(b) Fire map for February 2011. Figure from NASA (2013).

Figure 4.18 Additional plots for interpretation of the data collected during flight 330 from Cape Town to Frankfurt on 25.02.2011. (b) is a fire map showing the locations of actively burning fires for February 2011 based on MODIS observations on NASA's Terra satellite. The colors indicate numbers of fires observed within a 1000 km^2 area (NASA, 2013).

Chapter 5

Discussion

The amount of usable, accurate data collected by the PIUB measurement unit is lower than expected. In the light of the large uncertainties, many applications of O_2 and CO_2 data sets are rendered unfeasible. Due to several issues leading to inaccurate CO_2 measurements, the PIUB data set should at this point only be jointly used with the LSCE or flask data to assess the goodness. Based on the offsets variable with time, the present calibration procedure is questioned. With that in mind, the present data can provide insightful "snapshots" of the atmosphere and highlight structures. Individual in-flight measurements of CO_2 exhibited variations linked to whether the air sampled was of tropospheric or stratospheric nature, transport of air masses carrying different CO_2 loadings and to geographic location of the aircraft capturing latitude dependent seasonalities. The ratio in O_2/N_2 on the other hand revealed too much noise to be interpreted. Variable offsets render the data inappropriate for inter-flight comparisons and long-term analysis of the CO_2 evolution. According to Valentino (2007), constant conditions could be achieved in laboratory tests and the required precision in both O_2 and CO_2 could be obtained. The harsh and changing environment which the measurement unit is subjected to during flights however, introduced several challenges. The main problems that were encountered include short-term drift in the fuel cells, a temperature dependence, cycling associated with the switching of configurations, as well as inconstant inlet pressures during the calibrations. Tracking the causes is very challenging, particularly because the O_2 and CO_2 measurement unit is situated in Mainz, Germany and is obliged to be aboard every CARIBIC flight, limiting the time window for maintenance work to three weeks.

5.1 Issues in carbon dioxide data

Despite the quoted LI-6262 temperature range of 0 °C to 50 °C, the experienced temperatures of up to 50 °C within the unit might be too high for the LI-6262 to efficiently cool the detector with the

mounted peltier elements (LI-COR, 1996; Valentino, 2007). It is not expected that the averaged temperature correction is responsible for an offset, because the temperature correction is applied to the raw data including the calibration gases. Since by definition the use of calibration gases defines the absolute position of the sample gas values, any corrections applied prior to calibration should not affect the overall offset as defined through the calibration. This concept applies, if the entire range of CO_2 concentrations between HS and LS is equally influenced by changes in temperature, which was assumed. However, superimposed on top of the constant offset, there was also an inevitable remaining temperature dependence due to the fact that an average correction was performed on all flights, leading to changes in the offset. One might also suspect the assigned CG1 and CG2 gas cylinder CO_2 concentrations to be inaccurate. Calibration standards should always be determined to the highest precision possible because they have a large effect on the system error. Since the precision of the IRMS measurements becomes better with increasing sample sizes, the assignment of O_2, CO_2 and Ar concentrations to the standard cylinders are vague, if it is only based on four samples. An additional uncertainty involves gravitational and thermal fractionation or fractionation induced by the decreasing pressure in the standards. The 2.16 l aluminum cylinders are stored horizontally in the gas rack, but are not thermally insulated. Other high precision O_2 measurement projects use a threshold of 20 bar to 30 bar to determine when a standard needs to be replaced (e.g. Goto 2011). The WG in the CARIBIC setup is sometimes completely emptied during flights, likely fractionating as the pressure decreases. When they are measured back on the mass spectrometer after use, the CG1 and CG2 cylinders exhibit remaining pressures of less than 20 bar. As the effects of fractionation have not been measured for the 2.16 l cylinders, the determined concentrations when they were first measured prior to their deployment were assumed invariable throughout their employment in the container. The NDIR analyzer calibration only uses the two calibration gases CG1 and CG2, both of which typically last for more than 60 flights. One therefore would not expect a time-variant offset. In fact, both flights in figure 4.5 use the same set of calibration cylinders, albeit exhibiting not the same discrepancy to the LSCE CO_2 mixing ratios. The values in panel 4.5b agree with the LSCE values and even in the case of 4.5a, while there is an offset, the variations in CO_2 correspond well with each other.

A major drawback of the LI-6262 analyzer is that it only outputs the difference between the sample and the reference cell. This is problematic in that issues when obtaining data cannot be attributed to either the sample or reference cell. Running the LI-6262 analyzer in absolute mode means that the reference cell contains a zero concentration of CO_2 and H_2O, so that the signal from the sample cell is compared to the zero gas reference signal to provide absolute measurements of CO_2 and H_2O (LI-COR, 1996). In the CARIBIC setup, a zero gas is not used per se but the same sample gas after the CO_2 has been scrubbed using an Ascerite trap. This postulates that the Ascarite and the magnesium perchlorate between the two cells are able to effectively scrub all CO_2 and H_2O. For the Ascarite, this was tested in the laboratory at the PIUB by introducing outside air taken from the roof of the

PIUB building during the month of May in 2013 into a similar Li-7000 device and scrubbing the CO_2 using the same amount of Ascarite. This test revealed that the Ascarite appeared to be consistently effective in removing the CO_2 for about 135 h straight. Considering that even on campaigns covering longer distances the flight time is less than 50 h, one would not expect to find any drifts in the CO_2 signal caused by the sodium hydroxide-coated silica becoming saturated. Both traps not being 100 % effective in removing CO_2 and H_2O will lead to decreased sample cell - reference cell differences and could explain a constant offset. What speaks against this theory is that the CO_2 offset is variable. Another important consideration when trying to explain the offset in CO_2 is the differing conditions between the sample and the reference cell. The gas that is analyzed in the reference cell first needs to pass the H_2O trap, the fuel cells including the temperature controlled enclosure, and the CO_2 trap. The main concern is that there is a pressure difference between the sample and the reference cell with the reference cell pressure being about 450 hPa lower than the sample cell pressure. I do not account for this since I assume a zero CO_2 concentration in the reference cell and do not know the background voltage that is being measured in the reference cell, which is likely to be impacted by pressure. However, the fact that for most flights the strong fluctuations in the reference cell pressure when all the WG was used up, was not visible, is an argument to the contrary. Figure 4.7b revealed pressure changes induced by switching to the calibration gases. The pump does not seem to manage to suck enough air into the system to generate the desired pressure. Despite the inlet pressure being normalized to standard pressure in equation 3.5, this finding may also be causing the observed variable offset. Ultimately, the reason for the offset in CO_2 is not known but expected to be a mixture of the above mentioned factors.

There are three main factors that affect the Licor measurement: Temperature, pressure and to a lesser extent the flow through the system, which is basically controlled by pressure. A temperature effect can be ruled out as a reason for the visible mode switching because the Licor temperature is not expected to change in a step-wise fashion with the switching. One observes a difference in flow of $2\,\mathrm{ml\,min^{-1}}$ between configuration A and D in figure 4.7b, which only the reference cell is subjected to, as it is calculated as the difference between total flow and waste flux. However, this characteristic is commonly observed, including in flights with no cycling behavior. Furthermore, the normal values during modes B and C, despite exhibiting the same flow level as mode D, point to the possibility that the problem arises from something else. It is also important to note that the flow is not directly measured but calculated as the difference between total flow (MKS 179) and waste flux (AWM3100V), and that the waste flux values are averaged over each configuration due to the waste flux sensor being multiplexed. This introduces a rather large uncertainty in the flow estimates. CO_2 contents in the WG cylinders can be very high with values up to 509 ppmv (see Appendix D). Flight 385 employed a WG cylinder containing 403 ppmv of CO_2, which is above the expected ambient air mixing ratios. Since during configuration A sample air in the sample cell is compared to sample air in the reference

cell but during mode D sample air in the sample cell is compared to WG in the reference cell, this means that the Ascarite needs to remove two different amounts of CO_2 from the two gases passing through the CO_2 trap. The argument that the Ascarite is not able to fully remove the CO_2 contained in the WG as opposed to the sampled air can be rejected, given that during configuration B, when the HS with an even higher CO_2 concentration is swept through the reference cell, the CO_2 values agree with configuration A. This reasoning also does not work for the explanation of the cycling in H_2O because at cruise altitude the water content in the atmosphere is usually lower than in the standards. At this point, it remains puzzling as to what caused the cycling in the period February 2011 to April 2012.

5.2 Issues in oxygen data

Problems were also experienced for the oxygen determination during the flights. Variations in the atmospheric $\delta(O_2/N_2)$ were in the order of several hundred per meg and very difficult to interpret. Problematic is not necessarily the noise within a configuration but rather the drift occurring in-between the configurations, causing large fluctuations in the O_2/N_2 ratios. Valentino (2007) suggested that the temperature stability of 0.1 °C is not enough and still affects the fuel cell readings. Each fuel cell takes several hours until it is equilibrated with the temperature in the box, causing long-term drift. Consequently, fuel cell 2 had been adapted to record the temperature of the fuel cells. By subtracting a smoothing spline drift on longer time scales could be accounted for, but even so short-term drift smaller than 6 min remained.

At the example of flight 280 (figure 4.13b) it was checked whether it would be possible to correct for the small scale temperature variations as recorded by fuel cell 2. For that, the same cubic smoothing spline procedure was applied to the fuel cell 2 raw data and the spline subtracted to receive a base signal. Figure 5.1 depicts how fuel cell 1 and 4 behave very similarly after the spline had been subtracted, suggesting that both sensors are mutually affected by the same external sources. By discarding the first 30 min of flight 280 and correlating the last 110 s readings of configuration D (when WG is measured) with the temperature signal by fuel cell 2, it could be derived that temperature can explain 67 % of the remaining short-term variations in fuel cell 1 and 43 % of the drift in fuel cell 4. The $\delta(O_2/N_2)$ ratios that result after the fuel cells have been corrected with the derived linear relationship are plotted in figure 5.2. The variations are substantially lower but are still beyond interpretation. The fuel cells are still not able to resolve the pronounced trough in CO_2, where one would expect a peak in O_2. Based on this finding, it seems that the method of interpolating between previous and a following measurements of WG in order to determine the offset is not precise enough. Small temperature changes in the box further impact the oxygen signal indirectly via induced gas flow variations by pressure changes of the reference gas volume used by the differential pressure gauge. In

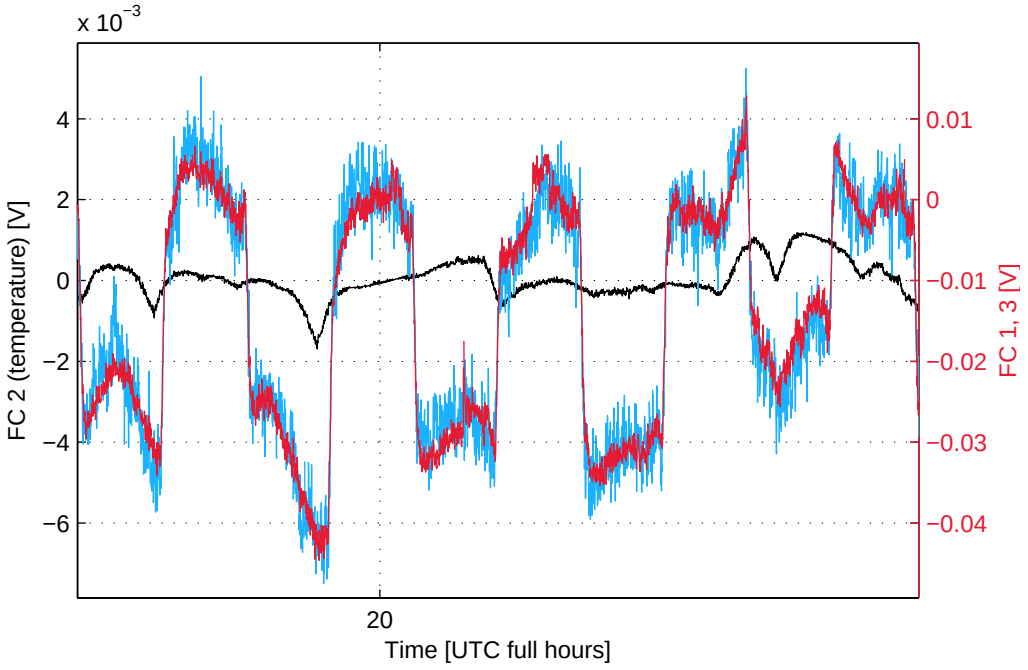

Figure 5.1 60 min extract of fuel cell data after the spline had been subtracted at the example of flight 280. Ten configurations are shown, with the upper values corresponding to configuration D and the lower values being associated with configuration A. Fuel cell 2, which was adapted to record the temperature, is plotted in black using the left y-axis, the fuel cells 1 and 4 are plotted in red and blue respectively and use the right y-axis.

addition to that, some of the drift in the fuel cells can possibly also be attributed to pressure changes measured at the differential pressure gauge directly. In the current setup, pressure values provided by the differential pressure gauge are only available in limited resolution since they are fed to the ADC via the multiplexer. The correction for pressure is therefore only based on averaged values over the active configuration. When correlating the multiplexed Baratron pressure readings to the remaining drift of fuel cell 1 during configuration D, they only explained 0.9 % of the variations in the signal. For fuel cell 4 this value was 0.7 %. It is also important to note that the manufacturer of the employed fuel cells specifies an operating temperature of 5 °C to 40 °C, substantially below the controlled conditions of 48 °C in the unit (Maxtec, 2003).

The required relative precision for atmospheric O_2 measurements is in a range where analytical artifacts such as fractionation play an increasingly important role (Popa, 2007). Various authors have described biases introduced by fractionation in O_2/N_2 measuring systems and have proposed ways to reduce them. Manning (2001) studied the fractionation occurring at intakes or T-junctions commonly used in plumbing systems and concluded that in order to be confident that no fractionation effects are present it is best to eliminate all the T-junctions from a system if possible. Keeling et al. (1998a) suggested the strategy of only subjecting gases to temperature, pressure and humidity gradients under

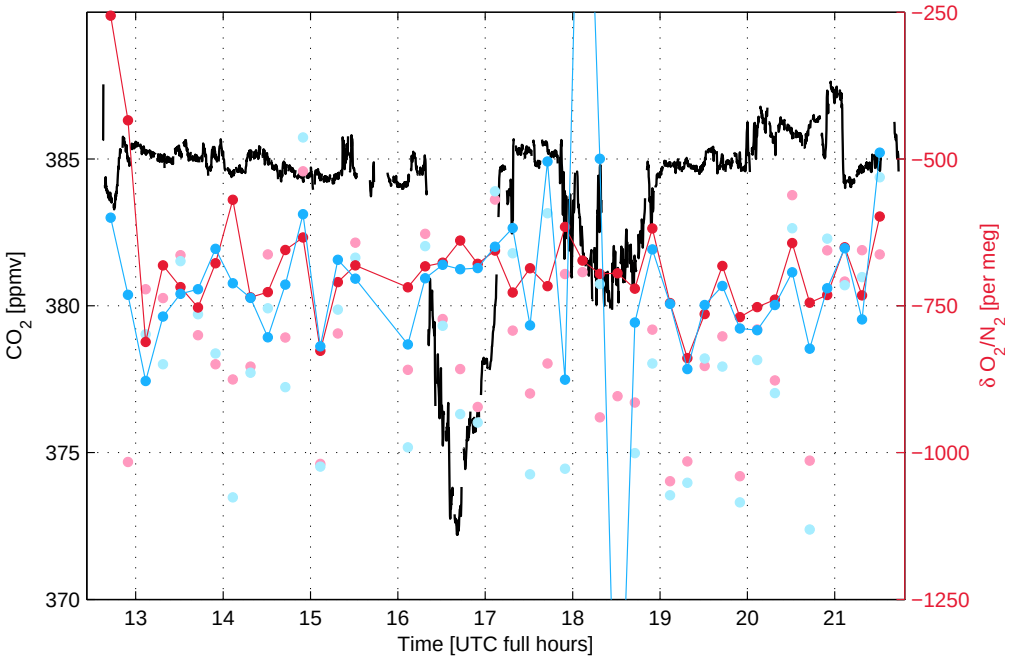

Figure 5.2 Temperature-corrected O_2 data for flight 280. The black line denotes the CO_2 data, light red and light blue dots denote the same uncorrected O_2 data by fuel cell 1 and 4 as in figure 4.13b, the red and blue connected dots denote the O_2 values with the above mentioned correction for short-term temperature changes applied.

conditions of steady flow, ensuring that the relative flows of O_2 and N_2 into a region equal the relative flows out of it even if gradients in concentration caused by temperature, pressure or humidity gradients are present in the region. Possible fractionations affecting the PIUB system include diffusive separation induced by temperature, pressure and humidity gradients resulting in the preferential accumulation of the heavier molecule—in this case O_2— in the region with lower temperatures, higher pressures or higher humidities (Keeling et al., 1998a). Any of these fractionations could lead to a deviation in the O_2/N_2 ratio to the expected values. Also, there are at least two T-junctions involved in the current setup, one being the split from the IMK water line, where a small portion of the flow is taken to feed the PIUB O_2 and CO_2 measurement unit, the other one being located at the differential pressure gauge, where excess air is allowed to vent to ensure constant pressure in the fuel cells. In theory, the extent of fractionation at these T-junctions depends on the geometry of the T and the flow ratio at the two branches, but little is known about the exact causes (Sturm et al., 2006). Fractionation in this case would have to be experimentally assessed. I suspect the jump in the O_2/N_2 after the switch of the inlet position in figure 4.8 to be caused by fractionation due to a change in the intake geometry. Furthermore, it cannot be ruled out that drying of the sample air with $Mg(ClO_4)_2$ can fractionate O_2 and N_2 chemically (Ishidoya et al., 2012). Whereas the flow through the fuel cells is controlled by

the differential pressure gauge, the $Mg(ClO_4)_2$ is upstream of the Baratron and therefore subjected to the changes in flow between configuration A and D. If we assume the alteration of the O_2/N_2 ratio by $Mg(ClO_4)_2$ to be pressure dependent, this could explain an offset in the O_2 data.

5.3 Potential improvements

The current setup employed in the CARIBIC aircraft has major potential for improvements. Compared to CO_2, in-situ measurements of O_2/N_2 are still a young field of research and precise data challenging to achieve, especially on a fast-moving platform. Rather than keep on collecting data that requires attempts of corrections, it is highly recommended that the system incorporate changes or be re-built from the ground up. While it is not guaranteed that all the shortcomings can be removed, some of the faults can be understood better. One has to bear in mind however, that any change concerning the electronic components of the O_2 and CO_2 analyzer unit means loss of the electromagnetic compatibility test for the entire CARIBIC container. Therefore, retrofitting with new equipment can only be performed by mutual agreement of all the partners, possibly during a longer scheduled grounding period of the aircraft.

In general, it is advised to use the down time to perform ground tests to determine the accuracy of the NDIR as well as the fuel cells with target gases, and to understand why some flights suffered from communication loss, missing data or pressure variations, and lower the equipment malfunction rate. In order to better understand the impacts of the pressure variations on the fuel cells and be able to correct for them, the Baratron pressure readings should be removed from the multiplexer and its temporal resolution increased. At its place, the temperature readings of the thermostable box could be added to the multiplexer. Instead of having a sensor to measure total flow and one to measure waste flux, the system could be simplified by only logging the flow passing the fuel cells.

The flask sample CO_2 values agree much better with the LSCE collected in-situ measurements of CO_2, despite using the same LI-6262 model NDIR analyzer. Notable differences between the two setups are that they dry the sample air prior to CO_2 analysis using a Nafion tube, keep the spectrometer temperature constant at 40 °C and calibrate more frequently (every 30 min) (Brenninkmeijer et al., 2007). At cruising altitude water vapor does not affect the CO_2 mixing ratio much (Schuck et al., 2009), but it does so during take-off and landing phases. The H_2O calibration that is applied in this setup is just an approximation given that equilibrated water values during configuration E and F are not always reached (figure 3.7). Uncertainties in CO_2, especially for vertical profiles, could therefore be lowered by placing the magnesium perchlorate upstream the NDIR analyzer. Nafion membrane tubes, as used in the CARIBIC container by the LSCE on their CO_2 measurements, have also been employed on precise, continuous O_2 measuring projects to dry sample air alongside cold traps (Goto, 2011; Laan-Luijkx et al., 2010a). Nafion tubes require a counter-flow of dry air to remove water vapor

from the sample air. Previously dried ambient or standard air after it has passed the analyses can be supplied along the outer side of the Nafion column to vent the water content. The use of Nafion membrane tubes instead of $Mg(ClO_4)_2$ might improve the O_2 and CO_2 measurements but both drying methods will have to be tested extensively to compare their efficiencies in removing water vapor in the air and to see their possible effects on O_2/N_2 ratios.

One of the biggest concerns that both the O_2 and CO_2 analyzer suffered from are temperature dependent effects. Temperature dependence of the NDIR analyzer can be avoided by extending the thermostable box to include the LI-6262 or placing it in its own. It is advised to add peltier elements to actively cool the system, which is something the fuel cells could also benefit from to reach an equilibrated temperature earlier and as the current 48 °C exceed the operating range by 8 °C. Incorporating these improvements would entail rearrangements within the unit's case and may require enhancements in the dissipation of thermal discharge. Should there still remain variations in temperature, they could be better taken into account by calibrating more frequently, like every hour. At the same time, this would also address the issue of missing calibrations on short flights. These have been proven problematic because hitherto the only way to obtain data for short flights was by assuming calibration values of other flights within the same campaign. With this approach many flights exhibited large deviations from the LSCE data, which indicated that calibration values are unique to each flight and did not seem stable enough over several legs of a campaign to be used interchangeably when no calibration procedures took place.

LI-COR (1996) recommend a re-calibration of the LI-6262 analyzer every two years. Factory calibration of the PIUB LI-6262 device was last carried out seven years ago in 2006. By processing CO_2 data using coefficients derived from a previous re-calibration routine conducted in 1999, mixing ratios were elevated by 0.24 ± 0.04 ppmv, which suggests that sensor re-calibration can have a small but significant effect on the measurements. The NDIR analyzer in use in the CARIBIC project has never been replaced. It is possible that the built-in thermoelectric sensor cooler is not working properly anymore and could have become sensitive to temperature drift. A replacement of the LI-6262 model could provide more information about whether some of the issues discussed above are device-specific. The preferred choice would be the newer Li-7000 model, which has the advantage of outputting sample and reference cell values individually. Due to its slightly larger dimensions however, the LI-7000 does not fit into the unit's case.

A means of reducing the cycling behavior when switching configuration often encountered in the current setup is to analyze the same type of gas in both sample and reference cell at all times. This would essentially halve the amount of CO_2 data collected on a flight because during every D configuration WG would need to be sampled rather than ambient air. On the contrary, the D configuration could then be used to correct the NDIR analyzer for any kinds of drift, for example caused by temperature. By scrubbing CO_2 directly after a gas has passed the sample cell and feeding

it into the reference cell immediately after, the conditions in the two cells would match each other more closely in terms of gas temperature and pressure, and could further help in improving the CO_2 measurements. This approach is likely to impede precise detection of O_2 using fuel cells, as they exhibit severe cross sensitivity towards sodium hydroxide (Maxtec, 2003). Thus, the best solution to eliminate drifts and cycling in CO_2 would be to use a different method of introducing the WG by creating two separate gas lines, with one being used by sample air and the other one by WG, allowing the NDIR analyzer to be run in differential mode. In differential mode, a non-zero gas of known CO_2 concentration is continuously passed through the reference cell (LI-COR, 1996). This way most errors emerging from changes in source output, filter transmission, detector response or temperature can be overcome since both cells are affected to similar extents. This would also make configuration D redundant and result in steady gas flows without 6 min switching cycles which were major sources of inconsistent conditions. Two steady streams of gas would also be greatly advantageous for the determination of O_2. To improve the precision and stability characteristics, many fuel cell-based projects incorporate a commercially available Oxzilla instrument (Laan-Luijkx et al., 2010a; Patecki and Manning, 2007; Stephens et al., 2007a; Thompson et al., 2007), whose default setup is capable of analyzing sample gas and a reference gas simultaneously using two fuel cells. Regularly switching the cell acting as the reference cell and the cell acting as the sample cell at a certain interval and deriving the change in the differences yields a double differential O_2 signal to eliminate bias arising from short-term baseline drifts due to differences in fuel cell sensitivities (Thompson et al., 2007). Another advantage of this approach is that the resolution of O_2 would essentially be doubled, because configuration D can be omitted. The limited space within the measurement unit prohibits the installation of a bulky Oxzilla device, but like in the current experimental design, a similar device can be custom made. However, this method also entails the disadvantage that the 2.16 l reference gas cylinder deployed in the CARIBIC container cannot hold adequate volumes of gas to support an uninterrupted reference gas flow. The gas cylinder rack in the container holds a special permit issued by the German civil aviation authority because the transport of high pressure cylinders on passenger aircrafts is forbidden, and therefore no changes can be made to the size or number of gas cylinders in use. Hence, the current problem of insufficient WG amount would be further aggravated. Reduced gas flow, omission of certain legs of a campaign and the activation of measurements only after stable conditions are reached, are potential ways to counteract this shortcoming. For running the NDIR device in differential mode it would be desirable to incorporate WG containing CO_2 concentrations in the range of the sampled air, rather than values up to 509 ppmv as is the case in the current WG cylinders. This implies that a new technique should be established for the preparation of the standards from natural air because the gas cylinders supplied by Carbagas may not be suitable for high precision measurements of atmospheric gases. The most elegant way to circumvent this problem would be the acquisition and employment of a compressor to collect natural air on top of the PIUB

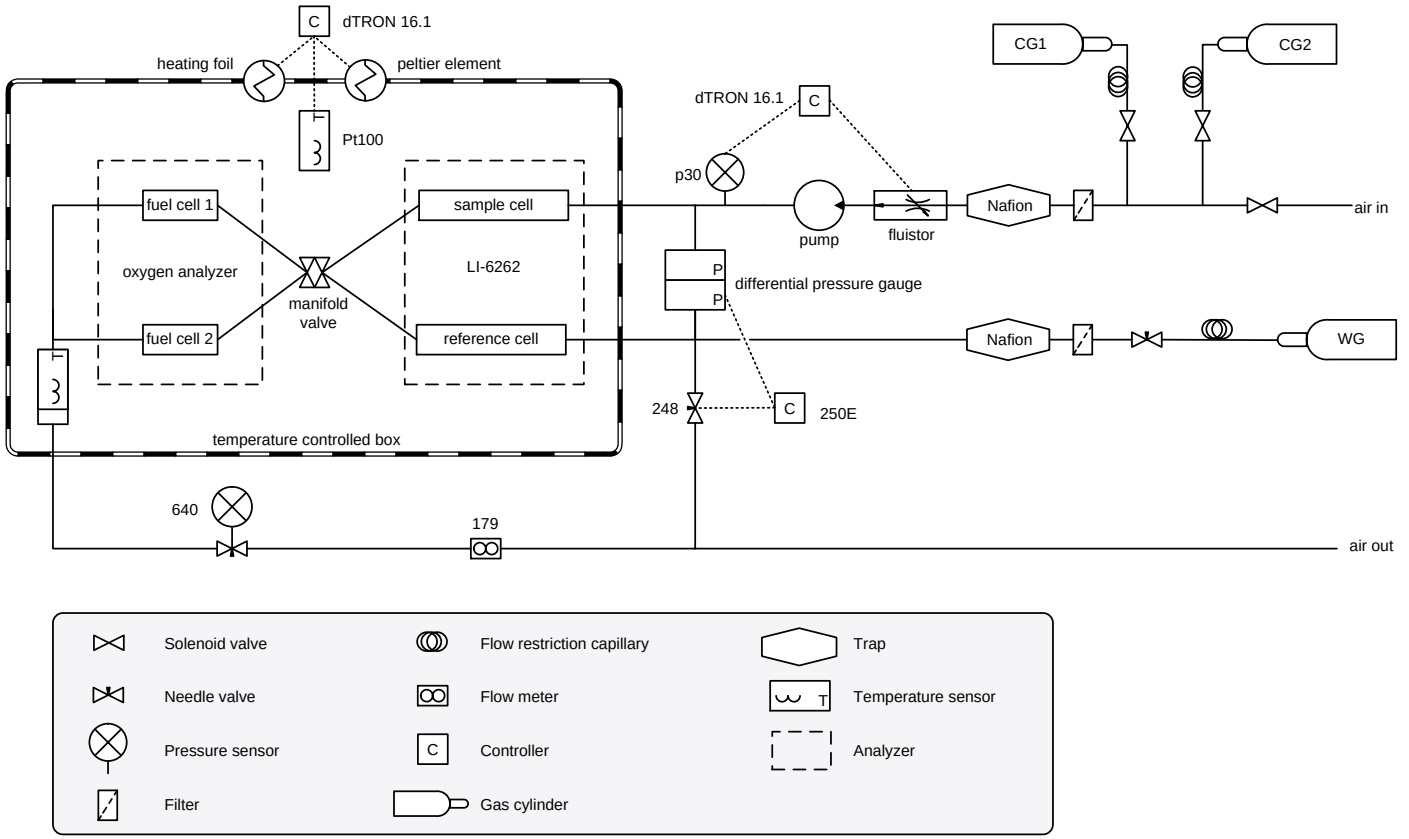

Figure 5.3 Suggestion for an improved plumbing scheme using two gas lines for a differential measurement design.

building. By compressing natural air in different seasons, HS and LS gases could be produced and the water vapor contained in the standard air could be removed cryogenically without altering the O_2/N_2 ratio (Goto, 2011). Using compressed natural air would further make corrections due to dilution by Ar abundant (Stephens et al., 2007a). The only solution for more precise measurements using the IRMS is to make the CARIBIC project higher priority and to allocate more time to measuring the standards. Additionally, it would be good to check the unit and the cylinders for sensitivity to fractionation and replace the calibration cylinders more frequently. Figure 5.3 shows a very tentative, future plumbing scheme for the implementation in the CARIBIC project to illustrate some of the above mentioned suggestions for improving the O_2 and CO_2 measurements.

One of the main differences in the proposed scheme compared to the current experimental design is the addition of a second gas line, allowing the NDIR to be run in differential mode and the fuel cells to measure a double differential signal. WG and sample gas flows are both constantly enabled. One of the fuel cells has been removed. Switching sample air and WG between the two cells is achieved using a four-way valve composed of two miniature solenoid valves and a manifold, following Stephens et al. (2007a). This adds the benefits of making configuration D superfluous and increasing the sensitivity of the measurement by a factor of 2, but it halves the amount of time before the WG runs out. A peltier-equipped thermo-controlled housing now surrounds the O_2 and the CO_2 analyzer to keep the temperature constant at 40 °C. Two Nafion tubes have been added upstream of the LI-6262 to remove water vapor beforehand. Due to the comparison of sample gas in the Licor sample cell to WG in the reference cell, the Ascarite CO_2 scrubber has been removed. In order to equalize the pressures in both lines before the NDIR analyzer, the pressure on the sample air line is reduced using a differential pressure gauge with the reference side connected to the WG line.

5.4 Conclusions

The civil aircraft-based global monitoring program CARIBIC is still in ongoing operation and has since 2005 convincingly demonstrated that for many different species valuable measurements can be conducted monthly aboard a passenger aircraft. Unfortunately, the PIUB has so far not been able to contribute to the success with its deployment of an O_2 analyzer based on fuel cell technology and a CO_2 measuring NDIR device. Foremost is the need for higher precision in the data and better reliability of the equipment. The analytical accuracies of the CO_2 and O_2 measurements were estimated to be 2.61 ppmv and 242 per meg, respectively. Given the expected variations in $\delta(O_2/N_2)$ in the order of a few per meg, O_2 data collected by the PIUB is not able to constrain the partitioning of the CO_2 uptake. The CO_2 data could not be treated as one single long-term record as variable offsets were discovered from flight to flight. However, relying on the CO_2 data by the LSCE for quality assessment, the CO_2 data could contribute to the understanding of observations made during single

flights. Problems were encountered in different stages of the measurement campaign including the preparation and determination of standard cylinders, the maintaining of appropriate measurement conditions in the container and drifts and fractionations in the fuel cells. The incorporation of analytical equipment in a civil aircraft poses a tremendous challenge due to numerous restrictions and extreme conditions. Instruments have to perform under large pressure, temperature and humidity variations, be insusceptible to vibration and shock, and manage to run on low power consumption levels. Restricted are also the number and size of transported gas cylinders, the amount of electromagnetic radiation of the equipment and the space within the container. Unlike research aircraft projects, CARIBIC has to be able to measure unattended for days at a stretch requiring low maintenance and an exceptionally high degree of automation. It is nearly impossible to test the equipment under such conditions in the lab. Several means of improvement of the measurement unit were presented. Of high priorities are the incorporation of a second gas line to run both analyzers in differential mode and the thermo-stabilization of the NDIR analyzer. I am confident that with the implementation of these proposed enhancements the combined O_2 and CO_2 data acquired by the PIUB can be improved so that it can add to the continuously growing CARIBIC data set in the future. It is hoped, that embedded in the CARIBIC project, information on these two gases can complement data collected by ground-based networks, satellite observations and other aircraft measurements and contribute to a better understanding of carbon cycle processes.

Appendix A

Plumbing schemes

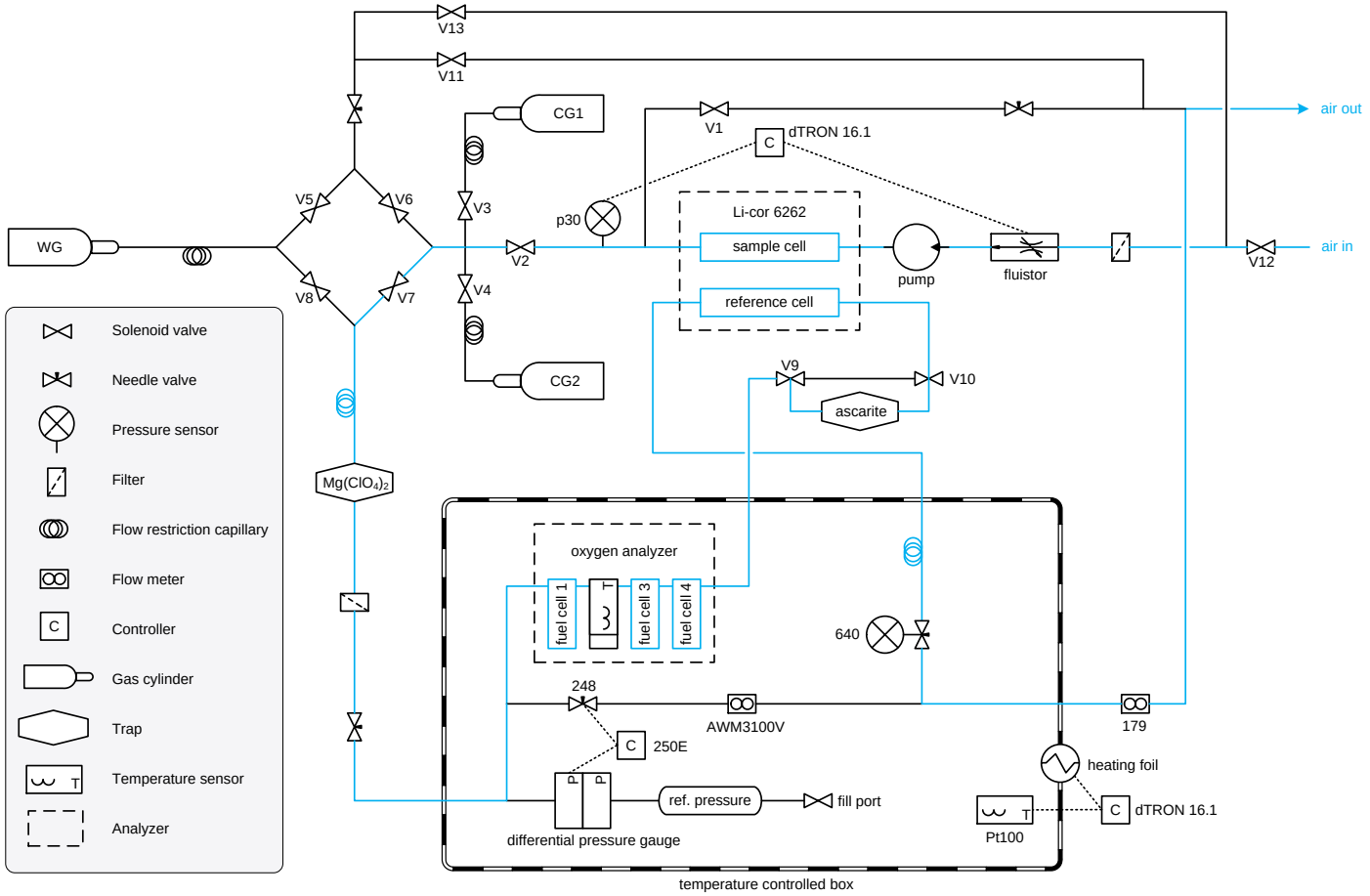

Figure A.1 Flow chart for configuration A. Blue, orange and red colors denote the path of flow of outside air sample, working gas and calibration gases, respectively.

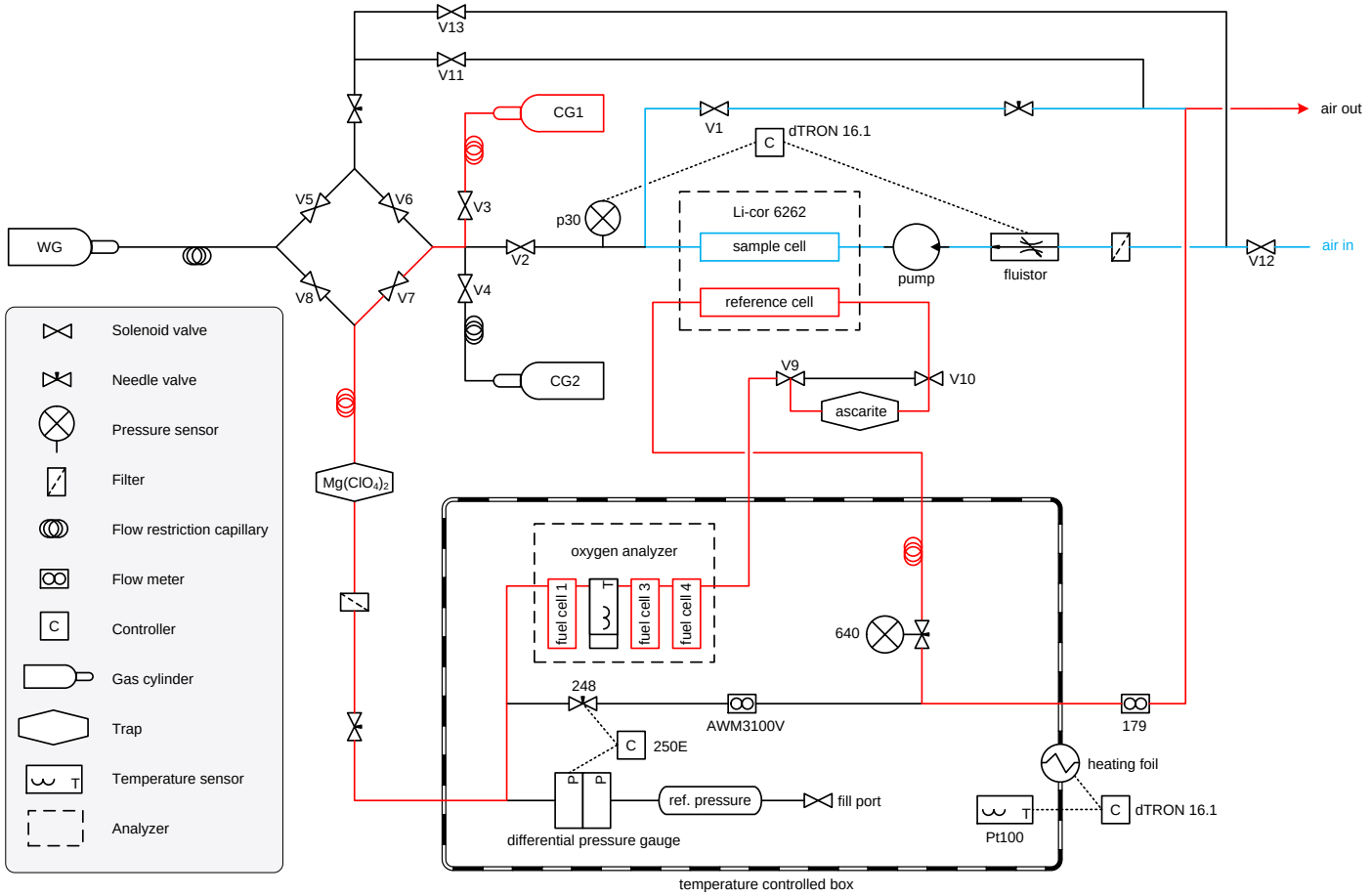

Figure A.2 Flow chart for configuration B. Blue, orange and red colors denote the path of flow of outside air sample, working gas and calibration gases, respectively.

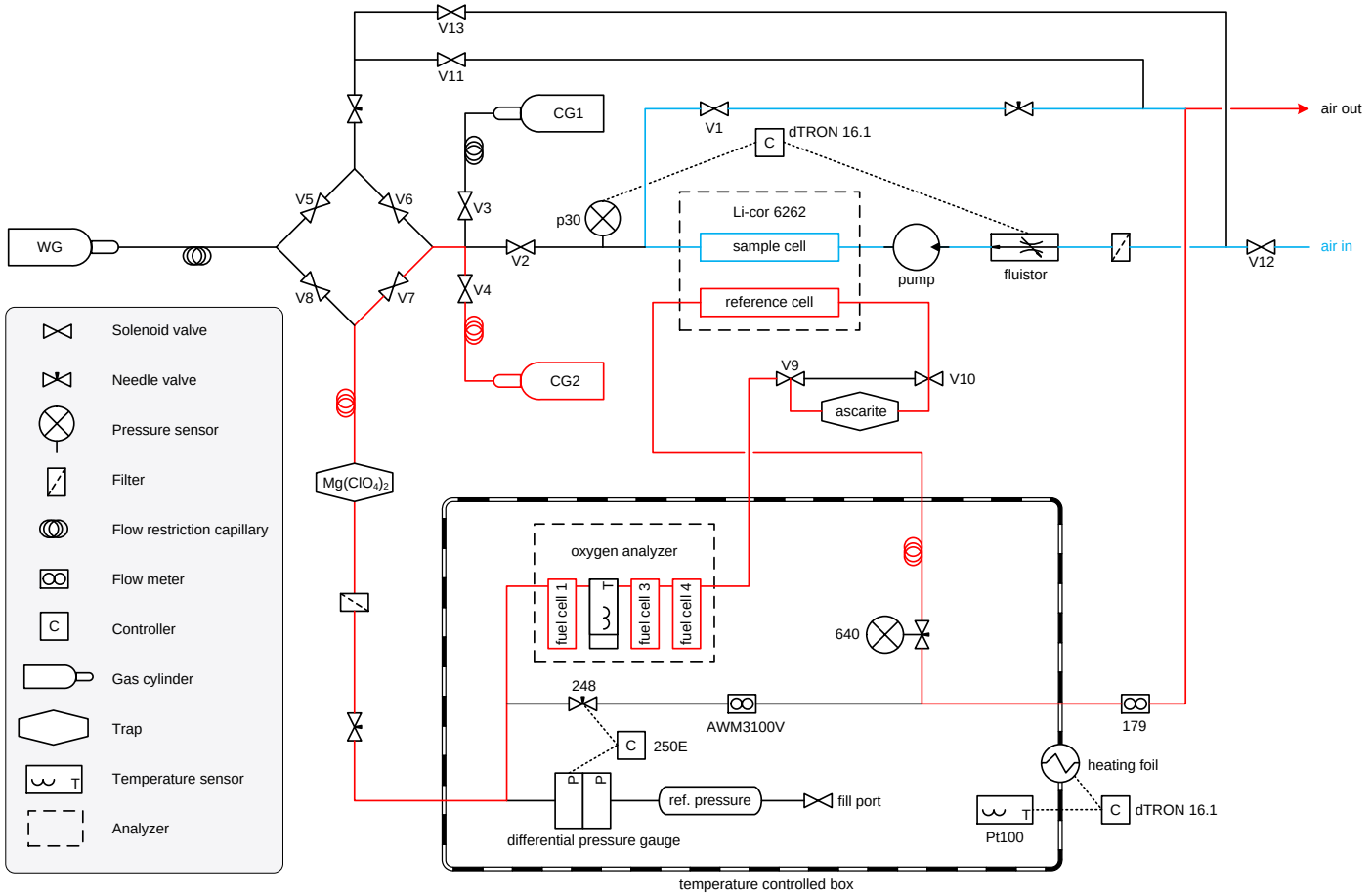

Figure A.3 Flow chart for configuration C. Blue, orange and red colors denote the path of flow of outside air sample, working gas and calibration gases, respectively.

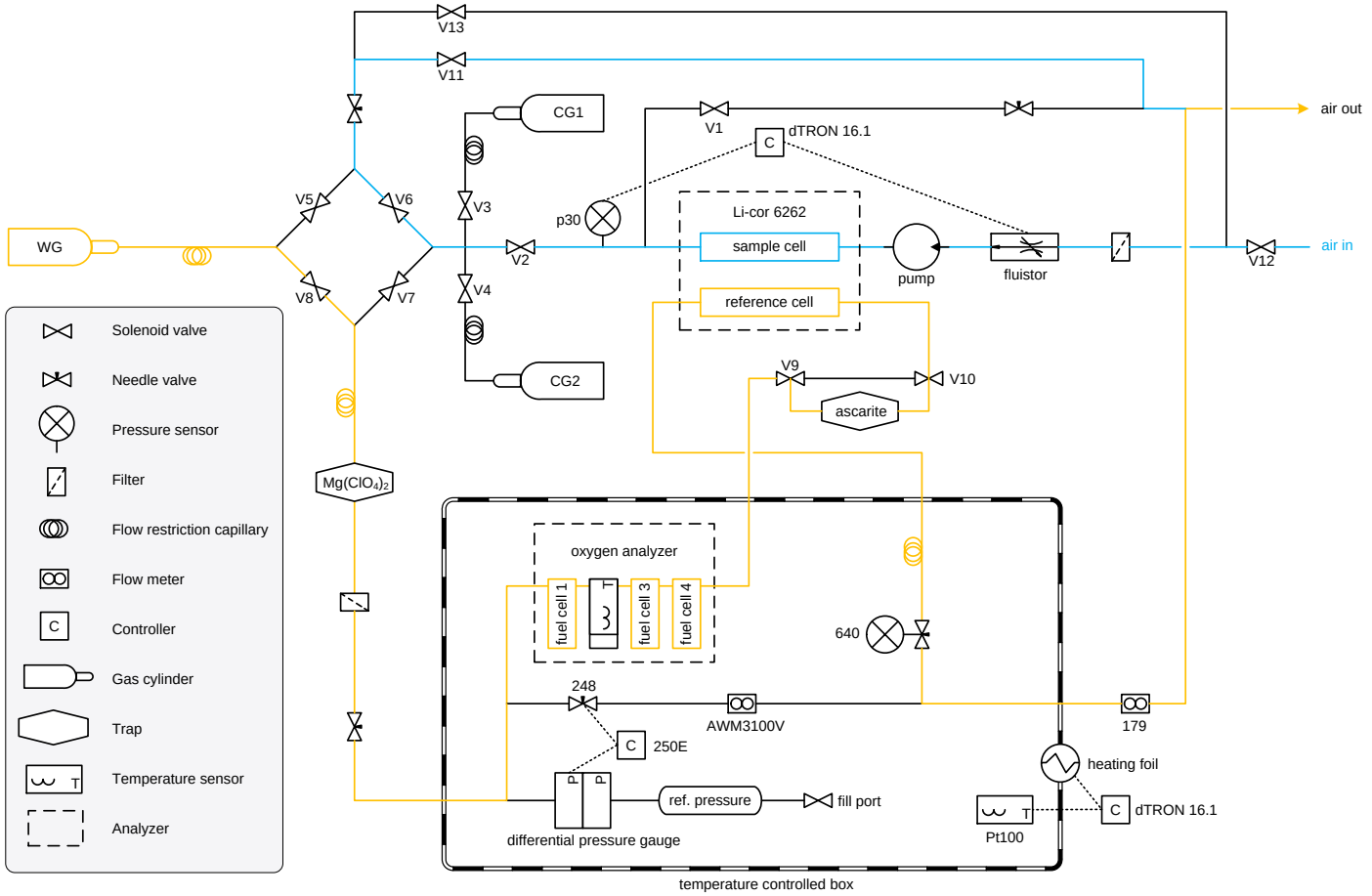

Figure A.4 Flow chart for configuration D. Blue, orange and red colors denote the path of flow of outside air sample, working gas and calibration gases, respectively.

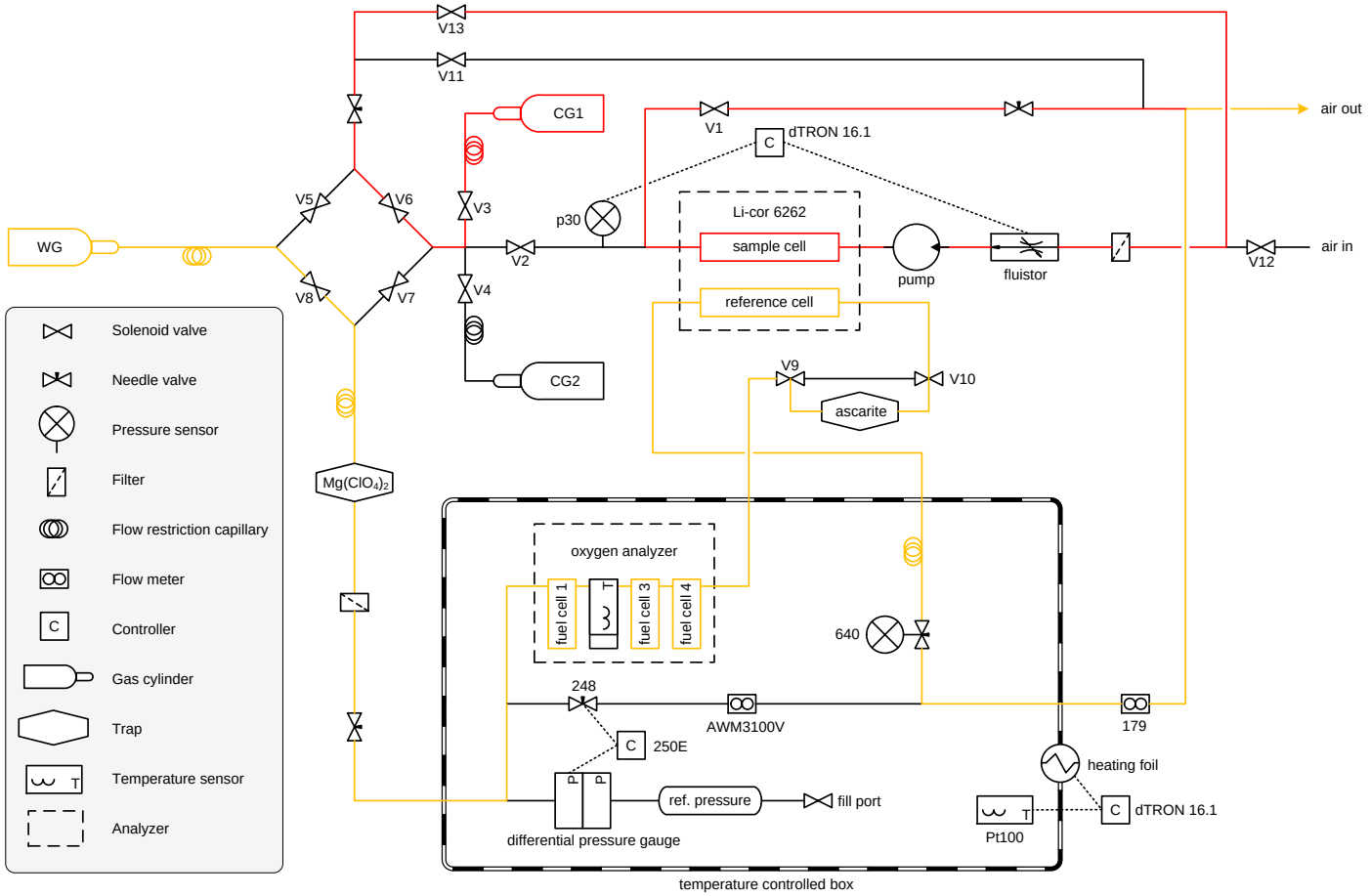

Figure A.5 Flow chart for configuration E. Blue, orange and red colors denote the path of flow of outside air sample, working gas and calibration gases, respectively.

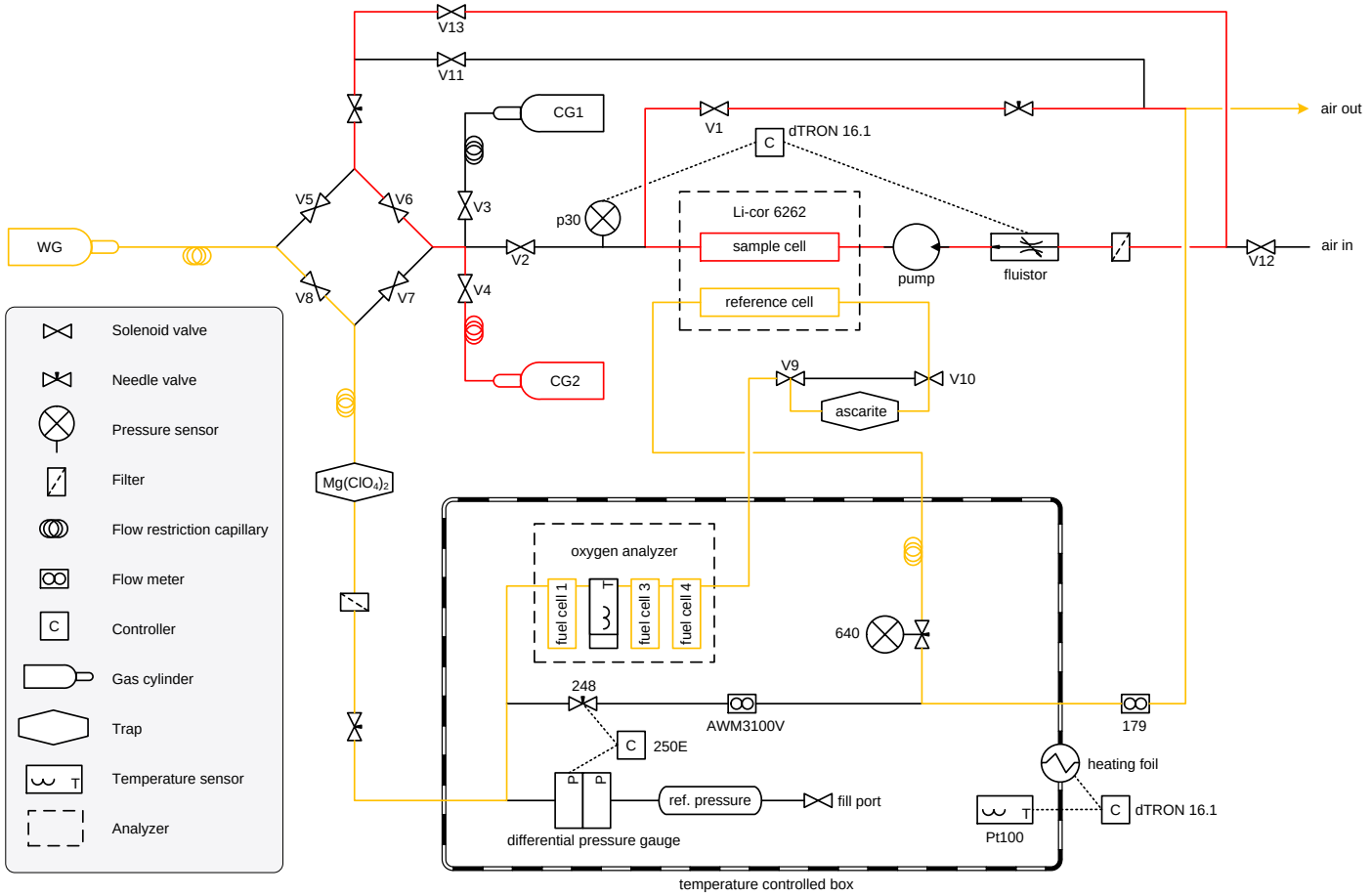

Figure A.6 Flow chart for configuration F. Blue, orange and red colors denote the path of flow of outside air sample, working gas and calibration gases, respectively.

Appendix B

Complete list of flights

Table B.1 Complete list of processed flights during the CARIBIC project undertaken since May 2007. Checked boxes indicate that data from the NDIR ("CO_2"), fuel cell 1 ("F1"), fuel cell 3 ("F3") and fuel cell 4 ("F4") were available, whereas unchecked boxes indicate missing, corrupt or removed data.

CARIBIC flight #	Lufthansa flight #	From	To	Date of departure	CO_2	F1	F3	F4	Notes
432	LH493	Toronto, Canada	Frankfurt, Germany	09.06.2013	☑	☐	☐	☑	
431	LH492	Frankfurt, Germany	Toronto, Canada	09.06.2013	☑	☐	☑	☑	
430	LH535	Caracas, Venezuela	Frankfurt, Germany	08.06.2013	☑	☐	☑	☑	
429	LH534	Frankfurt, Germany	Caracas, Venezuela	08.06.2013	☑	☐	☑	☑	
428	LH493	Toronto, Canada	Frankfurt, Germany	26.05.2013	☐	☐	☐	☐	No power
427	LH492	Frankfurt, Germany	Toronto, Canada	26.05.2013	☐	☐	☐	☐	No power
426	LH535	Caracas, Venezuela	Frankfurt, Germany	25.05.2013	☐	☐	☐	☐	No power
425	LH534	Frankfurt, Germany	Caracas, Venezuela	25.05.2013	☐	☐	☐	☐	No power
424	LH470	Toronto, Canada	Frankfurt, Germany	27.04.2013	☑	☑	☑	☑	
423	LH471	Frankfurt, Germany	Toronto, Canada	27.04.2013	☑	☑	☑	☑	
422	LH535	Caracas, Venezuela	Frankfurt, Germany	26.04.2013	☑	☐	☑	☑	
421	LH534	Frankfurt, Germany	Caracas, Venezuela	26.04.2013	☑	☐	☑	☑	
420	LH783	Bangkok, Thailand	Frankfurt, Germany	21.03.2013	☑	☐	☑	☑	
419	LH783	Kuala Lumpur, Malaysia	Bangkok, Thailand	21.03.2013	☑	☐	☑	☑	
418	LH782	Bangkok, Thailand	Kuala Lumpur, Malaysia	21.03.2013	☑	☐	☑	☑	
417	LH782	Frankfurt, Germany	Bangkok, Thailand	20.03.2013	☑	☐	☑	☑	
416	LH783	Bangkok, Thailand	Frankfurt, Germany	21.02.2013	☑	☐	☑	☑	
415	LH783	Kuala Lumpur, Malaysia	Bangkok, Thailand	21.02.2013	☑	☐	☑	☑	
414	LH782	Bangkok, Thailand	Kuala Lumpur, Malaysia	21.02.2013	☑	☑	☑	☑	
413	LH782	Frankfurt, Germany	Bangkok, Thailand	20.02.2013	☑	☑	☑	☑	
412	LH783	Bangkok, Thailand	Frankfurt, Germany	24.01.2013	☐	☐	☐	☐	No power
411	LH783	Kuala Lumpur, Malaysia	Bangkok, Thailand	24.01.2013	☐	☐	☐	☐	No power
410	LH782	Bangkok, Thailand	Kuala Lumpur, Malaysia	24.01.2013	☐	☐	☐	☐	No power

Continued on next page

Table B.1 – *Continued from previous page*

409	LH782	Frankfurt, Germany	Bangkok, Thailand	23.01.2013	☑	☑	☑	☑	
408	LH783	Bangkok, Thailand	Frankfurt, Germany	13.12.2012	☑	☑	☑	☑	
407	LH783	Kuala Lumpur, Malaysia	Bangkok, Thailand	13.12.2012	☑	☑	☑	☑	
406	LH782	Bangkok, Thailand	Kuala Lumpur, Malaysia	13.12.2012	☑	☑	☑	☑	
405	LH782	Frankfurt, Germany	Bangkok, Thailand	12.12.2012	☑	☑	☑	☑	
404	LH783	Bangkok, Thailand	Frankfurt, Germany	22.11.2012	☑	☑	☑	☑	
403	LH783	Kuala Lumpur, Malaysia	Bangkok, Thailand	22.11.2012	☑	☑	☑	☑	
402	LH782	Bangkok, Thailand	Kuala Lumpur, Malaysia	22.11.2012	☑	☑	☑	☑	
401	LH782	Frankfurt, Germany	Bangkok, Thailand	21.11.2012	☑	☑	☑	☑	
400	LH493	Vancouver, Canada	Frankfurt, Germany	17.10.2012	☑	☑	☑	☑	
399	LH492	Frankfurt, Germany	Vancouver, Canada	17.10.2012	☑	☑	☑	☑	
398	LH535	Caracas, Venezuela	Frankfurt, Germany	16.10.2012	☑	☑	☑	☑	
397	LH534	Frankfurt, Germany	Caracas, Venezuela	16.10.2012	☑	☑	☑	☑	
396	LH493	Vancouver, Canada	Frankfurt, Germany	19.09.2012	☑	☑	☑	☑	
395	LH492	Frankfurt, Germany	Vancouver, Canada	19.09.2012	☑	☑	☑	☑	
394	LH535	Caracas, Venezuela	Frankfurt, Germany	18.09.2012	☑	☑	☑	☑	
393	LH534	Frankfurt, Germany	Caracas, Venezuela	18.09.2012	☑	☑	☑	☑	
392	LH493	Vancouver, Canada	Frankfurt, Germany	08.08.2012	☑	☑	☑	☑	
391	LH492	Frankfurt, Germany	Vancouver, Canada	08.08.2012	☑	☑	☑	☑	
390	LH535	Caracas, Venezuela	Frankfurt, Germany	07.08.2012	☑	☑	☑	☑	
389	LH534	Frankfurt, Germany	Caracas, Venezuela	07.08.2012	☑	☑	☑	☑	
388	LH493	Seoul, South Korea	Frankfurt, Germany	23.05.2012	☑	☑	☑	☑	
387	LH492	Frankfurt, Germany	Seoul, South Korea	22.05.2012	☑	☑	☑	☑	
386	LH493	Vancouver, Canada	Frankfurt, Germany	25.04.2012	☑	☑	☑	☑	
385	LH492	Frankfurt, Germany	Vancouver, Canada	25.04.2012	☑	☑	☑	☑	
384	LH713	Seoul, South Korea	Frankfurt, Germany	29.03.2012	☑	☑	☑	☑	WG empty
383	LH712	Frankfurt, Germany	Seoul, South Korea	28.03.2012	☑	☑	☑	☑	
382	LH535	Caracas, Venezuela	Frankfurt, Germany	28.03.2012	☑	☑	☑	☑	

Continued on next page

Table B.1 – *Continued from previous page*

381	LH534	Frankfurt, Germany	Caracas, Venezuela	27.03.2012	☑	☑	☑	☑	
380	LH535	Caracas, Venezuela	Frankfurt, Germany	07.03.2012	☑	☑	☑	☑	
379	LH534	Frankfurt, Germany	Caracas, Venezuela	07.03.2012	☑	☑	☑	☑	
378	LH759	Chennai, India	Frankfurt, Germany	06.03.2012	☑	☑	☑	☑	
377	LH758	Frankfurt, Germany	Chennai, India	06.03.2012	☑	☑	☑	☑	
376	LH535	Caracas, Venezuela	Frankfurt, Germany	17.01.2012	☑	☑	☑	☑	
375	LH534	Frankfurt, Germany	Caracas, Venezuela	17.01.2012	☑	☑	☑	☑	
374	LH759	Chennai, India	Frankfurt, Germany	16.01.2012	☑	☑	☑	☑	
373	LH758	Frankfurt, Germany	Chennai, India	16.01.2012	☑	☑	☑	☑	
372	LH535	Caracas, Venezuela	Frankfurt, Germany	16.12.2011	□	□	□	□	Unit inoperable
371	LH534	Frankfurt, Germany	Caracas, Venezuela	16.12.2011	□	□	□	□	Unit inoperable
370	LH759	Chennai, India	Frankfurt, Germany	15.12.2011	□	□	□	□	Unit inoperable
369	LH758	Frankfurt, Germany	Chennai, India	15.12.2011	□	□	□	□	Unit inoperable
368	LH535	Caracas, Venezuela	Frankfurt, Germany	16.11.2011	□	□	□	□	Unit inoperable
367	LH534	Frankfurt, Germany	Caracas, Venezuela	16.11.2011	□	□	□	□	Unit inoperable
366	LH759	Chennai, India	Frankfurt, Germany	15.11.2011	□	□	□	□	Unit inoperable
365	LH758	Frankfurt, Germany	Chennai, India	15.11.2011	□	□	□	□	Unit inoperable
364	LH493	Vancouver, Canada	Frankfurt, Germany	25.10.2011	□	□	□	□	Equipment fail
363	LH492	Frankfurt, Germany	Vancouver, Canada	25.10.2011	☑	☑	☑	☑	
362	LH535	Caracas, Venezuela	Frankfurt, Germany	24.10.2011	☑	☑	☑	☑	
361	LH534	Frankfurt, Germany	Caracas, Venezuela	24.10.2011	☑	☑	☑	☑	
360	LH493	Vancouver, Canada	Frankfurt, Germany	21.09.2011	☑	☑	☑	☑	
359	LH492	Frankfurt, Germany	Vancouver, Canada	21.09.2011	☑	☑	☑	☑	
358	LH535	Caracas, Venezuela	Frankfurt, Germany	20.09.2011	☑	☑	☑	☑	
357	LH534	Frankfurt, Germany	Caracas, Venezuela	20.09.2011	☑	☑	☑	☑	
356	LH493	Vancouver, Canada	Frankfurt, Germany	18.08.2011	□	□	□	□	Equipment fail
355	LH492	Frankfurt, Germany	Vancouver, Canada	17.08.2011	□	□	□	□	Equipment fail
354	LH535	Caracas, Venezuela	Frankfurt, Germany	16.08.2011	☑	☑	☑	☑	

Continued on next page

Table B.1 – *Continued from previous page*

353	LH534	Frankfurt, Germany	Caracas, Venezuela	16.08.2011	☑	☑	☑	☑	
352	LH493	Vancouver, Canada	Frankfurt, Germany	21.07.2011	□	□	□	□	Equipment fail
351	LH492	Frankfurt, Germany	Vancouver, Canada	21.07.2011	□	□	□	□	Equipment fail
350	LH535	Caracas, Venezuela	Frankfurt, Germany	20.07.2011	□	□	□	□	Equipment fail
349	LH534	Frankfurt, Germany	Caracas, Venezuela	20.07.2011	□	□	□	□	Equipment fail
348	LH543	Bogotá, Columbia	Frankfurt, Germany	17.06.2011	☑	☑	☑	☑	
347	LH542	Frankfurt, Germany	Bogotá, Columbia	16.06.2011	□	□	□	□	Equipment fail
346	LH493	Vancouver, Canada	Frankfurt, Germany	15.06.2011	□	□	□	□	Equipment fail
345	LH492	Frankfurt, Germany	Vancouver, Canada	15.06.2011	☑	☑	☑	☑	
344	LH493	Vancouver, Canada	Frankfurt, Germany	17.05.2011	☑	☑	☑	☑	
343	LH492	Frankfurt, Germany	Vancouver, Canada	17.05.2011	☑	☑	☑	☑	
342	LH535	Caracas, Venezuela	Frankfurt, Germany	16.05.2011	☑	☑	☑	☑	
341	LH534	Frankfurt, Germany	Caracas, Venezuela	16.05.2011	☑	☑	☑	☑	
340	LH493	Vancouver, Canada	Frankfurt, Germany	19.04.2011	☑	☑	☑	☑	WG empty
339	LH492	Frankfurt, Germany	Vancouver, Canada	19.04.2011	☑	☑	☑	☑	
338	LH535	Caracas, Venezuela	Frankfurt, Germany	18.04.2011	☑	☑	☑	☑	
337	LH534	Frankfurt, Germany	Caracas, Venezuela	18.04.2011	☑	☑	☑	☑	
336	LH543	Bogotá, Columbia	Frankfurt, Germany	23.03.2011	☑	☑	☑	☑	WG empty
335	LH542	Frankfurt, Germany	Bogotá, Columbia	22.03.2011	☑	☑	☑	☑	
334	LH577	Cape Town, South Africa	Frankfurt, Germany	21.03.2011	☑	☑	☑	☑	
333	LH576	Frankfurt, Germany	Cape Town, South Africa	20.03.2011	☑	☑	☑	☑	
332	LH741	Osaka, Japan	Frankfurt, Germany	27.02.2011	☑	□	□	□	WG empty
331	LH740	Frankfurt, Germany	Osaka, Japan	26.02.2011	☑	□	☑	□	
330	LH577	Cape Town, South Africa	Frankfurt, Germany	25.02.2011	☑	☑	☑	☑	
329	LH576	Frankfurt, Germany	Cape Town, South Africa	24.02.2011	☑	☑	☑	□	
328	LH543	Bogotá, Columbia	Frankfurt, Germany	21.01.2011	☑	□	☑	☑	
327	LH542	Frankfurt, Germany	Bogotá, Columbia	20.01.2011	☑	□	☑	☑	
326	LH573	Johannesburg, South Africa	Frankfurt, Germany	19.01.2011	☑	☑	☑	☑	

Continued on next page

Table B.1 – *Continued from previous page*

325	LH572	Frankfurt, Germany	Johannesburg, South Africa	18.01.2011	☑	☑	☑	☐	
324	LH543	Bogotá, Columbia	Frankfurt, Germany	15.12.2010	☑	☑	☑	☐	WG empty
323	LH542	Frankfurt, Germany	Bogotá, Columbia	14.12.2010	☑	☑	☑	☑	
322	LH577	Cape Town, South Africa	Frankfurt, Germany	13.12.2010	☑	☑	☑	☑	
321	LH576	Frankfurt, Germany	Cape Town, South Africa	12.12.2010	☐	☐	☐	☐	Equipment fail
320	LH543	Bogotá, Columbia	Frankfurt, Germany	17.11.2010	☐	☐	☐	☐	No power
319	LH542	Frankfurt, Germany	Bogotá, Columbia	16.11.2010	☑	☑	☑	☐	
318	LH573	Johannesburg, South Africa	Frankfurt, Germany	15.11.2010	☐	☐	☐	☐	No power
317	LH572	Frankfurt, Germany	Johannesburg, South Africa	14.11.2010	☑	☑	☑	☐	
316	LH741	Osaka, Japan	Frankfurt, Germany	22.10.2010	☑	☑	☑	☑	WG empty
315	LH740	Frankfurt, Germany	Osaka, Japan	21.10.2010	☑	☑	☑	☑	
314	LH535	Caracas, Venezuela	Frankfurt, Germany	20.10.2010	☑	☑	☑	☑	
313	LH534	Frankfurt, Germany	Caracas, Venezuela	20.10.2010	☑	☑	☑	☑	
312	LH741	Osaka, Japan	Frankfurt, Germany	24.09.2010	☑	☑	☑	☑	WG empty
311	LH740	Frankfurt, Germany	Osaka, Japan	23.09.2010	☑	☑	☑	☑	
310	LH535	Caracas, Venezuela	Frankfurt, Germany	22.09.2010	☑	☑	☑	☑	
309	LH534	Frankfurt, Germany	Caracas, Venezuela	22.09.2010	☑	☑	☑	☑	
308	LH741	Osaka, Japan	Frankfurt, Germany	27.08.2010	☑	☑	☑	☑	WG empty
307	LH740	Frankfurt, Germany	Osaka, Japan	26.08.2010	☑	☑	☑	☑	
306	LH535	Caracas, Venezuela	Frankfurt, Germany	25.08.2010	☑	☑	☑	☑	
305	LH534	Frankfurt, Germany	Caracas, Venezuela	25.08.2010	☑	☑	☑	☑	
304	LH741	Osaka, Japan	Frankfurt, Germany	29.07.2010	☑	☑	☑	☑	WG empty
303	LH740	Frankfurt, Germany	Osaka, Japan	28.07.2010	☑	☑	☑	☑	
302	LH535	Caracas, Venezuela	Frankfurt, Germany	27.07.2010	☑	☑	☑	☑	
301	LH534	Frankfurt, Germany	Caracas, Venezuela	27.07.2010	☑	☑	☑	☑	
300	LH741	Osaka, Japan	Frankfurt, Germany	24.06.2010	☑	☑	☑	☑	Incomplete
299	LH740	Frankfurt, Germany	Osaka, Japan	23.06.2010	☑	☑	☑	☑	Incomplete
298	LH535	Caracas, Venezuela	Frankfurt, Germany	22.06.2010	☑	☑	☑	☑	Incomplete

Continued on next page

Table B.1 – *Continued from previous page*

297	LH534	Frankfurt, Germany	Caracas, Venezuela	22.06.2010	☑	☑	☑	☑	Incomplete
296	LH8850	Frankfurt, Germany	75N	19.05.2010	□	□	□	□	Volcanic flight
295	LH8850	Frankfurt, Germany	Ireland	16.05.2010	□	□	□	□	Volcanic flight
294	LH8936	Frankfurt, Germany	Baltic Sea - North Sea	20.04.2010	□	□	□	□	Volcanic flight
293	LH431	Chicago, USA	Frankfurt, Germany	29.10.2009	☑	☑	□	☑	
292	LH430	Frankfurt, Germany	Chicago, USA	29.10.2009	☑	☑	□	☑	
291	LH577	Cape Town, South Africa	Frankfurt, Germany	28.10.2009	☑	☑	□	☑	
290	LH576	Frankfurt, Germany	Cape Town, South Africa	27.10.2009	☑	☑	□	☑	
289	LH493	Vancouver, Canada	Frankfurt, Germany	24.09.2009	☑	☑	□	☑	
288	LH492	Frankfurt, Germany	Vancouver, Canada	24.09.2009	☑	☑	□	☑	
287	LH535	Caracas, Venezuela	Frankfurt, Germany	23.09.2009	☑	☑	□	☑	
286	LH534	Frankfurt, Germany	Caracas, Venezuela	23.09.2009	☑	☑	□	☑	
285	LH493	Vancouver, Canada	Frankfurt, Germany	28.08.2009	☑	☑	□	☑	
284	LH492	Frankfurt, Germany	Vancouver, Canada	27.08.2009	☑	☑	□	☑	
283	LH535	Caracas, Venezuela	Frankfurt, Germany	26.08.2009	☑	☑	□	☑	
282	LH534	Frankfurt, Germany	Caracas, Venezuela	26.08.2009	□	□	□	□	Missing data
281	LH493	Vancouver, Canada	Frankfurt, Germany	23.07.2009	☑	☑	☑	☑	
280	LH492	Frankfurt, Germany	Vancouver, Canada	23.07.2009	☑	☑	□	☑	
279	LH535	Caracas, Venezuela	Frankfurt, Germany	23.07.2009	☑	☑	□	☑	
278	LH534	Frankfurt, Germany	Caracas, Venezuela	22.07.2009	☑	☑	□	☑	
277	LH493	Vancouver, Canada	Frankfurt, Germany	25.06.2009	□	□	□	□	No power
276	LH492	Frankfurt, Germany	Vancouver, Canada	24.06.2009	□	□	□	□	No power
275	LH535	Caracas, Venezuela	Frankfurt, Germany	24.06.2009	□	□	□	□	Communication loss
274	LH534	Frankfurt, Germany	Caracas, Venezuela	23.06.2009	☑	☑	☑	□	
273	LH741	Osaka, Japan	Frankfurt, Germany	28.05.2009	□	□	□	□	Communication loss
272	LH740	Frankfurt, Germany	Osaka, Japan	27.05.2009	□	□	□	□	NDIR malfunction
271	LH447	Denver, USA	Frankfurt, Germany	27.05.2009	□	□	□	□	NDIR malfunction
270	LH446	Frankfurt, Germany	Denver, USA	26.05.2009	□	□	□	□	Communication loss

Continued on next page

Table B.1 – *Continued from previous page*

269	LH493	Vancouver, Canada	Frankfurt, Germany	24.04.2009	☑	☑	☑	☐	WG empty
268	LH492	Frankfurt, Germany	Vancouver, Canada	23.04.2009	☑	☑	☑	☐	
267	LH535	Caracas, Venezuela	Frankfurt, Germany	22.04.2009	☑	☑	☑	☐	
266	LH534	Frankfurt, Germany	Caracas, Venezuela	22.04.2009	☑	☑	☑	☐	
265	LH465	Orlando USA	Frankfurt, Germany	13.03.2009	☑	☑	☑	☐	WG empty
264	LH464	Frankfurt, Germany	Orlando USA	12.03.2009	☑	☑	☑	☐	
263	LH577	Cape Town, South Africa	Frankfurt, Germany	11.03.2009	☑	☑	☑	☐	
262	LH576	Frankfurt, Germany	Cape Town, South Africa	10.03.2009	☑	☑	☑	☑	
261	LH759	Chennai, India	Frankfurt, Germany	12.12.2008	☐	☐	☐	☐	NDIR malfunction
260	LH758	Frankfurt, Germany	Chennai, India	12.12.2008	☑	☑	☑	☐	
259	LH759	Chennai, India	Frankfurt, Germany	11.12.2008	☑	☑	☑	☐	
258	LH758	Frankfurt, Germany	Chennai, India	11.12.2008	☑	☑	☑	☐	
257	LH759	Chennai, India	Frankfurt, Germany	15.11.2008	☑	☑	☑	☐	Incomplete
256	LH758	Frankfurt, Germany	Chennai, India	15.11.2008	☑	☑	☑	☐	
255	LH759	Chennai, India	Frankfurt, Germany	14.11.2008	☑	☑	☑	☐	
254	LH758	Frankfurt, Germany	Chennai, India	14.11.2008	☑	☑	☑	☐	
253	LH759	Chennai, India	Frankfurt, Germany	15.10.2008	☑	☑	☑	☐	
252	LH758	Frankfurt, Germany	Chennai, India	15.10.2008	☑	☑	☑	☐	
251	LH759	Chennai, India	Frankfurt, Germany	11.09.2008	☑	☑	☑	☐	
250	LH758	Frankfurt, Germany	Chennai, India	11.09.2008	☑	☑	☑	☐	
249	LH759	Chennai, India	Frankfurt, Germany	10.09.2008	☑	☑	☑	☐	
248	LH758	Frankfurt, Germany	Chennai, India	10.09.2008	☑	☑	☑	☐	
247	LH759	Chennai, India	Frankfurt, Germany	14.08.2008	☑	☑	☑	☐	
246	LH758	Frankfurt, Germany	Chennai, India	14.08.2008	☑	☑	☑	☐	
245	LH759	Chennai, India	Frankfurt, Germany	13.08.2008	☑	☑	☑	☐	
244	LH758	Frankfurt, Germany	Chennai, India	13.08.2008	☑	☑	☑	☐	
243	LH447	Denver, USA	Frankfurt, Germany	17.07.2008	☑	☑	☑	☐	
242	LH446	Frankfurt, Germany	Denver, USA	16.07.2008	☐	☐	☐	☐	Missing data

Continued on next page

Table B.1 – *Continued from previous page*

241	LH759	Chennai, India	Frankfurt, Germany	15.07.2008	☑	☑	☑	☐	
240	LH758	Frankfurt, Germany	Chennai, India	15.07.2008	☑	☑	☑	☐	
239	LH759	Chennai, India	Frankfurt, Germany	19.06.2008	☐	☐	☐	☐	NDIR malfunction
238	LH758	Frankfurt, Germany	Chennai, India	19.06.2008	☐	☐	☐	☐	NDIR malfunction
237	LH759	Chennai, India	Frankfurt, Germany	18.06.2008	☐	☐	☐	☐	NDIR malfunction
236	LH758	Frankfurt, Germany	Chennai, India	18.06.2008	☐	☐	☐	☐	NDIR malfunction
235	LH759	Chennai, India	Frankfurt, Germany	29.05.2008	☑	☐	☐	☐	WG empty
234	LH758	Frankfurt, Germany	Chennai, India	29.05.2008	☑	☑	☑	☐	WG empty
233	LH759	Chennai, India	Frankfurt, Germany	28.05.2008	☑	☑	☑	☐	
232	LH758	Frankfurt, Germany	Chennai, India	28.05.2008	☑	☑	☑	☐	
231	LH759	Chennai, India	Frankfurt, Germany	24.04.2008	☑	☐	☐	☐	WG empty
230	LH758	Frankfurt, Germany	Chennai, India	24.04.2008	☑	☑	☐	☐	WG empty
229	LH759	Chennai, India	Frankfurt, Germany	23.04.2008	☑	☑	☐	☐	
228	LH758	Frankfurt, Germany	Chennai, India	23.04.2008	☑	☑	☑	☐	
227	LH789	Guangzhou, China	Frankfurt, Germany	27.03.2008	☑	☑	☐	☐	
226	LH789	Manila, Philippines	Guangzhou, China	27.03.2008	☑	☑	☐	☐	
225	LH788	Guangzhou, China	Manila, Philippines	27.03.2008	☑	☑	☐	☐	
224	LH788	Frankfurt, Germany	Guangzhou, China	26.03.2008	☑	☑	☐	☐	
223	LH789	Guangzhou, China	Frankfurt, Germany	26.02.2008	☑	☑	☐	☐	
222	LH789	Manila, Philippines	Guangzhou, China	26.02.2008	☑	☑	☐	☐	
221	LH788	Guangzhou, China	Manila, Philippines	26.02.2008	☑	☑	☐	☐	
220	LH788	Frankfurt, Germany	Guangzhou, China	25.02.2008	☑	☑	☐	☐	
219	LH447	Denver, USA	Frankfurt, Germany	18.12.2007	☑	☑	☐	☑	
218	LH446	Frankfurt, Germany	Denver, USA	17.12.2007	☑	☑	☐	☑	
217	LH789	Guangzhou, China	Frankfurt, Germany	14.11.2007	☐	☐	☐	☐	No power
216	LH789	Manila, Philippines	Guangzhou, China	14.11.2007	☑	☑	☐	☑	
215	LH788	Guangzhou, China	Manila, Philippines	14.11.2007	☑	☑	☐	☑	
214	LH788	Frankfurt, Germany	Guangzhou, China	13.11.2007	☑	☑	☐	☑	

Continued on next page

Table B.1 – *Continued from previous page*

213	LH789	Guangzhou, China	Frankfurt, Germany	25.10.2007	☑	☑	☐	☑	WG empty
212	LH789	Manila, Philippines	Guangzhou, China	25.10.2007	☑	☑	☐	☑	
211	LH788	Guangzhou, China	Manila, Philippines	25.10.2007	☑	☑	☐	☑	
210	LH788	Frankfurt, Germany	Guangzhou, China	24.10.2007	☑	☑	☐	☑	
209	LH441	Houston, USA	Frankfurt, Germany	18.09.2007	☐	☐	☐	☐	NDIR malfunction
208	LH440	Frankfurt, Germany	Houston, USA	18.09.2007	☑	☑	☐	☑	WG empty
207	LH471	Toronto, Canada	Frankfurt, Germany	18.09.2007	☑	☑	☐	☑	
206	LH470	Frankfurt, Germany	Toronto, Canada	17.09.2007	☑	☑	☐	☑	
205	LH789	Guangzhou, China	Frankfurt, Germany	15.08.2007	☑	☐	☑	☑	Incomplete
204	LH789	Manila, Philippines	Guangzhou, China	15.08.2007	☑	☐	☑	☑	
203	LH788	Guangzhou, China	Manila, Philippines	15.08.2007	☑	☐	☑	☑	
202	LH788	Frankfurt, Germany	Guangzhou, China	14.08.2007	☑	☐	☑	☑	
201	LH789	Guangzhou, China	Frankfurt, Germany	18.07.2007	☐	☐	☐	☐	Tubing broken
200	LH789	Manila, Philippines	Guangzhou, China	18.07.2007	☐	☐	☐	☐	Tubing broken
199	LH788	Guangzhou, China	Manila, Philippines	18.07.2007	☑	☐	☑	☑	
198	LH788	Frankfurt, Germany	Guangzhou, China	17.07.2007	☑	☐	☑	☑	
197	LH789	Guangzhou, China	Frankfurt, Germany	22.06.2007	☑	☑	☑	☑	
196	LH789	Manila, Philippines	Guangzhou, China	22.06.2007	☑	☑	☑	☑	
195	LH788	Guangzhou, China	Manila, Philippines	22.06.2007	☑	☐	☐	☐	
194	LH788	Frankfurt, Germany	Guangzhou, China	21.06.2007	☑	☐	☐	☐	
193	LH789	Guangzhou, China	Frankfurt, Germany	23.05.2007	☑	☑	☑	☑	
192	LH789	Manila, Philippines	Guangzhou, China	23.05.2007	☑	☑	☑	☐	
191	LH788	Guangzhou, China	Manila, Philippines	23.05.2007	☑	☑	☑	☐	
190	LH788	Frankfurt, Germany	Guangzhou, China	22.05.2007	☑	☑	☑	☑	

Appendix C

Data processing script

The following code is the main Matlab script, which was written to process the flights on a flight-by-flight basis.

```
% Program for the O2 analyser from Bern
%
clear all

% define colors for plotting
lightred = [1.000, 0.600, 0.750];
darkred  = [0.900, 0.100, 0.200];
lightblue = [0.650, 0.930, 1.000];
darkblue = [0.100, 0.700, 1.000];
lightorange = [1.000, 0.750, 0.500];
darkorange = [1.000, 0.500, 0.000];
lightgreen = [0.700, 1.000, 0.550];
darkgreen = [0.100, 0.900, 0.000];

datapath = '\\phkup4\ms\Bigler_Iwan\CARIBIC\data';

workdir=pwd();
cd(datapath);
[Files , Path] = uigetfile({'*.txt','Data_files';'*.*','All_files'}, 'Select_raw_data' , 'MultiSelect', 'on'
    );
cd(workdir);

Files = cellstr(Files);
Files = sort(Files);

if (isequal(Files, 0))
  uiwait(errordlg('No_file(s)_selected_!','File_selection_error'),'modal');
  return;
end

% Read flight number and destinations
[~, plotpathname] = fileparts(Path(1:end-1));
caribicno         = str2double(plotpathname(1:3));
destinationA      = plotpathname(5:7);
destinationB      = plotpathname(9:11);

% Loop over all selected files
%
fileno = numel(Files);
raw = cell(fileno , 1);
for i = 1 : fileno

  % Read file
  fid = fopen(fullfile(Path, Files{i}), 'r');
```

```
  line = fgets(fid);
  if (~isempty(strfind(line, 'Date')))
    headerline = 1;
  else
    headerline = 0;
  end
  frewind(fid);

  raw{i} = textscan(fid, '%s %s %s %f %f %f %f %f %f %f %f %f %f %f %f %f %f %f %f %f %f %f',...
                    'HeaderLines', headerline, 'MultipleDelimsAsOne', 1, 'CollectOutput', true);
  fclose(fid);
end

% Combine data from selected files
%
for i = 1 : fileno
  date = datenum(raw{i}{1}(:,1), 'dd.mm.yy', 2000) + ...
         datenum(raw{i}{1}(:,2), 'HH:MM:SS') - fix(datenum(raw{i}{1}(:,2), 'HH:MM:SS'));
  if (i == 1)
    alltimes = date;
    allmodes = raw{i}{1}(:,3);
    alldata = raw{i}{2};
  else
    if (date(1) <= alltimes(end))
      ind = find(date == alltimes(end));
    else
      ind = 0;
    end
    alltimes = [alltimes ; date(ind+1:end)];
    allmodes = [allmodes ; raw{i}{1}(ind+1:end,3)];
    alldata  = [alldata ; raw{i}{2}(ind+1:end, :)];
  end
end

timeno = numel(alltimes);

% Automatic time corrections
if (caribicno >= 224) && (caribicno <= 227)
    timecorr = (59+56*60+2*3600)/86400; % +2:56:59
    alltimes = alltimes + timecorr;
end;
if (caribicno == 295)
    timecorr = (1+59*60)/86400; % +0:59:01
    alltimes = alltimes + timecorr;
end;
if (caribicno >= 301) && (caribicno <= 304)
    timecorr = (49+58*60)/86400; % +0:58:49
    alltimes = alltimes + timecorr;
end;
if (caribicno >= 329) && (caribicno <= 332)
    timecorr = (7+59*60)/86400; % +0:59:07
    alltimes = alltimes + timecorr;
end;
if (caribicno >= 373) && (caribicno <= 378)
    alltimes = arrayfun(@(alltimes) addtodate(alltimes, 1, 'year'), alltimes);
end;
if (caribicno >= 379 && (caribicno <= 416))
    alltimes = arrayfun(@(alltimes) addtodate(alltimes, 1, 'year'), alltimes);
    alltimes = arrayfun(@(alltimes) addtodate(alltimes, -1, 'day'), alltimes);
end;
if (caribicno >= 417)
    alltimes = arrayfun(@(alltimes) addtodate(alltimes, 1, 'year'), alltimes);
end;

% de-MUX
alldata(alldata(:,12) ~= 0, 8)  = NaN; % Honeywell AWM3100
alldata(alldata(:,12) ~= 1, 9)  = NaN; % MKS Regler (Baratron)
alldata(alldata(:,12) ~= 2, 10) = NaN; % MKS 640
alldata(alldata(:,12) ~= 3, 11) = NaN; % Honeywell voltage input

FC1_original        = alldata(:,1);
```

```
FC2_original        = alldata(:,2);
FC3_original        = alldata(:,3);
FC4_original        = alldata(:,4);
p_original          = alldata(:,5);
boxt_original       = alldata(:,6);
messfluss_original  = alldata(:,7);
wasteflux_original  = alldata(:,8);
mksregler_original  = alldata(:,9);
mks640_original     = alldata(:,10);
CO2_original        = alldata(:,13);
H2O_original        = alldata(:,16);
t_original          = alldata(:,19);
refp_original       = alldata(:,20);

% Remove invalid fuel cell measurements
alldata(alldata(:,1) <= 0, 1)    = NaN;
alldata(alldata(:,2) <= 0, 2)    = NaN;
alldata(alldata(:,3) <= 0, 3)    = NaN;
alldata(alldata(:,4) <= 0, 4)    = NaN;
% Remove other invalid values (smaller/equal to 0)
alldata(alldata(:,5) <= 0, 5)    = NaN; % p30
alldata(alldata(:,6) <= 0, 6)    = NaN; % Temp FC box
alldata(alldata(:,7) <= 0, 7)    = NaN; % Messfluss MKS179
alldata(alldata(:,8) <= 0, 8)    = NaN; % Wastefluss AWM3100 (MUX)
alldata(alldata(:,9) <= 0, 9)    = NaN; % MKS differential (MUX)
alldata(alldata(:,10) <= 0, 10) = NaN; % MKS 640 (MUX)
alldata(alldata(:,11) <= 0, 11) = NaN; % Honeywell input (MUX)
alldata(alldata(:,13) <= 0, 13) = NaN; % Licor CO2 mV raw
alldata(alldata(:,14) <= 0, 14) = NaN; % Licor ppm calculated
alldata(alldata(:,15) <= 0, 15) = NaN; % Licor ppm calculated ref=395
alldata(alldata(:,16) <= 0, 16) = NaN; % Licor H2O mV raw
alldata(alldata(:,17) <= 0, 17) = NaN; % Licor H2O mmol/mol
alldata(alldata(:,18) <= 0, 18) = NaN; % Licor H2O mmol/mol d
alldata(alldata(:,19) <= 0, 19) = NaN; % Licor temp
alldata(alldata(:,20) <= 0, 20) = NaN; % Ref pressure

% Calculate parameters
flow_raw       = alldata(:, 7) .* 40;
wasteflux_raw = 9.3259 .* alldata(:, 8) .^ 2 - 8.0425 .* alldata(:, 8) + 0.6024;
mksregler_raw = 1120 / (273.15 + 20) * (273.15 + alldata(:,6)) + 2 * alldata(:,9);
mks640_raw     = alldata(:, 10) ./ 5 .* 1333;

% Export raw data as a single hires Excel-File (requires Excel)
filename = fullfile(Path, ['data_hires-' num2str(caribicno) '.xlsx']);
if exist(filename, 'file') == 0;
    excelexport = horzcat(vertcat('UTC', cellstr(datestr(alltimes, 'dd.mm.yyyy HH:MM:SS'))), vertcat('config
        ', allmodes), vertcat('FC1 [V]', num2cell(FC1_original)), vertcat('FC2 [V]', num2cell(FC2_original)
        ), vertcat('FC3 [V]', num2cell(FC3_original)), vertcat('FC4 [V]', num2cell(FC4_original)), vertcat(
        'Inlet p [hPa]', num2cell(p_original * 160)), vertcat('Box T [°C]', num2cell(boxt_original)),
        vertcat('Messfluss [ml/min]', num2cell(flow_raw)), vertcat('Wasteflux [ml/min]', num2cell(
        wasteflux_raw)), vertcat('MKS Regler [hPa]', num2cell(mksregler_raw)), vertcat('MKS640 [hPa]',
        num2cell(mks640_raw)), vertcat('CO2 [mV]', num2cell(CO2_original)), vertcat('H2O [mV]', num2cell(
        H2O_original)), vertcat('Licor T [°C]', num2cell(t_original)), vertcat('Ref p [hPa]', num2cell(
        refp_original*10)));
    xlswrite(filename, excelexport);
end

% Remove clipping FC measurements
alldata(alldata(:, 1) == 9.997559, 1) = NaN;
alldata(alldata(:, 3) == 9.997559, 3) = NaN;
alldata(alldata(:, 4) == 9.997559, 4) = NaN;

% Look for 1 min gaps and exclude O2 & CO2 data of the affected
% configuration after the occurrence
for i = 2 : timeno;
    if (alltimes(i)-alltimes(i-1))* 86400.0 > 20;
        uiwait(warndlg(sprintf('Gap found at %s. Press OK to continue.', datestr(alltimes(i))), 'data
            skipped warning'));
        indl = find(strcmp(allmodes{i}, allmodes(i:end)) == 0, 1, 'first') - 1; % find number of seconds
            until the last entry of the current configuration
```

```
        indf = find(strcmp(allmodes{i}, allmodes(1:i)) == 0, 1, 'last') + 1; % find first entry after config
            switch
        alldata(indf:i+ind1,13) = NaN; % Remove CO2 measurements of the entire affected config
        alldata(indf:i+ind1,1)  = NaN; % Remove O2 measurements of the entire config
        alldata(indf:i+ind1,3)  = NaN;
        alldata(indf:i+ind1,4)  = NaN;
    end
end

% Outlier removal for O2 (3 sigma)
i = 1;
ind110 = [];
while(i <= timeno)
  ind = find(strcmp(allmodes{i}, allmodes(i:end)) == 0, 1, 'first') - 1;
  if (isempty(ind))
    ind = numel(allmodes(i:end));
    if (allmodes{(i-1)+ind-120} ~= allmodes{i})
      break;
    end
  end
  t2 = alltimes((i-1)+ind) - 10.0/86400.0;
  t1 = t2 - 109.0/86400.0;
  ind2 = find(and(alltimes >= t1, alltimes <= t2));
  ind110 = vertcat(ind110, ind2);
  ind3 = alldata(ind2, 1) > nanmean(alldata(ind2, 1)) + 3 * nanstd(alldata(ind2, 1)) | alldata(ind2, 1) <
      nanmean(alldata(ind2, 1)) - 3 * nanstd(alldata(ind2, 1));
  alldata(ind2(ind3), 1) = NaN;
  ind3 = alldata(ind2, 3) > nanmean(alldata(ind2, 3)) + 3 * nanstd(alldata(ind2, 3)) | alldata(ind2, 3) <
      nanmean(alldata(ind2, 3)) - 3 * nanstd(alldata(ind2, 3));
  alldata(ind2(ind3), 3) = NaN;
  ind3 = alldata(ind2, 4) > nanmean(alldata(ind2, 4)) + 3 * nanstd(alldata(ind2, 4)) | alldata(ind2, 4) <
      nanmean(alldata(ind2, 4)) - 3 * nanstd(alldata(ind2, 4));
  alldata(ind2(ind3), 4) = NaN;
  i = i + ind;
end

% Outlier removal for CO2 (3 sigma)
i = 1;
while(i <= timeno)
  ind = find(strcmp(allmodes{i}, allmodes(i:end)) == 0, 1, 'first') - 1;
  if (isempty(ind))
    ind = numel(allmodes(i:end));
    if (allmodes{(i-1)+ind-300} ~= allmodes{i})
      break;
    end
  end
  % for the last 5 minutes: remove outliers (3sigma)
  t2 = alltimes((i-1)+ind) - 10.0/86400.0;
  t1 = t2 - 290.0/86400.0;
  ind2 = find(and(alltimes >= t1, alltimes <= t2));
  % remove outliers of CO2 measurements
  ind3 = alldata(ind2, 13) > nanmedian(alldata(ind2, 13)) + 3 * nanstd(alldata(ind2, 13)) | alldata(ind2,
      13) < nanmedian(alldata(ind2, 13)) - 3 * nanstd(alldata(ind2, 13));
  alldata(ind2(ind3), 13) = NaN;
  i = i + ind;
end

% Rough CO2 correction
% 30.5 and 0.26 are derived from averaging the corrections for first
% and last flights (T vs deltaCO2)
% 0.241 is the relationship mV -> ppm
alldata(:, 13) = alldata(:,13) + ((alldata(:, 19) - 30.055) * 0.244 / 0.241);

% Correlation temp with MKS Regler
ind = or(strcmp(allmodes, 'A'), strcmp(allmodes, 'D')) & and((alltimes >= alltimes(1)), (alltimes <=
    alltimes(1)+1.5/24)) & ~isnan(mksregler_raw) & ~isnan(alldata(:, 2));
coefficientsmks = polyfit(alldata(ind,2),mksregler_raw(ind),2);
mksregler_raw = mksregler_raw - (coefficientsmks(1) * alldata(:, 2) .^2 + coefficientsmks(2) * alldata(:, 2)
    + coefficientsmks(3)) + nanmedian(mksregler_raw);

% Calculate median for the muxed parameters
```

```
i = 1;
while(i <= timeno)
  indstart = find(strcmp(allmodes{i}, allmodes(1:i))   == 0, 1, 'last') + 1;
  if (isempty(indstart))
      indstart = 1;
  end
  indend   = find(strcmp(allmodes{i}, allmodes(i:end)) == 0, 1, 'first') - 1;
  if (isempty(indend))
    indend = numel(allmodes(i:end));
  end
  wasteflux(indstart:i + indend - 1) = nanmedian(wasteflux_raw(indstart:i + indend - 1));
  mksregler(indstart:i + indend - 1) = nanmedian(mksregler_raw(indstart:i + indend - 1));
  mks640   (indstart:i + indend - 1) = nanmedian(mks640_raw   (indstart:i + indend - 1));
  i = i + indend;
end
wasteflux = wasteflux';
mksregler = mksregler';

diffflow  = flow_raw - wasteflux;

% correction of FC for pressure
alldata(:, 1) = alldata(:, 1) .* (1013.25 ./ mksregler);
alldata(:, 3) = alldata(:, 3) .* (1013.25 ./ mksregler);
alldata(:, 4) = alldata(:, 4) .* (1013.25 ./ mksregler);

i = 1;
k = 0;
meantimes = zeros(1,1);
meanmode          = cell(1,1);
meanFCforspline   = zeros(1,4);
while(i <= timeno)
  ind = find(strcmp(allmodes{i}, allmodes(i:end)) == 0, 1, 'first') -1;
  if (isempty(ind))
    ind = numel(allmodes(i:end));
    if (allmodes{(i-1)+ind-120} ~= allmodes{i})
      break;
    end
  end
  % only include the last 110 seconds
  t2 = alltimes((i-1)+ind) - 10.0/86400.0;
  t1 = t2 - 109.0/86400.0;
  ind2 = find(and(alltimes >= t1, alltimes <= t2));
  k = k+1;
  meantimes(k)     = nanmean(alltimes(ind2));
  meanmode(k)              = allmodes(i);
  meanFCforspline(k, :)   = nanmean(alldata(ind2, 1:4));
  i = i + ind;
end

%FC1 spline
FC1spline = meanFCforspline(:,1);
FC1spline(~strcmp(meanmode, 'D') & ~strcmp(meanmode, 'E') & ~strcmp(meanmode, 'F')) = NaN;
FC1yesno = sum(~isnan(FC1spline)) > 4;
if FC1yesno == 1
    clear e_d;
    x_d=meantimes(~isnan(FC1spline));
    y_d=FC1spline(~isnan(FC1spline));
    e_d(1:length(x_d),1) = nanstd(FC1spline);
    cop=0.00833; % Cutoff period [years]
    resolution=length(alldata); % Number of points where spline is calculated
    [num_p,dummy]=size(x_d) % Evaluate number of data points
    w_d=rdivide(1,e_d.^2);
    w_d=w_d/sum(w_d)*num_p;
    dx=abs(x_d(1)-x_d(length(x_d)))/num_p; % Data spacing
    lambda=(cop/(2*pi))^4/dx; % Calculate lambda
    p=1/(1+lambda); % Calculate smoothing factor p
    x_gr=linspace(alltimes(1,1),alltimes(end),resolution); % Define grid where spline is calculated
    x_gr=x_gr.';
    data_sp=csaps(x_d,y_d,p,x_gr,w_d); % Spline through data
    % Plot data points
    hf = figure('Name', sprintf('FC1_spline_(%s)', plotpathname), ...
```

```
                'NumberTitle', 'off', ...
                'Position', [100 100 1100 750]);
    plot(x_d,y_d,'o-','color',darkred);
    xlabel('Time [d]');
    ylabel('FC1 signal [V]');
    hold on;
    plot(x_gr,data_sp,'-','color',darkblue,'LineWidth',2)
    grid on;
    alldata(:,1) = alldata(:,1) - data_sp;
    plot(x_gr,alldata(:,1),'-','color',darkred);
    hold off;
end

%FC3 spline
FC3spline = meanFCforspline(:,3);
FC3spline(~strcmp(meanmode, 'D') & ~strcmp(meanmode, 'E') & ~strcmp(meanmode, 'F')) = NaN;
FC3yesno = sum(~isnan(FC3spline)) > 4;
if FC3yesno == 1
    clear e_d;
    x_d=meantimes(~isnan(FC3spline));
    y_d=FC3spline(~isnan(FC3spline));
    e_d(1:length(x_d),1) = nanstd(FC3spline);
    cop=0.00833; % Cutoff period [years]
    resolution=length(alldata); % Number of points where spline is calculated
    [num_p,dummy]=size(x_d); % Evaluate number of data points
    w_d=rdivide(1,e_d.^2);
    w_d=w_d/sum(w_d)*num_p;
    dx=abs(x_d(1)-x_d(length(x_d)))/num_p;% Data spacing
    lambda=(cop/(2*pi))^4/dx; % Calculate lambda
    p=1/(1+lambda); % Calculate smoothing factor p
    x_gr=linspace(alltimes(1,1),alltimes(end),resolution); % Define grid where spline is calculated
    x_gr=x_gr.';
    data_sp=csaps(x_d,y_d,p,x_gr,w_d); % Spline through data
    % Plot data points
    hf = figure('Name', sprintf('FC3 spline (%s)', plotpathname), ...
                'NumberTitle', 'off', ...
                'Position', [100 100 1100 750]);
    plot(x_d,y_d,'o-','color',darkred);
    xlabel('Time [d]');
    ylabel('FC3 signal [V]');
    hold on;
    plot(x_gr,data_sp,'-','color',darkblue,'LineWidth',2)
    grid on;
    alldata(:,3) = alldata(:,3) - data_sp; % subtract spline from raw data
    plot(x_gr,alldata(:,3),'-','color',darkred);
    hold off;
end

%FC4 spline
FC4spline = meanFCforspline(:,4);
FC4spline(~strcmp(meanmode, 'D') & ~strcmp(meanmode, 'E') & ~strcmp(meanmode, 'F')) = NaN;
FC4yesno = sum(~isnan(FC4spline)) > 4;
if FC4yesno == 1
    clear e_d;
    x_d=meantimes(~isnan(FC4spline));
    y_d=FC4spline(~isnan(FC4spline));
    e_d(1:length(x_d),1) = nanstd(FC4spline);
    cop=0.00833; % Cutoff period [years]
    resolution=length(alldata); % Number of points where spline is calculated
    [num_p,dummy]=size(x_d); % Evaluate number of data points
    w_d=rdivide(1,e_d.^2);
    w_d=w_d/sum(w_d)*num_p;
    dx=abs(x_d(1)-x_d(length(x_d)))/num_p; % Data spacing
    lambda=(cop/(2*pi))^4/dx; % Calculate lambda
    p=1/(1+lambda); % Calculate smoothing factor p
    x_gr=linspace(alltimes(1,1),alltimes(end),resolution); % Define grid where spline is calculated
    x_gr=x_gr.';
    data_sp=csaps(x_d,y_d,p,x_gr,w_d); % Spline through data
    % Plot data points
    hf = figure('Name', sprintf('FC4 spline (%s)', plotpathname), ...
                'NumberTitle', 'off', ...
```

```
                'Position', [100 100 1100 750]);
    plot(x_d,y_d,'o-','color',darkred);
    xlabel('Time [d]');
    ylabel('FC4 signal [V]');
    hold on;
    plot(x_gr,data_sp,'-','color',darkblue,'LineWidth',2)
    grid on;
    alldata(:,4) = alldata(:,4) - data_sp; % subtract spline from raw data
    plot(x_gr,alldata(:,4),'-','color',darkred);
    hold off;
end

% Calculate averages for last 110 seconds for
% each measurement mode
%
i = 1;
k = 0;
meantimes = zeros(1,1);
meanmode  = cell(1,1);
meandata  = zeros(1,20);
meanstdev = zeros(1,20);
while(i <= timeno)
  ind = find(strcmp(allmodes{i}, allmodes(i:end)) == 0, 1, 'first') -1;
  if (isempty(ind))
    ind = numel(allmodes(i:end));
    if (allmodes{(i-1)+ind-120} ~= allmodes{i})
      break;
    end
  end
  % only include the last 110 seconds
  t2 = alltimes((i-1)+ind) - 10.0/86400.0;
  t1 = t2 - 109.0/86400.0;
  ind2 = find(and(alltimes >= t1, alltimes <= t2));
  k = k+1;
  meantimes(k)     = nanmean(alltimes(ind2));
  meanmode(k)      = allmodes(i);
  meandata(k, :)   = nanmean(alldata(ind2, :));
  meanstdev(k, :) = nanstd(alldata(ind2, :));
  i = i + ind;
end

meantimes = meantimes';

% Output result to file
%
meanno = k;
saveto = ['data_mean-' plotpathname(1:3) '.txt'];
filename = fullfile(Path, saveto);
fid = fopen(filename, 'w');
for i = 1 : meanno
  fprintf(fid, '%s\t%s', datestr(meantimes(i), 'dd.mm.yy\tHH:MM:SS', 2000), meanmode{i});
  for j = 1 : size(meandata, 2)
    fprintf(fid, '\t%f\t%f', meandata(i, j), meanstdev(i, j));
  end
  fprintf(fid, '\r\n');
end
fclose(fid);

% check for empty WG cylinder
nowg = 0;
i = 3;
while(i <= numel(meantimes) - 3)
    if meandata(i, 20) - meandata(i + 1, 20) > 0.2;
        nowg     = 1;
        indnowg = i - 2;
        break;
    end
    i = i + 1;
end

cylinders = importdata(fullfile(datapath, 'cylinders.txt'), '\t', 5);
```

```
ind_cyl = find(cylinders.data(:,1) == caribicno);

% CO2 calibration gases (default values)
CO2_high_span = cylinders.data(ind_cyl,2);
CO2_low_span  = cylinders.data(ind_cyl,3);
CO2_workgas   = cylinders.data(ind_cyl,4);

% Instrument CO2 calibration values
C2_T = 40.12;
C2_K = 18158;
C2_A = 1.35364e-1;
C2_B = 1.25591e-5;
C2_C = 4.37872e-9;
C2_D = -3.3379e-13;
C2_E = 1.90262e-17;

% Instrument water calibration values
H2_T = 40.22;
H2_K = 18401;
H2_A = 6.61436e-3;
H2_B = 2.17297e-6;
H2_C = 2.0124e-11;
Water_A = 1.57;

% calculate water mixing ratio (high resolution)
if (caribicno >= 162) && (caribicno <= 209)
    HSh2o = 0.05;
end
if (caribicno >= 210) && (caribicno <= 308)
    HSh2o = 0.076;
end
if (caribicno >= 309)
    HSh2o = 0.05;
end

if (caribicno >= 174) && (caribicno <= 328)
    LSh2o = 0.063;
end
if (caribicno >= 329)
    LSh2o = 0.059;
end

alldruck      = Calculate_Pressure_kPa(alldata(:, 5));
alltemperatur = alldata(:, 19);
allCO2_mV     = alldata(:, 13);

if (alltimes(end) - alltimes(1)) * 24 < 3.5;
    allwasser_raw = alldata(:, 16); - (min(alldata(:, 16))) + 1;
else
    allwasser_raw = alldata(:, 16);
end
allwasser_raw = allwasser_raw .* (101.325 ./ alldruck) .^ 0.9;
allwasser_raw = H2_A * allwasser_raw + H2_B * allwasser_raw.^2 + H2_C * allwasser_raw .^ 3;
allwasser_raw = allwasser_raw .* (H2_T + 273.15) ./ (alltemperatur + 273.15);

coefficientsh2o = [NaN NaN];
Rh2o = NaN(2,2);
if (alltimes(end) - alltimes(1)) * 24 > 3.5; % if the flight duration is less than 3.5 hours, skip the
     entire temp correction and offset correction (there are no calibrations)
    ind = or(strcmp(allmodes, 'A'), strcmp(allmodes, 'D')) & and((alltimes >= alltimes(1)+0.7/24), (alltimes
          <= alltimes(end)-0.7/24)) & ~isnan(alltimes) & ~isnan(allwasser_raw);
    wassermedian = nanmedian(allwasser_raw(ind));
    wassersigma  = mad(allwasser_raw(ind),1);
    ind = or(strcmp(allmodes, 'A'), strcmp(allmodes, 'D')) & and((alltimes >= alltimes(1)+0.7/24), (alltimes
          <= alltimes(end)-0.7/24)) & ~isnan(alltimes) & ~isnan(allwasser_raw) & allwasser_raw <
         wassermedian + 4 * wassersigma & allwasser_raw > wassermedian - 4 * wassersigma;

    coefficientsh2o = polyfit(alltemperatur(ind),allwasser_raw(ind),1);

    hf = figure('Name', sprintf('Temperature vs water mixing ratio (%s)', plotpathname), ...
                'NumberTitle', 'off', ...
```

```
                'Position', [100 100 1100 750]);
    scatter(alltemperatur(ind),allwasser_raw(ind),'.');
    lsline;
    hold on;
    title('Temperature vs water mixing ratio');
    xlabel('Temperature');
    ylabel('Water content [mmol/mol]');

    % Correction of water content with temperature
    Rh2o = corrcoef(alltemperatur(ind),allwasser_raw(ind));
    if Rh2o(2)^2 > 0.5
        allwasser = allwasser_raw - (coefficientsh2o(1) * alltemperatur + coefficientsh2o(2));
    else
        allwasser = allwasser_raw;
    end

    % Calculate mean water concentration for the calibration gases only
    meanEwater = [];
    indE = strcmp(allmodes, 'E');
    indEdouble = indE + 0;
    for i = 1 : numel(alltimes)-1
        if indEdouble(i) - indEdouble(i+1) == 1;
           t2 = alltimes(i) - 10.0/86400.0;
           t1 = t2 - 9.0/86400.0;
           ind = find(and(alltimes >= t1, alltimes <= t2));
           meanEwater = [meanEwater nanmean(allwasser(ind))];
        end
    end

    meanFwater = [];
    indF = strcmp(allmodes, 'F');
    indFdouble = indF + 0;
    for i = 1 : numel(alltimes)-1
        if indFdouble(i) - indFdouble(i+1) == 1;
            t2 = alltimes(i) - 10.0/86400.0;
            t1 = t2 - 9.0/86400.0;
            ind = find(and(alltimes >= t1, alltimes <= t2));
            meanFwater = [meanFwater nanmean(allwasser(ind))];
        end
    end

    differences = [meanEwater - HSh2o meanFwater - LSh2o];
    fprintf('differences = %.3f, %.3f, %.3f, %.3f \n', differences);
    allwasser = allwasser - min(differences);

else % if flight duration is less than 3.5 hours, just take the raw water values
    allwasser = allwasser_raw;
end

% if allwasser less than 0, set to 0
    allwasser(allwasser(:,1) < 0, 1)   = 0;

% Pressure in [kPa]
meandruck  = Calculate_Pressure_kPa(meandata(:,5));

% Calculate mean water values for last 110 seconds for
% each measurement mode
%
i = 1;
k = 0;
meanwasser = zeros(1,1);
while(i <= timeno)
  ind = find(strcmp(allmodes{i}, allmodes(i:end)) == 0, 1, 'first') -1;
  if (isempty(ind))
    ind = numel(allmodes(i:end));
    if (allmodes{(i-1)+ind-120} ~= allmodes{i})
      break;
    end
  end
  % only include the last 110 seconds
  t2 = alltimes((i-1)+ind) - 10.0/86400.0;
```

```
  t1 = t2 - 109.0/86400.0;
  ind2 = find(and(alltimes >= t1, alltimes <= t2));
  k = k+1;
  meanwasser(k, :) = nanmean(allwasser(ind2, :));
  i = i + ind;
end


% Calculate CO2 calibration from ppm to mV and
% corresponding span and offset
calno = 0;
for i = 5 : meanno
  if (meanmode{i} == 'E')
    indE = i;
    indF = i+2;

    if (indF > meanno)
      break;
    end

    CO2_high_mV = convert_Calibration_ppm_to_mV(CO2_high_span, meandata(indE, :), meanstdev(indE, :),
          meanwasser(indE), meandruck(indE), ...
                                        Water_A, C2_T, C2_A, C2_B, C2_C, C2_D, C2_E);
    CO2_low_mV  = convert_Calibration_ppm_to_mV(CO2_low_span, meandata(indF, :), meanstdev(indF, :),
          meanwasser(indF), meandruck(indF), ...
                                        Water_A, C2_T, C2_A, C2_B, C2_C, C2_D, C2_E);

    calno = calno+1;
    caltime(calno) = meantimes(indE+1);
    span(calno)    = (CO2_high_mV - CO2_low_mV)/(meandata(indE, 13) - meandata(indF, 13));
    offset(calno) = CO2_high_mV - span(calno) * meandata(indE, 13);

    fprintf('span = %.10f    offset = %.10f\n', span(calno), offset(calno));
  end
end

if (calno == 2)
    if (alltimes(end)-meantimes(indF))*24*60 < 42
        calno = 1;
%     else
%         answer = questdlg({sprintf('Second CO2 calibration at: %s UTC (%.0f min before last measurement).
      ', datestr(caltime(2)), (alltimes(end)-caltime(2))*24*60), ...
%                                 'Do you want to exclude the 2nd calibration ?'}, ...
%                               'CO2 calibration use', 'Yes', 'No', 'No');
%         if (strcmp(answer, 'Yes'))
%             calno = 1;
%         end
    end
end


% Interpolate/Extrapolate span and offset for all times
% in the high-resolution data
allspan   = zeros(timeno, 1);
alloffset = zeros(timeno, 1);

if (calno == 1)
  allspan(:)   = span(1);
  alloffset(:) = offset(1);
elseif (calno == 2)
  allspan   = span(1) + (span(2)-span(1))/(caltime(2)-caltime(1))*(alltimes - caltime(1));
  alloffset = offset(1) + (offset(2)-offset(1))/(caltime(2)-caltime(1))*(alltimes - caltime(1));
elseif (calno == 0)
    indlg_options.Resize       = 'on';
    indlg_options.WindowStyle = 'normal';
    indlg_options.Interpreter = 'none';
    answer = inputdlg({'Enter CO2 span:', 'Enter CO2 offset:'}, ...
                      'Flight contains no calibrations!', 1, ...
                      {'1.06', '-370'}, indlg_options);
    if (isempty(answer))
        return;
```

```
    end
    calno = 1;
    span(calno)    = str2double(answer{1});
    offset(calno) = str2double(answer{2});
    allspan(:)    =  span(1);
    alloffset(:) =  offset(1);
else
    fprintf('\nError: More than 2 calibrations found!\n\n');
end


% Convert high-resolution measurement values from mV(measured) to
% mV(assigned)
%
allCO2_mV = allspan .* allCO2_mV + alloffset;


% Calculate CO2 concentration in ppm
%
allCO2_mV = allCO2_mV ./ (1.0 + (Water_A - 1.0) * allwasser / 1000.0);
allCO2_mV = allCO2_mV .* (101.325 ./ alldruck);
% default: 101.3


allCO2_ppm = (C2_A * allCO2_mV + C2_B * allCO2_mV.^2 + C2_C * allCO2_mV.^3 + C2_D * allCO2_mV.^4 + C2_E *
     allCO2_mV.^5) ...
             .* (1.0 + (Water_A - 1.0) * allwasser / 1000.0) ...
             .* (alldata(:,19) + 273.15) / (C2_T + 273.15) ...
             ./ (1.0 - allwasser / 1000);


% Calculate average CO2 values over last 110s per mode
i = 1;
k = 0;
meanCO2_ppm = NaN*ones(meanno, 1);
while(i <= timeno)
  ind = find(strcmp(allmodes{i}, allmodes(i:end)) == 0, 1, 'first') -1;
  if (isempty(ind))
    ind = numel(allmodes(i:end));
    if (allmodes{(i-1)+ind-120} ~= allmodes{i})
      break;
    end
  end
  % only include the last 110 seconds
  t2 = alltimes((i-1)+ind) - 10.0/86400.0;
  t1 = t2 - 110.0/86400.0;
  ind2 = find(and(alltimes >= t1, alltimes <= t2));
  k = k+1;
  meanCO2_ppm(k) = nanmean(allCO2_ppm(ind2));
  i = i + ind;
end


% Calculate oxygen concentrations
%
%
fprintf('\nOxygen calculation:\n\n');

% Calibration gases
O2_low_span  = cylinders.data(ind_cyl,11);
O2_high_span = cylinders.data(ind_cyl,12);
O2_workgas   = cylinders.data(ind_cyl,13);

% default values for the HS calibration mode C
modeshift = 2; % config C is 2 steps after B
timeshift = 1; % the meantime of the calibration is inbetween B and C

% Possibility to use WG as HS if its O2 content is higher
% if O2_workgas > O2_high_span
%      answer = questdlg({sprintf('Workgas contains more O2 than high span'), ...
```

```
%                                   'Do you want to use the working gas also as the high span for the calibration
    ?'}, ...
%                                   'WG calibration use', 'Yes', 'No', 'No');
% end
% if (strcmp(answer, 'Yes'))
%     O2_high_span  = O2N2_workgas;
%     modeshift     = -3; % -3 for the last D config before the B config, +3 for the first config after the
    calibration
%     timeshift     = -1; % -/+ 1.5 doesn't work as it requires an integer. -1 if the previous D config is
    used
% end

% Calculate O2 calibration from ppm to V and corresponding span
O2calno = 0;
indBs = [];
indHSs = [];
for i = 5 : meanno
  if (meanmode{i} == 'B')
    indB = i; % LS
    indBs = [indBs i];
    indHS = i + modeshift; % HS; normally this is indC, but in case the WG is to be used as the HS this is
        indD
    indHSs = [indHSs i + modeshift];
    if (indHS+1 > meanno) % because of calculation below which requires a WG afterwards
      break;
    end

    fprintf('indB = %d\n', indB);

    O2calno = O2calno+1;
    O2caltime(O2calno) = meantimes(indB + timeshift);
    spanF1(O2calno)    = ((O2_high_span - O2_workgas) + (O2_workgas - O2_low_span)) / ((meandata(indHS, 1) -
        nanmean([meandata(indHS-1, 1) meandata(indHS+1, 1)])) + (nanmean([meandata(indB-1, 1) meandata(
        indB+1, 1)]) - meandata(indB, 1)));
   if spanF1(O2calno) <= 0;
       spanF1(O2calno) = NaN;
    end

    spanF3(O2calno)    = ((O2_high_span - O2_workgas) + (O2_workgas - O2_low_span)) / ((meandata(indHS, 3) -
        nanmean([meandata(indHS-1, 3) meandata(indHS+1, 3)])) + (nanmean([meandata(indB-1, 3) meandata(
        indB+1, 3)]) - meandata(indB, 3)));
  if spanF3(O2calno) <= 0;
       spanF3(O2calno) = NaN;
  end

    spanF4(O2calno)    = ((O2_high_span - O2_workgas) + (O2_workgas - O2_low_span)) / ((meandata(indHS, 4) -
        nanmean([meandata(indHS-1, 4) meandata(indHS+1, 4)])) + (nanmean([meandata(indB-1, 4) meandata(
        indB+1, 4)]) - meandata(indB, 4)));
   if spanF4(O2calno) <= 0;
       spanF4(O2calno) = NaN;
    end

    fprintf('spanF1 = %.5f   spanF3 = %.5f   spanF4 = %.5f\n', spanF1(O2calno), spanF3(O2calno), spanF4(
        O2calno));
  end
end


if (O2calno == 2) % remove NaN values from span
    if isnan(spanF1(1)) && ~isnan(spanF1(2))
        spanF1(1) = spanF1(2)
    end
    if isnan(spanF1(2)) && ~isnan(spanF1(1))
        spanF1(2) = spanF1(1)
    end

    if isnan(spanF3(1)) && ~isnan(spanF3(2))
        spanF3(1) = spanF3(2)
    end
    if isnan(spanF3(2)) && ~isnan(spanF3(1))
        spanF3(2) = spanF3(1)
```

```
    end

    if isnan(spanF4(1)) && ~isnan(spanF4(2))
        spanF4(1) = spanF4(2)
    end
    if isnan(spanF4(2)) && ~isnan(spanF4(1))
        spanF4(2) = spanF4(1)
    end
end

if (O2calno == 2)
    if (alltimes(end)-meantimes(indB + 2))*24*60 < 42
        O2calno = 1;
    elseif nowg == 1 && indnowg < indB + 2;
        O2calno = 1;
%     else
%         answer = questdlg({sprintf('Second O2 calibration at: %s UTC (%.0f min before last measurement).
     ', datestr(O2caltime(2)), (alltimes(end)-O2caltime(2))*24*60), ...
%                            'Do you want to exclude the 2nd calibration ?'}, ...
%                            'O2 calibration use', 'Yes', 'No', 'No');
%         if (strcmp(answer, 'Yes'))
%             O2calno = 1;
%         end
    end
end

% Interpolate/Extrapolate O2 span for all times
% in the low-resolution data
meanO2spanF1 = zeros(meanno, 1);
meanO2spanF3 = zeros(meanno, 1);
meanO2spanF4 = zeros(meanno, 1);

if (O2calno == 1)
  meanO2spanF1(:) = spanF1(1);
  meanO2spanF3(:) = spanF3(1);
  meanO2spanF4(:) = spanF4(1);
elseif (O2calno == 2)
  meanO2spanF1 = spanF1(1) + (spanF1(2) - spanF1(1))/(O2caltime(2)-O2caltime(1))*(meantimes - O2caltime(1));
  meanO2spanF3 = spanF3(1) + (spanF3(2) - spanF3(1))/(O2caltime(2)-O2caltime(1))*(meantimes - O2caltime(1));
  meanO2spanF4 = spanF4(1) + (spanF4(2) - spanF4(1))/(O2caltime(2)-O2caltime(1))*(meantimes - O2caltime(1));
elseif (O2calno == 0)
    indlg_options.Resize       = 'on';
    indlg_options.WindowStyle = 'normal';
    indlg_options.Interpreter = 'none';
    answer = inputdlg({'Enter O2 span (FC1):', 'Enter O2 span (FC3):', 'Enter O2 span (FC4):'}, ...
                      'Flight contains no calibrations!', 1, ...
                      {'3500', '3500', '3500'}, indlg_options);
    if (isempty(answer))
        return;
    end
    O2calno = 1;
    spanF1(O2calno) = str2double(answer{1});
    spanF3(O2calno) = str2double(answer{2});
    spanF4(O2calno) = str2double(answer{3});
    meanO2spanF1(:) = spanF1(1);
    meanO2spanF3(:) = spanF3(1);
    meanO2spanF4(:) = spanF4(1);
else
    fprintf('\nError: More than 2 calibrations found!\n\n');
end

meanFC1    = NaN*ones(meanno, 1);
meanFC3    = NaN*ones(meanno, 1);
meanFC4    = NaN*ones(meanno, 1);
meanFCmean = NaN*ones(meanno, 1);

% Calibration gases
Ar_low_span  = cylinders.data(ind_cyl,5);
Ar_high_span = cylinders.data(ind_cyl,6);
Ar_workgas   = cylinders.data(ind_cyl,7);
```

```
for i = 2 : meanno-1
  if meanmode{i} == 'A'
    meanFC1(i) = ((meandata(i, 1) - nanmean([meandata(i-1, 1) meandata(i+1, 1)])) * meanO2spanF1(i) +
         O2_workgas) / ((1.0 - 0.20946) * 0.20946) ...
        + (meanCO2_ppm(i) - 384.5) / (1.0 - 0.20946);
    meanFC1(i) = ((meanFC1(i) / 10^6 + 1.0) * (-550.0 / 10^6 + 1.0) - 1.0) * 10^6; % conversion PIUB -->
         SCRIPPS scale

    meanFC3(i) = ((meandata(i, 3) - nanmean([meandata(i-1, 3) meandata(i+1, 3)])) * meanO2spanF3(i) +
         O2_workgas) / ((1.0 - 0.20946) * 0.20946) ...
        + (meanCO2_ppm(i) - 384.5) / (1.0 - 0.20946);
    meanFC3(i) = ((meanFC3(i) / 10^6 + 1.0) * (-550.0 / 10^6 + 1.0) - 1.0) * 10^6; % conversion PIUB -->
         SCRIPPS scale

    meanFC4(i) = ((meandata(i, 4) - nanmean([meandata(i-1, 4) meandata(i+1, 4)])) * meanO2spanF4(i) +
         O2_workgas) / ((1.0 - 0.20946) * 0.20946) ...
        + (meanCO2_ppm(i) - 384.5) / (1.0 - 0.20946);
    meanFC4(i) = ((meanFC4(i) / 10^6 + 1.0) * (-550.0 / 10^6 + 1.0) - 1.0) * 10^6; % conversion PIUB -->
         SCRIPPS scale

    meanFCmean(i) = nanmean([meanFC1(i) meanFC3(i) meanFC4(i)]);

  elseif meanmode{i} == 'B'
    meanFC1(i) = ((meandata(i, 1) - nanmean([meandata(i-1, 1) meandata(i+1, 1)])) * meanO2spanF1(i) +
         O2_workgas) / ((1.0 - 0.20946) * 0.20946) ...
        + (meanCO2_ppm(i-1) - 384.5) / (1.0 - 0.20946) ...
        + (Ar_low_span * 0.009393) / (1.0 - 0.20946);
    meanFC1(i) = ((meanFC1(i) / 10^6 + 1.0) * (-550.0 / 10^6 + 1.0) - 1.0) * 10^6; % conversion PIUB -->
         SCRIPPS scale

    meanFC3(i) = ((meandata(i, 3) - nanmean([meandata(i-1, 3) meandata(i+1, 3)])) * meanO2spanF3(i) +
         O2_workgas) / ((1.0 - 0.20946) * 0.20946) ...
        + (meanCO2_ppm(i-1) - 384.5) / (1.0 - 0.20946)...
        + (Ar_low_span * 0.009393) / (1.0 - 0.20946);
    meanFC3(i) = ((meanFC3(i) / 10^6 + 1.0) * (-550.0 / 10^6 + 1.0) - 1.0) * 10^6; % conversion PIUB -->
         SCRIPPS scale

    meanFC4(i) = ((meandata(i, 4) - nanmean([meandata(i-1, 4) meandata(i+1, 4)])) * meanO2spanF4(i) +
         O2_workgas) / ((1.0 - 0.20946) * 0.20946) ...
        + (meanCO2_ppm(i-1) - 384.5) / (1.0 - 0.20946)...
        + (Ar_low_span * 0.009393) / (1.0 - 0.20946);
    meanFC4(i) = ((meanFC4(i) / 10^6 + 1.0) * (-550.0 / 10^6 + 1.0) - 1.0) * 10^6; % conversion PIUB -->
         SCRIPPS scale

    meanFCmean(i) = nanmean([meanFC1(i) meanFC3(i) meanFC4(i)]);

    elseif meanmode{i} == 'C'
    meanFC1(i) = ((meandata(i, 1) - nanmean([meandata(i-1, 1) meandata(i+1, 1)])) * meanO2spanF1(i) +
         O2_workgas) / ((1.0 - 0.20946) * 0.20946) ...
        + (meanCO2_ppm(i-1) - 384.5) / (1.0 - 0.20946) ...
        + (Ar_high_span * 0.009393) / (1.0 - 0.20946);
    meanFC1(i) = ((meanFC1(i) / 10^6 + 1.0) * (-550.0 / 10^6 + 1.0) - 1.0) * 10^6; % conversion PIUB -->
         SCRIPPS scale

    meanFC3(i) = ((meandata(i, 3) - nanmean([meandata(i-1, 3) meandata(i+1, 3)])) * meanO2spanF3(i) +
         O2_workgas) / ((1.0 - 0.20946) * 0.20946) ...
        + (meanCO2_ppm(i-1) - 384.5) / (1.0 - 0.20946)...
        + (Ar_high_span * 0.009393) / (1.0 - 0.20946);
    meanFC3(i) = ((meanFC3(i) / 10^6 + 1.0) * (-550.0 / 10^6 + 1.0) - 1.0) * 10^6; % conversion PIUB -->
         SCRIPPS scale

    meanFC4(i) = ((meandata(i, 4) - nanmean([meandata(i-1, 4) meandata(i+1, 4)])) * meanO2spanF4(i) +
         O2_workgas) / ((1.0 - 0.20946) * 0.20946) ...
        + (meanCO2_ppm(i-1) - 384.5) / (1.0 - 0.20946)...
        + (Ar_high_span * 0.009393) / (1.0 - 0.20946);
    meanFC4(i) = ((meanFC4(i) / 10^6 + 1.0) * (-550.0 / 10^6 + 1.0) - 1.0) * 10^6; % conversion PIUB -->
         SCRIPPS scale

    meanFCmean(i) = nanmean([meanFC1(i) meanFC3(i) meanFC4(i)]);
  else
  meanFC1(i)     = NaN;
```

```
  meanFC3(i)     = NaN;
  meanFC4(i)     = NaN;
  meanFCmean(i) = NaN;
  end
end

% Interpolate/Extrapolate O2 span for all times
% in the high-resolution data
allO2spanF1 = zeros(timeno, 1);
allO2spanF3 = zeros(timeno, 1);
allO2spanF4 = zeros(timeno, 1);

if (O2calno == 1)
  allO2spanF1(:) = spanF1(1);
  allO2spanF3(:) = spanF3(1);
  allO2spanF4(:) = spanF4(1);
elseif (O2calno == 2)
  allO2spanF1 = spanF1(1) + (spanF1(2) - spanF1(1))/(O2caltime(2)-O2caltime(1))*(alltimes - O2caltime(1));
  allO2spanF3 = spanF3(1) + (spanF3(2) - spanF3(1))/(O2caltime(2)-O2caltime(1))*(alltimes - O2caltime(1));
  allO2spanF4 = spanF4(1) + (spanF4(2) - spanF4(1))/(O2caltime(2)-O2caltime(1))*(alltimes - O2caltime(1));
else
  fprintf('\nError: No/more than 2 calibrations found!\n\n');
end


allFC1     = NaN*ones(timeno, 1);
allFC3     = NaN*ones(timeno, 1);
allFC4     = NaN*ones(timeno, 1);
allFCmean = NaN*ones(timeno, 1);
diff_time = NaN;
ind = or(strcmp(meanmode, 'D'), or(strcmp(meanmode, 'E'), strcmp(meanmode, 'F')));
for i = 2 : timeno-1
  if strcmp(allmodes{i}, 'A');
    diff_time(ind) = meantimes(ind) - alltimes(i);
    i1 = find(diff_time < 0, 1, 'last');
    i2 = find(diff_time > 0, 1, 'first');
    meanD1 = nanmean([meandata(i1, 1) meandata(i2, 1)]);
    if sum(isnan(meanD1)) > 1
        meanD1 = NaN;
    end
    meanD3 = nanmean([meandata(i1, 3) meandata(i2, 3)]);
    if sum(isnan(meanD3)) > 1
        meanD3 = NaN;
    end
    meanD4 = nanmean([meandata(i1, 4) meandata(i2, 4)]);
    if sum(isnan(meanD4)) > 1
        meanD4 = NaN;
    end
    if ((~isnan(meanD1)) || (~isnan(alldata(i, 1))))
      allFC1(i) = ((alldata(i, 1) - meanD1) * allO2spanF1(i) + O2_workgas) / ((1.0 - 0.20946) * 0.20946) ...
          + (allCO2_ppm(i) - 384.5) / (1.0 - 0.20946);
      allFC1(i) = ((allFC1(i) / 10^6 + 1.0) * (-550.0 / 10^6 + 1.0) - 1.0) * 10^6; % conversion PIUB -->
          SCRIPPS
    end

    if ((~isnan(meanD3)) || (~isnan(alldata(i, 3))))
      allFC3(i) = ((alldata(i, 3) - meanD3) * allO2spanF3(i) + O2_workgas) / ((1.0 - 0.20946) * 0.20946) ...
          + (allCO2_ppm(i) - 384.5) / (1.0 - 0.20946);
      allFC3(i) = ((allFC3(i) / 10^6 + 1.0) * (-550.0 / 10^6 + 1.0) - 1.0) * 10^6; % conversion PIUB -->
          SCRIPPS
    end

    if ((~isnan(meanD4)) || (~isnan(alldata(i, 4))))
      allFC4(i) = ((alldata(i, 4) - meanD4) * allO2spanF4(i) + O2_workgas) / ((1.0 - 0.20946) * 0.20946) ...
          + (allCO2_ppm(i) - 384.5) / (1.0 - 0.20946);
      allFC4(i) = ((allFC4(i) / 10^6 + 1.0) * (-550.0 / 10^6 + 1.0) - 1.0) * 10^6; % conversion PIUB -->
          SCRIPPS
    end

    if isinf(allFC1(i)) == 1 % set inf values to NaN to exclude them from mean calculation below
        allFC1(i) = NaN;
```

```
    end
    if isinf(allFC3(i)) == 1
        allFC3(i) = NaN;
    end
    if isinf(allFC4(i)) == 1
        allFC4(i) = NaN;
    end

    allFCmean(i) = nanmean([allFC1(i) allFC3(i) allFC4(i)]);

  elseif strcmp(allmodes{i}, 'B')
      diff_time(ind) = meantimes(ind) - alltimes(i);
    i1 = find(diff_time < 0, 1, 'last');
    i2 = find(diff_time > 0, 1, 'first');
    meanD1 = nanmean([meandata(i1, 1) meandata(i2, 1)]);
    if sum(isnan(meanD1)) > 1
        meanD1 = NaN;
    end
    meanD3 = nanmean([meandata(i1, 3) meandata(i2, 3)]);
    if sum(isnan(meanD3)) > 1
        meanD3 = NaN;
    end
    meanD4 = nanmean([meandata(i1, 4) meandata(i2, 4)]);
    if sum(isnan(meanD4)) > 1
        meanD4 = NaN;
    end
    if ((~isnan(meanD1)) || (~isnan(alldata(i, 1))))
      allFC1(i) = ((alldata(i, 1) - meanD1) * allO2spanF1(i) + O2_workgas) / ((1.0 - 0.20946) * 0.20946) ...
          + (CO2_high_span - 384.5) / (1.0 - 0.20946);
          + (Ar_low_span * 0.009393) / (1.0 - 0.20946);
      allFC1(i) = ((allFC1(i) / 10^6 + 1.0) * (-550.0 / 10^6 + 1.0) - 1.0) * 10^6; % conversion PIUB -->
          SCRIPPS
    end

    if ((~isnan(meanD3)) || (~isnan(alldata(i, 3))))
      allFC3(i) = ((alldata(i, 3) - meanD3) * allO2spanF3(i) + O2_workgas) / ((1.0 - 0.20946) * 0.20946) ...
          + (CO2_high_span - 384.5) / (1.0 - 0.20946);
          + (Ar_low_span * 0.009393) / (1.0 - 0.20946);
      allFC3(i) = ((allFC3(i) / 10^6 + 1.0) * (-550.0 / 10^6 + 1.0) - 1.0) * 10^6; % conversion PIUB -->
          SCRIPPS
    end

    if ((~isnan(meanD4)) || (~isnan(alldata(i, 4))))
      allFC4(i) = ((alldata(i, 4) - meanD4) * allO2spanF4(i) + O2_workgas) / ((1.0 - 0.20946) * 0.20946) ...
          + (CO2_high_span - 384.5) / (1.0 - 0.20946);
          + (Ar_low_span * 0.009393) / (1.0 - 0.20946);
      allFC4(i) = ((allFC4(i) / 10^6 + 1.0) * (-550.0 / 10^6 + 1.0) - 1.0) * 10^6; % conversion PIUB -->
          SCRIPPS
    end

    if isinf(allFC1(i)) == 1 % set inf values to NaN to exclude them from mean calculation below
        allFC1(i) = NaN;
    end
    if isinf(allFC3(i)) == 1
        allFC3(i) = NaN;
    end
    if isinf(allFC4(i)) == 1
        allFC4(i) = NaN;
    end

    allFCmean(i) = nanmean([allFC1(i) allFC3(i) allFC4(i)]);

  elseif strcmp(allmodes{i}, 'C')
    diff_time(ind) = meantimes(ind) - alltimes(i);
    i1 = find(diff_time < 0, 1, 'last');
    i2 = find(diff_time > 0, 1, 'first');
    meanD1 = nanmean([meandata(i1, 1) meandata(i2, 1)]);
    if sum(isnan(meanD1)) > 1
        meanD1 = NaN;
    end
    meanD3 = nanmean([meandata(i1, 3) meandata(i2, 3)]);
```

```
    if sum(isnan(meanD3)) > 1
        meanD3 = NaN;
    end
    meanD4 = nanmean([meandata(i1, 4) meandata(i2, 4)]);
    if sum(isnan(meanD4)) > 1
        meanD4 = NaN;
    end
    if ((~isnan(meanD1)) || (~isnan(alldata(i, 1))))
      allFC1(i) = ((alldata(i, 1) - meanD1) * allO2spanF1(i) + O2_workgas) / ((1.0 - 0.20946) * 0.20946) ...
          + (CO2_low_span - 384.5) / (1.0 - 0.20946);
          + (Ar_high_span * 0.009393) / (1.0 - 0.20946);
      allFC1(i) = ((allFC1(i) / 10^6 + 1.0) * (-550.0 / 10^6 + 1.0) - 1.0) * 10^6; % conversion PIUB -->
          SCRIPPS
    end

    if ((~isnan(meanD3)) || (~isnan(alldata(i, 3))))
      allFC3(i) = ((alldata(i, 3) - meanD3) * allO2spanF3(i) + O2_workgas) / ((1.0 - 0.20946) * 0.20946) ...
          + (CO2_low_span - 384.5) / (1.0 - 0.20946);
          + (Ar_high_span * 0.009393) / (1.0 - 0.20946);
      allFC3(i) = ((allFC3(i) / 10^6 + 1.0) * (-550.0 / 10^6 + 1.0) - 1.0) * 10^6; % conversion PIUB -->
          SCRIPPS
    end

    if ((~isnan(meanD4)) || (~isnan(alldata(i, 4))))
      allFC4(i) = ((alldata(i, 4) - meanD4) * allO2spanF4(i) + O2_workgas) / ((1.0 - 0.20946) * 0.20946) ...
          + (CO2_low_span - 384.5) / (1.0 - 0.20946);
          + (Ar_high_span * 0.009393) / (1.0 - 0.20946);
      allFC4(i) = ((allFC4(i) / 10^6 + 1.0) * (-550.0 / 10^6 + 1.0) - 1.0) * 10^6; % conversion PIUB -->
          SCRIPPS
    end

    if isinf(allFC1(i)) == 1 % set inf values to NaN to exclude them from mean calculation below
        allFC1(i) = NaN;
    end
    if isinf(allFC3(i)) == 1
        allFC3(i) = NaN;
    end
    if isinf(allFC4(i)) == 1
        allFC4(i) = NaN;
    end

    allFCmean(i) = nanmean([allFC1(i) allFC3(i) allFC4(i)]);

  end
end

plottimes      = alltimes;
plotCO2_ppm    = allCO2_ppm;

% Remove first minute and last 10 seconds of CO2 measurements based on time
i = 1;
while(i <= timeno)
  indl = find(strcmp(allmodes{i}, allmodes(i:end)) == 0, 1, 'first') - 1; % find number of seconds until the
      last entry of the current configuration
  if (isempty(indl)) % for the last configuration just take the number of elements in the current config
    indl = numel(allmodes(i:end));
%     if (allmodes{(i-1)+ind-120} ~= allmodes{i})
%       break;
%     end
  end
  indf = find(strcmp(allmodes{i}, allmodes(1:i)) == 0, 1, 'last') + 1; % find first entry after config
      switch
  if (isempty(indf)) % for the first config this is simply the first entry
      indf = 1;
  end
 % set the limits for data exclusion
  t2 = alltimes((i-1)+indl) - 9.0/86400.0; % last 10 seconds
  if allmodes{i} == 'B' || allmodes{i} == 'C'
      t1 = t2 - 171.0/86400.0; % for the configurations after the HS and LS, it takes longer to re-
          equilibrate (-> remove first 3 mins)
  else
```

```
        t1 = t2 - 291.0/86400.0; % first 60 seconds
    end

    % exclude last seconds
    endtime = alltimes((i-1)+indl);
    ind2 = find(and(alltimes >= t2, alltimes <= endtime));
    plotCO2_ppm(ind2) = NaN;

    % exclude first seconds
    starttime = alltimes(indf);
    ind3 = find(and(alltimes >= starttime, alltimes <= t1));
    plotCO2_ppm(ind3) = NaN;
    i = i + indl;
end

% remove first 6 mins of the flight (manual states warm-up effect of 5 min)
    ind = alltimes >= alltimes(1) & alltimes <= alltimes(1) + 359/60/60/24;
    plotCO2_ppm(ind) = NaN;


% outlier removal of CO2
for i = 1 : numel(plotCO2_ppm) - 3;
    if abs(plotCO2_ppm(i + 2) - plotCO2_ppm(i + 1)) > 1 || abs(plotCO2_ppm(i + 2) - plotCO2_ppm(i + 3)) > 1;
        plotCO2_ppm(i + 2) = NaN;
    end
end


% START PLOTTING
%
%
% PLOT CO2
%

% finished = 0;
hf        = NaN;
t0        = datenum(2004, 1, 1);    % time reference is 01.01.2004 00:00:00
% while(~finished)
    ind = find(~isnan(plottimes));
    CO2_ts = timeseries(plotCO2_ppm(ind), plottimes(ind) - t0);
    ti            = get(CO2_ts, 'TimeInfo');
    ti.Units      = 'days';
    ti.StartDate = datestr(t0);
    ti.Format     = 'HH:MM';
    set(CO2_ts, 'TimeInfo', ti);


    if (isnan(hf))
      hf = figure('Name', sprintf('CO2 measurement high-res (%s)', plotpathname), ...
                  'NumberTitle', 'off', ...
                  'Position', [100 100 1100 750]);
    else
      figure(hf);
    end
    plot(CO2_ts, '-','color',darkred);
    title('CO2 measurement');
    xlabel(sprintf('Time UTC [starting %s]', datestr(plottimes(1), 'dd.mm.yyyy')));
    xlim([plottimes(1)-t0 plottimes(end)-t0]);
    ylabel('CO2 [ppm]');

    %Removal of CO2 data
    %
%    answer = questdlg('Remove CO2 data ?', 'Data check', 'Yes', 'No', 'No');
%    if (strcmp(answer, 'Yes'))
%      indlg_options.Resize       = 'on';
%      indlg_options.WindowStyle = 'normal';
%      indlg_options.Interpreter = 'none';
%      answer = inputdlg({'Data removal start:', 'Data removal end:'}, ...
%                        'Enter period for CO2 data removal', 1, ...
%                        {datestr(plottimes(1), 'dd.mm.yyyy HH:MM:SS'), datestr(plottimes(end), 'dd.mm.yyyy
     HH:MM:SS')}, ...
```

```
%                           indlg_options);
%       if (~isempty(answer))
%         t1 = datenum(answer{1}, 'dd.mm.yyyy HH:MM:SS');
%         t2 = datenum(answer{2}, 'dd.mm.yyyy HH:MM:SS');
%         ind = and((alltimes >= t1), (alltimes <= t2));
%         plotCO2_ppm(ind) = NaN;
%       else
%         finished = 1;
%       end
%     else
%       finished = 1;
%     end
% end

% Save figure
filename = fullfile(Path, ['plot_' plotpathname(1:3) '-' destinationA '_' destinationB '_CO2']);
saveas(hf,filename,'fig');


plotO2_permeg = allFCmean;

% Remove O2 measurements in case WG has run out

if nowg == 1 && abs(meandata(end - 4, 20) - meandata(end - 3, 20)) > 0.2;
     meanFCmean(indnowg:end) = NaN; % remove low resolution O2
     meanFC1(indnowg:end)    = NaN;
     meanFC3(indnowg:end)    = NaN;
     meanFC4(indnowg:end)    = NaN;

     plotO2_permeg(meantimes(indnowg) < alltimes) = NaN;
     allFC1(meantimes(indnowg) < alltimes)        = NaN;
     allFC3(meantimes(indnowg) < alltimes)        = NaN;
     allFC4(meantimes(indnowg) < alltimes)        = NaN;
end

% Remove first 239 sec and last 10 sec of O2 measurements based on time

i = 1;
while(i <= timeno)
  indl = find(strcmp(allmodes{i}, allmodes(i:end)) == 0, 1, 'first') - 1; % find number of seconds until the
       last entry of the current configuration
  if (isempty(indl)) % for the last configuration just take the number of elements in the current config
    indl = numel(allmodes(i:end));
  end
  indf = find(strcmp(allmodes{i}, allmodes(1:i)) == 0, 1, 'last') + 1; % find first entry after config
       switch
  if (isempty(indf)) % for the first config this is simply the first entry
      indf = 1;
  end
 % set the limits for data exclusion
  t2 = alltimes((i-1)+indl) - 9.0/86400.0; % last 10 seconds
  t1 = t2 - 111.0/86400.0; % first 4 min
  % exclude last seconds
  endtime = alltimes((i-1)+indl);
  ind2 = find(and(alltimes >= t2, alltimes <= endtime));
  plotO2_permeg(ind2) = NaN;
  allFC1(ind2)        = NaN;
  allFC3(ind2)        = NaN;
  allFC4(ind2)        = NaN;
  % exclude first seconds
  starttime = alltimes(indf);
  ind3 = find(and(alltimes >= starttime, alltimes <= t1));
  plotO2_permeg(ind3) = NaN;
  allFC1(ind3)        = NaN;
  allFC3(ind3)        = NaN;
  allFC4(ind3)        = NaN;
  i = i + indl;
end


% PLOT O2
```

```
%
% create time series
  ind = find(~isnan(plottimes));
  O2_ts = timeseries(plotO2_permeg(ind), plottimes(ind) - t0);
  ti           = get(O2_ts, 'TimeInfo');
  ti.Units     = 'days';
  ti.StartDate = datestr(t0);
  ti.Format    = 'HH:MM';
  set(O2_ts, 'TimeInfo', ti);


ind = find(~isnan(plottimes));
O2_FC1_ts    = timeseries(allFC1(ind), plottimes(ind) - t0);
O2_FC3_ts    = timeseries(allFC3(ind), plottimes(ind) - t0);
O2_FC4_ts    = timeseries(allFC4(ind), plottimes(ind) - t0);
ti           = get(O2_FC1_ts, 'TimeInfo');
ti.Units     = 'days';
ti.StartDate = datestr(t0);
ti.Format    = 'HH:MM';
set(O2_FC1_ts, 'TimeInfo', ti);
set(O2_FC3_ts, 'TimeInfo', ti);
set(O2_FC4_ts, 'TimeInfo', ti);


hf = figure('Name', sprintf('Individual FC O2 measurements hi-res (%s)', plotpathname), ...
                'NumberTitle', 'off', ...
                'Position', [100 100 1100 750]);

plot(O2_FC1_ts, '-','color',darkred);
hold('on');
plot(O2_FC3_ts, '-','color',darkgreen);
hold('on');
plot(O2_FC4_ts, '-','color',darkblue);
hold('on');
plot(O2_ts, '-k');
title('O2 measurement');
xlabel(sprintf('Time UTC [starting %s]', datestr(plottimes(1), 'dd.mm.yyyy')));
xlim([plottimes(1)-t0 plottimes(end)-t0]);
ylabel('\delta O2/N2 [per meg]');
legend({'FC1', 'FC3', 'FC4', 'mean'}, 'Location', 'BestOutside');
hold('off');

% Save plot
filename = fullfile(Path, ['plot_' plotpathname(1:3) '-' destinationA '_' destinationB '_O2']);
saveas(hf,filename,'fig');

%
 removeFC = [];
% answer = inputdlg('Enter space-separated FC numbers for removal (1 3 or 4):', 'Select FCs to remove', [1
    60], {''}, indlg_options);
%     if (~isempty(answer))
%         removeFC = str2num(answer{:});
%         plotFC1low = meanFC1;
%         plotFC3low = meanFC3;
%         plotFC4low = meanFC4;
%         plotFC1hi  = allFC1;
%         plotFC3hi  = allFC3;
%         plotFC4hi  = allFC4;
%         if ismember(1,removeFC)
%             plotFC1low = NaN*ones(length(meanFC1),1);
%             plotFC1hi  = NaN*ones(length(allFC1),1);
%         end
%         if ismember(3,removeFC)
%             plotFC3low = NaN*ones(length(meanFC3),1);
%             plotFC3hi  = NaN*ones(length(allFC3),1);
%         end
%         if ismember(4,removeFC)
%             plotFC4low = NaN*ones(length(meanFC4),1);
%             plotFC4hi  = NaN*ones(length(allFC4),1);
%         end
```

```
        % overwrite meanFCmean (low res)
%           for i = 2 : meanno-1
%               if meanmode{i} == 'A' || meanmode{i} == 'B' || meanmode{i} == 'C'
%                 meanFCmean(i) = nanmean([plotFC1low(i) plotFC3low(i) plotFC4low(i)]);
%               else
%               plotFC1low(i) = NaN;
%               plotFC3low(i) = NaN;
%               plotFC4low(i) = NaN;
%               meanFCmean(i) = NaN;
%               end
%           end

        % overwrite plotO2_permeg (hi res)
%           for i = 2 : timeno-1
%               if or(strcmp(allmodes{i}, 'A'), or(strcmp(allmodes{i}, 'B'), strcmp(allmodes{i}, 'C')));
%                   plotO2_permeg(i) = nanmean([plotFC1hi(i) plotFC3hi(i) plotFC4hi(i)]);
%               end
%           end

        % Remove first 239 sec and last 10 sec of O2 measurements based on time

%               i = 1;
%               while(i <= timeno)
%                   indl = find(strcmp(allmodes{i}, allmodes(i:end)) == 0, 1, 'first') - 1; % find number of
    seconds until the last entry of the current configuration
%                   if (isempty(indl)) % for the last configuration just take the number of elements in the
    current config
%                       indl = numel(allmodes(i:end));
%               %       if (allmodes{(i-1)+ind-120} ~= allmodes{i})
%               %         break;
%               %       end
%                   end
%                   indf = find(strcmp(allmodes{i}, allmodes(1:i)) == 0, 1, 'last') + 1; % find first entry
    after config switch
%                   if (isempty(indf)) % for the first config this is simply the first entry
%                       indf = 1;
%                   end
%                  % set the limits for data exclusion
%                   t2 = alltimes((i-1)+indl) - 9.0/86400.0; % last 10 seconds
%                   t1 = t2 - 111.0/86400.0; % first 4 min
%                   % exclude last seconds
%                   endtime = alltimes((i-1)+indl);
%                   ind2 = find(and(alltimes >= t2, alltimes <= endtime));
%                   plotO2_permeg(ind2) = NaN;
%                   % exclude first seconds
%                   starttime = alltimes(indf);
%                   ind3 = find(and(alltimes >= starttime, alltimes <= t1));
%                   plotO2_permeg(ind3) = NaN;
%                   i = i + indl;
%               end
%
%           ind = find(~isnan(plottimes));
%           O2_ts = timeseries(plotO2_permeg(ind), plottimes(ind) - t0);
    %end

%finished = 0;
hf = NaN;
%while(~finished)

  % only modes A
  ind = strcmp(meanmode, 'A');
  O2low_ts = timeseries(meanFCmean(ind), meantimes(ind) - t0);
  ti             = get(O2low_ts, 'TimeInfo');
  ti.Units       = 'days';
  ti.StartDate = datestr(t0);
  ti.Format      = 'HH:MM';
  set(O2low_ts, 'TimeInfo', ti);

  % modes B and C
  ind = or(strcmp(meanmode, 'B'), strcmp(meanmode, 'C'));
  O2low_cal_ts = timeseries(meanFCmean(ind), meantimes(ind) - t0);
```

```
  ti            = get(O2low_cal_ts, 'TimeInfo');
  ti.Units      = 'days';
  ti.StartDate = datestr(t0);
  ti.Format     = 'HH:MM';
  set(O2low_cal_ts, 'TimeInfo', ti);

  if (isnan(hf))
    hf = figure('Name', sprintf('O2 measurement hi-res (%s)', plotpathname), ...
                'NumberTitle', 'off', ...
                'Position', [100 100 1100 750]);
  else
    figure(hf);
  end
  plot(O2_ts, '-k');
  hold('on');
  plot(O2low_ts, '*','color',darkblue);
  hold('on');
  plot(O2low_cal_ts, '*','color',darkred);
  title('O2 measurement');
  xlabel(sprintf('Time UTC [starting %s]', datestr(plottimes(1), 'dd.mm.yyyy')));
  xlim([plottimes(1)-t0 plottimes(end)-t0]);
  ylabel('\delta O2/N2 [per meg]');
  hold('off');

%    answer = questdlg('Remove O2 data ?', 'Data check', 'Yes', 'No', 'No');
%    if (strcmp(answer, 'Yes'))
%      indlg_options.Resize       = 'on';
%      indlg_options.WindowStyle = 'normal';
%      indlg_options.Interpreter = 'none';
%      answer = inputdlg({'Data removal start:', 'Data removal end:'}, ...
%                        'Enter period for O2 data removal', 1, ...
%                        {datestr(plottimes(1), 'dd.mm.yyyy HH:MM:SS'), datestr(plottimes(end), 'dd.mm.yyyy
     HH:MM:SS')}, ...
%                        indlg_options);
%      if (~isempty(answer))
%        t1 = datenum(answer{1}, 'dd.mm.yyyy HH:MM:SS');
%        t2 = datenum(answer{2}, 'dd.mm.yyyy HH:MM:SS');
%        ind = and((alltimes >= t1), (alltimes <= t2));
%        ind2= and((meantimes>= t1), (meantimes<= t2));
%        allFC1(ind)          = NaN;
%        allFC3(ind)          = NaN;
%        allFC4(ind)          = NaN;
%        plotO2_permeg(ind) = NaN;
%        meanFCmean(ind2)    = NaN;
%      else
%        finished = 1;
%      end
%    else
%      finished = 1;
%    end
%end

O2low_permeg  = NaN*ones(length(alldata),1); % to have the low res O2 data in hires
O2low1_permeg = NaN*ones(length(alldata),1);
O2low3_permeg = NaN*ones(length(alldata),1);
O2low4_permeg = NaN*ones(length(alldata),1);
i = 1;
for i = 1 : meanno
    diff_time = meantimes(i) - alltimes;
    ind = find(diff_time < 0, 1, 'first');
    O2low_permeg(ind)  = meanFCmean(i);
    O2low1_permeg(ind) = meanFC1(i);
    O2low3_permeg(ind) = meanFC3(i);
    O2low4_permeg(ind) = meanFC4(i);
end

if calno == 1
    span(2) = NaN;
    offset(2) = NaN;
end
```

```
if O2calno == 1
    spanF1(2) = NaN;
    spanF3(2) = NaN;
    spanF4(2) = NaN;
end

% excel export parameters
% if isempty(indBs)
%     o2calvaluelow = NaN;
%     o2calvaluehigh = NaN;
% else
%     o2calvaluelow = meanFCmean(indBs(1));
%     o2calvaluehigh = meanFCmean(indHSs(1));
% end
% flightparam = [coefficientsmks R1(2)^2 calno O2calno span(1) offset(1) span(2) offset(2) coefficientsh2o
    (1) coefficientsh2o(2) Rh2o(2)^2 FC1yesno FC3yesno FC4yesno ismember(1, removeFC) ismember(3, removeFC)
     ismember(4, removeFC) spanF1(1) spanF1(2) spanF3(1) spanF3(2) spanF4(1) spanF4(2) o2calvaluelow
    o2calvaluehigh nowg];
% num = xlsread(fullfile(datapath,'allflights'));
% position = find(num(:) == caribicno);
% xlrange = ['B' num2str(position+1) ':AC' num2str(position+1)];
% xlswrite(fullfile(datapath,'allflights'),flightparam,1,xlrange)

% Export data to NASA AMES
%
% answer = questdlg('Do you want to export data to NASA AMES ?', ...
%                   'NASA AMES export', 'Yes', 'No', 'No');
% if (strcmp(answer, 'Yes'))
  data.alltimes       = alltimes;
% remove configs E and F for CO2
  ind = or(strcmp(allmodes, 'E'), strcmp(allmodes, 'F'));
  plotCO2_ppm(ind)    = NaN;
% remove everything but config A for O2
  ind = find(~strcmp(allmodes, 'A'));
  plotO2_permeg(ind) = NaN; % hires means of o2
  O2low_permeg(ind)  = NaN; % lowres means of o2
  O2low1_permeg(ind) = NaN;
  O2low3_permeg(ind) = NaN;
  O2low4_permeg(ind) = NaN;

  data.allCO2_ppm     = plotCO2_ppm;
  data.allO2_permeg   = plotO2_permeg;
  data.O2low_permeg   = O2low_permeg;
  data.meantimes      = meantimes;
  data.meanO2_permeg  = meanFCmean;
  data.allwasserppm   = allwasser*1000;
  data.alltemperatur  = alltemperatur;
  data.alldruck       = alldruck*10;
  data.mksregler      = mksregler;
  data.refp           = alldata(:,20)*10;
  data.mks640         = mks640;
  data.boxt           = alldata(:,6);
  data.FC2            = alldata(:,2);
  data.allFC1         = allFC1;
  data.FC1            = O2low1_permeg;
  data.allFC3         = allFC3;
  data.FC3            = O2low3_permeg;
  data.allFC4         = allFC4;
  data.FC4            = O2low4_permeg;

  Export_to_AMES_file_GUI(data, Path, caribicno, destinationA, destinationB);
% end


% Merge with MS Nasa AMES data
%
% answer = questdlg('Do you want to merge with the MS data?', ...
%                   'Data merge', 'Yes', 'No', 'No');
% if (strcmp(answer, 'Yes'))
    mspath    = '\\phkup4\ms\Bigler_Iwan\CARIBIC\data\ms_files';
    ghgpath   = '\\phkup4\ms\Bigler_Iwan\CARIBIC\data\ghg_files';
```

```
cd(Path);
[File, Path] = uigetfile({'*.txt','Data files';'*.*','All files'}, 'Select Bern data file', '
    MultiSelect', 'off');
cd(workdir);
if (isequal(File, 0))
    uiwait(errordlg('No file selected!','File selection error'),'modal');
    return;
end

% Import the selected Bern file
data_BERN = CARIBIC_ReadData(fullfile(Path, File));

% MS file

% Get file names in MS folder
listing_ms  = dir(fullfile(mspath));
allnames_ms = {listing_ms.name};
% Look for matching flight numbers (MS)
for i = 1 : numel(allnames_ms)
    if cell2mat(strfind(allnames_ms(i), plotpathname(1:3))) == 13;
        msfile = char(allnames_ms(i));
    end
end
% Import MS file
data_CARIBIC = CARIBIC_ReadData(fullfile(mspath, msfile));


% GHG file

% Get file names in GHG folder
listing_ghg  = dir(fullfile(ghgpath));
allnames_ghg = {listing_ghg.name};
% Look for matching flight numbers (GHG)
for i = 1 : numel(allnames_ghg)
    if cell2mat(strfind(allnames_ghg(i), plotpathname(1:3))) == 14;
        ghgfile = char(allnames_ghg(i));
    end
end
% Import GHG file
if exist('ghgfile', 'var') ~= 0;
    data_GHG = CARIBIC_ReadData(fullfile(ghgpath, ghgfile));
end
% Merge the 2 files
ind = find(data_CARIBIC.times(:,1) == data_BERN.times(1,1)); % look for overlap in both files
if isempty(ind)
    uiwait(warndlg(sprintf('No time overlap was found between the files. Press OK to continue.')));
end
alldatamerged = [data_CARIBIC.times NaN*ones(size(data_CARIBIC.data,1), size(data_BERN.data,2))
    data_CARIBIC.data]; % append a matrix of size databern + 1 (for times) containing NaN
if length(data_BERN.times) + ind-1 > length(data_CARIBIC.times)
    alldatamerged = vertcat(alldatamerged, NaN*ones(length(data_BERN.times) + ind-1 - length(
        data_CARIBIC.times),size(alldatamerged,2))); % append a matrix of NaNs of the height (length(
        data_BERN.times) + ind-1) - length(data_CARIBIC.times)
    alldatamerged(ind:(ind+size(data_BERN.times,1)-1), 1:1) = data_BERN.times; % overwrite CARIBIC times
        with BERN times (since BERN times are often longer for 2 mins)
end
alldatamerged(ind:(ind+size(data_BERN.data,1)-1), 2:size(data_BERN.data,2)+1) = data_BERN.data; %
    overwrite the values with databern matrix

% add GHG flask CO2 values
if exist('ghgfile', 'var') ~= 0;
    alldatamerged = [alldatamerged NaN*ones(size(alldatamerged,1),1)];
    i = 1;
    for i = 1 : size(data_GHG.data,1)
        diff_time = data_GHG.times(i) - alldatamerged(:,1);
        ind = find(diff_time < 0, 1, 'first');
        alldatamerged(ind,end) = data_GHG.data(i,find(ismember(data_GHG.names,'co2')));
    end
end

newheader = ['UTC' data_BERN.names' data_CARIBIC.names']; % combine headers
```

```
    if exist('ghgfile', 'var') ~= 0;
        newheader = [newheader 'CO2_flask'];
    end

    filename = ['../' plotpathname(1:3) '-' destinationA '_' destinationB '_merged.txt'];

    write = 1;
%     if (exist(fullfile(Path, filename), 'file'))
%       answer = questdlg(sprintf('Merged file already exists! Do you want to overwrite it?'), ...
%                 'Overwrite', 'Yes', 'No', 'No');
%       if (strcmp(answer, 'No'))
%         write = 0;
%         return;
%       end
%     end
    if write == 1;
        % Write all data to file
         fid = fopen(fullfile(Path, filename),'w');
         for i=1:size(newheader,1) % write header
           fprintf(fid,'%s\t',newheader{i,1:end-1});
           fprintf(fid,'%s\n',newheader{i,end});
         end
        y = repmat('%.11f\t',1,(size(alldatamerged,2)-1)); % write data
        fprintf(fid,[y,'%d\n'],alldatamerged');
        fclose(fid);
    end
% end
```

Appendix D

Standard cylinders

Table D.1 List of the values assigned to the standard cylinders employed during the CARIBIC project. The $\delta(O_2/N_2)$ ratios are expressed on the local PIUB O_2/N_2 scale. The δX_{O_2} values in the last three columns are apparent mole fraction differences corrected for CO_2 and Ar using equation 3.1.

CARIBIC flight #	CO_2 [ppmv]			$\delta(Ar/N_2)$ [per meg]			$\delta(O_2/N_2)$ PIUB [per meg]			δX_{O_2} [ppmv]		
	CG1	CG2	WG	CG1	CG2	WG	CG1	CG2	WG	CG1	CG2	WG
178	433.13	357.50	400.04	-1720.10	45.57	-552.46	-1257.66	85.49	-698.92	-215.05	19.72	-117.90
179	433.13	357.50	400.04	-1720.10	45.57	-552.46	-1257.66	85.49	-698.92	-215.05	19.72	-117.90
180	433.13	357.50	400.04	-1720.10	45.57	-552.46	-1257.66	85.49	-698.92	-215.05	19.72	-117.90
181	433.13	357.50	400.04	-1720.10	45.57	-552.46	-1257.66	85.49	-698.92	-215.05	19.72	-117.90
182	433.13	357.50	400.07	-1720.10	45.57	-525.06	-1257.66	85.49	-689.97	-215.05	19.72	-116.48
183	433.13	357.50	400.07	-1720.10	45.57	-525.06	-1257.66	85.49	-689.97	-215.05	19.72	-116.48
184	433.13	357.50	400.07	-1720.10	45.57	-525.06	-1257.66	85.49	-689.97	-215.05	19.72	-116.48
185	433.13	357.50	400.07	-1720.10	45.57	-525.06	-1257.66	85.49	-689.97	-215.05	19.72	-116.48
186	433.13	357.50	395.36	-1720.10	45.57	-556.69	-1257.66	85.49	-716.84	-215.05	19.72	-119.88
187	433.13	357.50	395.36	-1720.10	45.57	-556.69	-1257.66	85.49	-716.84	-215.05	19.72	-119.88
188	433.13	357.50	395.36	-1720.10	45.57	-556.69	-1257.66	85.49	-716.84	-215.05	19.72	-119.88
189	433.13	357.50	395.36	-1720.10	45.57	-556.69	-1257.66	85.49	-716.84	-215.05	19.72	-119.88
190	433.13	357.50	395.46	-1720.10	45.57	-540.05	-1257.66	85.49	-707.86	-215.05	19.72	-118.45
191	433.13	357.50	395.46	-1720.10	45.57	-540.05	-1257.66	85.49	-707.86	-215.05	19.72	-118.45
192	433.13	357.50	395.46	-1720.10	45.57	-540.05	-1257.66	85.49	-707.86	-215.05	19.72	-118.45
193	433.13	357.50	395.46	-1720.10	45.57	-540.05	-1257.66	85.49	-707.86	-215.05	19.72	-118.45
194	433.13	357.50	395.55	-1720.10	45.57	-519.23	-1257.66	85.49	-686.03	-215.05	19.72	-114.89
195	433.13	357.50	395.55	-1720.10	45.57	-519.23	-1257.66	85.49	-686.03	-215.05	19.72	-114.89
196	433.13	357.50	395.55	-1720.10	45.57	-519.23	-1257.66	85.49	-686.03	-215.05	19.72	-114.89
197	433.13	357.50	395.55	-1720.10	45.57	-519.23	-1257.66	85.49	-686.03	-215.05	19.72	-114.89
198	433.13	357.50	396.13	-1720.10	45.57	-575.45	-1257.66	85.49	-708.58	-215.05	19.72	-118.64
199	433.13	357.50	396.13	-1720.10	45.57	-575.45	-1257.66	85.49	-708.58	-215.05	19.72	-118.64

Continued on next page

Table D.1 – *Continued from previous page*

200	433.13	357.50	396.13	-1720.10	45.57	-575.45	-1257.66	85.49	-708.58	-215.05	19.72	-118.64
201	433.13	357.50	396.13	-1720.10	45.57	-575.45	-1257.66	85.49	-708.58	-215.05	19.72	-118.64
202	433.13	357.50	396.13	-1720.10	45.57	-575.45	-1257.66	85.49	-708.58	-215.05	19.72	-118.64
203	433.13	357.50	396.13	-1720.10	45.57	-575.45	-1257.66	85.49	-708.58	-215.05	19.72	-118.64
204	433.13	357.50	396.13	-1720.10	45.57	-575.45	-1257.66	85.49	-708.58	-215.05	19.72	-118.64
205	433.13	357.50	396.13	-1720.10	45.57	-575.45	-1257.66	85.49	-708.58	-215.05	19.72	-118.64
206	433.13	357.50	396.13	-1720.10	45.57	-575.45	-1257.66	85.49	-708.58	-215.05	19.72	-118.64
207	433.13	357.50	396.13	-1720.10	45.57	-575.45	-1257.66	85.49	-708.58	-215.05	19.72	-118.64
208	433.13	357.50	396.13	-1720.10	45.57	-575.45	-1257.66	85.49	-708.58	-215.05	19.72	-118.64
209	433.13	357.50	396.13	-1720.10	45.57	-575.45	-1257.66	85.49	-708.58	-215.05	19.72	-118.64
210	432.00	357.50	396.13	-1719.80	45.57	-575.45	-1273.31	85.49	-708.58	-217.41	19.72	-118.64
211	432.00	357.50	396.13	-1719.80	45.57	-575.45	-1273.31	85.49	-708.58	-217.41	19.72	-118.64
212	432.00	357.50	396.13	-1719.80	45.57	-575.45	-1273.31	85.49	-708.58	-217.41	19.72	-118.64
213	432.00	357.50	396.13	-1719.80	45.57	-575.45	-1273.31	85.49	-708.58	-217.41	19.72	-118.64
214	432.00	357.50	401.59	-1719.80	45.57	-1414.74	-1273.31	85.49	-318.98	-217.41	19.72	-53.61
215	432.00	357.50	401.59	-1719.80	45.57	-1414.74	-1273.31	85.49	-318.98	-217.41	19.72	-53.61
216	432.00	357.50	401.59	-1719.80	45.57	-1414.74	-1273.31	85.49	-318.98	-217.41	19.72	-53.61
217	432.00	357.50	401.59	-1719.80	45.57	-1414.74	-1273.31	85.49	-318.98	-217.41	19.72	-53.61
218	432.00	357.50	399.32	-1719.80	45.57	-1154.10	-1273.31	85.49	-465.54	-217.41	19.72	-77.92
219	432.00	357.50	399.32	-1719.80	45.57	-1154.10	-1273.31	85.49	-465.54	-217.41	19.72	-77.92
220	432.00	357.50	400.76	-1719.80	45.57	-1334.10	-1273.31	85.49	-375.02	-217.41	19.72	-62.88
221	432.00	357.50	400.76	-1719.80	45.57	-1334.10	-1273.31	85.49	-375.02	-217.41	19.72	-62.88
222	432.00	357.50	400.76	-1719.80	45.57	-1334.10	-1273.31	85.49	-375.02	-217.41	19.72	-62.88
223	432.00	357.50	400.76	-1719.80	45.57	-1334.10	-1273.31	85.49	-375.02	-217.41	19.72	-62.88
224	432.00	357.50	401.15	-1719.80	45.57	-1335.59	-1273.31	85.49	-362.64	-217.41	19.72	-60.91
225	432.00	357.50	401.15	-1719.80	45.57	-1335.59	-1273.31	85.49	-362.64	-217.41	19.72	-60.91
226	432.00	357.50	401.15	-1719.80	45.57	-1335.59	-1273.31	85.49	-362.64	-217.41	19.72	-60.91
227	432.00	357.50	401.15	-1719.80	45.57	-1335.59	-1273.31	85.49	-362.64	-217.41	19.72	-60.91

Continued on next page

Table D.1 – *Continued from previous page*

228	432.00	357.50	399.81	-1719.80	45.57	-1205.60	-1273.31	85.49	-447.22	-217.41	19.72	-74.89
229	432.00	357.50	399.81	-1719.80	45.57	-1205.60	-1273.31	85.49	-447.22	-217.41	19.72	-74.89
230	432.00	357.50	399.81	-1719.80	45.57	-1205.60	-1273.31	85.49	-447.22	-217.41	19.72	-74.89
231	432.00	357.50	399.81	-1719.80	45.57	-1205.60	-1273.31	85.49	-447.22	-217.41	19.72	-74.89
232	432.00	357.50	398.90	-1719.80	45.57	-1113.03	-1273.31	85.49	-494.95	-217.41	19.72	-82.78
233	432.00	357.50	398.90	-1719.80	45.57	-1113.03	-1273.31	85.49	-494.95	-217.41	19.72	-82.78
234	432.00	357.50	398.90	-1719.80	45.57	-1113.03	-1273.31	85.49	-494.95	-217.41	19.72	-82.78
235	432.00	357.50	398.90	-1719.80	45.57	-1113.03	-1273.31	85.49	-494.95	-217.41	19.72	-82.78
236	432.00	357.50	408.33	-1719.80	45.57	-3269.74	-1273.31	85.49	385.20	-217.41	19.72	65.23
237	432.00	357.50	408.33	-1719.80	45.57	-3269.74	-1273.31	85.49	385.20	-217.41	19.72	65.23
238	432.00	357.50	408.33	-1719.80	45.57	-3269.74	-1273.31	85.49	385.20	-217.41	19.72	65.23
239	432.00	357.50	408.33	-1719.80	45.57	-3269.74	-1273.31	85.49	385.20	-217.41	19.72	65.23
240	432.00	357.50	407.44	-1719.80	45.57	-3003.24	-1273.31	85.49	313.96	-217.41	19.72	53.09
241	432.00	357.50	407.44	-1719.80	45.57	-3003.24	-1273.31	85.49	313.96	-217.41	19.72	53.09
242	432.00	357.50	407.44	-1719.80	45.57	-3003.24	-1273.31	85.49	313.96	-217.41	19.72	53.09
243	432.00	357.50	407.44	-1719.80	45.57	-3003.24	-1273.31	85.49	313.96	-217.41	19.72	53.09
244	432.00	357.50	408.79	-1719.80	45.57	-3471.22	-1273.31	85.49	389.47	-217.41	19.72	66.23
245	432.00	357.50	408.79	-1719.80	45.57	-3471.22	-1273.31	85.49	389.47	-217.41	19.72	66.23
246	432.00	357.50	408.79	-1719.80	45.57	-3471.22	-1273.31	85.49	389.47	-217.41	19.72	66.23
247	432.00	357.50	408.79	-1719.80	45.57	-3471.22	-1273.31	85.49	389.47	-217.41	19.72	66.23
248	432.00	357.50	407.22	-1719.80	45.57	-2886.29	-1273.31	85.49	224.01	-217.41	19.72	38.01
249	432.00	357.50	407.22	-1719.80	45.57	-2886.29	-1273.31	85.49	224.01	-217.41	19.72	38.01
250	432.00	357.50	407.22	-1719.80	45.57	-2886.29	-1273.31	85.49	224.01	-217.41	19.72	38.01
251	432.00	357.50	407.22	-1719.80	45.57	-2886.29	-1273.31	85.49	224.01	-217.41	19.72	38.01
252	432.00	357.50	408.85	-1719.80	45.57	-3420.73	-1273.31	85.49	428.62	-217.41	19.72	72.60
253	432.00	357.50	408.85	-1719.80	45.57	-3420.73	-1273.31	85.49	428.62	-217.41	19.72	72.60
254	432.00	357.50	408.62	-1719.80	45.57	-3442.13	-1273.31	85.49	360.71	-217.41	19.72	61.45
255	432.00	357.50	408.62	-1719.80	45.57	-3442.13	-1273.31	85.49	360.71	-217.41	19.72	61.45

Continued on next page

Table D.1 – *Continued from previous page*

256	432.00	357.50	408.62	-1719.80	45.57	-3442.13	-1273.31	85.49	360.71	-217.41	19.72	61.45
257	432.00	357.50	408.62	-1719.80	45.57	-3442.13	-1273.31	85.49	360.71	-217.41	19.72	61.45
258	432.00	357.50	408.62	-1719.80	45.57	-3447.38	-1273.31	85.49	386.40	-217.41	19.72	65.71
259	432.00	357.50	408.62	-1719.80	45.57	-3447.38	-1273.31	85.49	386.40	-217.41	19.72	65.71
260	432.00	357.50	408.62	-1719.80	45.57	-3447.38	-1273.31	85.49	386.40	-217.41	19.72	65.71
261	432.00	357.50	408.62	-1719.80	45.57	-3447.38	-1273.31	85.49	386.40	-217.41	19.72	65.71
262	432.00	357.50	408.63	-1719.80	45.57	-3291.43	-1273.31	85.49	434.50	-217.41	19.72	73.37
263	432.00	357.50	408.63	-1719.80	45.57	-3291.43	-1273.31	85.49	434.50	-217.41	19.72	73.37
264	432.00	357.50	408.63	-1719.80	45.57	-3291.43	-1273.31	85.49	434.50	-217.41	19.72	73.37
265	432.00	357.50	408.63	-1719.80	45.57	-3291.43	-1273.31	85.49	434.50	-217.41	19.72	73.37
266	432.00	357.50	408.58	-1719.80	45.57	-3313.74	-1273.31	85.49	444.66	-217.41	19.72	75.11
267	432.00	357.50	408.58	-1719.80	45.57	-3313.74	-1273.31	85.49	444.66	-217.41	19.72	75.11
268	432.00	357.50	408.58	-1719.80	45.57	-3313.74	-1273.31	85.49	444.66	-217.41	19.72	75.11
269	432.00	357.50	408.58	-1719.80	45.57	-3313.74	-1273.31	85.49	444.66	-217.41	19.72	75.11
270	432.00	357.50	408.38	-1719.80	45.57	-3365.15	-1273.31	85.49	374.45	-217.41	19.72	63.62
271	432.00	357.50	408.38	-1719.80	45.57	-3365.15	-1273.31	85.49	374.45	-217.41	19.72	63.62
272	432.00	357.50	408.38	-1719.80	45.57	-3365.15	-1273.31	85.49	374.45	-217.41	19.72	63.62
273	432.00	357.50	408.38	-1719.80	45.57	-3365.15	-1273.31	85.49	374.45	-217.41	19.72	63.62
274	432.00	357.50	408.27	-1719.80	45.57	-3286.75	-1273.31	85.49	468.68	-217.41	19.72	79.10
275	432.00	357.50	408.27	-1719.80	45.57	-3286.75	-1273.31	85.49	468.68	-217.41	19.72	79.10
276	432.00	357.50	408.27	-1719.80	45.57	-3286.75	-1273.31	85.49	468.68	-217.41	19.72	79.10
277	432.00	357.50	408.27	-1719.80	45.57	-3286.75	-1273.31	85.49	468.68	-217.41	19.72	79.10
278	432.00	357.50	428.72	-1719.80	45.57	57.38	-1273.31	85.49	320.03	-217.41	19.72	43.62
279	432.00	357.50	428.72	-1719.80	45.57	57.38	-1273.31	85.49	320.03	-217.41	19.72	43.62
280	432.00	357.50	428.72	-1719.80	45.57	57.38	-1273.31	85.49	320.03	-217.41	19.72	43.62
281	432.00	357.50	428.72	-1719.80	45.57	57.38	-1273.31	85.49	320.03	-217.41	19.72	43.62
282	432.00	357.50	426.64	-1719.80	45.57	-302.37	-1273.31	85.49	322.33	-217.41	19.72	45.14
283	432.00	357.50	426.64	-1719.80	45.57	-302.37	-1273.31	85.49	322.33	-217.41	19.72	45.14

Continued on next page

Table D.1 – *Continued from previous page*

284	432.00	357.50	426.64	-1719.80	45.57	-302.37	-1273.31	85.49	322.33	-217.41	19.72	45.14
285	432.00	357.50	426.64	-1719.80	45.57	-302.37	-1273.31	85.49	322.33	-217.41	19.72	45.14
286	432.00	357.50	428.73	-1719.80	45.57	35.93	-1273.31	85.49	309.22	-217.41	19.72	41.87
287	432.00	357.50	428.73	-1719.80	45.57	35.93	-1273.31	85.49	309.22	-217.41	19.72	41.87
288	432.00	357.50	428.73	-1719.80	45.57	35.93	-1273.31	85.49	309.22	-217.41	19.72	41.87
289	432.00	357.50	428.73	-1719.80	45.57	35.93	-1273.31	85.49	309.22	-217.41	19.72	41.87
290	432.00	357.50	428.70	-1719.80	45.57	22.13	-1273.31	85.49	303.28	-217.41	19.72	40.92
291	432.00	357.50	428.70	-1719.80	45.57	22.13	-1273.31	85.49	303.28	-217.41	19.72	40.92
292	432.00	357.50	428.70	-1719.80	45.57	22.13	-1273.31	85.49	303.28	-217.41	19.72	40.92
293	432.00	357.50	428.70	-1719.80	45.57	22.13	-1273.31	85.49	303.28	-217.41	19.72	40.92
294	432.00	357.50	446.38	-1719.80	45.57	-1355.94	-1273.31	85.49	115.91	-217.41	19.72	8.90
295	432.00	357.50	446.38	-1719.80	45.57	-1355.94	-1273.31	85.49	115.91	-217.41	19.72	8.90
296	432.00	357.50	446.38	-1719.80	45.57	-1355.94	-1273.31	85.49	115.91	-217.41	19.72	8.90
297	432.00	357.50	451.32	-1719.80	45.57	-1544.06	-1273.31	85.49	67.73	-217.41	19.72	0.26
298	432.00	357.50	451.32	-1719.80	45.57	-1544.06	-1273.31	85.49	67.73	-217.41	19.72	0.26
299	432.00	357.50	451.32	-1719.80	45.57	-1544.06	-1273.31	85.49	67.73	-217.41	19.72	0.26
300	432.00	357.50	451.32	-1719.80	45.57	-1544.06	-1273.31	85.49	67.73	-217.41	19.72	0.26
301	432.00	357.50	439.13	-1719.80	45.57	-2366.74	-1273.31	85.49	146.89	-217.41	19.72	17.54
302	432.00	357.50	439.13	-1719.80	45.57	-2366.74	-1273.31	85.49	146.89	-217.41	19.72	17.54
303	432.00	357.50	439.13	-1719.80	45.57	-2366.74	-1273.31	85.49	146.89	-217.41	19.72	17.54
304	432.00	357.50	439.13	-1719.80	45.57	-2366.74	-1273.31	85.49	146.89	-217.41	19.72	17.54
305	432.00	357.50	453.74	-1719.80	45.57	-1787.87	-1273.31	85.49	19.52	-217.41	19.72	-7.75
306	432.00	357.50	453.74	-1719.80	45.57	-1787.87	-1273.31	85.49	19.52	-217.41	19.72	-7.75
307	432.00	357.50	453.74	-1719.80	45.57	-1787.87	-1273.31	85.49	19.52	-217.41	19.72	-7.75
308	432.00	357.50	453.74	-1719.80	45.57	-1787.87	-1273.31	85.49	19.52	-217.41	19.72	-7.75
309	432.25	357.50	452.71	-1813.29	45.57	-1739.95	-1333.99	85.49	15.25	-227.32	19.72	-8.34
310	432.25	357.50	452.71	-1813.29	45.57	-1739.95	-1333.99	85.49	15.25	-227.32	19.72	-8.34
311	432.25	357.50	452.71	-1813.29	45.57	-1739.95	-1333.99	85.49	15.25	-227.32	19.72	-8.34

Continued on next page

Table D.1 – *Continued from previous page*

312	432.25	357.50	452.71	-1813.29	45.57	-1739.95	-1333.99	85.49	15.25	-227.32	19.72	-8.34
313	432.25	357.50	419.14	-1813.29	45.57	-1485.54	-1333.99	85.49	409.47	-227.32	19.72	63.47
314	432.25	357.50	419.14	-1813.29	45.57	-1485.54	-1333.99	85.49	409.47	-227.32	19.72	63.47
315	432.25	357.50	419.14	-1813.29	45.57	-1485.54	-1333.99	85.49	409.47	-227.32	19.72	63.47
316	432.25	357.50	419.14	-1813.29	45.57	-1485.54	-1333.99	85.49	409.47	-227.32	19.72	63.47
317	432.25	357.50	509.09	-1813.29	45.57	-2662.38	-1333.99	85.49	249.09	-227.32	19.72	20.39
318	432.25	357.50	509.09	-1813.29	45.57	-2662.38	-1333.99	85.49	249.09	-227.32	19.72	20.39
319	432.25	357.50	509.09	-1813.29	45.57	-2662.38	-1333.99	85.49	249.09	-227.32	19.72	20.39
320	432.25	357.50	509.09	-1813.29	45.57	-2662.38	-1333.99	85.49	249.09	-227.32	19.72	20.39
321	432.25	357.50	509.31	-1813.29	45.57	-2662.38	-1333.99	85.49	249.09	-227.32	19.72	20.34
322	432.25	357.50	509.31	-1813.29	45.57	-2662.38	-1333.99	85.49	249.09	-227.32	19.72	20.34
323	432.25	357.50	509.31	-1813.29	45.57	-2662.38	-1333.99	85.49	249.09	-227.32	19.72	20.34
324	432.25	357.50	509.31	-1813.29	45.57	-2662.38	-1333.99	85.49	249.09	-227.32	19.72	20.34
325	432.25	357.50	509.31	-1813.29	45.57	-2681.20	-1333.99	85.49	236.61	-227.32	19.72	18.31
326	432.25	357.50	509.31	-1813.29	45.57	-2681.20	-1333.99	85.49	236.61	-227.32	19.72	18.31
327	432.25	357.50	509.31	-1813.29	45.57	-2681.20	-1333.99	85.49	236.61	-227.32	19.72	18.31
328	432.25	357.50	509.31	-1813.29	45.57	-2681.20	-1333.99	85.49	236.61	-227.32	19.72	18.31
329	432.25	357.47	509.63	-1813.29	9.13	-2632.07	-1333.99	78.23	276.10	-227.32	18.60	24.69
330	432.25	357.47	509.63	-1813.29	9.13	-2632.07	-1333.99	78.23	276.10	-227.32	18.60	24.69
331	432.25	357.47	509.63	-1813.29	9.13	-2632.07	-1333.99	78.23	276.10	-227.32	18.60	24.69
332	432.25	357.47	509.63	-1813.29	9.13	-2632.07	-1333.99	78.23	276.10	-227.32	18.60	24.69
333	432.25	357.47	485.96	-1813.29	9.13	-2098.20	-1333.99	78.23	249.19	-227.32	18.60	24.14
334	432.25	357.47	485.96	-1813.29	9.13	-2098.20	-1333.99	78.23	249.19	-227.32	18.60	24.14
335	432.25	357.47	485.96	-1813.29	9.13	-2098.20	-1333.99	78.23	249.19	-227.32	18.60	24.14
336	432.25	357.47	485.96	-1813.29	9.13	-2098.20	-1333.99	78.23	249.19	-227.32	18.60	24.14
337	432.25	357.47	477.46	-1813.29	9.13	-1916.77	-1333.99	78.23	277.80	-227.32	18.60	30.30
338	432.25	357.47	477.46	-1813.29	9.13	-1916.77	-1333.99	78.23	277.80	-227.32	18.60	30.30
339	432.25	357.47	477.46	-1813.29	9.13	-1916.77	-1333.99	78.23	277.80	-227.32	18.60	30.30

Continued on next page

Table D.1 – *Continued from previous page*

340	432.25	357.47	477.46	-1813.29	9.13	-1916.77	-1333.99	78.23	277.80	-227.32	18.60	30.30
341	432.25	357.47	455.35	-1813.29	9.13	-1703.62	-1333.99	78.23	213.36	-227.32	18.60	23.84
342	432.25	357.47	455.35	-1813.29	9.13	-1703.62	-1333.99	78.23	213.36	-227.32	18.60	23.84
343	432.25	357.47	455.35	-1813.29	9.13	-1703.62	-1333.99	78.23	213.36	-227.32	18.60	23.84
344	432.25	357.47	455.35	-1813.29	9.13	-1703.62	-1333.99	78.23	213.36	-227.32	18.60	23.84
345	432.25	357.47	455.28	-1813.29	9.13	-1614.66	-1333.99	78.23	281.51	-227.32	18.60	34.96
346	432.25	357.47	455.28	-1813.29	9.13	-1614.66	-1333.99	78.23	281.51	-227.32	18.60	34.96
347	432.25	357.47	455.28	-1813.29	9.13	-1614.66	-1333.99	78.23	281.51	-227.32	18.60	34.96
348	432.25	357.47	455.28	-1813.29	9.13	-1614.66	-1333.99	78.23	281.51	-227.32	18.60	34.96
349	432.25	357.47	455.43	-1813.29	9.13	-1663.35	-1333.99	78.23	236.97	-227.32	18.60	27.65
350	432.25	357.47	455.43	-1813.29	9.13	-1663.35	-1333.99	78.23	236.97	-227.32	18.60	27.65
351	432.25	357.47	455.43	-1813.29	9.13	-1663.35	-1333.99	78.23	236.97	-227.32	18.60	27.65
352	432.25	357.47	455.43	-1813.29	9.13	-1663.35	-1333.99	78.23	236.97	-227.32	18.60	27.65
353	432.25	357.47	455.42	-1813.29	9.13	-1676.08	-1333.99	78.23	233.23	-227.32	18.60	27.06
354	432.25	357.47	455.42	-1813.29	9.13	-1676.08	-1333.99	78.23	233.23	-227.32	18.60	27.06
355	432.25	357.47	455.42	-1813.29	9.13	-1676.08	-1333.99	78.23	233.23	-227.32	18.60	27.06
356	432.25	357.47	455.42	-1813.29	9.13	-1676.08	-1333.99	78.23	233.23	-227.32	18.60	27.06
357	432.25	357.47	391.02	-1813.29	9.13	-3145.48	-1333.99	78.23	24.27	-227.32	18.60	8.84
358	432.25	357.47	391.02	-1813.29	9.13	-3145.48	-1333.99	78.23	24.27	-227.32	18.60	8.84
359	432.25	357.47	391.02	-1813.29	9.13	-3145.48	-1333.99	78.23	24.27	-227.32	18.60	8.84
360	432.25	357.47	391.02	-1813.29	9.13	-3145.48	-1333.99	78.23	24.27	-227.32	18.60	8.84
361	432.25	357.47	389.52	-1813.29	9.13	-1583.27	-1333.99	78.23	-164.86	-227.32	18.60	-25.24
362	432.25	357.47	389.52	-1813.29	9.13	-1583.27	-1333.99	78.23	-164.86	-227.32	18.60	-25.24
363	432.25	357.47	389.52	-1813.29	9.13	-1583.27	-1333.99	78.23	-164.86	-227.32	18.60	-25.24
364	432.25	357.47	389.52	-1813.29	9.13	-1583.27	-1333.99	78.23	-164.86	-227.32	18.60	-25.24
365	432.25	357.47	390.81	-1813.29	9.13	-1636.98	-1333.99	78.23	-190.39	-227.32	18.60	-29.63
366	432.25	357.47	390.81	-1813.29	9.13	-1636.98	-1333.99	78.23	-190.39	-227.32	18.60	-29.63
367	432.25	357.47	390.81	-1813.29	9.13	-1636.98	-1333.99	78.23	-190.39	-227.32	18.60	-29.63

Continued on next page

Table D.1 – *Continued from previous page*

368	432.25	357.47	390.81	-1813.29	9.13	-1636.98	-1333.99	78.23	-190.39	-227.32	18.60	-29.63
369	432.25	357.47	390.81	-1813.29	9.13	-1636.98	-1333.99	78.23	-190.39	-227.32	18.60	-29.63
370	432.25	357.47	390.81	-1813.29	9.13	-1636.98	-1333.99	78.23	-190.39	-227.32	18.60	-29.63
371	432.25	357.47	390.81	-1813.29	9.13	-1636.98	-1333.99	78.23	-190.39	-227.32	18.60	-29.63
372	432.25	357.47	390.81	-1813.29	9.13	-1636.98	-1333.99	78.23	-190.39	-227.32	18.60	-29.63
373	432.25	357.47	392.92	-1813.29	9.13	-1684.68	-1333.99	78.23	-190.32	-227.32	18.60	-29.96
374	432.25	357.47	392.92	-1813.29	9.13	-1684.68	-1333.99	78.23	-190.32	-227.32	18.60	-29.96
375	432.25	357.47	392.92	-1813.29	9.13	-1684.68	-1333.99	78.23	-190.32	-227.32	18.60	-29.96
376	432.25	357.47	392.92	-1813.29	9.13	-1684.68	-1333.99	78.23	-190.32	-227.32	18.60	-29.96
377	432.25	357.47	398.48	-1813.29	9.13	-1679.87	-1333.99	78.23	-152.25	-227.32	18.60	-24.83
378	432.25	357.47	398.48	-1813.29	9.13	-1679.87	-1333.99	78.23	-152.25	-227.32	18.60	-24.83
379	432.25	357.47	398.48	-1813.29	9.13	-1679.87	-1333.99	78.23	-152.25	-227.32	18.60	-24.83
380	432.25	357.47	398.48	-1813.29	9.13	-1679.87	-1333.99	78.23	-152.25	-227.32	18.60	-24.83
381	432.25	357.47	399.33	-1813.29	9.13	-1645.38	-1333.99	78.23	-132.94	-227.32	18.60	-21.88
382	432.25	357.47	399.33	-1813.29	9.13	-1645.38	-1333.99	78.23	-132.94	-227.32	18.60	-21.88
383	432.25	357.47	399.33	-1813.29	9.13	-1645.38	-1333.99	78.23	-132.94	-227.32	18.60	-21.88
384	432.25	357.47	399.33	-1813.29	9.13	-1645.38	-1333.99	78.23	-132.94	-227.32	18.60	-21.88
385	432.25	357.47	403.75	-1813.29	9.13	-1545.32	-1333.99	78.23	-29.01	-227.32	18.60	-5.79
386	432.25	357.47	403.75	-1813.29	9.13	-1545.32	-1333.99	78.23	-29.01	-227.32	18.60	-5.79
387	432.25	357.47	390.55	-1813.29	9.13	-1888.72	-1333.99	78.23	-206.05	-227.32	18.60	-31.67
388	432.25	357.47	390.55	-1813.29	9.13	-1888.72	-1333.99	78.23	-206.05	-227.32	18.60	-31.67
389	432.25	357.47	390.46	-1813.29	9.13	-1626.19	-1333.99	78.23	-225.14	-227.32	18.60	-35.33
390	432.25	357.47	390.46	-1813.29	9.13	-1626.19	-1333.99	78.23	-225.14	-227.32	18.60	-35.33
391	432.25	357.47	390.46	-1813.29	9.13	-1626.19	-1333.99	78.23	-225.14	-227.32	18.60	-35.33
392	432.25	357.47	390.46	-1813.29	9.13	-1626.19	-1333.99	78.23	-225.14	-227.32	18.60	-35.33
393	432.25	357.47	454.41	-1813.29	9.13	-1641.40	-1333.99	78.23	232.78	-227.32	18.60	27.13
394	432.25	357.47	454.41	-1813.29	9.13	-1641.40	-1333.99	78.23	232.78	-227.32	18.60	27.13
395	432.25	357.47	454.41	-1813.29	9.13	-1641.40	-1333.99	78.23	232.78	-227.32	18.60	27.13

Continued on next page

Table D.1 – *Continued from previous page*

396	432.25	357.47	454.41	-1813.29	9.13	-1641.40	-1333.99	78.23	232.78	-227.32	18.60	27.13
397	432.25	357.47	435.76	-1813.29	9.13	-1732.23	-1333.99	78.23	87.68	-227.32	18.60	7.19
398	432.25	357.47	435.76	-1813.29	9.13	-1732.23	-1333.99	78.23	87.68	-227.32	18.60	7.19
399	432.25	357.47	435.76	-1813.29	9.13	-1732.23	-1333.99	78.23	87.68	-227.32	18.60	7.19
400	432.25	357.47	435.76	-1813.29	9.13	-1732.23	-1333.99	78.23	87.68	-227.32	18.60	7.19
401	432.25	357.47	454.85	-1813.29	9.13	-1670.55	-1333.99	78.23	222.48	-227.32	18.60	25.39
402	432.25	357.47	454.85	-1813.29	9.13	-1670.55	-1333.99	78.23	222.48	-227.32	18.60	25.39
403	432.25	357.47	454.85	-1813.29	9.13	-1670.55	-1333.99	78.23	222.48	-227.32	18.60	25.39
404	432.25	357.47	454.85	-1813.29	9.13	-1670.55	-1333.99	78.23	222.48	-227.32	18.60	25.39
405	432.25	357.47	453.64	-1813.29	9.13	-1664.81	-1333.99	78.23	211.83	-227.32	18.60	23.87
406	432.25	357.47	453.64	-1813.29	9.13	-1664.81	-1333.99	78.23	211.83	-227.32	18.60	23.87
407	432.25	357.47	453.64	-1813.29	9.13	-1664.81	-1333.99	78.23	211.83	-227.32	18.60	23.87
408	432.25	357.47	453.64	-1813.29	9.13	-1664.81	-1333.99	78.23	211.83	-227.32	18.60	23.87
409	429.58	357.47	454.85	-1725.49	9.13	-1670.55	-1304.15	78.23	222.48	-222.00	18.60	25.39
410	429.58	357.47	454.85	-1725.49	9.13	-1670.55	-1304.15	78.23	222.48	-222.00	18.60	25.39
411	429.58	357.47	454.85	-1725.49	9.13	-1670.55	-1304.15	78.23	222.48	-222.00	18.60	25.39
412	429.58	357.47	454.85	-1725.49	9.13	-1670.55	-1304.15	78.23	222.48	-222.00	18.60	25.39
413	429.58	357.47	390.46	-1725.49	9.13	-1626.19	-1304.15	78.23	-225.14	-222.00	18.60	-35.33
414	429.58	357.47	390.46	-1725.49	9.13	-1626.19	-1304.15	78.23	-225.14	-222.00	18.60	-35.33
415	429.58	357.47	390.46	-1725.49	9.13	-1626.19	-1304.15	78.23	-225.14	-222.00	18.60	-35.33
416	429.58	357.47	390.46	-1725.49	9.13	-1626.19	-1304.15	78.23	-225.14	-222.00	18.60	-35.33
417	429.58	357.47	454.85	-1725.49	9.13	-1670.55	-1304.15	78.23	222.48	-222.00	18.60	25.39
418	429.58	357.47	454.85	-1725.49	9.13	-1670.55	-1304.15	78.23	222.48	-222.00	18.60	25.39
419	429.58	357.47	454.85	-1725.49	9.13	-1670.55	-1304.15	78.23	222.48	-222.00	18.60	25.39
420	429.58	357.47	454.85	-1725.49	9.13	-1670.55	-1304.15	78.23	222.48	-222.00	18.60	25.39
421	429.58	357.47	390.48	-1725.49	9.13	-1619.66	-1304.15	78.23	-195.75	-222.00	18.60	-30.48
422	429.58	357.47	390.48	-1725.49	9.13	-1619.66	-1304.15	78.23	-195.75	-222.00	18.60	-30.48
423	429.58	357.47	390.48	-1725.49	9.13	-1619.66	-1304.15	78.23	-195.75	-222.00	18.60	-30.48

Continued on next page

Table D.1 – *Continued from previous page*

424	429.58	357.47	390.48	-1725.49	9.13	-1619.66	-1304.15	78.23	-195.75	-222.00	18.60	-30.48
425	429.58	357.47	454.41	-1725.49	9.13	-1641.40	-1304.15	78.23	232.78	-222.00	18.60	27.13
426	429.58	357.47	454.41	-1725.49	9.13	-1641.40	-1304.15	78.23	232.78	-222.00	18.60	27.13
427	429.58	357.47	454.41	-1725.49	9.13	-1641.40	-1304.15	78.23	232.78	-222.00	18.60	27.13
428	429.58	357.47	454.41	-1725.49	9.13	-1641.40	-1304.15	78.23	232.78	-222.00	18.60	27.13
429	429.58	357.47	454.41	-1725.49	9.13	-1641.40	-1304.15	78.23	232.78	-222.00	18.60	27.13
430	429.58	357.47	454.41	-1725.49	9.13	-1641.40	-1304.15	78.23	232.78	-222.00	18.60	27.13
431	429.58	357.47	454.41	-1725.49	9.13	-1641.40	-1304.15	78.23	232.78	-222.00	18.60	27.13
432	429.58	357.47	454.41	-1725.49	9.13	-1641.40	-1304.15	78.23	232.78	-222.00	18.60	27.13

References

Anderson, B. E., Gregory, G. L., Collins, J. E., Sachse, G. W., Conway, T. J., and Whiting, G. P. (1996). "Airborne observations of spatial and temporal variability of tropospheric carbon dioxide". *J. Geophys. Res.-Atmos.*, *101*, 1985–1997. DOI: 10.1029/95JD00413.

Assonov, S., Taylor, P., and Brenninkmeijer, C. A. M. (2009). "A system for high-quality CO_2 isotope analyses of air samples collected by the CARIBIC Airbus A340-600". *Rapid Commun. Mass Spectrom.*, *23*, 1347–1363. DOI: 10.1002/rcm.4008.

Barnola, J. M. (1999). "Status of the atmospheric CO_2 reconstruction from ice cores analyses". *Tellus, Ser. B*, *51*, 151–155. DOI: 10.1034/j.1600-0889.1999.t01-1-00002.x.

Battle, M., Fletcher, S. E. M., Bender, M. L., Keeling, R. F., Manning, A. C., Gruber, N., Tans, P. P., Hendricks, M. B., Ho, D. T., Simonds, C., Mika, R., and Paplawsky, B. (2006). "Atmospheric potential oxygen: New observations and their implications for some atmospheric and oceanic models". *Global Biogeochem. Cycles*, *20*, GB1010. DOI: 10.1029/2005GB002534.

Bender, M. L., Tans, P. P., Ellis, J. T., Orchardo, J., and Habfast, K. (1994). "A high-precision isotope ratio mass-spectrometry method for measuring the O_2/N_2 ratio of air". *Geochim. Cosmochim. Acta*, *58*, 4751–4758. DOI: 10.1016/0016-7037(94)90205-4.

Bender, M. L., Ho, D. T., Hendricks, M. B., Mika, R., Battle, M. O., Tans, P. P., Conway, T. J., Sturtevant, B., and Cassar, N. (2005). "Atmospheric O_2/N_2 changes, 1993-2002: Implications for the partitioning of fossil fuel CO_2 sequestration". *Global Biogeochem. Cycles*, *19*, GB4017. DOI: 10.1029/2004GB002410.

Bender, M. (2006). *The distribution of O_2 in air*. Princeton University, Department of Geosciences. URL: http://geoweb.princeton.edu/people/bender/lab/research_o2n2.html (visited on 08/10/2013).

Bender, M., Ellis, T., Tans, P., Francey, R., and Lowe, D. (1996). "Variability in the O_2/N_2 ratio of southern hemisphere air, 1991-1994: Implications for the carbon cycle". *Global Biogeochem. Cycles*, *10*, 9–21. DOI: 10.1029/95GB03295.

Bischof, W. (1970). "Carbon dioxide measurements from aircraft". *Tellus*, *22*, 545–549. DOI: 10.1111/j.2153-3490.1970.tb00521.x.

Boenisch, H., Engel, A., Curtius, J., Birner, Th., and Hoor, P. (2009). "Quantifying transport into the lowermost stratosphere using simultaneous in-situ measurements of SF_6 and CO_2". *Atmos. Chem. Phys.*, *9*, 5905–5919. DOI: 10.5194/acp-9-5905-2009.

Boering, K. A., Wofsy, S. C., Daube, B. C., Schneider, H. R., Loewenstein, M., and Podolske, J. R. (1996). "Stratospheric mean ages and transport rates from observations of carbon dioxide and nitrous oxide". *Science*, *274*, 1340–1343. DOI: 10.1126/science.274.5291.1340.

Boettern, L. (2000). *How sensors work*. Tech. rep. Biosystems, Inc.

Brenninkmeijer, C. A. M., Crutzen, P. J., Fischer, H., Gusten, H., Hans, W., Heinrich, G., Heintzenberg, J., Hermann, M., Immelmann, T., Kersting, D., Maiss, M., Nolle, M., Pitscheider, A., Pohlkamp, H., Scharffe, D., Specht, K., and Wiedensohler, A. (1999). "CARIBIC - Civil aircraft for global measurement of trace gases and aerosols in the tropopause region". *J. Atmos. Oceanic Technol.*, *16*, 1373–1383. DOI: 10.1175/1520-0426(1999)016<1373:CCAFGM>2.0.CO;2.

Brenninkmeijer, C. A. M., Crutzen, P., Boumard, F., Dauer, T., Dix, B., Ebinghaus, R., Filippi, D., Fischer, H., Franke, H., Friess, U., Heintzenberg, J., Helleis, F., Hermann, M., Kock, H. H., Koeppel, C., Lelieveld, J., Leuenberger, M., Martinsson, B. G., Miemczyk, S., Moret, H. P., Nguyen, H. N., Nyfeler, P., Oram, D., O'Sullivan, D., Penkett, S., Platt, U., Pupek, M., Ramonet, M., Randa, B., Reichelt, M., Rhee, T. S., Rohwer, J., Rosenfeld, K., Scharffe, D., Schlager, H., Schumann, U., Slemr, F., Sprung, D., Stock, P., Thaler, R., Valentino, F., Velthoven, P. van, Waibel, A., Wandel, A., Waschitschek, K., Wiedensohler, A., Xueref-Remy, I., Zahn, A., Zech, U., and Ziereis, H. (2007). "Civil aircraft for the regular investigation of the atmosphere based on an instrumented container: The new CARIBIC system". *Atmos. Chem. Phys.*, *7*, 4953–4976. DOI: 10.5194/acp-7-4953-2007.

Chen, H., Winderlich, J., Gerbig, C., Hoefer, A., Rella, C. W., Crosson, E. R., Van Pelt, A. D., Steinbach, J., Kolle, O., Beck, V., Daube, B. C., Gottlieb, E. W., Chow, V. Y., Santoni, G. W., and Wofsy, S. C. (2010). "High-accuracy continuous airborne measurements of greenhouse gases (CO_2 and CH_4) using the cavity ring-down spectroscopy (CRDS) technique". *Atmos. Meas. Tech.*, *3*, 375–386. DOI: 10.5194/amt-3-375-2010.

Ciais, P., Tans, P. P., White, J. W. C., Trolier, M., Francey, R. J., Berry, J. A., Randall, D. R., Sellers, P. J., Collatz, J. G., and Schimel, D. S. (1995). "Partitioning of ocean and land uptake of CO_2 as inferred by $\delta^{13}C$ measurements from the NOAA Climate Monitoring and Diagnostics Laboratory Global Air Sampling Network". *J. Geophys. Res.-Atmos.*, *100*, 5051–5070. DOI: 10.1029/94JD02847.

Dattore, B. (2011). *Global Change Master Directory (GCMD)*. NASA. URL: http://gcmd.nasa.gov/records/GCMD_NCAR_DS368.0.html (visited on 11/12/2012).

Dias-Lalcaca, P., Brunner, D., Imfeld, W., Moser, W., and Staehelin, J. (1998). "An automated system for the measurement of nitrogen oxides and ozone concentrations from a passenger aircraft: Instrumentation and first results of the NOXAR project". *Environ. Sci. Technol.*, *32*, 3228–3236. DOI: 10.1021/es980119w.

Falconer, P. D. and Holdeman, J. D. (1976). "Measurements of atmospheric ozone made from a GASP-equipped 747-airliner - mid-March, 1975". *Geophys. Res. Lett.*, *3*, 101–104. DOI: 10.1029/GL003i002p00101.

Gibert, F., Joly, L., Xueref-Remy, I., Schmidt, M., Royer, A., Flamant, P. H., Ramonet, M., Parvitte, B., Durry, G., and Zeninari, V. (2009). "Inter-comparison of 2 µm Heterodyne Differential Absorption Lidar, Laser Diode Spectrometer, LICOR NDIR analyzer and flasks measurements of near-ground atmospheric CO_2 mixing ratio". *Spectrochim. Acta A*, *71*, 1914–1921. DOI: 10.1016/j.saa.2008.07.010.

Goto, D. (2011). "Observations of temporal and spatial variations of the atmospheric oxygen concentration and estimation of global carbon budget". PhD thesis. Tohoku University, Sendai, Japan.

Gurk, Ch., Fischer, H., Hoor, P., Lawrence, M. G., Lelieveld, J., and Wernli, H. (2008). "Airborne in-situ measurements of vertical, seasonal and latitudinal distributions of carbon dioxide over Europe". *Atmos. Chem. Phys.*, *8*, 6395–6403. DOI: 10.5194/acp-8-6395-2008.

Hintsa, E. J., Boering, K. A., Weinstock, E. M., Anderson, J. G., Gary, B. L., Pfister, L., Daube, B. C., Wofsy, S. C., Loewenstein, M., Podolske, J. R., Margitan, J. J., and Bui, T. P. (1998). "Troposphere-to-stratosphere transport in the lowermost stratosphere from measurements of H_2O, CO_2, N_2O and O_3". *Geophys. Res. Lett.*, *25*, 2655–2658. DOI: 10.1029/98GL01797.

Hoor, P., Gurk, C., Brunner, D., Hegglin, M. I., Wernli, H., and Fischer, H. (2004). "Seasonality and extent of extratropical TST derived from in-situ CO measurements during SPURT". *Atmos. Chem. Phys.*, *4*, 1427–1442. DOI: 10.5194/acp-4-1427-2004.

IAGOS (2012). *Related Projects*. IAGOS. URL: http://www.iagos.org/Related_Projects (visited on 01/31/2013).

IPCC (2003). *Climate Change 2001: The Scientific Basis. Contribution of Working Group I to the Third Assessment Report of the Intergovernmental Panel on Climate Change*. Ed. by J. T. Houghton, Y. Ding, D. J. Griggs, M. Noguer, P. J. van der Linden, X. Dai, K. Maskell, and C. A. Johnson. Cambridge University Press, Cambridge, UK, pp. 19–91.

IPCC (2007). *Climate Change 2007: The Physical Science Basis. Contribution of Working Group I to the Fourth Assessment Report of the Intergovernmental Panel on Climate Change*. Ed. by S. Solomon, D. Qin, M. Manning, Z. Chen, M. Marquis, K. B. Averyt, M. Tignor, and H. L. Miller. Cambridge University Press, Cambridge, UK and New York, NY, USA, pp. 19–91.

Ishidoya, S., Sugawara, S., Hashida, G., Morimoto, S., Aoki, S., Nakazawa, T., and Yamanouchi, T. (2006). "Vertical profiles of the O_2/N_2 ratio in the stratosphere over Japan and Antarctica". *Geophys. Res. Lett.*, *33*, 4. DOI: 10.1029/2006gl025886.

Ishidoya, S., Aoki, S., Goto, D., Nakazawa, T., Taguchi, S., and Patra, P. K. (2012). "Time and space variations of the O_2/N_2 ratio in the troposphere over Japan and estimation of the global CO_2 budget for the period 2000-2010". *Tellus, Ser. B*, *64*, 18964. DOI: 10.3402/tellusb.v64i0.18964.

James, R. and Legras, B. (2009). "Mixing processes and exchanges in the tropical and the subtropical UT/LS". *Atmos. Chem. Phys.*, *9*, 25–38.

Joos, F. (2012). *Introduction to the carbon cycle*. lecture notes, Physics Institute, University of Bern, Switzerland.

Keeling, C. D. and Whorf, T. P. (2000). *Trends: A compendium of data on global change*. Carbon Dioxide Information Analysis Center, Oak Ridge National Laboratory, US Department of Energy, Oak Ridge, Tennessee. URL: http://cdiac.esd.ornl.gov/ndps/ndp001.html.

Keeling, C. D., Bacastow, R. B., Bainbridge, A. E., Ekdahl, C. A., Guenther, P. R., Waterman, L. S., and Chin, J. F. S. (1976). "Atmospheric carbon-dioxide variations at Mauna-Loa observatory, Hawaii". *Tellus*, *28*, 538–551.

Keeling, C. D., Chin, J. F. S., and Whorf, T. P. (1996). "Increased activity of northern vegetation inferred from atmospheric CO_2 measurements". *Nature*, *382*, 146–149. DOI: 10.1038/382146a0.

Keeling, R. F. (1988a). "Development of an interferometric oxygen analyzer for precise measurement of the atmospheric O_2 mole fraction". PhD thesis. Harvard University, Cambridge, USA.

Keeling, R. F. (1988b). "Measuring correlations between atmospheric oxygen and carbon-dioxide mole fractions - a preliminary-study in urban air". *J. Atmos. Chem.*, *7*, 153–176. DOI: 10.1007/BF00048044.

Keeling, R. F. and Shertz, S. R. (1992). "Seasonal and interannual variations in atmospheric oxygen and implications for the global carbon-cycle". *Nature*, *358*, 723–727. DOI: 10.1038/358723a0.

Keeling, R. F., Najjar, R. P., Bender, M. L., and Tans, P. P. (1993). "What atmospheric oxygen measurements can tell us about the global carbon-cycle". *Global Biogeochem. Cycles*, *7*, 37–67. DOI: 10.1029/92gb02733.

Keeling, R. F., Manning, A. C., McEvoy, E. M., and Shertz, S. R. (1998a). "Methods for measuring changes in atmospheric O_2 concentration and their application in southern hemisphere air". *J. Geophys. Res.-Atmos.*, *103*, 3381–3397. DOI: 10.1029/97JD02537.

Keeling, R. F., Manning, A. C., Paplawsky, W. J., and Cox, A. C. (2007). "On the long-term stability of reference gases for atmospheric O_2/N_2 and CO_2 measurements". *Tellus, Ser. B*, *59*, 3–14. DOI: 10.1111/j.1600-0889.2006.00228.x.

Keeling, R. (2010). *Atmospheric Oxygen Research Group - Data*. Scripps Institution of Oceanography. URL: http://bluemoon.ucsd.edu/data.html (visited on 08/10/2013).

Keeling, RF, Stephens, BB, Najjar, RG, Doney, SC, Archer, D, and Heimann, M (1998b). "Seasonal variations in the atmospheric O_2/N_2 ratio in relation to the kinetics of air-sea gas exchange". *Global Biogeochem. Cycles*, *12*, 141–163. DOI: 10.1029/97GB02339.

LI-COR (1996). *LI-6262 CO_2/H_2O Analyzer Instruction Manual*. Tech. rep. LI-COR, Inc.

Laan-Luijkx, I. T. van der, Neubert, R. E. M., Laan, S. van der, and Meijer, H. A. J. (2010a). "Continuous measurements of atmospheric oxygen and carbon dioxide on a North Sea gas platform". *Atmos. Meas. Tech.*, *3*, 113–125. DOI: 10.5194/amt-3-113-2010.

Laan-Luijkx, I. T. van der, Karstens, U., Steinbach, J., Gerbig, C., Sirignano, C., Neubert, R. E. M., Laan, S. van der, and Meijer, H. A. J. (2010b). "CO_2, delta O_2/N_2 and APO: observations from the Lutjewad, Mace Head and F3 platform flask sampling network". *Atmos. Chem. Phys.*, *10*, 10691–10704. DOI: 10.5194/acp-10-10691-2010.

Laan-Luijkx, I. van der (2010). "Atmospheric oxygen and the global carbon cycle. Observations from the new F3 North Sea platform monitoring station and 6 additional locations in Europe and Siberia". PhD thesis. University of Groningen, Groningen, Netherlands.

Langenfelds, R. L. (2002). "Studies of the global carbon cycle using atmospheric oxygen and associated tracers". PhD thesis. University of Tasmania, Hobart, Australia.

Le Quéré, C., Orr, J. C., Monfray, P., Aumont, O., and Madec, G. (2000). "Interannual variability of the oceanic sink of CO_2 from 1979 through 1997". *Global Biogeochem. Cycles*, *14*, 1247–1265. DOI: 10.1029/1999GB900049.

Leuenberger, M., Nyfeler, P., Moret, H. P., Sturm, P., Indermuhle, A., and Schwander, J. (2000). "CO_2 concentration measurements on air samples by mass spectrometry". *Rapid Commun. Mass Spectrom.*, *14*, 1552–1557. DOI: 10.1002/1097-0231(20000830)14:16<1552::AID-RCM63>3.0.CO;2-C.

Liu, B. Y. H., Zhang, Z. Q., and Kuehn, T. H. (1989). "A numerical study of inertial errors in anisokinetic sampling". *J. Aerosol Sci.*, *20*, 367–380. DOI: 10.1016/0021-8502(89)90012-8.

Machida, T., Kita, K., Kondo, Y., Blake, D., Kawakami, S., Inoue, G., and Ogawa, T. (2002). "Vertical and meridional distributions of the atmospheric CO_2 mixing ratio between northern midlatitudes and southern subtropics". *J. Geophys. Res.-Atmos.*, *108*, 9. DOI: 10.1029/2001jd000910.

Machida, T., Matsueda, H., Sawa, Y., Nakagawa, Y., Hirotani, K., Kondo, N., Goto, K., Nakazawa, T., Ishikawa, K., and Ogawa, T. (2008). "Worldwide measurements of atmospheric CO_2 and other trace gas species using commercial airlines". *J. Atmos. Oceanic Technol.*, *25*, 1744–1754. DOI: 10.1175/2008jtecha1082.1.

Machta, L. and Hughes, E. (1970). "Atmospheric oxygen in 1967 to 1970". *Science*, *168*, 1582–1584. DOI: 10.1126/science.168.3939.1582.

Malhi, Y. (2002). "Carbon in the atmosphere and terrestrial biosphere in the 21st century". *Proc. R. Soc. Lond. A Math. Phys. Eng. Sci.*, *360*, 2925–2945. DOI: 10.1098/rsta.2002.1098.

Manning, A. C. (2001). "Temporal variability of atmospheric oxygen from both continuous measurements and a flask sampling network: Tools for studying the global carbon cycle". PhD thesis. University of California San Diego, La Jolla, California, USA.

Manning, A. C. and Keeling, R. F. (2006). "Global oceanic and land biotic carbon sinks from the Scripps atmospheric oxygen flask sampling network". *Tellus, Ser. B*, *58*, 95–116. DOI: 10.1111/j.1600-0889.2006.00175.x.

Manning, A. C., Keeling, R. F., and Severinghaus, J. P. (1999). "Precise atmospheric oxygen measurements with a paramagnetic oxygen analyzer". *Global Biogeochem. Cycles*, *13*, 1107–1115. DOI: 10.1029/1999GB900054.

Matsueda, H., Taguchi, S., Inoue, H. Y., and Ishii, M. (2002a). "A large impact of tropical biomass burning on CO and CO_2 in the upper troposphere". *Sci. China Ser. C*, *45*, 116–125.

Matsueda, H., Inoue, H. Y., and Ishii, M. (2002b). "Aircraft observation of carbon dioxide at 8-13 km altitude over the western Pacific from 1993 to 1999". *Tellus, Ser. B*, *54*, 1–21. DOI: 10.1034/j.1600-0889.2002.00304.x.

Matsueda, H., Machida, T., Sawa, Y., Nakagawa, Y., Hirotani, K., Ikeda, H., Kondo, N., and Goto, K. (2008). "Evaluation of atmospheric CO_2 measurements from new flask air sampling of JAL airliner observations". *Pap. Meteor. Geophys.*, *59*, 1–17. DOI: 10.2467/mripapers.59.1.

Maxtec (2003). *New, motion stable weak acid electrolyte oxygen sensor MAX-250 series*. Tech. rep. Maxtec, Inc.

McGuire, A. D., Sitch, S., Clein, J. S., Dargaville, R., Esser, G., Foley, J., Heimann, M., Joos, F., Kaplan, J., Kicklighter, D. W., Meier, R. A., Melillo, J. M., Moore, B., Prentice, I. C., Ramankutty, N., Reichenau, T., Schloss, A., Tian, H., Williams, L. J., and Wittenberg, U. (2001). "Carbon balance of the terrestrial biosphere in the twentieth century: Analyses of CO_2, climate and land use effects with four process-based ecosystem models". *Global Biogeochem. Cycles*, *15*, 183–206. DOI: 10.1029/2000GB001298.

NASA (2013). *Fire: Global maps*. NASA Earth Observatory. URL: http://earthobservatory.nasa.gov/GlobalMaps/view.php?d1=MOD14A1_M_FIRE (visited on 08/15/2013).

NOAA (2012). *ESRL Global Monitoring Division - Globalview*. NOAA. URL: http://www.esrl.noaa.gov/gmd/ccgg/globalview/ (visited on 08/15/2012).

Nakazawa, T., Miyashita, K., Aoki, S., and Tanaka, M. (1991). "Temporal and spatial variations of upper tropospheric and lower stratospheric carbon-dioxide". *Tellus, Ser. B*, *43*, 106–117. DOI: 10.1034/j.1600-0889.1991.t01-1-00005.x.

Pandey, S. K. and Kim, K. H. (2007). "The relative performance of NDIR-based sensors in the near real-time analysis of CO_2 in air". *Sensors*, *7*, 1683–1696. DOI: 10.3390/s7091683.

Park, S., Jimenez, R., Daube, B. C., Pfister, L., Conway, T. J., Gottlieb, E. W., Chow, V. Y., Curran, D. J., Matross, D. M., Bright, A., Atlas, E. L., Bui, T. P., Gao, R. S., Twohy, C. H., and Wofsy, S. C. (2007). "The CO_2 tracer clock for the tropical tropopause layer". *Atmos. Chem. Phys.*, *7*, 3989–4000. DOI: 10.5194/acp-7-3989-2007.

Patecki, M. and Manning, A. C. (2007). "First results from shipboard atmospheric O_2 and CO_2 measurements over the North Atlantic Ocean". *Oceans 2007 - Europe, Vols. 1-3*. 345 E 47th St, New York, NY 10017 USA: IEEE, pp. 864–869.

Plattner, G. K., Joos, F., and Stocker, T. F. (2002). "Revision of the global carbon budget due to changing air-sea oxygen fluxes". *Global Biogeochem. Cycles*, *16*, 43. DOI: 10.1029/2001GB001746.

Popa, M. E. (2007). "Continuous tall tower multispecies measurements in Europe for quantifying and understanding land-atmosphere carbon exchange". PhD thesis. Friedrich-Schiller-Universität, Jena, Germany.

Regnier, P., Friedlingstein, P., Ciais, P., Mackenzie, F. T., Gruber, N., Janssens, I. A., Laruelle, G. G., Lauerwald, R., Luyssaert, S., Andersson, A. J., Arndt, S., Arnosti, C., Borges, A. V., Dale, A. W., Gallego-Sala, A., Godderis, Y., Goossens, N., Hartmann, J., Heinze, C., Ilyina, T., Joos, F., LaRowe, D. E., Leifeld, J., Meysman, F. J. R., Munhoven, G., Raymond, P. A., Spahni, R.,

Suntharalingam, P., and Thullner, M. (2013). "Anthropogenic perturbation of the carbon fluxes from land to ocean". *Nat. Geosci.*, *6*, 597–607. DOI: 10.1038/ngeo1830.

Sarmiento, J. L. and Gruber, N. (2002). "Sinks for anthropogenic carbon". *Phys. Today*, *55*, 30–36. DOI: 10.1063/1.1510279.

Sawa, Y., Machida, T., and Matsueda, H. (2008). "Seasonal variations of CO_2 near the tropopause observed by commercial aircraft". *J. Geophys. Res.-Atmos.*, *113*, D23301. DOI: 10.1029/2008jd010568.

Sawa, Y., Machida, T., and Matsueda, H. (2012). "Aircraft observation of the seasonal variation in the transport of CO_2 in the upper atmosphere". *J. Geophys. Res.-Atmos.*, *117*, D05305. DOI: 10.1029/2011jd016933.

Scharffe, D., Slemr, F., Brenninkmeijer, C. A. M., and Zahn, A. (2012). "Carbon monoxide measurements onboard the CARIBIC passenger aircraft using UV resonance fluorescence". *Atmos. Meas. Tech.*, *5*, 1753–1760. DOI: 10.5194/amt-5-1753-2012.

Schuck, T. J., Brenninkmeijer, C. A. M., Slemr, F., Xueref-Remy, I., and Zahn, A. (2009). "Greenhouse gas analysis of air samples collected onboard the CARIBIC passenger aircraft". *Atmos. Meas. Tech.*, *2*, 449–464. DOI: 10.5194/amt-2-449-2009.

Severinghaus, J. P. (1995). "Studies of the terrestrial O_2 and carbon cycles in sand dune gases and in biosphere 2". PhD thesis. Columbia University, New York, USA.

Siegenthaler, U. and Sarmiento, J. L. (1993). "Atmospheric carbon-dioxide and the ocean". *Nature*, *365*, 119–125. DOI: 10.1038/365119a0.

Sprung, D. and Zahn, A. (2010). "Acetone in the upper troposphere/lowermost stratosphere measured by the CARIBIC passenger aircraft: distribution, seasonal cycle, and variability". *J. Geophys. Res.-Atmos.*, *115*, 12. DOI: 10.1029/2009JD012099.

Stephens, B. B. (1999). "Field-based atmospheric oxygen measurements and the ocen carbon cycle". PhD thesis. University of California, San Diego, USA.

Stephens, B. B., Keeling, R. F., Heimann, M., Six, K. D., Murnane, R., and Caldeira, K. (1998). "Testing global ocean carbon cycle models using measurements of atmospheric O_2 and CO_2 concentration". *Global Biogeochem. Cycles*, *12*, 213–230. DOI: 10.1029/97GB03500.

Stephens, B. B., Keeling, R. F., and Paplawsky, W. J. (2003). "Shipboard measurements of atmospheric oxygen using a vacuum-ultraviolet absorption technique". *Tellus, Ser. B*, *55*, 857–878. DOI: 10.1046/j.1435-6935.2003.00075.x.

Stephens, B. B., Bakwin, P. S., Tans, P. P., Teclaw, R. M., and Baumann, D. D. (2007a). "Application of a differential fuel-cell analyzer for measuring atmospheric oxygen variations". *J. Atmos. Oceanic Technol.*, *24*, 82–94. DOI: 10.1175/JTECH1959.1.

Stephens, B. B., Gurney, K. R., Tans, P. P., Sweeney, C., Peters, W., Bruhwiler, L., Ciais, P., Ramonet, M., Bousquet, P., Nakazawa, T., Aoki, S., Machida, T., Inoue, G., Vinnichenko, N., Lloyd, J., Jordan, A., Heimann, M., Shibistova, O., Langenfelds, R. L., Steele, L. P., Francey, R. J., and Denning, A. S. (2007b). "Weak northern and strong tropical land carbon uptake from vertical profiles of atmospheric CO_2". *Science*, *316*, 1732–1735. DOI: 10.1126/science.1137004.

Sturm, P. (2001). "Entwicklung eines neuen Einlasssystems für die massenspektrometrische Messung des O_2/N_2 Verhältnisses". MA thesis. University of Bern.

Sturm, P. (2005). "Atmospheric oxygen and associated tracers from flask sampling and continuous measurements: Tools for studying the global carbon cycle". PhD thesis. University of Bern, Bern, Switzerland.

Sturm, P., Leuenberger, M., Moncrieff, J., and Ramonet, M. (2005). "Atmospheric O_2, CO_2 and $\delta^{13}C$ measurements from aircraft sampling over Griffin Forest, Perthshire, UK". *Rapid Commun. Mass Spectrom.*, *19*, 2399–2406. DOI: 10.1002/rcm.2071.

Sturm, P., Leuenberger, M., Valentino, F. L., Lehmann, B., and Ihly, B. (2006). "Measurements of CO_2, its stable isotopes, O_2/N_2, and ^{222}Rn at Bern, Switzerland". *Atmos. Chem. Phys.*, *6*, 1991–2004.

Tans, P. P., Fung, I. Y., and Takahashi, T. (1990). "Observational constraints on the global atmospheric CO_2 budget". *Science*, *247*, 1431–1438. DOI: 10.1126/science.247.4949.1431.

Thompson, R. L., Manning, A. C., Lowe, D. C., and Weatherburn, D. C. (2007). "A ship-based methodology for high precision atmospheric oxygen measurements and its application in the Southern Ocean region". *Tellus, Ser. B*, *59*, 643–653. DOI: 10.1111/j.1600-0889.2007.00292.x.

Thoning, K. W., Conway, T. J., Zhang, N., and Kitzis, D. (1995). "Analysis system for measurement of CO_2 mixing ratios in flask air samples". *J. Atmos. Oceanic Technol.*, *12*, 1349–1356. DOI: 10.1175/1520-0426(1995)012<1349:ASFMOC>2.0.CO;2.

Tohjima, Y. (2000). "Method for measuring changes in the atmospheric O_2/N_2 ratio by a gas chromatograph equipped with a thermal conductivity detector". *J. Geophys. Res.-Atmos.*, *105*, 14575–14584. DOI: 10.1029/2000JD900057.

Tohjima, Y., Mukai, H., Machida, T., Nojiri, Y., and Gloor, M. (2005). "First measurements of the latitudinal atmospheric O_2 and CO_2 distributions across the western Pacific". *Geophys. Res. Lett.*, *32*, L17805. DOI: 10.1029/2005gl023311.

Tohjima, Y., Mukai, H., Nojiri, Y., Yamagishi, H., and Machida, T. (2008). "Atmospheric O_2/N_2 measurements at two Japanese sites: estimation of global oceanic and land biotic carbon sinks and analysis of the variations in atmospheric potential oxygen (APO)". *Tellus, Ser. B*, *60*, 213–225. DOI: 10.1111/j.1600-0889.2007.00334.x.

Uglietti, C. (2009). "Understanding the carbon cycle through atmospheric carbon dioxide and oxygen observations". PhD thesis. University of Bern, Bern, Switzerland.

Valentino, F. L. (2007). "A method to partition the measured atmospheric CO_2 based on oxygen measurements". PhD thesis. University of Bern, Bern, Switzerland.

Volz-Thomas, A., Smit, H., Cammas, J., Nedelec, P., Karcher, F., Stoll, M., Jones, R. L., Gallagher, M., Petzold, A., Schlager, H., Bickerstaff, C. M., Kershaw, A., Gerbig C. Waibel, A., Franke, H, Hermann, M., Barrie, L., Henshaw, T., and Girod, F. (2007). "In-service Aircraft for Global Oobservations – the future". *IGACtivities Newsletter*, *37*, 18–22.

Wada, A., Sawa, Y., Matsueda, H., Taguchi, S., Murayama, S., Okubo, S., and Tsutsumi, Y. (2007). "Influence of continental air mass transport on atmospheric CO_2 in the western North Pacific". *J. Geophys. Res.-Atmos.*, *112*, D07311. DOI: 10.1029/2006JD007552.

Waugh, D. W. and Hall, T. M. (2002). "Age of stratospheric air: Theory, observations, and models". *Rev. Geophys.*, *40*, 1010. DOI: 10.1029/2000RG000101.

Yates, E. L., Iraci, L. T., Roby, M. C., Pierce, R. B., Johnson, M. S., Reddy, P. J., Tadić, J. M., Loewenstein, M., and Gore, W. (2013). "Airborne observations and modeling of springtime stratosphere-to-troposphere transport over California". *Atmospheric Chemistry and Physics Discussions*, *13*, 10157–10192. DOI: 10.5194/acpd-13-10157-2013.

Erklärung

gemäss Art. 28 Abs. 2 RSL 05

Name, Vorname: Bigler, Iwan

Matrikelnummer: 06-919-047

Studiengang: Climate Sciences

Bachelor ☐ Master ☒ Dissertation ☐

Titel der Arbeit: Evaluation of combined CO_2 and O_2 measurements taken by the CARIBIC passenger aircraft

Leiter der Arbeit: Prof. Markus Leuenberger

Ich erkläre hiermit, dass ich diese Arbeit selbständig verfasst und keine anderen als die angegebenen Quellen benutzt habe. Alle Stellen, die wörtlich oder sinngemäss aus Quellen entnommen wurden, habe ich als solche gekennzeichnet. Mir ist bekannt, dass andernfalls der Senat gemäss Artikel 36 Absatz 1 Buchstabe o des Gesetzes vom 5. September 1996 über die Universität zum Entzug des auf Grund dieser Arbeit verliehenen Titels berechtigt ist.

Bern, 23.08.2013

Unterschrift